Characterisation of *Burkholderia pseudomallei* type III secretion system III components

Puthayalai Treerat

B.Sc. (Medical Technology), M.Sc. (by research)

A Thesis presented for the degree of

Doctor of Philosophy

May 2014

Department of Microbiology

Monash University

Clayton Campus, Melbourne 3800

Australia

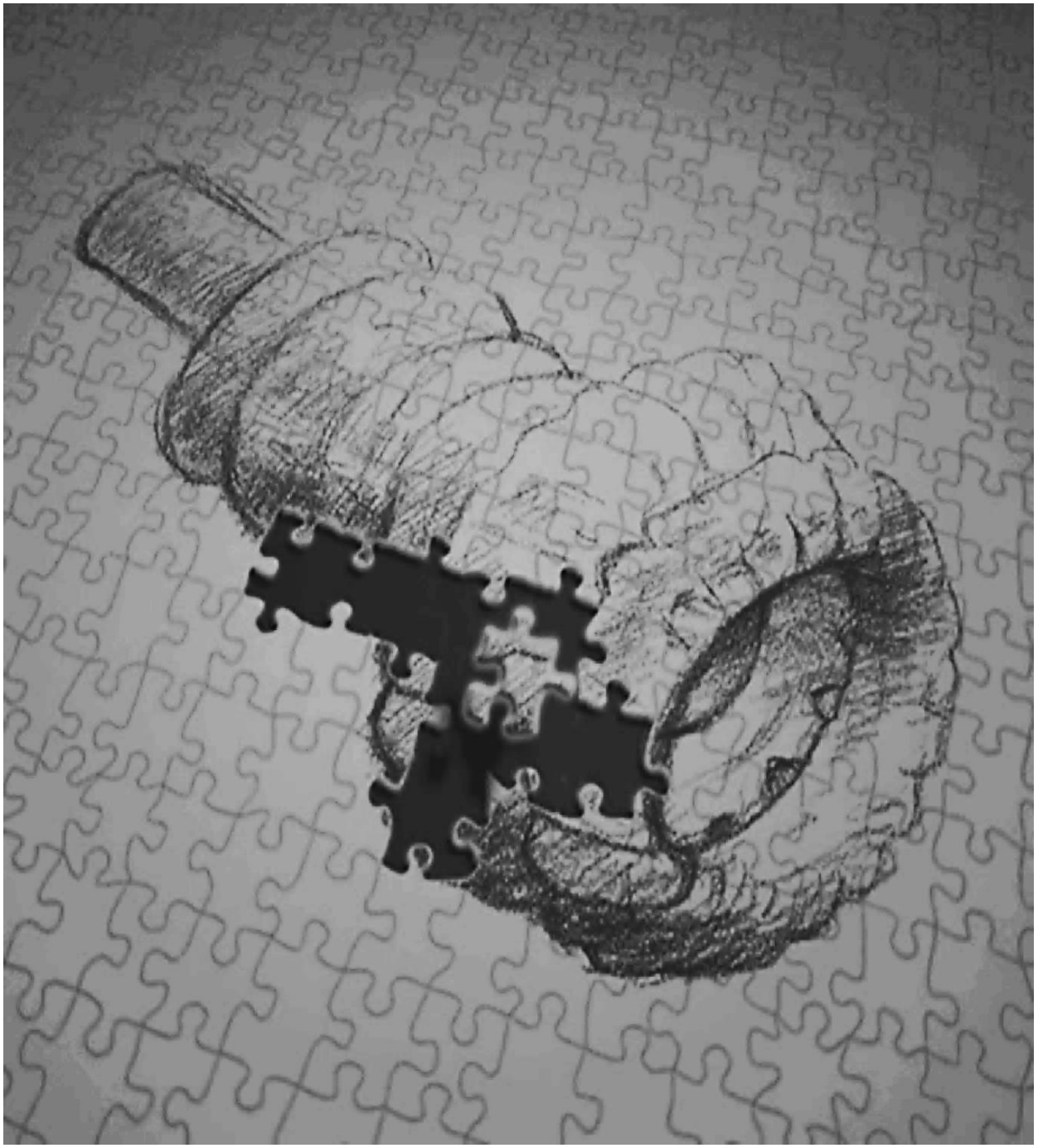

(http://thomas.marlovits.myresearchlab.org)

“Strength does not come from physical capacity. It comes from an indomitable will”

- Mahatma Gandhi

“Do not go where the path may lead, go instead where there is no path and leave a trail”

- Ralph Waldo Emerson

“Our greatest glory is not in never failing, but in rising up every time we fail”

- Ralph Waldo Emerson

“Success consists of going from failure to failure without loss of enthusiasm”

- Winston Churchill

Table of contents

Summary

In many intracellular pathogens, the type III secretion system (TTSS) plays an important role in virulence by secreting effector molecules directly across the host cell membrane. These effectors subsequently interact with, and alter, host signalling pathways for the benefit of the pathogen. *Burkholderia pseudomallei*, an intracellular pathogen that is the causative agent of the potentially fatal disease melioidosis, utilises a TTSS for its survival and replication in both phagocytic and non-phagocytic cells. Although this pathogen contains three TTSS gene clusters, the Type III Secretion System 3 (TTSS3) is critical for bacterial infectivity and pathogenesis. , However, to date, only BopE, BopA and BopC are characterised effectors of the TTSS-3. This research aimed to identify and characterise the putative TTSS3 proteins BapA, BapB and BapC with regard to their possible functions as bacterial effectors involved in either modulation of host cell functions for bacterial survival, replication or escape from host endosomal vacuoles, or the secretion of the other TTSS3 effectors. By using a double cross-over allelic exchange approach, *bapA, bapB, bapC* and double *bapBC* mutant strains were generated and assayed for their *in vivo* and *in vitro* phenotypes. Competitive growth assays in BALB/c mice showed reduced growth of each of the mutants compared to the wild-type. Furthermore, all showed reduced virulence in the acute mouse infection model, indicating possible roles in bacterial virulence. Complementation was attempted but was unsuccessful. Therefore, independent mutants were constructed. The independent mutants were all tested for virulence in the BALB/c acute model but only the *bapA_2* mutant showed reduced virulence compared to the wild-type strain. These data suggest that BapA likely plays a minor role in virulence, although successful complementation is required to conclusively prove this. To determine whether BapA, BapB and BapC were secreted effectors, the TC-FlAsH^{TM} labelling technique was used to monitor the secretion of tetracysteine-tagged fusion proteins. It was demonstrated that BapA and BapC are secreted *in vitro*. These proteins were secreted in a TTSS3-dependant manner as they were not secreted by mutant *B. pseudomallei* expressing a non-functional TTSS3. To further investigate any potential involvement of BapA, BapB and BapC in the TTSS3 secretion process, the well-characterised TTSS3 effector BopE was used as a marker to examine TTSS secretion in each of the mutant strains compared to the wild-type and the *bopE* mutant. The level of transcription of *bopE* was also assessed in certain strains in order to determine if there was any difference in the transcriptional regulation of this gene. It was demonstrated that, although BapA, BapB and BapC are not required for TTSS function, BapB appears to be necessary for normal secretion of BopE. Therefore, this study defines BapA and BapC as *B. pseudomallei* TTSS-3 effectors, and BapB as

a possible regulator of BopE secretion that may play a role in the pathogenicity of *B. pseudomallei*.

General declaration

In accordance with Monash University Doctorate Regulations, the following declarations are made:

I hereby declare that this thesis contains no material which has been accepted for the award of any other degree or diploma at any university or other institution and affirm that, to the best of my knowledge and belief, this thesis contains no material previously published or written by another person, except where due reference is made in the text of the thesis.

This thesis contains six chapters, compromising of Introduction (*Chapter 1*), Materials and methods (*Chapter 2*), three result chapters (*Chapter 3*, *4* and *5*) and General discussion and future directions (*Chapter 6*) with unpublished data. The core theme of the thesis is **characterising *Burkholderia pseudomallei* type III secretion system III components**. The ideas, development and writing of the chapters in the thesis were the principal responsibility of me, the candidate, working within the Department of Microbiology under the supervision of Dr. John D. Boyce and Professor Ben Adler.

The inclusion of co-authors reflects the fact that the work came from active collaboration between researchers and acknowledges input into team-based research.

In the case of *Chapters 3*, *4* and *5*, I was solely responsible for the collection of data. I was primarily responsible for data analysis and interpretation. A contribution to the conception of experimental questions and interpretation of data was made by Dr. John D. Boyce and Professor Ben Adler.

Signed:_____Puthayalai Treerat_____

Date:_____07/03/2014_____

Acknowledgements

Effective supervision is crucial in a student's path to successful completion. I was very fortunate to have the great opportunity to work with two wonderful supervisors, Dr. John D. Boyce and Professor Ben Adler, which has been invaluable on an academic and a personal level. To John, there are no proper words to convey my deepest gratitude and respect. You have always been knowledgeable, patient, extremely supportive, tolerant, kind and encouraging. I deeply thank you for having faith in me and giving me the freedom to pursue various skills/techniques without objection. To Ben, I cannot thank you enough for your expertise, understanding, patience, caring and unconditional support.

It has been an honour to be a member of Adler/Boyce Laboratory. These amazing and brilliant friends and colleagues (former and current) have always inspired and immensely supported me, and contributed to making this journey a rewarding experience. To Dr. Meabh Cullinane, Dr. Rebekah Henry (my all-time lifesaver), Dr. Xenia Gatsos (my coffee buddy), Dr. Gerald Murray and Dr. Marina Harper, I sincerely thank you for being knowledgeable in just about everything, your invaluable comments and advice toward improving my work and helping me to shape and guide the direction of the work. To Vicki Vallance, Saw Eng Tan and Ian McPherson, I deeply thank you for your tremendous support, encouragement and positive attitudes. Special thanks must also go to my invaluable network of supportive, helpful, cheerful, generous and loving friends: Priya Alwis (my 'partner in crime'), Amy King (my great officemate and attack buddy), Mark Edmunds (my coffee buddy with whom I can always talk about cars and motorcycles), Kate Rainczuk (my concert buddy), Rhys Dunstan (my heavy metal buddy), Alicia Shu-chin Lai (my lunch buddy), Jennifer Moffatt, Deanna Deveson, Dr. Elizabeth Alexander, Dr. Miranda Lo, Dr. Tim Witchell, Dr. Renee Marcsisin-Rogers, Joy Tong Chen Ai, Dr. Kunkun Zhang, Desmond Gul, Nathalie Uwamahoro and Amrei Jaenicke. I am also grateful to my collaborators in the Department of Biochemistry: Professor Rodney Devenish, Dr. Mark Prescott, Dr. Lan Gong, Dr. Xuelei Li, for the assistance they provided at all levels of my project, scientific advice, knowledge and many insightful discussions. To the members of my PhD committee: Professor Brian Cooke, Dr. David Sheffield and Dr. Xiao Yan Han, for invaluable advice and support. My special appreciations must also go to my beloved (and gorgeous) Mrs. "Clooney" Young (my ROCK!) for her never ending efforts to assist me on everything before I even began my PhD. To Dr. Candida da Fonseca Pereira, I deeply thank you for your prompt responses and extremely helpful advice with the FlAsH work. To Irene Hatzinisiriou, for always being so helpful with

imaging requests. To all members of Department of Microbiology, Micromon and SOBS Store, for invaluable support, help and advice. To all members of Monash Micro Imaging (MMI), for giving me the permission to use all required equipment and the necessary materials, being extremely helpful and knowledgeable (and for not kicking me out when I overbooked the FV1000!). To Dr. Jamuna Vadivelu, for generating the K96243*ΔbapA* strain. To Dr. Christopher French, for kindly sending the pBBR1 vector and invaluable advice. To Assistant Professor Jonathan Warawa, for kindly sending the pBHR1 vector. To Professor Mark Stevens, for kindly sending the BopE-specific antiserum. To Vicky Dimitriou, Liz Kemp, Jessica William, Rachel Cawsey and Jennifer Scott, for being so helpful with the administrative tasks necessary for completing my doctoral program. I would also like to express my heartfelt gratitude to ARC/NHMRC for funding the project and to MGS/MIPRS for the scholarships.

Friendship is not about whom you have known the longest, it's about who came, and never left your side. To my dearest friend Marietta John, I sincerely thank you for being extremely helpful, supportive, kind, and always standing beside me since I first arrived in Melbourne (best of luck for your PhD!). To Dr. Tanya D'Cruze, I deeply thank you for being so helpful, supportive, kind and friendly. To Dr. Miguel Shingu-Vazquez (my "mishin"), for always being my shadow buddy. Special thanks must also go to all my gym buddies for energy, friendship, joy and incredible fun: Shar, Teresa, Christelle, Kamil, Bianca, Thanh, Nazra, Jenny, May and Dini. Most importantly, to my dearest friend in Bangkok, Tomtam, I am truly grateful to have you as my like-minded buddy despite the distance.

Family is where life begins and love never ends, so last but not least, I am forever grateful to my parents for your unconditional love, never ending support and trust, and for never giving up on me. There are no words that can truly express the level of gratitude and appreciation I have for you, and I never could have come this far without you. To my beloved brother (my X-box buddy), who has always stood beside me despite the long distance between us and been my best friend since the day I was born. I will never truly be able to express my love to you and how much you mean to me. Thank you for your unwavering love and your faith in me, and for making me laugh and distracting me when I have been too focused.

Publications and conference proceedings

Journal publications:

- D'Cruze, T., Gong, L., **Treerat, P.**, Ramm, G., Boyce, J. D., Prescott, M., Adler, B. and Devenish, R. J., (2011), Role for the *Burkholderia pseudomallei* type three secretion system cluster 1 *bpscN* gene in virulence. *Infect Immun.,* **79,** 3659-3664.
- Gong, L., Cullinane, M., **Treerat, P.**, Ramm, G., Prescott, M., Adler, B., Boyce, J. D. and Devenish, R. J., (2011), The *Burkholderia pseudomallei* type III secretion system and BopA are required for evasion of LC3-associated phagocytosis, PLoS One, **6**, p e17852.

Conference proceedings:

- **Treerat, P.**, Alwis, P., D'Cruze, T., Cullinane, M., Vadivelu, J., Gong, L., Devenish, R. J., Prescott, M., Adler, B. and Boyce, J. D., (2012), As simple as *bapABC*: A new insight into the virulence of the human pathogen *Burkholderia pseudomallei*, *The 11th Awaji International Forum on Infection and Immunity*, Osaka, Japan.
- **Treerat, P.**, Alwis, P., D'Cruze, T., Cullinane, M., Vadivelu, J., Gong, L., Devenish, R. J., Prescott, M., Adler, B. and Boyce, J. D., (2012), As simple as *bapABC*: A new insight into the virulence of the human pathogen *Burkholderia pseudomallei*, *The 2nd Microbiology Student Conference*, Melbourne, Australia.
- **Treerat, P.**, Alwis, P., D'Cruze, T., Cullinane, M., Vadivelu, J., Devenish, R. J., Prescott, M., Adler, B. and Boyce, J. D., (2011), As simple as *bapABC*: A new insight into the virulence of the human pathogen *Burkholderia pseudomallei*. *BacPath 11: Molecular Biology of Bacterial Pathogens*, Wyong, Australia.
- **Treerat, P.**, Alwis, P., Prescott, M., Devenish, R. J., Adler, B. and Boyce, J., (2010), Importance of the type III secretion system genes *bapA*, *bapB* and *bapC* in the virulence of *Burkholderia pseudomallei*, *The 6th World Melioidosis Congress*, Townsville, Australia.
- **Treerat, P.**, Alwis, P., D'Cruze, T., Cullinane, M., Vadivelu, J., Devenish, R. J., Prescott, M., Adler, B. and Boyce, J. D., (2010), A new insight in the virulence of human pathogen *Burkholderia pseudomallei*, *The 1st Microbiology Student Conference*, Melbourne, Australia.

Abbreviations and definitions

μg	Microgram
μL	Microlitre
μM	Micromolar
ACP	Acyl carrier protein
ALP	Alkaline phosphatase
Amp^R	Ampicillin resistance
ANOVA	Analysis of Variance
ASC	Apoptosis associated speck-like protein containing a caspase recruitment domain
ATP	Adenosine triphosphate
B. mallei	*Burkholderia mallei*
B. pseudomallei	*Burkholderia pseudomallei*
B. thailandensis	*Burkholderia thailandensis*
BAL	2,3-dimercapto-1-propanol
Bap	Bsa associated protein
Bim	*Burkholderia* intracellular motility
Bip	*Burkholderia* invasion protein
BME	β-mercaptoethanol
Bop	*Burkholderia* outer protein
bp	Base pairs
bsa	*Burkholderia* secretion apparatus
BSA	Bovine serum albumin
^oC	Degrees Celsius

CARD	Caspase activation and recruitment domain
Cat	Chloramphenicol acetyl transferase
CDC	the Centers for Disease Control and Prevention
cDNA	Complementary DNA
CFU	Colony forming unit
Chl/Chl^R	Chloramphenicol resistance
CI	Competitive index
CpG	Cytosine-phosphate-guanine
CT	Computerised tomography
DAPI	4',6-diamidino-2-phenylindole
DEPC	Diethylpyrocarbonate
dH_2O	Distilled water
ddH_2O	Double-distilled water
DIC	Differential interference contrast
DIG	Digoxigenin
DMEM	Dulbecco's Modified Eagle Medium
DMSO	Dimethyl sulfoxide
DNA	Deoxyribonucleic acid
DNAse	Deoxyribonuclease
dNTPs	Deoxynucleotide triphosphates
DOC	Sodium deoxycholate
DTT	DL-Dithiothreitol
E. coli	*Escherichia coli*
ECL	Electrochemiluminescence

EDTA	Ethylenediaminetetraacetic acid
ELISA	Enzyme-linked immunosorbent assay
EPEC	Enteropathogenic *E. coli*
FCS	Fetal calf serum
FITC	Fluorescein isothiocyanate
FlAsH	4’,5’-bis(bis1,3,2-dithioarsolan-2-yl) fluorescein
g	Grams
GC	Guanine Cytosine
GFP	Green fluorescent protein
h	Hour(s)
HCl	Hydrochloric acid
HEPES	4-(2-hydroxyethyl)-1-piperazineethanesulfonic acid
HRP	Horseradish peroxidase
i.p.	Intraperitoneal
Iag	Invasion-associated gene
IFN-γ	Interferon-gamma
IgG	Immunoglobulin G
IL	Interleukin
IM	Inner membrane
iNOS	Inducible nitric oxide synthase
Inv	Invasion
Ipa	Invasion plasmid antigen
Ipg	Invasion plasmid gene
IRAK	Interleukin 1 receptor associated kinase

IRAK-M	Interleukin 1 receptor associated kinase-like molecule
IRF-1	Interferon-regulatory factor 1
Kan/Kan^{R}	Kanamycin resistance
kDa	KiloDalton
kb	Kilobase
L	Litre
L. monocytogenes	*Listeria monocytogenes*
LAMP-1	Lysosomal associated membrane protein-1
LAP	LC3-associated phagocytosis
LB	Luria-Bertani broth
LC3	Light chain 3
LD	Lactate dehydrogenase
LPS	Lipopolysaccharide
LT	Lytic transglycosylase
M	Molar
M. tuberculosis	*Mycobacterium tuberculosis*
MAPK	Mitogen-activated protein kinase
Mb	Mega base
MBC	Minimum bactericidal concentration
MCS	Multiple cloning site
min	Minute(s)
mL	Millilitre
mM	Millimolar
MNGC	Multinucleated giant cell

MOI	Multiplicity of infection
mRNA	Messenger RNA
MTOC	Microtubule-organising centre
Mxi	Membrane expression of Ipa
MyD88	Myeloid differentiation factor 88
NaCl	Sodium chloride
NF-κB	Nuclear factor-kappa B
NK	Natural killer
NLR	NOD-like receptor
NLRC4	NOD-like receptor family, CARD domain containing 4
NLRP3	NOD-like receptor family, pyrin domain containing 3
nm	Nanometre
NO	Nitric oxide
NOD	Nucleotide-binding oligomerisation domain
OD_{600}	Optical density at 600 nm
OM	Outer membrane
P. aeruginosa	*Pseudomonas aeruginosa*
PAGE	Polyacrylamide gel electrophoresis
PAMP	Pathogen-associated molecular patterns
PBS	Phosphate buffer saline
PCR	Polymerase chain reaction
PFA	Paraformaldehyde
pg	Picograms
PG	Peptidoglycan

pH	Potential of hydrogen
p.i.	Post infection
PP	Pantetheine 4' phosphate
PRR	Pattern recognition receptor
PVDF	Polyvinylidene difluoride
QS	Quorum sensing
RE	Restriction enzyme
RNA	Ribonucleic acid
RNase	Ribonuclease
ROS	Reactive oxygen species
rpm	Revolutions per minute
RPMI	Roswell Park Memorial Institute
RT	Room temperature
RT-PCR	Reverse transcription - polymerase chain reaction
S. enterica	*Salmonella enterica*
S. flexneri	*Shigella flexneri*
S. typhi	*Salmonella typhi*
SCV	*Salmonella* containing vacuole
SDS	Sodium dodecyl sulfate
sec	Second(s)
Sip	*Salmonella* invasion protein
Sm^R	Streptomycin resistance
SOB	Super optimal broth
Sop	*Salmonella* outer protein

SPI1	*Salmonella* pathogenicity island 1
SPI2	*Salmonella* pathogenicity island 2
Spa	Surface presentation of antigen
SSC	Saline-sodium citrate
TAE	Tris-acetate-EDTA
TBS	Tris-buffered saline
TC	Tetracysteine
TCA	Trichloroacetic acid
TCEP	Tris(2-carboxyethyl) phosphine
TEMED	N,N,N,N'-tetramethylenediamine
Temp	Temperature
Tet/Tet^R	Tetracycline resistance
TLR	Toll-like receptor
Tp^R	Trimethoprim resistance
TNF-α	Tumour necrosis factor-α
TREM-1	Triggering receptor expressed on myeloid cells-1
TRITC	Tetramethylrhodamine isothiocyanate
TTSS	Type III secretion system
TTSS1	Type III secretion system cluster 1
TTSS2	Type III secretion system cluster 2
TTSS3	Type III secretion system cluster 3
UV	Ultraviolet
V	Volt
v/v	Volume/volume

w/v	Mass/volume
WT	Wild-type
X. campestris	*Xanthomonas campestris*
X. oryzae	*Xanthomonas oryzae*
Yop	*Yersinia* outer protein

Chapter 1

Introduction

Chapter 1: Introduction

In this Chapter, information on the human pathogen *Burkholderia pseudomallei* is summarised with regard to the disease caused by this bacterium and pathogenicity. Some important virulence factors, especially the type III secretion system (TTSS), are described in more detail. Furthermore, the techniques employed for characterising the target genes in this study are also summarised and compared with other techniques.

1.1 Melioidosis

Melioidosis is an emerging infectious disease caused by the Gram-negative pathogen *B. pseudomallei*, that was first reported by Major Alfred Whitmore and Dr. C. S. Krishnaswami in 1912 (Whitmore, 1913). The disease is prevalent in tropical environments, especially Southeast Asia and Northern Australia (*Figure 1.1.1*), with increased numbers of cases reported after the rainy season (Meumann *et al.*, 2012). Cases have recently been reported in countries where they have not previously been recognised (Cheng & Currie, 2005). Clinical manifestations of melioidosis are diverse (*Figure 1.1.2*), due to a range of factors including the ability of the pathogen to disseminate and cause infection in almost any host tissue, and different presentations in hosts with underlying predisposing conditions (Currie *et al.*, 2004; Wiersinga *et al.*, 2012). Nonetheless, cutaneous, pneumonic and the often fatal septicaemic melioidosis are the three most common manifestations reported (Currie, 2003). Such diversity in manifestations can lead to misdiagnosis resulting in delayed, absent, and/or inappropriate treatments. Recurrent infection is common, possibly due to the ability of the bacterium to remain dormant within the host, and infection may reactivate later in life (Hayden *et al.*, 2012; Ngauy *et al.*, 2005). Direct cutaneous inoculation and inhalation are the two major transmission modes of melioidosis (Cheng & Currie, 2005). The incubation period also varies due mainly to the different routes of transmission and host health conditions − the longest incubation period reported is 62 years (Ngauy *et al.*, 2005). The mortality rate varies depending upon several factors, including the rapidity and accuracy of disease diagnosis and host underlying diseases (Wiersinga *et al.*, 2012). The overall mortality rates in endemic areas such as Thailand and Northern Australia are approximately 40% and 20%, respectively (Meumann *et al.*, 2012; Wiersinga *et al.*, 2006). Treatment of melioidosis and prevention of recurrent infections can be difficult due to misdiagnosis of melioidosis, intrinsic antibiotic resistance of the organism and inappropriate antibiotic treatment regimens that result in acquired-antibiotic resistance (Estes *et al.*, 2010; Wiersinga *et al.*, 2012). Intravenous administration of ceftazidime in combination with meropenem followed by oral administration of trimethoprim/sulfamethoxazole appears to be the

most effective treatment regimen (Wuthiekanun & Peacock, 2006); however, ceftazidime resistance has been observed following ceftazidime chemotherapy (Sarovich *et al.*, 2012). Vaccination has been extensively studied as a prevention strategy for melioidosis (Atkins *et al.*, 2002a; Atkins *et al.*, 2002b). However, there are currently no licensed vaccines and no experimental vaccines that can generate solid cross-protective immunity against multiple *B. pseudomallei* strains without causing adverse effects (Peacock *et al.*, 2012).

1.2 *Burkholderia pseudomallei*

B. pseudomallei, the causative agent of melioidosis, is a Gram-negative, motile, saprophytic and non-spore forming bacillus found in tropical environments (Galyov *et al.*, 2010; Peacock, 2006). The bacterium is classified in the Phylum Proteobacteria, Class Betaproteobacteria, Order Burkholderiales, Family *Burkholderiaceae*, Genus *Burkholderia*, Species group *pseudomallei* (Yabuuchi *et al.*, 1992). It has been classified as a category B bioterrorism agent by the Centers for Disease Control and Prevention (CDC) (Atlas, 2003). The complete 7.25-megabase pair (Mb) genome of *B. pseudomallei* strain K96243, a clinical isolate from a diabetic patient in Thailand, is composed of two chromosomes of 4.07- and 3.17-Mb pairs. The large chromosome, or chromosome 1, encodes proteins primarily involved in the essential functions of central metabolism and cell growth while the small chromosome, or chromosome 2, encodes many proteins associated with accessory functions including bacterial virulence and adaptation and survival in different niches (Holden *et al.*, 2004). This may explain why *B. pseudomallei* is capable of persisting in a range of niches including under anaerobic conditions (Hamad *et al.*, 2011) or even in non-nutrient conditions such as distilled water (Moore *et al.*, 2008; Pumpuang *et al.*, 2011). In addition, such unique genotypes allow this bacterium to adapt and reside in many host cell types (Chieng *et al.*, 2012; Jones *et al.*, 1996; Pilatz *et al.*, 2006) and also overcome antimicrobial mechanisms of the host (Galyov *et al.*, 2010; Wiersinga *et al.*, 2006). Key features of the intracellular lifestyle of *B. pseudomallei* and the host immune response to infection are summarised in *Figure 1.2.1*.

B. pseudomallei is a facultative intracellular pathogen that is capable of invading and replicating within many host cells, including non-phagocytic and phagocytic cells (Jones *et al.*, 1996; Kespichayawattana *et al.*, 2000). Once internalised in the host cells, *B. pseudomallei* utilises several mechanisms for lysing host endosomal membranes, resulting in the escape from the host endosomal vacuole into the cytoplasm (Chieng *et al.*, 2012; Galyov *et al.*, 2010). In addition, this bacterium is able to modulate actin polymerisation resulting in membrane protrusion,

intercellular migration, cell-to-cell fusion and multinucleated giant cell (MNGC) formation (Kespichayawattana *et al.*, 2000; Stevens *et al.*, 2006). In addition, to avoid bacterial clearance and promote bacterial persistence within the host, *B. pseudomallei* has evolved a number of strategies for suppression of host immune responses (Chieng *et al.*, 2012; Gan, 2005). Intracellular *B. pseudomallei* can down-regulate key virulence genes, including those involved in synthesis of LPS and flagellin, in order to avoid stimulation of host innate immunity especially through toll-like receptors (TLRs), which are essential for the recognition of pathogens and initiation of the innate immune response (Chieng *et al.*, 2012). Furthermore, failure to induce the production of IFN-β, resulting in reduced production of inducible nitric oxide synthase (iNOS), is a key bacterial defence against phagocytic killing, since both molecules are required for bacterial elimination by macrophages (Ceballos-Olvera *et al.*, 2011; Tangsudjai *et al.*, 2010). In addition, the ability to induce the expression of sterile-α and Armadillo motif (SARM) protein, a key negative regulator of the MyD88-independent pathway, in a time-dependent manner, appears to be another key bacterial factor for suppressing host immunity (Pudla *et al.*, 2011). As well as suppression of the host immune response, *B. pseudomallei* is intrinsically multi-drug resistant and can acquire further antibiotic resistance following exposure to various antibiotics (Cheng & Currie, 2005; Godfrey *et al.*, 1991; Sawasdidoln *et al.*, 2010).

1.3 Virulence factors of *B. pseudomallei*

To fully understand bacterial pathogenesis, it is important to understand the virulence mechanisms of the aetiologic agents. Similar to most pathogenic bacteria, *B. pseudomallei* possesses a large number of virulence factors that are necessary for the ability of the bacterium to cause disease, to survive intracellularly during latent periods and to allow reactivation (Ernst *et al.*, 1999; Galyov *et al.*, 2010; Moore *et al.*, 2004; Schroeder & Hilbi, 2008). By employing signature-tagged mutagenesis (STM), a number of genes required for bacterial pathogenicity have been identified, including those involved in capsular biosynthesis, DNA replication and repair, and aromatic amino acid biosynthesis (Cuccui *et al.*, 2007). Moreover, several genes, including *BPSS1539* encoding a hypothetical protein within the type III secretion system cluster 3 (TTSS3; *bsa*TTSS), have been found to play an important role in *in vitro* plaque formation, an indicator for intracellular survival and intercellular spreading of *B. pseudomallei* (Pilatz *et al.*, 2006). A summary of key virulence factors of *B. pseudomallei* especially TTSS is provided below.

1.3.1 Polysaccharides

In contrast to other Gram-negative pathogens, *B. pseudomallei* LPS appears to stimulate a reduced host innate immune response, resulting in enhanced host immune evasion (Sarkar-Tyson *et al.*, 2007). The unique LPS structure, consisting of 3-hydroxyhexadecanoic acid, an amide-linked fatty acid, and an acid-stable structure attached to lipid A at the inner core region, helps the bacterium to suppress the host immune response (Kawahara *et al.*, 1992). In addition, the long chain fatty acid $C_{14:0}$(2-OH) and Ara4N-modified phosphate groups of the lipid A species identified in *B. pseudomallei* also play a key role in host immune evasion; these groups are absent in the avirulent strain *B. thailandensis* (Novem *et al.*, 2009). Characterisation of four gene clusters encoding type I, II, III and IV surface polysaccharides has shown an essential role for each in bacterial virulence and these polysaccharides have also been tested as vaccine candidates (DeShazer *et al.*, 1998; DeShazer *et al.*, 2001; Sarkar-Tyson *et al.*, 2007). The O-antigen polysaccharide moiety of *B. pseudomallei* has been shown to alter the host innate immune response, at least in part by suppressing interferon-regulatory factor 1 (IRF-1) expression, an essential transcription factor of iNOS, thereby interfering with the bactericidal activities of macrophages (Arjcharoen *et al.*, 2007). Thus, it is clear that *B. pseudomallei* uses its unique LPS as one of the key virulence factors mainly for host innate immune suppression contributing to long-term persistence in the host. In addition to LPS, capsular polysaccharide, another key virulence factor, enables the bacterium to resist phagocytosis and contributes to bacterial persistence by inhibiting the deposition of host complement factor C3b on the bacteria. Inactivation of capsular production directly affects bacterial survival and replication (Reckseidler-Zenteno *et al.*, 2005).

1.3.2 Quorum sensing (QS)

QS is also an important mechanism involved in bacterial pathogenicity (Galyov *et al.*, 2010). QS is a type of two-component system for the control of gene expression in response to cell density. In *B. pseudomallei* two main molecules, LuxR and LuxI, are responsible for transcriptional regulation and production of QS molecules (Poole, 2001). Inactivation of the *B. pseudomallei* QS networks results in a decrease in bacterial localisation in the lungs, but not in the liver and spleen, suggesting either an essential role of bacterial QS with regard to organ-specificity, or bacterial survival and multiplication, but not dissemination (Ulrich *et al.*, 2004). *B. pseudomallei* possesses at least five LuxR and three LuxI homologs which can produce up to seven QS molecules, including *N*-octanoyl-homoserine lactone (C8-HSL), *N*-(3-hydroxyoctanoyl)-L-homoserine lactone (3-hydroxy-C8-HSL), 3-oxo-C8-HSL, *N*-decanoyl-homoserine lactone

(C10-HSL), 3-hydroxy-C10-HSL, 3-oxo-C10-HSL, 3-hydroxy-C12-HSL and 3-oxo-C14-HSL (Ulrich *et al.*, 2004), indicating the complexity of the QS network of this bacterium.

1.3.3 Efflux pumps

Efflux pumps are also key factors contributing to the inherent and acquired aminoglycoside and macrolide antibiotic resistance observed in this bacterium (Poole, 2001) but also have direct role in virulence. These systems generally consist of at least three subunits: a cytoplasmic transporter protein, an outer membrane channel and a periplasmic linker protein, and function by excreting different molecules, including antibiotics, in a proton motive force-dependent manner (Nikaido, 1998). The *B. pseudomallei* AmrAB-OprA complex is specific for excreting aminoglycoside and macrolide antibiotics and shows significant similarity to multidrug efflux systems found in *P. aeruginosa* and *E. coli* (Moore et al., 1999). Another efflux pump in the same family, named BpeAB-OprB, has specificity for aminoglycosides, except for spectinomycin, and macrolides, except for clarithromycin (Chan et al., 2004). This suggests a possible synergistic activity between both efflux pumps, resulting in the high intrinsic resistance to aminoglycoside and macrolide antibiotics, and may be part of the reason why antibiotic combination regimens for treatment of melioidosis are often ineffective. The *B. pseudomallei* BpeAB-OprB efflux pump can also excrete some QS molecules (Chan et al., 2007). This efflux pump has been found to play an essential role in bacterial invasion, cytotoxicity, biofilm formation and siderophore and phospholipase production, possibly via the QS mechanism (Chan & Chua, 2005), suggesting how cross-talk between two different mechanisms can contribute to bacterial survival and virulence.

1.3.4 Biofilm production

The ability to form biofilms is an important virulence mechanism that is likely to be associated with chronic infections and/or avoidance of killing by the host immune response and by antibiotics (Joo & Otto, 2012). The formation and maturation of biofilms, including detachment from biofilm matrix, appears be regulated by QS systems (Ramli *et al.*, 2012). This relationship demonstrates an important cross-talk between two virulence factors with regard to survival and multiplication of the bacteria within the host. In *B. pseudomallei*, there seems to be a significant correlation between ability to form biofilms and strain virulence, since biofilm formation has been found only in clinical isolates, and not in the non-pathogenic strain *B. thailandensis*. However, there seems to be no correlation between biofilm formation and virulence in the acute BALB/c mouse infection model (Taweechaisupapong *et al.*, 2005). Given that biofilm formation

is more frequently associated with chronic infection, using the chronic mouse infection model may be more appropriate. Furthermore, it has been suggested that, instead of the biofilm itself, other factors activated and produced during or after biofilm formation may also play important roles in promoting acquired antibiotic resistance (Sawasdidoln *et al.*, 2010).

1.3.5 Flagella

Many Gram-negative pathogens employ flagella as essential tools for bacterial motility and adhesion, thereby contributing to bacterial colonisation and dissemination of disease (Bucior *et al.*, 2012; Ibarra & Steele-Mortimer, 2009; Kutsukake, 1997). *B. pseudomallei* possesses a number of proteins with similarity to flagellar structural and biosynthesis proteins, and both swimming motility and adhesion have been linked with virulence *in vivo* (Chua *et al.*, 2003; Wiersinga *et al.*, 2006; Yu *et al.*, 2010a). A role has been reported for the *B. pseudomallei* FliC protein in bacterial virulence in the BALB/c mouse infection model even though this flagellin protein does not seem to be involved in bacterial invasion and intracellular replication *in vitro* (Chua *et al.*, 2003). Moreover, post-translational processes, such as glycosylation, of flagellin protiens appear to be key factors in determining virulent and non-virulent strains of *B. pseudomallei* (Scott *et al.*, 2011). The components of the flagella are closely related to type III secretion system (TTSS) components; indeed, flagella can be additionally employed for secretion of various proteins including those required for the biogenesis and operation of flagella, such as flagellin, and this system has been called the flagella-mediated TTSS (Büttner, 2012). The fundamental components of the flagella-mediated TTSS are illustrated in *Figure 1.3.1*. Several proteins are required for the formation and assembly of the flagellar structure, which crosses the bacterial inner membrane, periplasmic space and outer membrane (Homma *et al.*, 1990; Minamino *et al.*, 2000). Of these proteins, FlgJ is one of the key molecules required for efficient assembly since its C-terminal muramidase domain, also known as a soluble lytic transglycosylase, is involved in degradation of the peptidoglycan layer during the early stage of flagellar assembly and its N-terminal domain is involved in the formation of the basal body structure (de la Mora *et al.*, 2007; Hirano *et al.*, 2001; Nambu *et al.*, 1999). In addition, flagella-specific chaperones are essential not only for preventing the premature degradation/aggregation of their cognate proteins in the cytoplasm, but are also involved in regulation of flagellar-associated gene expression during the assembly process (Aldridge *et al.*, 2006; Bennett *et al.*, 2001; Imada *et al.*, 2010). After basal body formation, specific flagellar-associated proteins are activated or inactivated in order to control the flagellar hook length, ensure the completion of the assembly process or trigger flagellar function (Aldridge & Hughes, 2002). The expression of

various flagellar components is tightly regulated at both the transcriptional and translational level (Aldridge *et al.*, 2006; Kutsukake, 1997; Kutsukake *et al.*, 1990; McCarter, 2006).

Several flagellar components have been shown to be important for bacterial pathogenesis. Flagellin, the key structural protein which forms the major part of the filament body, plays important roles in bacterial motility and colonisation, but is also a target for the host innate and adaptive immune responses (Hayashi *et al.*, 2001; Ramos *et al.*, 2004). In addition to flagellin itself, some additional molecules resulting from the post-translational modification of flagellin, such as the glycans used to glycosylate flagellin appear to be involved in bacterial virulence and host immune interaction (Logan, 2006; Scott *et al.*, 2011). Flagellin is a critical virulence factor, since all BALB/c mice infected with a *B. pseudomallei fliC* mutant survived and did not show any signs of infection, whereas all mice infected with the wild-type succumbed to disease (Chua *et al.*, 2003). Moreover, flagellin-specific antiserum obtained from rabbits immunised with purified flagellin, confers passive protection against an intraperitoneal *B. pseudomallei* challenge in the diabetic rat melioidosis model (Brett *et al.*, 1994). These results suggest that flagellin components may have potential as vaccine candidates for melioidosis prevention. However, conversely, the *fliC* mutant showed no difference in *B. pseudomallei* virulence in either the diabetic rat or Syrian hamster infection model (DeShazer *et al.*, 1997). These contradictory results could result from the variation of using different bacterial strains, or the different importance of the flagella in the different animal models.

1.3.6 Type III secretion system (TTSS)

The type III secretion system (TTSS), evolved from the flagellar TTSS, is a key virulence factor required for delivering effector proteins from the bacterial cell directly into the eukaryotic cell cytosol (Abby & Rocha, 2012; Aizawa, 2001; Galan & Collmer, 1999; Gophna *et al.*, 2003; Plano *et al.*, 2001). These effectors subsequently interact with, and subvert, an array of host cell functions for the benefit of the bacteria (Coombes & Pilar, 2011; Dean, 2011). Similar to the flagellar TTSS, the core structure of TTSS consists of three main parts: the basal body spanning the bacterial inner and outer membranes; the needle-like apparatus or injectisome, which allows for the direct translocation of effectors; and the translocon, a set of proteins located at the tip of the injectisome that makes a direct connection with the host cell (Blocker *et al.*, 2003; Cornelis, 2006; Galan & Wolf-Watz, 2006). Similar to bacterial flagella, the TTSS assembly and operation processes are required to be precisely regulated (Brutinel & Yahr, 2008; Deane *et al.*, 2010; Deng *et al.*, 2005). The components required for formation of the TTSS basal body appear to be

exported by the Sec secretion machinery, and the subsequent components are secreted by the TTSS itself (Blocker *et al.*, 2003; He *et al.*, 2004). Following the basal body formation, the injectisome is assembled as a conduit-like helical structure by polymerisation of several subunits of a single molecule, and its length is appropriately controlled by the translocon protein complex located at the tip of the injectisome (Fujii *et al.*, 2012; Journet *et al.*, 2003; Marlovits *et al.*, 2004; Wagner *et al.*, 2010; Worrall *et al.*, 2011). After formation of the TTSS fundamental structure, there seem to be two distinct functional modes of TTSS secretion; the first involves the secretion of translocons for penetrating and forming the pore in the host cell membrane. Hence, these act as the tip complex and block secretion of bacterial effectors. The second involves the release of the tip complex and the secretion of effectors through the pore into the host cell (Deane *et al.*, 2010; Galan & Wolf-Watz, 2006; Matteï *et al.*, 2011; Mueller *et al.*, 2008). Importantly, the TTSS structure proteins are well-conserved among different Gram-negative bacteria whereas the effector proteins are not (Arnold *et al.*, 2009).

Upon receiving the appropriate TTSS stimulation signal, including the cholesterol-rich membrane of the host, the TTSS secretion is triggered to deliver destined effectors into the host cell cytosol for manipulation of host cell functions (Buchrieser *et al.*, 2000; Coburn *et al.*, 2007; Figueira & Holden, 2012; Ghosh, 2004). The secretion of effectors may follow a TTSS-specific chaperone-dependent pathway; the chaperones help to prevent the premature folding of the effectors, protect against unintentional interactions of the effectors, or ensure the efficient secretion of the effectors (Costa *et al.*, 2012; Francis *et al.*, 2001; Ho Lee & Galan, 2003; Ogawa *et al.*, 2003; Parsot *et al.*, 2003). However, some effectors are capable of being delivered into the target cells without any requirement for chaperone interaction (Johnson *et al.*, 2007). Interestingly, some cross-talk between flagella-dependent motility and TTSS function has been reported as, in the absence of flagella, TTSS gene expression and secretion was increased, whereas a decrease in expression of flagellar genes was observed in a strain with overproduction of ExsA, a crucial protein required for regulation of TTSS transcription (Brutinel *et al.*, 2009; Soscia *et al.*, 2007). These data suggest that there is negative cross-regulation between both systems.

1.3.7 *B. pseudomallei* and TTSS

B. pseudomallei possesses three TTSS gene clusters, the third of these is designated TTSS3 and contains 35 genes (Holden *et al.*, 2004; Wiersinga *et al.*, 2006). The TTSS3 is closely related to the Inv/Mxi-Spa systems of *Salmonella* and *Shigella*, which are required for bacterial invasion

and virulence, indicating a role for this cluster in *B. pseudomallei* pathogenesis (Stevens *et al.*, 2002; Stevens *et al.*, 2004). Proteins encoded by the TTSS cluster 1 (TTSS1) and 2 (TTSS2) show significant similarity to TTSS proteins in the plant pathogens *Ralstonia solanacearum* and *Xanthomonas* spp., suggesting that these *B. pseudomallei* systems may also be involved in infection of plants even though no change in plant pathogenicity phenotype was observed for a *B. thailandensis* TTSS2 mutant (Attree & Attree, 2001; Rainbow *et al.*, 2002; Winstanley *et al.*, 1999). Recently, the TTSS1 was shown to be important for *B. pseudomallei* virulence in the BALB/c mouse model (D'Cruze *et al.*, 2011). The TTSS1 is present only in *B. pseudomallei* while the TTSS2 and TTSS3 are present in *B. pseudomallei*, *B. mallei* and the avirulent strain *B. thailandensis* (Wiersinga *et al.*, 2006). Although *B. pseudomallei* and *B. thailandensis* possess both TTSS2 and TTSS3, transcription of TTSS3 genes in *B. thailandensis* is negatively regulated by L-arabinose. The genes responsible for arabinose assimilation are absent in *B. pseudomallei* (Moore *et al.*, 2004), suggesting a direct link between loss-of-function of this locus and virulence of *B. pseudomallei*.

1.3.8 The TTSS cluster 3 (TTSS3; *bsa*TTSS)

Sun and Gan (2010) proposed a putative structure for the *B. pseudomallei* TTSS3 complex (*Figure 1.3.2*) based on information obtained from well-characterised TTSS proteins in other organisms. The genetic organisation of the genes involved in TTSS3 biogenesis and their predicted function is illustrated in *Figure 1.3.3.* The expression of the genes encoding the TTSS3 structural proteins, translocons, effectors, chaperones and transcriptional regulators is precisely regulated; some chaperones may play additional roles, either direct or indirect, as transcription factors for regulating the expression of other TTSS components during infection (Büttner, 2012; Francis *et al.*, 2002). During *B. pseudomallei* pathogenesis, TTSS genes are expressed sequentially in order to allow for their specific functions (Sun & Gan, 2010; Sun *et al.*, 2010). The injectisome is composed of a two-helix bundle of polymerised BsaL which is stabilised by interhelix hydrophobic contacts (Zhang *et al.*, 2006). The basal body, consisting of the inner ring (BsaM and BsaJ), export apparatus (BsaQWXYZ), minor subunit (BsaK) and outer ring (BsaO), crosses the bacterial inner membrane, peptidoglycan and outer membrane (*Figure 1.3.2*). These export apparatus proteins, in collaboration with BsaY and BsaS proteins, are required for promoting effector secretion (Sun & Gan, 2010). In addition, the needle assembly proteins BsaU and BsaT have been suggested to be involved in regulation of the injectisome length and the secretory function, respectively (Muangsombut *et al.*, 2008; Sun & Gan, 2010). The complete TTSS comprises the needle tip complex, injectisome, basal body, cytoplasmic domain,

transcriptional regulators, chaperones and effectors (Sun & Gan, 2010). The needle tip complex is composed of three core proteins BipD, BipB and BipC; the homologous proteins in *Salmonella* are the translocons SipD, SipB and SipC, and these play a key role in forming the TTSS pore in the host cell membrane (Stevens *et al.*, 2002). BipD, in addition, has been shown to be essential for a range of functions *in vitro*, including invasion of epithelial cells, survival and multiplication in macrophages, bacterial escape from host endosomes and actin-mediated motility. Furthermore, BipD is required for full bacterial virulence in the BALB/c and C57BL/6 mouse infection models (Stevens *et al.*, 2002; Stevens *et al.*, 2004). *B. pseudomallei bipB* mutants are also attenuated for virulence and show reduced MNGC formation and cell-to-cell spread, although these last two phenotypes are likely due specifically to the inability of the *bipB* mutant to escape from the endosome (Suparak *et al.*, 2005).

Many studies have analysed the role of the *B. pseudomallei* TTSS3 or its components in pathogenesis (Burtnick *et al.*, 2008; Cullinane *et al.*, 2008; Druar *et al.*, 2008; French *et al.*, 2011; Gong *et al.*, 2011; Muangman *et al.*, 2011; Muangsombut *et al.*, 2008; Stevens *et al.*, 2002; Warawa & Woods, 2005). It was initially reported that the TTSS3 was associated with *B. pseudomallei* invasion of non-phagocytic cells (Stevens *et al.*, 2003). However, it has been recently argued that the TTSS3 does not play a direct role in bacterial invasion (French *et al.*, 2011). However, the TTSS3 promotes escape of the bacterium from the phagosomes of phagocytic cells and is therefore an essential prerequisite for replication within the cytoplasm of these cells (Stevens *et al.*, 2002). Once in the cytoplasm, *B. pseudomallei* can move by actin-mediated motility; leading to intercellular and/or intracellular movement and the induction of multinucleated giant cell (MNGC) formation, which allows cell to cell spread without exposure to the host immune response (Kespichayawattana *et al.*, 2000; Stevens *et al.*, 2006; Suparak *et al.*, 2005). Several genes in this cluster are required for full bacterial virulence. Furthermore, specific antibodies against some TTSS3 proteins can be detected in patient sera, confirming the expression of the TTSS3 *in vivo* (Felgner *et al.*, 2009). TTSS3 components have also been shown to be specifically targeted by $CD4^+$ and/or $CD8^+$ T cell responses (Haque *et al.*, 2006), indicating a role of TTSS3 in host adaptive immune response.

Following physical contact with the host cell, the TTSS3 effectors, with or without interaction of specific TTSS3 chaperones, are delivered into the host cytoplasm where there is a direct interaction between effectors and host cell proteins (Dean, 2011). To date, only three putative TTSS3 effectors, BopE, BopA and BopC, have been characterised (Cullinane *et al.*, 2008; Gong

et al., 2011; Muangman *et al.*, 2011; Stevens *et al.*, 2003). BopE was the first TTSS3 effector shown to be secreted in a TTSS3-dependent manner (Stevens *et al.*, 2003). BopE is a guanine nucleotide exchange factor, which can activate two host cell molecules, Cdc42 and Rac1. Cdc42 and Rac1 are members of the Rho family of GTPase molecules, and induce rearrangement of actin in the host cell leading to membrane ruffling. Interestingly, the *bopE* mutant retains the ability to cause wild-type levels of disease, at least in the BALB/c mouse infection model (Stevens *et al.*, 2004). Therefore, it is possible that BopE is not required for bacterial virulence, or that *B. pseudomallei* has functionally redundant proteins which can compensate for the absence of BopE.

BopA was the second putative effector identified, and while secretion has not experimentally been proved, BopA is clearly required for efficient escape of *B. pseudomallei* from host endosomes and avoidance of host LC3-associated phagocytosis (Cullinane *et al.*, 2008; Gong *et al.*, 2011). Moreover, *bopA* mutants show partial attenuation for virulence, indicating an involvement in bacterial pathogenesis (Stevens *et al.*, 2004). Recently, a third TTSS3 effector, BopC, was shown to be secreted *in vitro* in a TTSS3-dependent manner (Muangman *et al.*, 2011). The *bopC* (*BPSS1516*) gene is located beside the *BPSS1517* gene predicted to encode its cognate chaperone. Disruption of *bopC* decreased invasion of *B. pseudomallei* into human lung epithelial cells *in vitro*, suggesting an important role of BopC in virulence (Muangman *et al.*, 2011). Another *B. pseudomallei* effector CHBP has been shown to inhibit ubiquitination process by specifically targeting host glutamine Gln-40 in ubiquitin and NEDD8 (Cui *et al.*, 2010). This effector is a cycle inhibiting factor (Cif) homolog that contains a conserved catalytic triad essential for inducing eukaryotic cell cycle arrest, thereby inactivation of the normal cell cycle progression (Yao *et al.*, 2009). However, specific secretion of this effector by the TTSS has not been demonstrated.

1.4 Analysis of the secretion of TTSS effectors

Several techniques have been used to investigate the secretion and translocation of TTSS effectors in different Gram-negative pathogens (Bobard *et al.*, 2011; Enninga & Rosenshine, 2009; Giepmans *et al.*, 2006; Rodrigues & Enninga, 2010). Due to the fact that the inner diameter of TTSS needle-like apparatus is very narrow (approximately 2 nm), it is crucial that any technique being used should not impede the secretion process (Blocker *et al.*, 2003; Ghosh, 2004). The use of antibodies directed against specific effectors, or the use of epitope-tagged effectors, are potential direct methods to monitor the secretion. However, both are limited in

their sensitivity (Jarvik & Telmer, 1998). Fusion of predicted effectors with fluorescent proteins, such as green fluorescent protein (GFP), appears to be another useful approach to investigate the secretion and localisation; however, the size of GFP itself can obstruct the TTSS secretion and/or interfere with effector function inside host cells (Bobard *et al.*, 2011; Enninga & Rosenshine, 2009).

The β-lactamase reporter system has been extensively used to monitor the dynamic translocation of effectors into host cells, by using the catalytic domain of TEM-1 β-lactamase (*blaM*) as the reporter gene and the fluorescent β-lactamase substrate CCF2/AM as the detector (Charpentier & Oswald, 2004; McCann *et al.*, 2007; Mills *et al.*, 2008). Upon the translocation of an effector fused with β-lactamase into the host cell loaded with the substrate CCF2/AM, the lactamase enzyme hydrolyses the lactam ring in the substrate and undergoes an elimination reaction, resulting in the change of CCF2 fluorescence from green to blue (Charpentier & Oswald, 2004). By employing this technique, many TTSS effectors have been characterised, for instance, *E. coli* Cif, Tir, Map and EspF (Charpentier & Oswald, 2004), *Yersinia* YopH and YopE (Akopyan *et al.*, 2011), *Vibrio* VopX (Alam *et al.*, 2011) and *Salmonella* SteA, SlrP, SteC, and SseJ (Geddes *et al.*, 2007). However, given that this technique is dependent upon both the detection of products in the host cells and the stability and half-life of the fused proteins, it is essential to know the time frame of protein secretion/translocation. This may limit the usefulness of employing this β-lactamase reporter system (Bobard *et al.*, 2011; Briones *et al.*, 2006).

Another approach is based on fusion of a tetracysteine (TC) motif to putative effectors so that the reaction with the fluorescent FlAsH substrate can be analysed to directly monitor the effector-secretion kinetics (Enninga *et al.*, 2005). As the TC tag is very small, secretion efficiency is unlikely to be affected by the presence of the tag (Machleidt *et al.*, 2006). The arsenic molecules of the FlAsH reagent form a covalent bond with the TC tag (*Figure 1.3.4*), leading to high affinity binding (Adams *et al.*, 2002). This technique has been used to show that the two putative *S. flexneri* effectors, IpaB and IpaC, were secreted at approximately 240 seconds post infection (p.i.), and the entire pool of IpaB was secreted within 10 min p.i., indicating a role of these effectors at an early stage of infection (Enninga *et al.*, 2005; Simpson *et al.*, 2010). This technique has been also used with live cell imaging to show that the putative effector SopE2 of *S. enterica* serovar Typhimurium was secreted at 1 min p.i., and the entire pool accumulated in the HeLa epithelial cell line at 35 min p.i. (VanEngelenburg & Palmer, 2008). Moreover, data obtained from time course analysis of HeLa cells infected with *S. enterica* serovar Typhimurium

demonstrated that, after effector secretion, the bacterium caused host membrane ruffling, bacterial internalisation and host membrane restoration at 6, 15 and 21 min p.i. (VanEngelenburg & Palmer, 2008).

1.5 Scope and aim of this study

The TTSS is critical for *B. pseudomallei* virulence and appears to be involved at many stages of pathogenesis, including initial invasion, intracellular survival, multiplication, and cell-to-cell spread. Thus, structural and effector components of this system could be potential candidates for targets of antimicrobial therapy or as possible vaccine targets. However, many of the *B. pseudomallei* TTSS structural components, the proteins that regulate TTSS expression and many of the effector proteins have not yet been identified or fully characterised. Additionally, the mechanisms by which many injected effector molecules modulate host signalling pathways remains unclear. Therefore, characterising the function of other TTSS3 effectors and accessory proteins will advance the understanding of the molecular mechanisms of TTSS in relation to the pathogenicity of *B. pseudomallei*, and may give rise to new targets for therapeutic intervention.

In this study, three putative effectors of the *B. pseudomallei* TTSS3, namely BapA, BapB and BapC, were characterised with regard to their secretion, involvement in bacterial virulence and modulation of host cell functions. The *bapA*, *bapB* and *bapC* genes are located between *bipD*, which encodes a TTSS3 translocon component and *bopE*, which encodes a well-characterised TTSS3 effector (*Figure 1.3.3*). The *bapA*, *bapB* and *bapC* genes likely form an operon as the last bp of the *bapA* coding sequence overlaps the first bp of *bapB* and the last bp of the *bapB* coding sequence overlaps the first bp of *bapC*. This arrangement also suggests possible translational coupling. BapA (2,643 bp) is an 87.4-kDa hypothetical protein which currently has no predicted functional domains. However, BapB (9.6 kDa) contains a domain with homology to acyl carrier proteins (ACPs), based on its phosphopantetheine attachment site, which are generally required for transferring acyl molecules during fatty acid biosynthesis. It shares 33% identity to the TTSS acyl carrier protein IacP of *Salmonella enterica* serovar Typhimurium, which is involved in host actin modification resulting in facilitating bacterial invasion during infection (Kim *et al.*, 2011), suggesting that BapB could play a similar role. BapC (20.2 kDa) contains a signal peptide domain at the N-terminal region, suggesting that it could be secreted, and a lytic transglycosylase domain, which is generally involved in cleavage of β-1,4-glycosidic bonds of bacterial peptidoglycan. It shares approximately 37% identity with the *Salmonella* TTSS protein IagB, which has been shown to be involved in bacterial invasion in cultured epithelial cells

(Koraimann, 2003). In addition, *bapC* has been shown to be up-regulated in infected hamster livers (Tuanyok *et al.*, 2006). These data suggest that BapC could function as an effector during bacterial invasion, contributing to the virulence of *B. pseudomallei*. However, based on *in silico* analyses (http://gecco.org.chemie.uni-frankfurt.de and http://www.effectors.org) only BapA is strongly predicted to be a TTSS effector whereas BapB and BapC are not. However, it should be noted that these bioinformatic tools use similar prediction approaches and are unlikely to accurately predict all effectors (McDermott *et al.*, 2011). Taken together, these data suggest that BapA, BapB and BapC could be TTSS3 effectors and/or play roles in *B. pseudomallei* virulence.

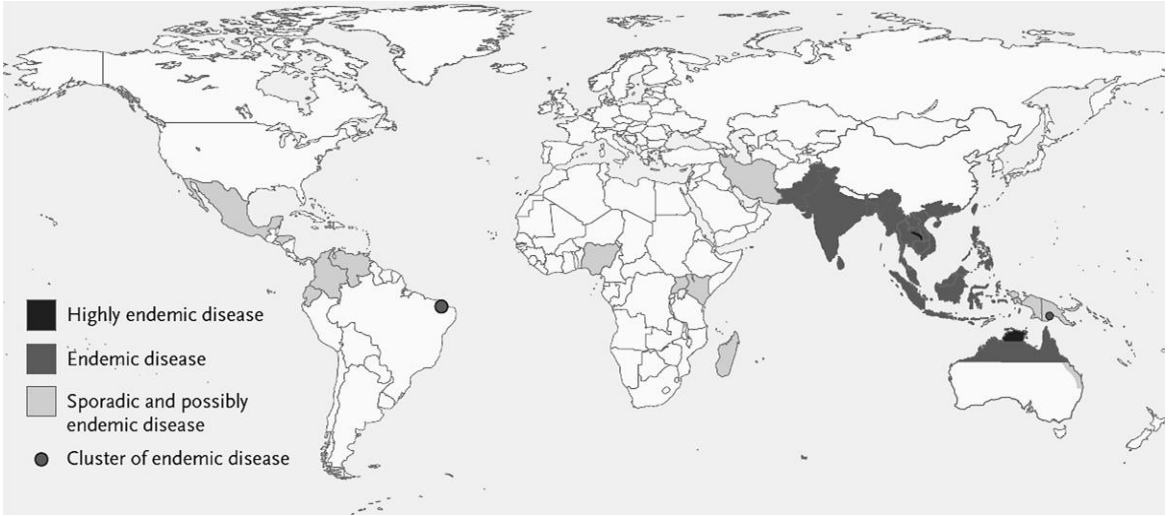

Figure 1.1.1 Distribution of melioidosis. Southeast Asia and Northern Australia are highly endemic areas, with the highest incidence of cases observed following the rainy season (Wiersinga *et al.*, 2012).

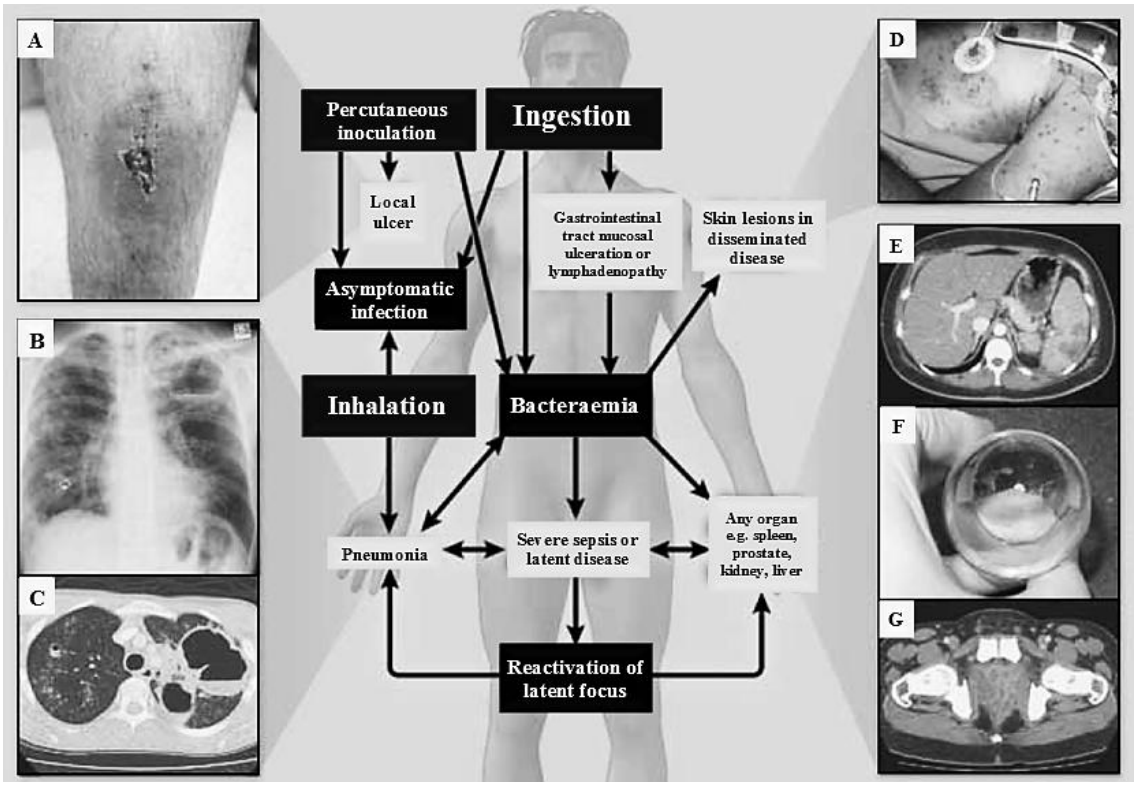

Figure 1.1.2 Clinical manifestations and major routes of transmission of melioidosis. Cutaneous infection (A), pneumonia (B) and a computed tomographic (CT) scan demonstrating lung abscesses (C), disseminated skin infection (D), spleen infection (E), aspirated pus obtained from a patient with peritonitis (F) and a CT scan displaying an accumulation of abscesses (G). Blue boxes represent major routes of disease transmission. Black boxes indicate latent, asymptomatic and/or history of infection. White boxes indicate the diverse clinical manifestations (Wiersinga *et al.*, 2012).

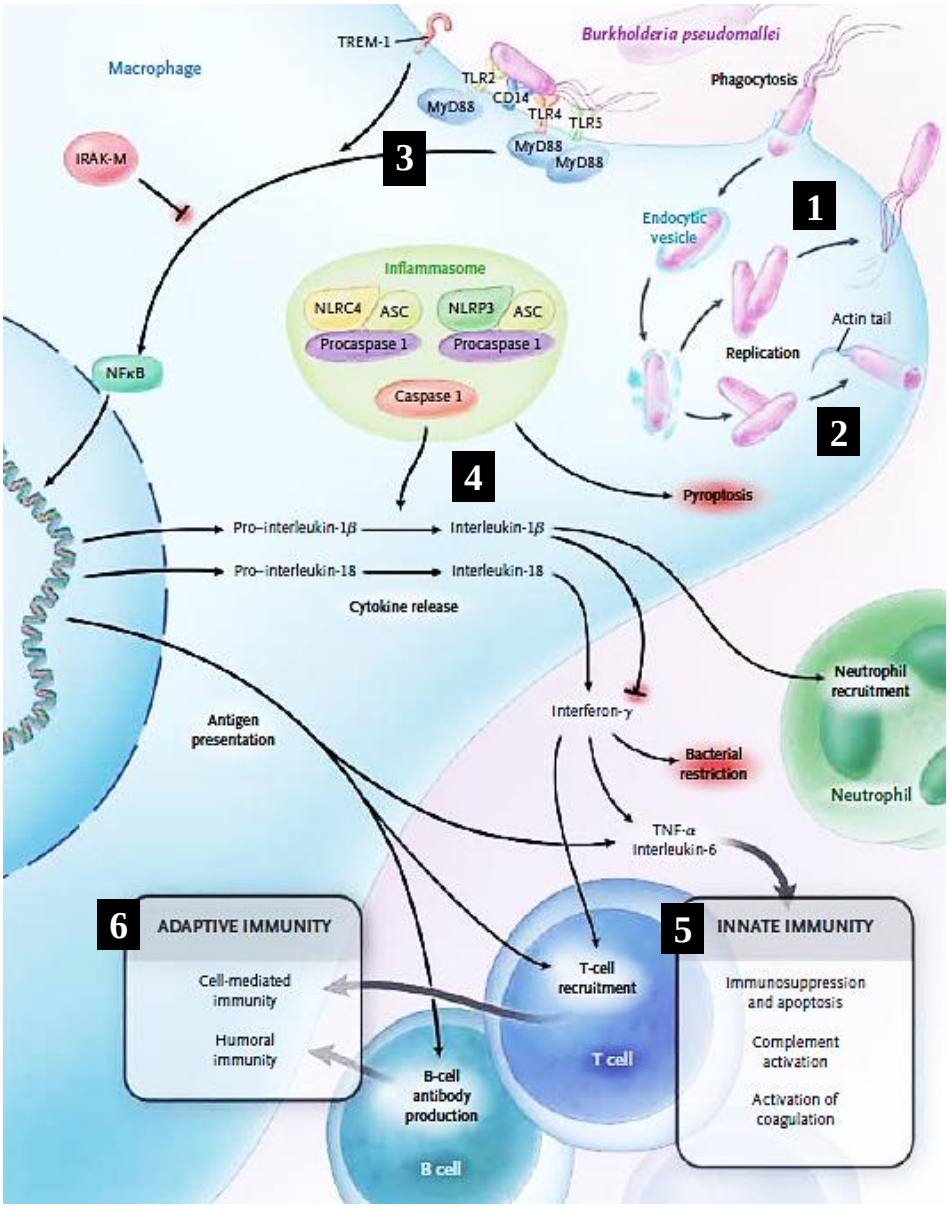

Figure 1.2.1 Summary of *B. pseudomallei* pathogenesis and host immune response in melioidosis. After bacterial internalisation, *B. pseudomallei* escapes from the host endosome and begins to multiply, either emerging to become free-living in the host cytoplasm (1) or invading adjacent cells in an actin-based motility dependent manner (2). Toll-like receptors (TLRs) expressed on host cells are involved in bacterial invasion by sending the signal to nuclear factor-κB (NF-κB) for activating the immune response through the release of proinflammatory cytokines. This signalling pathway is tightly regulated by triggering receptor expressed on myeloid cells 1 (TREM-1), as an amplifier molecule, and interleukin 1 receptor associated kinase-like molecule (IRAK-M), as an inhibitor. Myeloid differentiation factor 88 (MyD88) functions as the central TLR adaptor molecule (3). The host inflammasome, mainly the nucleotide-binding oligomerization domain (NOD)-like receptors (NLRs) NLRC4 and NLRP3 (Ceballos-Olvera *et al.*, 2011), recognise various bacterial virulence factors and send a signal in a caspase 1-dependent manner for triggering the release of interleukin (IL)-1β and IL-18. In addition to pyroptosis, a caspase-dependent cell death specific for bacterial growth can stimulate the production of interferon (IFN)-γ. The apoptosis associated speck-like protein containing a caspase recruitment domain (ACS) acts as an NLR adaptor molecule (4). As a result, neutrophil accumulation and several innate immunity cascades are triggered (5). During progression of infection, host adaptive immunity cascades are also activated resulting in T-cell recruitment in response to IFN-γ production, as a cell-mediated immune response, and the production of antibodies by B cells, as a humoral immune response (6) (Wiersinga *et al.*, 2012).

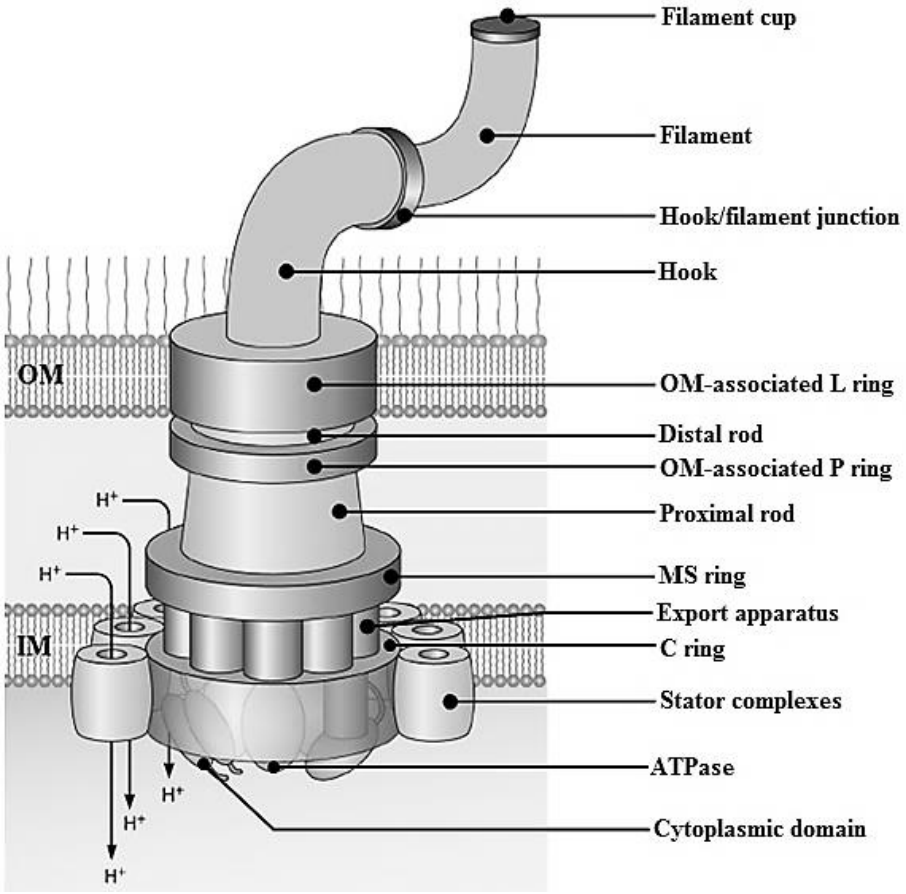

Figure 1.3.1 Overview of the flagellar TTSS components. The entire apparatus is composed of the filament structure, the hook-basal body, the cytoplasmic C ring, the ATPase and the export apparatus. The hook-basal body consists of two outer membrane (OM) rings, namely the lipopolysaccharide (L) and periplasmic peptidoglycan (P) rings, which are connected via a distal and proximal rod to the inner membrane (IM) ring (MS ring). The MS ring is surrounded by 8 to 11 stator complexes containing proton-conducting channels which are responsible for converting the energy of the proton flux into a mechanical force, hence, driving flagellum rotation. In addition to these membrane-embedded stator complexes, the flagellar TTSS-associated ATPase is involved in providing the energy required for the secretion, especially the initial process. The export apparatus and cytoplasmic domain play a key role in docking flagella-associated proteins and chaperones during the secretion process (Büttner, 2012).

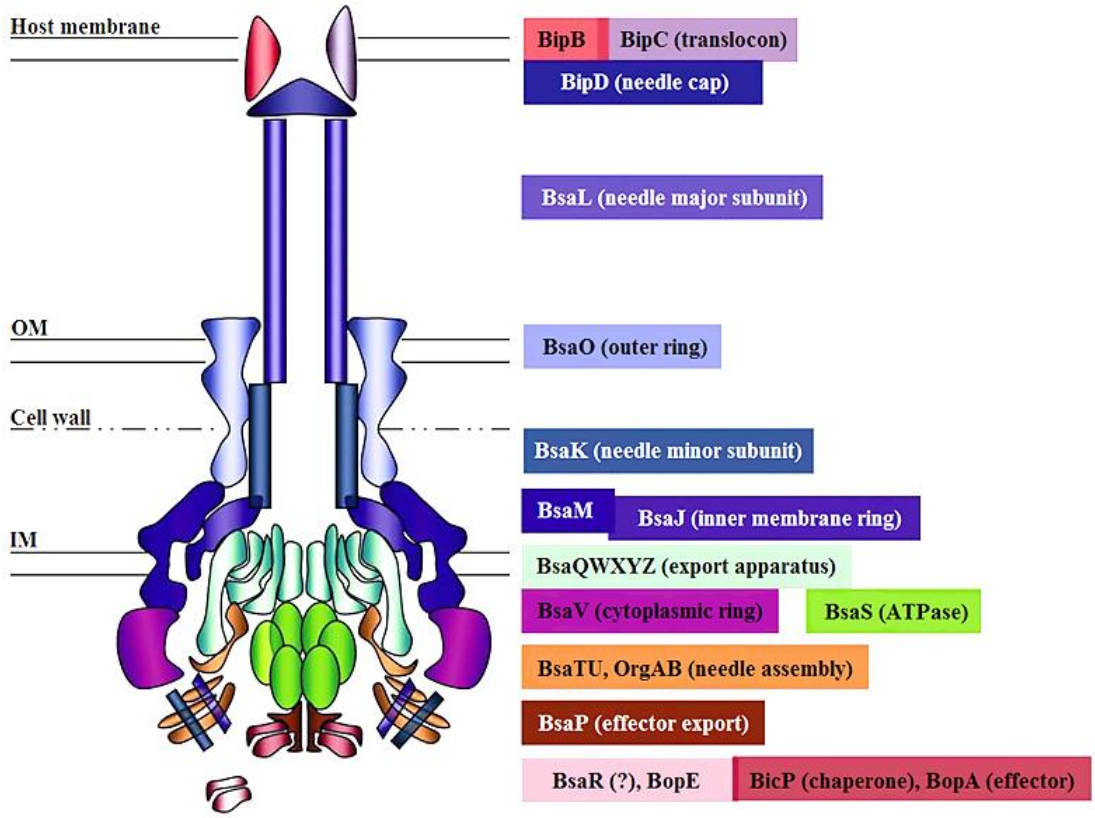

Figure 1.3.2 Proposed model of the TTSS3 needle-like apparatus. Components are illustrated based on their possible functions and colour coded with their identities on the right panel (Sun & Gan, 2010).

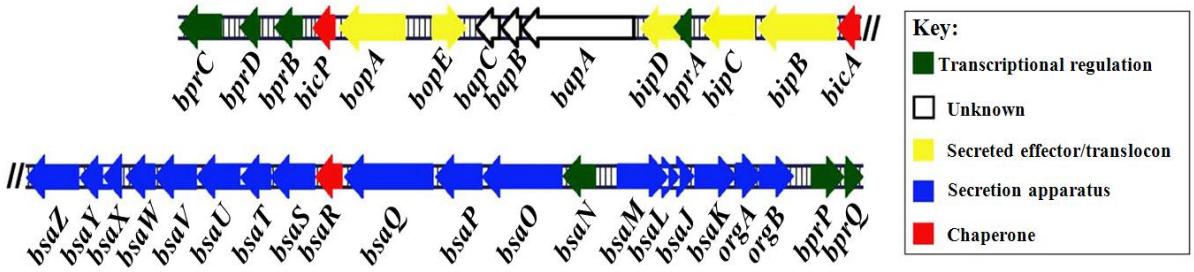

Figure 1.3.3 Organisation of *B. pseudomallei* TTSS3 gene cluster. Putative functions of the genes are colour-coded and indicated in the box on the right panel. Arrow directions indicate the orientation of the genes. The two sections shown are contiguous, as indicated by oblique double lines (Sun & Gan, 2010).

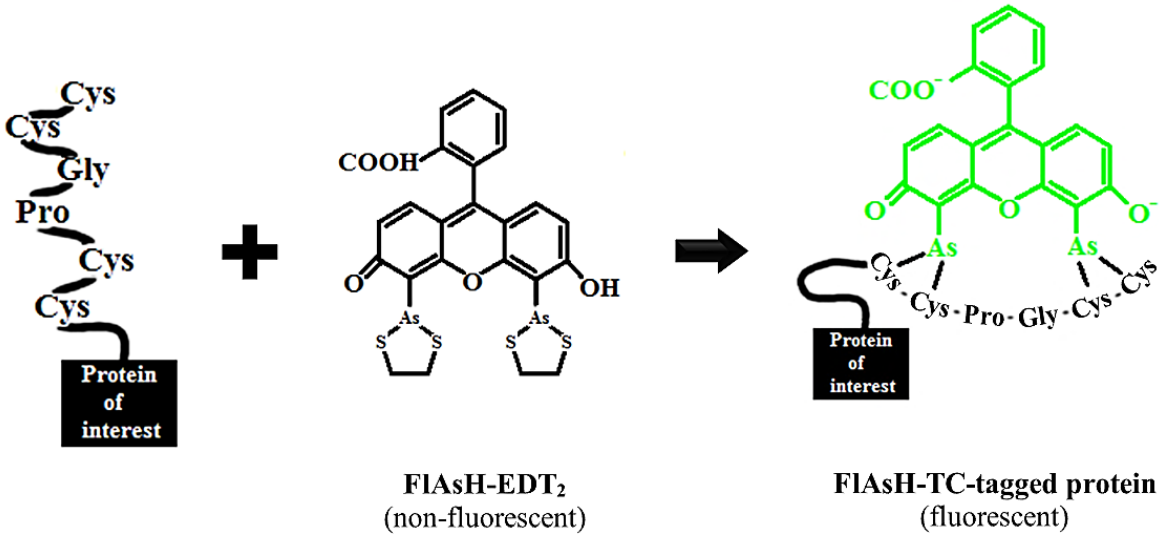

FlAsH-EDT$_2$
(non-fluorescent)

FlAsH-TC-tagged protein
(fluorescent)

Figure 1.3.4 The tetracysteine-FlAsH labelling system. The protein of interest is genetically fused to a tetracysteine motif (CysCysProGlyCysCys) is bound and forms covalent bonds with the biarsenical molecules (As-As) of non-fluorescent, FlAsH compound (FlAsH-EDT$_2$), causing it to become the fluorescent protein complex. The level of fluorescence is measured immediately at 520 nm with an excitation at 488 nm (GFP/FITC filter set) (modified from Adams *et al.*, 2002).

Chapter 2

Materials and methods

Chapter 2: Materials and methods

2.1 Bacterial strains, eukaryotic cell lines and primers

All bacterial strains and plasmids used in this study are described in *Table 2.1*. The *B. pseudomallei* wild-type strain K96243 (kindly provided by Dr. Brenda Govan, James Cook University, Townsville, Australia) was used as the parent strain for mutagenesis. This strain was originally isolated from a human melioidosis patient and its genome sequence has been determined and annotated (Holden *et al.*, 2004).

The *Escherichia coli* strain DH5α (*Table 2.1*) was primarily used for growth and amplification of plasmids. *E. coli* strain S17-1/λ*pir* harbouring pDM4 or pBHR1 constructs and strain SM10/λ*pir* harbouring pTNS3 or the mini-Tn*7* constructs (*Table 2.1*) were used for mobilisation of DNA into *B. pseudomallei* by conjugation (Szpirer *et al.*, 2001).

The murine RAW264.7 macrophage-like cell line and the human respiratory epithelial A549 cell line were obtained from the American Type Culture Collection (Manassas, VA). The RAW264.7 cell line stably expressing GFP-LC3 was obtained as described previously (Cullinane *et al.*, 2008).

All primer sequences for generation and verification of constructs and for nucleotide sequencing used in this study are listed and described in *Table 2.2*, *Table* 2.3 and *Table 2.4*.

2.2 Growth media and conditions

All chemical reagents and solvents, unless otherwise stated, were purchased from Merck (Victoria, Australia). Bacterial culture media were purchased from Oxoid (Hampshire, UK) and autoclaved at 121°C, 405-506 kPa for 20 min. Agar plates were made by adding 1.5% (w/v) agar. All antibiotics were purchased from Sigma-Aldrich (MO, USA) and added to the culture medium after autoclaving, when it had cooled to 50°C. Unless otherwise indicated, *E. coli* was cultured in Luria-Bertani (LB) broth (*Appendix 1, A1.1*) with ampicillin (100 μg/mL), chloramphenicol (20 μg/mL), kanamycin (50 μg/mL) or tetracycline (12.5 μg/mL) added when required. *B. pseudomallei* was cultured in LB broth supplemented with gentamicin (8 μg/mL), chloramphenicol (50 or 100 μg/mL), kanamycin (1 mg/mL) or tetracycline (25 μg/mL) added when required. All bacterial cultures were grown at 37°C; broth cultures were incubated with

shaking at 200 rpm. For long-term storage, strains were kept in glycerol broth (*Appendix 1, A1.2*) and stored at -80^{o}C.

RAW264.7 and RAW264.7 cells stably expressing GFP-LC3 (Cullinane *et al.*, 2008; D'Cruze *et al.*, 2011) were maintained at 37ºC in 5% CO_2 without antibiotics in RPMI 1640 Medium (D'Cruze *et al.*, 2011), GlutaMAX™, HEPES (GIBCO® Laboratories, Life Technologies™, USA) supplemented with 10% (v/v) heat-inactivated fetal calf serum (FCS) (GIBCO® Laboratories). A549 cells were maintained at 37ºC in 5% CO_2 without antibiotics in Dulbecco's Modified Eagle Medium DMEM, High Glucose, GlutaMAX™, HEPES (GIBCO® Laboratories), supplemented with 10% (v/v) heat-inactivated FCS. For long-term storage, all cell lines were stored at -80ºC in appropriate tissue culture media supplemented with 10% (v/v) tissue-culture grade dimethyl sulfoxide (DMSO; ≥99.9%) (Sigma-Aldrich, USA).

2.3 Polymerase chain reaction

Polymerase chain reaction (PCR), using Taq DNA polymerase (*Appendix 3, Table A3.1*) or Expand High Fidelity polymerase system (Roche Diagnostics Australia, NSW, Australia) (*Appendix 3, Table A3.2*) was carried out, according to the manufacturer's protocols. Gradient PCRs were carried out to identify the optimum annealing temperature for primer pairs. The KOD polymerase system (Novagen, Madison, USA) (*Appendix 3, Table A3.3*) was chosen to amplify the GC-rich template of *B. pseudomallei* genomic DNA.

2.4 DNA sequencing

Nucleotide sequencing was conducted using the Applied Biosystems BigDye Terminator mix (Life Technologies™, USA). The sequencing reaction protocol and clean-up procedures are available at: (https://platforms.monash.edu/micromon/). In brief, sequencing reactions were prepared and conducted as described in *Appendix 3, Table A3.4*. Reaction products were purified using the sodium acetate-ethanol method (*Appendix 3, Table A3.5*) prior to analysis on the Applied Biosystems 3730s Genetic Analyser (Life Technologies™, USA).

2.5 Agarose gel electrophoresis

DNA products, derived from PCR amplification, restriction enzyme digestion or purification processes, were separated by gel electrophoresis on 1% (w/v) agarose gel in 1X TAE (*Appendix 2, A2.4*). For DNA visualisation, SYBR® Safe DNA gel stain (Life Technologies™, USA) was used to stain DNA samples according to the manufacturer's instructions. DNA standard size

markers (New England Biolabs®, USA) were used to estimate DNA size and concentration in unknown samples. Gels were run at 100 V for 30 min and visualised using a Fujifilm LAS-3000 Imager (SYBR Green filter). DNA fragments excised from agarose gels were purified using NucleoSpin® Gel and PCR Clean-up kits (MACHEREY-NAGEL, Düren, Germany), according to the manufacturer's protocol.

2.6 DNA restriction endonuclease (RE) digestion

All restriction endonucleases were purchased from New England Biolabs® (MA, USA). Restriction endonuclease reactions were performed in appropriate buffers according to the manufacturer's instructions. For cloning reactions, digested vector DNA was dephosphorylated with calf intestinal alkaline phosphatase (Promega, WI, USA) to prevent re-ligation. The dephosphorylation reactions were incubated at 37°C for 30 min and then the enzyme was inactivated by heating to 65°C for 10 min. The dephosphorylated DNA was then purified using NucleoSpin® Gel and PCR Clean-up kits according to the manufacturer's protocol.

2.7 DNA ligation and transformation

Ligation reactions were carried out with T4 DNA ligase (Roche Diagnostics Australia, NSW, Australia) according to the manufacturer's instructions with a vector-insert ratio of 1:3, if the insert was <1.5-kb or 1:5, if the insert was >1.5-kb. Ligation reactions were incubated at 4°C for 16 h and then introduced by transformation into competent *E. coli* DH5α (*Section 2.8*). In brief, 5-10 μL of each ligation reaction was incubated on ice for 1 h with 100 μL of competent *E. coli* DH5α cells. The mixture was then heat-shocked at 42°C for 1 min and then returned to ice for a further 5 min prior to addition of 1 mL of SOB broth (*Appendix 1, A1.3*). The cells were recovered at 37°C for 1 h, with shaking at 200 rpm. A 100 μL of aliquot of the transformed cells was then plated onto LB agar containing appropriate antibiotic(s) to select for colonies harbouring specific plasmids. Plates were incubated at 37°C, overnight.

2.8 Preparation of competent *E. coli* cells

E. coli DH5α, SM10/λ*pir* and S17-1/λ*pir*, were made competent using rubidium chloride treatment (Glover, 1985). In brief, *E. coli* cells were grown to an OD_{600} of approximately 0.3 in SOB medium prior to chilling on ice for 15 min. Cells were collected by centrifugation at 1,157 x *g* (3,000 rpm), for 15 min, at 4°C. Cells were gently resuspended with pre-chilled RF1 buffer (*Appendix 2, A2.25*) and incubated on ice for 1 h prior to harvesting by centrifugation again at

1,157 x *g* (3,000 rpm), for 15 min, at 4^{o}C. Supernatant was discarded, and cells were resuspended with pre-chilled RF2 buffer (*Appendix 2, A2.26*) and incubated on ice for 15 min. The suspension was divided into 100 μL aliquots in pre-chilled microfuge tubes and immediately stored at -80^{o}C.

2.9 Mutagenesis of TTSS3 genes

B. pseudomallei bapA, *bapB*, and *bapC* mutant strains were generated by double-crossover allelic exchange using the *λ-pir* dependent vector pDM4 (*Table 2.1*) which contains the *sacB* gene for counter selection (Milton *et al.*, 1996). Specific primer pairs (*Table 2.2*) were used to amplify separate sequences upstream and downstream of the target genes. In brief, for *bapA* mutagenesis, the primers MC5532 and MC5533 were used to amplify the upstream fragment of *bapA*, and the primers MC5516 and MC5517 were used to amplify the downstream fragments encompassing the entire *bapB* and *bapC* genes. Both fragments were cloned into *Spe*I-/*Xba*I-digested pDM4. For *bapB* mutagenesis, two sets of primer pairs, JT6156/JT6157 and JT6175/JT6176, were used to amplify the upstream and downstream fragments, and both fragments were cloned into *Sph*I-/*Spe*I-digested pDM4. For *bapC* mutagenesis, two primer pairs, JT6319/JT6320 and JT6179/JT6180, were used to amplify the upstream and downstream fragments which were cloned sequentially into *Sac*I-/*Xba*I-digested and *Sal*I-digested pDM4. The tetracycline resistance gene *tetA*(C), recovered from pUTminiTn*5*Tc (de Lorenzo *et al.*, 1990), was then ligated into the central *Bgl*II site of pDM4 in order to generate the mutant constructs pDM4::*bapA*::*tetA*(C), pDM4::*bapB*::*tetA*(C) and pDM4::*bapC*::*tetA*(C). The constructs were introduced by transformation into the conjugative donor strain *E. coli* S17-1/λ*pir*, and then introduced into *B. pseudomallei* by conjugation. Each conjugation reaction was plated on LB agar containing 8 μg/mL gentamicin and 25 μg/mL tetracycline, and plates were incubated at 37^{o}C for up to 2 days. To confirm that the transconjugants had the correct antibiotic profile, colonies were patched onto LB agar containing 8 μg/mL gentamicin and 25 μg/mL tetracycline. Any transconjugants showing tetracycline resistance were subsequently patched onto LB agar supplemented with 20% (w/v) sucrose in order to select for the loss of the suicide vector pDM4 as described previously (Logue *et al.*, 2009), based on a *sacB* counter-selection protocol acting through the activation of the *sacB* gene of pDM4. The resulting colonies were characterised by PCR and sequence analysis using the primers flanking the mutated regions.

2.10 Conjugation between *E. coli* and *B. pseudomallei*

Overnight cultures of the donor strain *E. coli* SM10/λ*pir* or S17-1/λ*pir*, containing pDM4 or pBHR1 constructs, and the recipient strain *B. pseudomallei* K96243 were subcultured separately and incubated at 37^{o}C with shaking at 200 rpm, to obtain an OD_{600} of 0.6. Cells were collected by centrifugation at 4,293 x *g* (8,000 rpm) for 5 min, washed by resuspending in 1 mL of sterile 1X PBS, pH 7.4 (*Appendix 2, A2.8*) and then centrifuged at 4,293 x *g* (8,000 rpm) for 5 min to remove the antibiotic prior to resuspending in 1 mL of sterile PBS, pH 7.4. An equal amount of the donor (200 µL) and recipient (200 µL) suspensions was then mixed prior to spotting on LB agar plates. The conjugation reactions were incubated at 30^{o}C for 2 days, resuspended in 2 mL of sterile PBS, pH 7.4 and then plated onto LB agar containing appropriate antibiotics. Plates were incubated at 37^{o}C for up to 2 days. Transconjugants were subsequently verified for the presence of the appropriate construct by patching on LB agar containing appropriate antibiotics and characterised by PCR.

Complementation of the K96243*ΔbapA*, *ΔbapB* and *ΔbapC* strains was carried out by introduction of the appropriate genes cloned into the plasmid pBHR1 (*Table 2.1*). The empty pBHR1 plasmid was additionally introduced into each of the mutants and the wild-type strain as negative controls. Due to the instability of the plasmid pBHR1 (see *Chapter 3.6*), complementation using the mini-Tn*7* vector was also carried out using triparental mating which requires the co-conjugation of the helper plasmid pTNS3, a crucial construct for integration of the transposon into the bacterial genome, and the appropriate complementation construct.

2.11 Minimum bactericidal concentration (MBC) assays

MBC assays were performed as described elsewhere (Treerat *et al.*, 2008). In brief, overnight cultures of *B. pseudomallei* strains were subcultured 1:50 into fresh LB broth containing appropriate antibiotics and grown to an OD_{600} of 0.8 which was equivalent to 10^8 CFU/mL. The cultures were then diluted 1 in 10 with fresh LB broth to give a culture of 10^7 CFU/mL. The stock antibiotic solutions required for each experiment were freshly prepared and then serially diluted in LB broth as specified. Each of the antibiotic dilutions (100 µL) was added to sterile BD Falcon^{TM}, clear 96-well, flat bottom plates (BD Biosciences, Australia) prior to addition of 100 µL of bacterial cell suspension (10^6 CFU). A well with cells but no antibiotic was used as a growth control and a well with medium but no cells was used as a negative control. The plates were incubated at 37^{o}C on an orbital shaker (100 rpm) overnight. The lowest concentration of antibiotic that showed no visible bacterial growth was taken as the MBC. For verification of the MBC results, a culture from the well showing no visible growth was subsequently inoculated

into fresh LB broth and incubated at 37°C for up to 2 days. This assay was performed in technical triplicates on biological duplicates.

2.12 RNA extraction and reverse transcription-PCR (RT-PCR)

Total RNA was extracted using TRIzol® (Life Technologies™, USA), and cDNA was produced by reverse transcription using random hexamers as described previously (Lo *et al.*, 2006). In brief, bacterial strains were cultured to the desired growth phase and cells harvested by centrifugation at 4,293 x *g* (8,000 rpm) for 5 min. The cell pellet was resuspended in 1 mL of pre-chilled TRIzol® reagent and incubated at 65°C with shaking at 1,000 rpm, for 15 min. RNase-free chloroform:isoamyl alcohol mix (24:1) was added in a ratio of 200 μL to 1 mL of TRIzol® reagent. The reaction was mixed vigorously for 15 sec and then incubated at room temperature for 10 min. The mixed emulsion was separated by centrifugation at 11,337 x *g* (13,000 rpm), for 15 min, at 4°C. The upper aqueous phase was carefully transferred, without disturbing the interface, to a new sterile tube containing 1 μL of Protector RNase Inhibitor (Roche Diagnostics Australia, Australia). RNA was precipitated by addition of RNase-free isopropanol (300 μL) and incubated for 10 min. The RNA was collected by centrifugation at 11,337 x *g* (13,000 rpm), for 10 min, at 4°C. The RNA pellet was washed twice in 500 μL of RNase-free 75% ethanol. The final RNA pellet was air-dried at room temperature for 30 min and then resuspended in 50 μL of nuclease-free DEPC-treated Ambion® water (Life Technologies™, USA) containing 2 μL of Protector RNase Inhibitor. Contaminating DNA was removed by treatment with the RNase-Free DNase Set (QIAGEN®, Australia) according to the manufacturer's instructions. The RNA was then purified using the RNeasy Mini Kit (QIAGEN®, Australia) according to the manufacturer's instructions, and the RNA was eluted by addition of 50 μL of nuclease-free DEPC-treated Ambion® water to the column and centrifugation at 11,337 x *g* (13,000 rpm) for 1 min. The elution step was repeated using 50 μL of the previous elution and a second centrifugation at 11,337 x *g* (13,000 rpm) for 1 min. The DNase digestion treatment and RNA purification steps were repeated a second time to obtain DNA-free RNA samples.

Reverse Transcription was performed with the SuperScript™ III Reverse Transcriptase (Life Technologies™, USA) according to the manufacturer's instructions. In brief, RNA samples were mixed with 2.5 μL of random hexamers (pdN6) (supplied by Micromon, Monash University), and 2 μL of Protector RNase Inhibitor. RNA concentration of each mutant sample (10 ng) was normalised to the wild-type concentration prior to adjusting the total volume of the reaction to 16

μL using nuclease-free DEPC-treated Ambion® water. The reactions were then incubated at 70°C, for 10 min followed by immediate cooling on ice for 10 min. Each reaction was then split in half, and one half used for a reverse transcription reaction (RT+), and the other (RT-) as a negative control. The RT reactions contained:

RT+ (sample)		**RT- (negative control)**
8 μl	RNA/pdN6 mixture	8 μl
0.5 μl	Protector RNase Inhibitor	0.5 μl
2 μl	dNTP (10 mM)	2 μl
4 μl	5X RTC buffer	4 μl
2 μl	DTT (100 mM)	2 μl
1.5 μl	SuperScript™ III Reverse Transcriptase	- μl
2 μl	Nuclease-free DEPC-treated Ambion® water	3.5 μl

The reactions were subsequently incubated at 42°C for 2 h 30 min, and then the temperature increased to 70°C for 15 min. The synthesised cDNA (RT+) and the negative control reaction (RT-) were stored at -20°C. The RT reactions were used as the template for RT-PCR using the amplification protocol described in *Appendix 3, Table A3.1* with a 58°C annealing temperature, and a 2 min extension time. Primers JT6073 and JT6321 (*Table 2.2*) were used to investigate co-transcription of *bapA*, *bapB* and *bapC*, and primers JT6640 and JT6180 (*Table 2.2*) were used to investigate the co-transcription of *bapB* and *bapC*. The primers JT6079 and JT6080 (*Table 2.4*) were used to investigate the transcription of *bopE*.

2.13 Quantitative real-time RT-PCR

Semi-quantitative real-time RT-PCR was conducted with the Mastercycler® ep *realplex* PCR system (Eppendorf South Pacific, Australia) using FastStart Universal SYBR Green Master mix (Rox) (Roche Diagnostics Australia, Australia). The primer pairs JT7472/JT7473 and JT7474/JT7475 (*Table 2.4*) were designed for the amplification of *bopE* and the internal control *rpoA* (*BPSL3187*), respectively, using the Primer3 primer design software (http://simgene.com/Primer3). These primer pairs amplified PCR products of 119 and 90 bp, respectively. Each *bopE* or *rpoA* real-time RT-PCR mixture was prepared by addition of 5 μL of 1:10 dilution of cDNA to 15 μL of PCR master mixture (10 μL of FastStart Universal SYBR Green Master mix (Rox), 0.2 μL of 100 μM of each primer and 4.6 μL of nuclease-free DEPC-treated Ambion® water). The genomic DNA of the *B. pseudomallei* wild-type K96243 and the

RT- sample were used as positive and negative controls, respectively. The cycling parameters for amplification were as follows: 1 cycle of polymerase activation at 95°C for 2 min, 40 cycles of 95°C for 15 sec and 60°C for 1 min. A final melting curve to check the specificity of amplified products was set up as follows: 95°C for 15 sec, 60°C for 15 sec, and then the temperature was increased to 95^{o}C within 20 min, and held at 95^{o}C for 15 sec before immediate cooling to 10°C. All real-time PCR was carried out in technical triplicates on biological duplicates.

2.14 *In vitro* growth curves

The growth of the mutant and wild-type strains was assessed in LB broth. The optical density of overnight cultures of each of the strains was measured (OD_{600}) and diluted to give an OD_{600} of 0.05 in 20 mL of LB broth. Broth cultures were subsequently incubated at 37^{o}C with shaking at 200 rpm, and the absorbance of each of the cultures (OD_{600}) measured at 30 min time intervals for at least 12 h. The experiments were performed in technical and biological triplicates.

2.15 *In vivo* competitive growth assays

In vivo competitive growth assays were carried out in BALB/c mice, and the competitive index (CI) of each mutant was calculated as described previously (Auerbuch *et al.*, 2001; D'Cruze *et al.*, 2011; Harper *et al.*, 2004) with minor modifications. Each of the mutant and the wild-type strains was cultured in LB with antibiotics as appropriate to obtain an OD_{600} of 0.2 (corresponding to 2 x 10^8 CFU/mL). Bacterial cells were harvested by centrifugation at 4,293 x *g* (8,000 rpm) for 5 min. Pellets were subsequently washed in 1 mL of sterile PBS, pH 7.4 to remove antibiotics and centrifuged at 4,293 x *g* (8,000 rpm) for 5 min prior to resuspension in 1 mL of sterile PBS, pH 7.4. Equal volumes of the mutant and the wild-type cultures were combined and ten-fold serial dilutions of the combined mixture were prepared; the 10^{-2} dilution was used for *in vitro* growth analysis, and 100 μL of the 10^{-5} dilution plated on LB agar. These plates represented the *in vitro* and input samples, respectively.

For the *in vitro* growth analysis, 10 μL of the 10^{-2} dilution (corresponding to 4 x 10^4 CFU) was inoculated in LB broth and then incubated at 37^{o}C, with shaking at 200 rpm for up to 20 h. Ten-fold serial dilutions were prepared, and 100 μL of appropriate dilutions plated on LB agar.

For the *in vivo* growth analysis, each of the mixed cultures was inoculated intranasally into three to five, 6- to 8-week-old, female BALB/c mice. The infection was allowed to proceed for 20 h, and mice were then euthanised in an ethically approved manner (Monash University Animal

Ethics Committee approval #SOBS/M/2008/2). Spleens were removed aseptically, homogenised in 3 mL of sterile PBS, pH 7.4 and then plated onto LB agar.

Plates were incubated at 37^{o}C for up to 2 days. One hundred colonies from the input and *in vivo* analyses were patched onto LB agar with or without 25 μg/mL tetracycline. The CI was defined as the ratio of mutant to wild-type bacteria in the output pool divided by the ratio of mutant to wild-type bacteria in the input pool. The statistical significance of a reduction in CI was determined by a one sided z-test, as used previously (Harper *et al.*, 2003; Harper *et al.*, 2004).

2.16 Mouse virulence trials

To investigate the role of *bapA*, *bapB* and *bapC* in virulence, each of the mutant strains was used in virulence trials in the BALB/c mouse acute infection model and compared with the wild-type strain as described previously (Leakey *et al.*, 1998; Lever *et al.*, 2009; Liu *et al.*, 2002; Tan *et al.*, 2008) with minor modifications. Overnight cultures of the mutant and the wild-type strains were grown in LB with or without antibiotics as appropriate, and then incubated at 37^{o}C with shaking at 200 rpm to obtain an OD_{600} of 0.8 (corresponding to approximately 5 x 10^8 CFU/mL). Cells were concentrated by centrifugation at 4,293 x *g* (8,000 rpm) for 5 min. Pellets were washed with 1 mL of sterile PBS, pH 7.4 and harvested by centrifugation at 4,293 x *g* (8,000 rpm) for 5 min prior to resuspension in 1 mL of sterile PBS, pH 7.4. Groups of seven mice were inoculated intranasally with 20 μL of 10^5 or 10^7 CFU of each of the mutants or the wild-type strain. All infected mice were monitored carefully for signs of infection (ruffled fur, reduced movement and responsiveness) for up to 10 days and euthanized when moribund, in accordance with animal ethics requirements (Monash University Animal Ethics Committee approval # SOBS/M/2008/2). The stability of the mutants was verified by patching mutant colonies recovered from the spleens of mutant-infected mice onto LB and LB containing 25 μg/mL tetracycline. DNA isolated from tetracycline resistant colonies was analysed by PCR for retention of the mutagenesis insert using the primers flanking the mutated regions.

2.17 Cell invasion assays

The ability of each of the mutant and the wild-type *B. pseudomallei* strains to the invade human respiratory epithelial cell line A549 was determined as described previously (Jones *et al.*, 1996; Kespichayawattana *et al.*, 2000; Muangman *et al.*, 2011; Muangsombut *et al.*, 2008) with minor modifications. A549 cells were seeded in 24-well plates (5 x 10^5 cells per well) in DMEM supplemented with 10% (v/v) heat-inactivated FCS and grown at 37^{o}C, 5% CO_2 overnight. Prior

to infection assays, the monolayers were washed twice with 500 μL of pre-warmed PBS, pH 7.4, and then covered with 300 μL of DMEM supplemented with 10% (v/v) heat-inactivated FCS.

For infections, overnight cultures of the mutants, the wild-type (the positive control) and *E. coli* DH5α (the negative control) were subcultured in appropriate antibiotics and then incubated at 37°C with shaking at 200 rpm, to obtain an OD_{600} of 0.8 (corresponding to approximately 5 x 10^8 CFU/mL). Cells were concentrated by centrifugation at 4,293 x *g* (8,000 rpm) for 5 min and then resuspended in 1 mL of DMEM supplemented with 10% (v/v) heat-inactivated FCS. The A549 monolayers were infected with each of the strains at an MOI of 100, and incubated for 2 h to allow for bacterial adherence and invasion. At 2 h p.i., the infected monolayers were washed four times with pre-warmed sterile PBS, pH 7.4 and then overlaid with fresh DMEM containing 900 μg/mL kanamycin and 90 μg/mL ceftazidime for 2 h to kill extracellular bacteria. The monolayers were lysed with 1X PBS/0.1% (v/v) Triton X-100 (*Appendix 2, A2.9*) to liberate the intracellular bacteria. The number of viable cells released from the lysed monolayers was determined by direct plating. The assays were performed in technical triplicates on three separate days for each strain.

2.18 Intracellular survival assays in murine macrophages cells

The ability of mutant and the wild-type strains to survive and replicate in murine macrophage-like RAW264.7 cells was determined as described previously (D'Cruze *et al.*, 2011; Muangman *et al.*, 2011; Stevens *et al.*, 2002) with minor modifications. To ensure that intracellular bacteria were completely released, a range of saponin (Chieng *et al.*, 2012) and Triton X-100 concentrations was first assessed for lysis of the infected monolayers. A 1X PBS/0.5% (w/v) saponin (*Appendix 2, A2.10*) wash solution showed the most effective lytic activity without having an impact on bacterial growth and survival (data not shown). The murine macrophage-like RAW264.7 cells were seeded in 24-well plates (5 x 10^5 cells per well) in RPMI supplemented with 10% (v/v) heat-inactivated FCS and grown at 37°C, 5% CO_2 overnight. The monolayers were washed twice with 500 μL of pre-warmed sterile PBS, pH 7.4, and then covered with 300 μL of RPMI supplemented with 10% (v/v) heat-inactivated FCS before performing infections.

Overnight cultures of the mutants and the wild-type (the positive control) strain were subcultured in appropriate antibiotics and then incubated at 37°C with shaking at 200 rpm, to obtain an OD_{600} of 0.8 (corresponding to approximately 5 x 10^8 CFU/mL). Cells were concentrated by

centrifugation at 4,293 x *g* (8,000 rpm) for 5 min and then resuspended in 1 mL of RPMI supplemented with 10% (v/v) heat-inactivated FCS. The monolayers were subsequently infected with each of the mutants or the wild-type strain at an MOI of 10:1, and incubated for 1 h. The infected monolayers were then washed four times with pre-warmed sterile PBS, pH 7.4 and then overlaid with fresh RPMI containing 900 μg/mL kanamycin and 90 μg/mL ceftazidime to kill extracellular bacteria. At 2, 4 and 6 h post infection, wells were washed four times with 500 μL pre-warmed sterile PBS, pH 7.4 to remove any extracellular bacteria, and 50 μL of the final wash was plated on LB agar and incubated at 37^{o}C for up to 2 days, designated as 'wash' plates. The infected RAW264.7 macrophages were incubated with 200 μL of pre-warmed 1X PBS/0.5% (w/v) saponin for 10 min at 37^{o}C to release the intracellular bacteria. 100 μL of the lysate was plated on LB agar and grown at 37^{o}C for up to 2 days, designated as 'lysis' plates. Numbers of bacterial colonies recovered from 'wash' and 'lysis' were tallied and statistically analysed using T-tests and one-way ANOVA. Assays were performed on at least three different days, each in technical triplicates.

2.19 Immunofluorescence and confocal microscopy

2.19.1 Bacterial co-localisation with GFP-LC3

Co-localisation of bacteria with the autophagy marker protein LC3 (Kuma *et al.*, 2007) was conducted as described previously, with some alterations (Cullinane *et al.*, 2008; D'Cruze *et al.*, 2011; Gong *et al.*, 2011). Mutant and wild-type *B. pseudomallei* strains were grown to an OD_{600} of 0.8, and RAW264.7 cells expressing LC3-GFP were seeded and prepared in 24-well trays containing cover slips. The monolayers were infected for 1 h with bacterial strains at an MOI of 10:1. Infected monolayers were then washed and treated with antibiotics as described previously for intracellular survival assay (*Chapter 2.18*). At 2, 4 and 6 h post-infection, the monolayers were washed four times with pre-warmed sterile PBS, pH 7.4 to remove extracellular bacteria. The PBS was then replaced with 500 μL of 100% methanol and incubated at 37^{o}C for 10 min in order to fix the cells. The infected monolayers on the cover slips were then analysed by immunofluorescence.

For IFN-γ stimulation, RAW264.7 or RAW264.7 cells stably transfected with LC3-GFP, were treated with 200 U/mL of recombinant mouse IFN-γ (ProSpec-Tany TechnoGene, Israel) for 3 h prior to infections.

For immunofluorescent labelling, antibody solutions and washes were prepared in 1X PBS/1% (w/v) BSA (*Appendix 2, A2.11*). Unless otherwise indicated, washing steps were performed at room temperature with shaking. The methanol-fixed monolayers were incubated with rabbit antiserum raised against *B. pseudomallei* outer membrane proteins (Cullinane *et al.*, 2008) at a dilution of 1:100 at 37^{o}C for 1 h. The monolayers were washed four times with 1X PBS/1% (w/v) BSA for 10 min and then incubated with the secondary goat anti-rabbit IgG Texas Red® antiserum (Molecular Probes®, OR, USA) at a 1:250 dilution, for a further 1 h at room temperature. The monolayers were washed four times, as described above, prior to mounting the cover slips containing the infected macrophages on glass slides using PermaFluor™ Aqueous Mounting Medium (Thermo Fisher Scientific, CA, USA). Internalised *B. pseudomallei* and cytoplasmic LC3 were visualised by confocal microscopy (see *Chapter 2.19.3*). The images were scored for the total number of internalised bacteria and the number of internalised bacteria that co-localised with LC3. The ratio of bacterial co-localisation, obtained from technical triplicate and biological triplicate experiments, was identified for the wild-type and mutant strains, and statistical significance of differences in co-localisation determined using Student's *t*-tests.

2.19.2 Visualisation of actin tails via immunofluorescent phalloidin labelling

Intracellular motility of the wild-type and the mutant strains was assessed in RAW264.7 cells by immunofluorescence as described in *Chapter 2.19.1* with minor modifications. At 2, 4 and 6 h post-infection, the monolayers were washed four times with pre-warmed sterile PBS, pH 7.4, to remove extracellular bacteria. The PBS was replaced with 500 μL of 1X PBS/3.5% (v/v) paraformaldehyde (PFA; *Appendix 2, A2.12*) and incubated at 37°C for 15 min to fix the cells prior to permeabilising with 1X PBS/0.1% (v/v) Triton X-100 (*Appendix 2, A2.9*) at 37°C for 10 min. For immunofluorescent-labelling and actin staining, antibody solutions and washes were prepared in 1X PBS/1% (w/v) BSA. Unless otherwise indicated, all washing steps were performed at room temperature with shaking. The PFA-fixed monolayers were incubated with the primary and secondary antibodies as described in *Chapter 2.19.1*. Following immunofluorescent labelling, the monolayers were incubated with Alexa Fluor® 647 Phalloidin (Molecular Probes®, OR, USA) at a dilution of 1:250 for a further 1 h at RT to stain intracellular actin. The monolayers were washed and mounted on the cover slips as described previously. Actin-tail formation was visualised by confocal microscopy (see *Chapter 2.19.3*).

2.19.3 Confocal laser scanning microscopy

An Olympus FV-1000 confocal laser scanning fluorescence microscope (Monash Micro Imaging, Monash University, Australia) equipped with a 1.2 NA water immersion lens (Olympus 60X UPlanapo), was used for all fluorescent imaging. Image analysis and processing was performed using Olympus FV1000 Viewer software (Ver.2.0b) and the public domain software Fiji. Internalised *B. pseudomallei* and cytoplasmic LC3 were visualised using the red TRITC and green FITC channel, respectively. The far-red fluorescent Alexa Fluor® 647 dye (excitation/emission: 650/668 nm) was used to visualise intracellular actin in macrophage cells.

2.20 Cytokine assays

RAW264.7 cells, with or without IFN-γ pre-treatment, were infected with each of the mutants or the wild-type strain as described in *Chapter 2.18*. At the indicated time points, the mammalian cell culture supernatants were filtered using a 0.22 µm, 4 mm, Millex® syringe filter (Merck Millipore, USA). The cultured supernatants were used to determine the level of the proinflammatory cytokines TNF-α and IL-6 present in each supernatant by ELISA. The BD OptEIA™ mouse TNF and IL-6 ELISA Kits (BD Biosciences, USA) were used according to the manufacturer's protocols. The data were obtained from technical triplicates and biological duplicates.

2.21 Sodium deoxycholate/trichloroacetic acid (DOC/TCA) precipitation of proteins

For precipitation of very low amounts of protein, DOC was used, in combination with TCA, to act as a co-precipitant to enhance the interaction between the protein and TCA through hydrophobic interactions (Arnold & Ulbrich-Hofmann, 1999; Chang, 1992; Chevallet *et al.*, 2007). Bacterial strains were grown to the appropriate growth phase and the cells removed by centrifugation at 4,293 x *g* (8,000 rpm) for 5 min. The supernatant was filtered through a sterile 0.45-µM syringe filter (Pall Life Science, USA) to eliminate bacterial cells. DOC was subsequently added and mixed with total culture and supernatant samples to obtain a final concentration of 0.02% (w/v), and incubated at room temperature for 15 min. Total protein was precipitated by incubation with 10% (w/v, final concentration) TCA overnight at 4°C. The precipitated protein was subsequently collected by centrifugation at 10,000 x *g* (8,819 rpm), for 20 min, at 4°C. The supernatant was discarded, and the pellet washed twice with 1 mL of ice-chilled methanol with 15 min incubation on ice prior to centrifugation at 10,000 x *g* (8,819 rpm), for 20 min, at 4°C. The precipitated proteins were air-dried to eliminate any methanol residue. Laemmli sample buffer (1X) was freshly prepared by diluting the 5X Laemmli sample buffer

(containing β-mercaptoethanol (BME)) (*Appendix 2, A2.15*) with 1 M Tris-HCl, pH 7.5 (*Appendix 2, A2.1*), and used to resuspend the air-dried protein pellet. The sample was subsequently denatured by boiling at 99^{o}C for 10 min and cooled to room temperature before performing further experiments. Total protein in the samples was determined using the 2-D Quant Kit (GE Healthcare, NSW, Australia) according to the manufacturer's instructions.

2.22 TC-FlAsH™-based fluorescence labelling

Live *B. pseudomallei* expressing TC-tagged BapA, BapB, BapC or BopE were visualised using FlAsH-labelling as described previously (Enninga *et al.*, 2005; Simpson *et al.*, 2010) with some modifications. *B. pseudomallei* strains were cultured in LB broth containing appropriate antibiotics, and grown at 37°C with shaking at 200 rpm to an OD_{600} of 0.8. The FlAsH positive control DH5α[pJP117] strain (*Table 2.1*), which expresses a TC-tagged GspD, was induced for expression as described previously (Dunstan *et al.*, 2013). In brief, an overnight culture was subcultured (1:100 dilution) in fresh LB broth supplemented with 100 μg/mL ampicillin and incubated at 37°C with shaking at 200 rpm for 1 h. The expression of the TC-tagged GspD was induced by addition of arabinose (0.1% w/v, final concentration) and further incubation for another 2 h until the culture reached an OD_{600} of 0.8. All exponential growth phase cultures (1 mL each) were harvested by centrifugation at 4,293 x *g* (8,000 rpm) for 5 min. Cells were washed with 1 mL of sterile PBS, pH 7.4 to remove the culture medium and antibiotics prior to resuspension in 50 μL of sterile PBS, pH 7.4. Stock FlAsH reagent, from the TC-FlAsH™ II In-Cell Tetracysteine Tag Detection Kit (Life Technologies™, USA), was added to the bacterial cell suspension to obtain a final concentration of 5 μM prior to incubation at 37°C with shaking at 1,000 rpm, for 1 h. Sample labelling was performed in the dark, and direct light contact was avoided during all later manipulations. During live cell labelling, sample buffer (1X) was freshly prepared by diluting the Laemmli sample buffer (without reducing agent) (*Appendix 2, A2.16*) 5-fold with 1 M Tris-HCl, pH 7.5. DL-Dithiothreitol (DTT; 10 mM, final concentration) was added to be used as the reducing agent, and this diluted sample buffer was kept on ice until use. Labelled samples were washed to remove unbound FlAsH reagent by addition of 1.5 mL of sterile PBS, pH 7.4, followed by centrifugation at 4,293 x *g* (8,000 rpm) for 5 min to concentrate the cells. Each of the pellets was resuspended in 30 μL of 1X sample buffer containing 10 mM DTT and heated at 99°C for 10 min, before cooling in the dark, at room temperature, for 5 min. Labelled samples (15 μL each) were separated by sodium dodecyl sulfate-polyacrylamide gel electrophoresis (SDS-PAGE) as described in *Chapter 2.23*, and the level of fluorescence measured immediately at 520 nm with an excitation at 488 nm (GFP/FITC filter set) with the Typhoon Trio imager (Department of Biochemistry and Molecular Biology, Monash University, Melbourne, Australia) using Image Quant software (GE Healthcare, NSW, Australia). Total proteins were visualised by SDS-PAGE (15 μL each) followed by staining with Coomassie Brilliant Blue (see *Chapter 2.25*).

For direct FlAsH visualisation of proteins, DOC/TCA-precipitated protein samples were labelled with FlAsH reagent as described in the manufacturer's protocol, with minor modifications. In brief, each of the precipitated protein samples (15 μL) was transferred to a new, sterile 1.5 mL microcentrifuge tube, and FlAsH reagent added (20 μM, final concentration) and incubated at 70^{o}C with shaking at 1,000 rpm, for 10 min. Samples were cooled to room temperature for 5 min and then separated by SDS-PAGE. Following electrophoresis, the fluorescence was immediately measured at 520 nm with excitation at 488 nm. Total protein in the samples was visualised by SDS-PAGE, using the remainder of the samples (15 μL each), followed by Coomassie Brilliant Blue staining as described above.

2.23 Sodium dodecyl sulfate-polyacrylamide gel electrophoresis (SDS-PAGE)

Proteins were separated by SDS-PAGE with polyacrylamide gels consisting of 10% resolving gels (containing 4.42 mL of ddH_2O, 2.5 mL of resolving gel buffer (*Appendix 2, A2.13*), 2.48 mL of ACRYL/BIS™ 37.5:1 (30:0.8) 40% (w/v) solution (AMRESCO, USA), 50 μL of 10% (w/v) ammonium persulphate and 10 μL of N,N,N,N'-tetramethylenediamine (TEMED)) and 4% stacking gels (comprising 6.4 mL of ddH_2O, 2.5 mL of stacking gel buffer (*Appendix 2, A2.14*), 1 mL of ACRYL/BIS™ 37.5:1, 40% (w/v) solution, 50 μL of 10% (w/v) ammonium persulphate and 10 μL of TEMED). Gels were run in 1X Tris-Glycine running buffer (*Appendix 2, A2.17*) at 150 V for 90 min. Gels were then used for further experiments, including detection of the FlAsH fluorescent complex, Western blot analysis or Coomassie Brilliant Blue staining.

2.24 Western blotting and enhanced chemiluminescence (ECL) detection

Following SDS-PAGE, proteins were transferred to PVDF membranes (Merck Millipore, USA) by electroblotting at 100 V, for 1 h, at 4^{o}C in Transblot buffer (*Appendix 2, A2.19*). All antibody solutions and washes were prepared in 1X TBS/0.1% (v/v) Tween-20 buffer (*Appendix 2, A2.21*). Washing steps, unless otherwise indicated, were performed at room temperature with shaking. Membranes were blocked in Blocking buffer (*Appendix 2, A2.22*) at 4^{o}C for 16 h with shaking and washed twice with 1X TBS/0.1% (v/v) Tween-20 buffer for 5 min prior to incubation with a 1:1,000 dilution of the rabbit polyclonal anti- $BopE_{78-261}$ antiserum (Stevens *et al.*, 2003) at 37^{o}C for 1 h with shaking. The membranes were then washed four times for 10 min and incubated with a 1:5,000 dilution of the secondary goat anti-rabbit IgG antibody, HRP-conjugate (Merck Millipore, Australia) at room temperature for 1 h with shaking. Membranes

were washed as described earlier and antibody binding was analysed with the Amersham ECL Western Blotting Detection Reagent (GE Healthcare, NSW, Australia), and visualised by expose to X-ray film (Kodak, NY, USA).

2.25 Coomassie Brilliant Blue staining

To visualise total proteins following separation by SDS-PAGE, gels were stained with Coomassie Brilliant Blue solution (*Appendix 2, A2.23*) at room temperature for 16 h with shaking at approximately 100 rpm. Gels were subsequently destained with Destaining solution (*Appendix 2, A2.24*) until excess stain was removed, and the stained gels were then scanned with an Epson Perfection 4990 Photo Scanner for further analysis.

2.26 Southern blotting

Bacterial genomic DNA samples from either *E. coli* or *B. pseudomallei* strains were purified using a HiYield^{TM} Genomic DNA Mini Kit (Real Biotech Corporation, Taipei, Taiwan) according to the manufacturer's instructions. Genomic DNA was digested at 37^{o}C, overnight, with the appropriate restriction enzyme(s) in a total volume of 20 μL (per reaction) as described below:

- Genomic DNA (10 μg) 10 μL
- Restriction buffer 2 μL
- Restriction enzyme (10 U/μL) 1 μL
- ddH_2O 7 μL

Digested DNA samples were separated by agarose gel electrophoresis together with a sample of the Digoxigenin (DIG)-labelled (Roche Diagnostics Australia, NSW, Australia) DNA molecular weight standard marker II, a 1:10 dilution of DIG-labelled PCR product, as a positive control, and a non DIG-labelled PCR product, as a negative control. DNA samples were visualised as described in *Chapter 2.5*. Gels were then incubated in depurination solution (*Appendix 2, A2.27*) at room temperature for 15 min with shaking prior to rinsing in ddH_2O. The gel was then incubated in denaturation solution (*Appendix 2, A2.28*) at room temperature for 30 min with shaking and washed briefly with ddH_2O prior to incubation in neutralisation solution (*Appendix 2, A2.29*) at room temperature for at least 30 min with shaking. Denaturation and neutralisation steps were repeated, if required, before Southern capillary transfer of DNA.

DIG-labelled DNA probes were prepared by PCR with the addition of DIG-labelled dNTPs (Roche Diagnostics Australia, NSW, Australia) (*Appendix 3, Table A3.6*). The PCR products were visualised following agarose electrophoresis in 1% (w/v) gels in 1X TAE buffer at 100 V, for 30 min. PCR products (DIG-labelled and non DIG-labelled) were excised and purified using QIAquick Gel Extraction Kit (QIAGEN®, Australia). The DIG-labelled probe was added to 20 mL of pre-hybridisation solution (*Appendix 2, A2.33*), boiled for 10 min and the solution immediately chilled on ice for 10 min.

Following DNA transfer, membranes were rinsed briefly in 2X SCC solution (*Appendix 2, A2.31*) prior to drying between Whatman™ 3 MM filter paper at room temperature for 10 min. DNA was cross-linked to the membrane for 3 min using a UVIlink CL508 Crosslinker (UVItec Limited, Cambridge, United Kingdom). The membrane was then incubated in pre-hybridisation solution for at least 3 h at 65°C. The pre-hydridisation solution was then replaced with the DIG-labelled DNA probe solution (see above) and hybridised at 65°C, overnight. Following hybridisation, the membrane was washed twice in 2X Wash solution (*Appendix 2, A2.34*) at room temperature for 5 min. The membrane was subsequently washed twice with 0.2X Wash solution (*Appendix 2, A2.35*) at 65°C for 15 min prior to rinsing in Washing buffer (*Appendix 2, A2.37*) at room temperature for 5 min. The membrane was then incubated in Blocking buffer (*Appendix 2, A2.38*) at room temperature for at least 30 min with shaking. Following blocking, the membrane was incubated with a 1:10,000 dilution of anti-DIG-alkaline phosphatase conjugate (Roche Diagnostics Australia, NSW, Australia) in Blocking buffer at room temperature for 30 min with shaking. The membrane was then washed twice in Washing solution at room temperature for 15 min prior to incubation in Detection solution (*Appendix 2, A2.39*) at room temperature for 5 min. The hybridising bands were visualised by addition of a 1:100 dilution of CDP-*Star* (Roche Diagnostics Australia, NSW, Australia) in Detection solution and the membrane exposed to X-ray film (Kodak, NY, USA) for an appropriate time.

2.27 Statistical analysis

Differences in survival of mice infected with the wild-type strain or mutant *B. pseudomallei* strains were assessed using Fisher's exact test. Kaplan–Meier survival curves were used to display time-to-death data for virulence trials and the curves for different strains compared using Log-rank (Mantel-Cox) test. Two-way ANOVA was used to analyse intracellular survival assays, and Student's unpaired *t*-test was used to compare means between each mutant and the

wild-type strain. A *P* value of less than 0.05 was accepted as indicating a statistically significant difference between samples.

Table 2.1 Strains and plasmids used in this study.

Strains or plasmids	Description	Reference
***B. pseudomallei* strains**		
K96243	Wild-type, clinical isolate from Thailand	(Holden *et al.*, 2004)
K96243*ΔbapA*	K96243 derivative with a 1,565-bp deletion within *bapA* replaced by a 1.3-kb tetracycline resistance cassette derived from pUTminiTn*5*Tc, Tet^R	This study
K96243*ΔbapA*_2	The independently derived K96243*ΔbapA* strain	This study
K96243*ΔbapB*	K96243 derivative with a central fragment of *bapB* replaced by a 1.3-kb tetracycline resistance cassette derived from pUTminiTn*5*Tc, Tet^R	This study
K96243*ΔbapB*_2	The independently derived K96243*ΔbapB* strain	This study
K96243*ΔbapC*	K96243 derivative with a central fragment of *bapC* replaced by a 1.3-kb tetracycline resistance cassette derived from pUTminiTn*5*Tc, Tet^R	This study
K96243*ΔbapC*_2	The independently derived K96243*ΔbapC* strain	This study
K96243*ΔbapBC*	K96243 derivative with a 510-bp deletion encompassing the 3'-end of *bapB* and the 5'-end of *bapC* replaced by a 1.3-kb tetracycline resistance cassette derived from pUTminiTn*5*Tc, Tet^R	This study
K96243*ΔbapA-bapA*	The K96243*ΔbapA* strain complemented with the pUC18Tmini-Tn*7*T::*cat*::P_{glmS2}::*bapA* construct, Tet^R, Cm^R	This study
K96243*ΔbapB-bapABC*	The K96243*ΔbapB* strain complemented with the pUC18Tmini-Tn*7*T::*cat*::P_{glmS2}::*bapABC* construct, Tet^R, Cm^R	This study
K96243*ΔbapC-bapABC*	The K96243*ΔbapC* strain complemented with the pUC18Tmini-Tn*7*T::*cat*::P_{glmS2}::*bapABC* construct, Tet^R, Cm^R	This study
K96243*ΔbapBC-bapABC*	The K96243*ΔbapBC* strain complemented with the pUC18Tmini-Tn*7*T::*cat*::P_{glmS2}::*bapABC* construct, Tet^R, Cm^R	This study
K96243*ΔbapA*[*bapA*]	The K96243*ΔbapA* strain complemented with the pBHR::*bapA* construct, Tet^R, Kan^R	This study
K96243*ΔbapB*[*bapB*]	The K96243*ΔbapB* strain complemented with the pBHR::*bapB* construct, Tet^R, Kan^R	This study
K96243*ΔbapC*[*bapC*]	The K96243*ΔbapC* strain complemented with the pBHR::*bapC* construct, Tet^R, Kan^R	This study
K96243*ΔbapA*[pBHR1]	The K96243*ΔbapA* strain harbouring empty pBHR1 vector, Tet^R, Kan^R, Cm^R	This study
K96243*ΔbapB*[pBHR1]	The K96243*ΔbapB* strain harbouring empty pBHR1 vector, Tet^R, Kan^R, Cm^R	This study

Table 2.1 Strains and plasmids used in this study (cont.).

Strains or plasmids	Description	Reference
K96243*ΔbapC*[pBHR1]	The K96243*ΔbapC* strain harbouring empty pBHR1 vector, Tet^R, Kan^R, Cm^R	This study
K96243[pBHR1]	K96243 derivative harbouring empty pBHR1 vector, Kan^R, Cm^R	This study
K96243*bopE*TC	K96243 derivative with a tetracysteine (TC) tagged *bopE*. Insertion of the pUC18Tmini-Tn*7*T::*tetA*(C):: P_{glmS2}::*bopE*TC construct into the bacterial genome at a site other than the *glmS1, glmS2* and *glmS3* downstream regions, Tet^R	This study
K96243[*bopE*TC]	K96243 derivative harbouring the pBHR1::P_{glmS2} ::*bopE*TC construct, Kan^R	This study
K96243[*bapA*TC]	K96243 derivative harbouring the pBHR1::*bapA*TC construct, Kan^R	This study
K96243[*bapB*TC]	K96243 derivative harbouring the pBHR1::*bapB*TC construct, Kan^R	This study
K96243[*bapC*TC]	K96243 derivative harbouring the pBHR1::*bapC*TC construct, Kan^R	This study
K96243*ΔbsaS*	K96243 derivative with a central fragment of *bsaS* replaced by a 1.3-kb tetracycline resistance cassette derived from pUTminiTn*5*Tc, Tet^R	Gong *et al.*, manuscript in preparation
K96243*ΔbsaS*[*bopE*TC]	K96243*ΔbsaS* derivative harbouring the pBHR1:: P_{glmS2}::*bopE*TC construct, Tet^R, Kan^R	This study
K96243*ΔbsaS*[*bapA*TC]	K96243*ΔbsaS* derivative harbouring the pBHR1:: *bapA*TC construct, Tet^R, Kan^R	This study
K96243*ΔbsaS*[*bapB*TC]	K96243*ΔbsaS* derivative harbouring the pBHR1:: *bapB*TC construct, Tet^R, Kan^R	This study
K96243*ΔbsaS*[*bapC*TC]	K96243*ΔbsaS* derivative harbouring the pBHR1:: *bapC*TC construct, Tet^R, Kan^R	This study
K96243*ΔbsaS*[pBHR1]	K96243*ΔbsaS* derivative harbouring empty pBHR1 vector, Tet^R, Kan^R, Cm^R	This study
K96243*ΔbopE*::pDM4	K96243 derivative harbouring the pDM4::*bopE* construct, Cm^R	This study
***E. coli* strains**		
S17-1/λ*pir*	Strain for propagation of pDM4 and pBHR1, contains RP4 transfer genes integrated into the chromosome, expresses *λpir* replication protein: *recA, thi, pro, hsdR-M⁺RP4: 2-Tc:Mu: Km, Tn7, λpir*, Tp^R, Sm^R	(Simon *et al.*, 1983)
SM10/λ*pir*	Strain for propagation of pUC18Tmini-Tn*7*T constructs and pTNS3, expresses *λpir* replication protein: *thi-1, thr, leu, tonA, lacY, supE, recA::RP4-2-Tc::Mu, λpir*, Kan^R	(Simon *et al.*, 1983)

Table 2.1 Strains and plasmids used in this study (cont.).

Strains or plasmids	Description	Reference
DH5α	General *E. coli* strain used for plasmid amplification, transformation and storage: *F⁻, ø80dlacZΔM15, Δ(lacZYA-argF)U169, recA1, endA1, hsdR17(rK⁻, mK⁺), phoA, supE44, λ–, thi-1, deoR, gyrA96, relA1*	(Grant *et al.*, 1990)
DH5α[pJP117]	Strain for FlAsH optimisation containing the plasmid pJP117: *F⁻, ø80dlacZΔM15, Δ(lacZYA-argF)U169, recA1, endA1, hsdR17 (rK⁻, mK⁺), phoA, supE44, λ–, thi-1, deoR, gyrA96, relA1, bla, araC*, TC-tagged *gspD*, Amp^R	(Dunstan *et al.*, 2013)
Plasmids		
pDM4	*λpir*-dependent replication, suicide vector in *B. pseudomallei*, *oriR6K*, *mobRP4*, *sacBR*, Cm^R	(Milton *et al.*, 1996)
pDM4::*bapA*::*tetA*(C)	pDM4 containing a 918-bp fragment harbouring the 5' region of *bapA*, tetracycline resistance cassette and a 1,241-bp fragment encompassing the 3' region of *bapA* and the entire *bapB* and *bapC* genes, Cm^R, Tet^R	This study
pDM4::*bapB*::*tetA*(C)	pDM4 containing a 1,093-bp fragment encompassing the 3' region of *bapA* and the 5' region of *bapB*, tetracycline resistance cassette and a 662-bp fragment containing the 3' region of *bapB* and the entire *bapC* gene, Cm^R, Tet^R	This study
pDM4::*bapC*::*tetA*(C)	pDM4 containing a 753-bp fragment encompassing the 3' region of *bapA*, the entire *bapB* and the 5' region of *bapC*, tetracycline resistance cassette and a 755-bp fragment containing the 3' region of *bapC* and the downstream region, Cm^R, Tet^R	This study
pDM4::*bapBC*::*tetA*(C)	pDM4 containing a 448-bp fragment encompassing the 3' region of *bapA* and the 5' region of *bapB*, tetracycline resistance cassette and a 775-bp fragment containing the 3' region and downstream region of *bapC*, Cm^R, Tet^R	This study
pDM4::*bopE*	pDM4 containing a 367-bp internal fragment of *bopE* derived from *B. pseudomallei* strain 10276 for generating the K96243*ΔbopE*::pDM4 strain, Cm^R	(Stevens *et al.*, 2002)
pUTminiTn*5*Tc	Mini-Tn*5*Tc in plasmid pUT, Amp^R Tet^R	(de Lorenzo *et al.*, 1990)
pUC18Tmini-Tn*7*T	Mini-Tn*7* based broad-host-range transposon vector, Amp^R	(Choi *et al.*, 2005)
pUC18Tmini-Tn*7*T::P_{glmS2}	pUC18Tmini-Tn*7*T containing *glmS2* promoter derived from *B. pseudomallei* strain K96243, Amp^R	Alwis *et al.* unpublished data
pUC18Tmini-Tn*7*T::*tetA*(C)::P_{glmS2}	pUC18Tmini-Tn*7*T containing tetracycline resistance cassette derived from pUTminiTn*5* Tc and *glmS2* promoter, Amp^R, Tet^R	Alwis *et al.* unpublished data

Table 2.1 Strains and plasmids used in this study (cont.).

Strains or plasmids	Description	Reference
pUC18Tmini-Tn*7*T:: P_{glmS2}::*bapA*	pUC18Tmini-Tn*7*T containing *glmS2* promoter and the full length *bapA* gene derived from *B. pseudomallei* strain K96243, Amp^R	This study
pUC18Tmini-Tn*7*T:: P_{glmS2}::*bapABC*	pUC18Tmini-Tn*7*T containing *glmS2* promoter and the full length *bapA*, *bapB* and *bapC* genes derived from *B. pseudomallei* strain K96243, Amp^R	This study
pUC18Tmini-Tn*7*T::*cat*:: P_{glmS2}::*bapA*	pUC18Tmini-Tn*7*T containing the chloramphenicol acetyl transferase (*cat*) gene derived from pDM4, *glmS2* promoter and the full length *bapA* derived from *B. pseudomallei* strain K96243, Amp^R, Cm^R	This study
pUC18Tmini-Tn*7*T::*cat*:: P_{glmS2}::*bapABC*	pUC18Tmini-Tn*7*T containing the chloramphenicol acetyl transferase (*cat*) gene derived from pDM4, *glmS2* promoter and the full length *bapA*, *bapB* and *bapC* genes derived from *B. pseudomallei* strain K96243, Amp^R, Cm^R	This study
pUC18Tmini-Tn*7*T:: *tetA*(C)::P_{glmS2}::*bopE*	pUC18Tmini-Tn*7*T containing tetracycline resistance cassette derived from pUTminiTn*5*Tc, *glmS2* promoter and the full length *bopE* derived from *B. pseudomallei* strain K96243, Amp^R, Tet^R	This study
pUC18Tmini-Tn*7*T:: *tetA*(C)::P_{glmS2}::*bopE*TC	pUC18Tmini-Tn*7*T containing tetracycline resistance cassette derived from pUTminiTn*5*Tc, *glmS2* promoter and the full length *bopE* derived from *B. pseudomallei* strain K96243 and fused with the TC motif, Amp^R, Tet^R	This study
pTNS3	A helper plasmid for mini-Tn*7* transposition vector contains Tn*7* transposase gene, Amp^R	(Choi *et al.*, 2005)
pBHR1	A mobilisable *B. pseudomallei* and *E. coli* shuttle vector: the genotype: *mob*, *rep*, Cm^R, Kan^R	(Szpirer *et al.*, 2001)
pBHR1::*bapA*	pBHR1 containing full length *bapA* derived from *B. pseudomallei* strain K96243, Kan^R	This study
pBHR1::*bapB*	pBHR1 containing full length *bapB* derived from *B. pseudomallei* strain K96243, Kan^R	This study
pBHR1::*bapC*	pBHR1 containing full length *bapC* derived from *B. pseudomallei* strain K96243, Kan^R	This study
pBHR1::P_{glmS2}::*bopE*TC	pBHR1 containing a 1,411-bp fragment, derived from *B. pseudomallei* strain K96243 *bopE*TC, harbouring *glmS2* promoter, full length *bopE* tagged with the TC motif and two transcriptional terminators T_0 and T_1, Kan^R	This study
pBHR1::*bapA*TC	pBHR1 containing full length *bapA*, derived from *B. pseudomallei* strain K96243, and fused with the TC motif, Kan^R	This study
pBHR1::*bapB*TC	pBHR1 containing full length *bapB*, derived from *B. pseudomallei* strain K96243, and fused with the TC motif, Kan^R	This study

Table 2.1 Strains and plasmids used in this study (cont.).

Strains or plasmids	Description	Reference
pBHR1::*bapC*TC	pBHR1 containing full length *bapC*, derived from *B. pseudomallei* strain K96243, and fused with the TC motif, Kan^R	This study
pJP117	pBAD24 containing the *araBAD* promoter and full length *gspD*, derived from *E. coli enteropathogenic* strain *E2348/69*, and fused with the TC motif, Amp^R	(Dunstan *et al.*, 2013)

Table 2.2 Mutagenesis primers used to generate the K96243*ΔbapA*, K96243*ΔbapB*, K96243*ΔbapC* and K96243*ΔbapBC* strains.

Primer name	Sequence (5' – 3')*	Description
MC5532	GGGCCCACTAGTCCGATCCGAAGCAACCGACAAGA	Forward primer for amplification of the 5' region of *bapA*, specifying a *Spe*I site
MC5533	GGGCCCAGATCTACCATGTCGACGAGATTCGTC	Reverse primer for amplification of the 5' region of *bapA*, specifying a *Bgl*II site
MC5516	GGGCCCAGATCTCTTTATCCGCTCGTCGACGATGCTT	Forward primer for amplification of the 3' region of *bapA* and the entire *bapB* and *bapC* genes, specifying a *Bgl*II site
MC5517	GGGCCCTCTAGATTGGCGTATTGGCGTATTGGCGTA	Reverse primer for amplification of the 3' region of *bapA* and the entire *bapB* and *bapC* genes, specifying an *Xba*I site
JT6156	CGGCTGACGCAATCGCG	Forward primer for amplification of the 1,093-bp 3' region of *bapA* and the 5' region of *bapB*, containing a native *Sph*I site
JT6157	ATCCATCGCCAGGTCGTCGA	Reverse primer for amplification of the 1,093-bp 3' region of *bapA* and the 5' region of *bapB*, containing a native *Sph*I site
JT6175	GGGCCCACTAGTCAGATCGCGCCGCCGCA	Forward primer for amplification of the 662-bp 3' region of *bapB* and the entire *bapC* gene, specifying a *Spe*I site
JT6176	GGGCCCACTAGTGGGCCGCGCGACATAGA	Reverse primer for amplification of the 662-bp 3' region of *bapB* and the entire *bapC* gene, specifying a *Spe*I site
JT6319	GGGCCCCCCGGGGTCACATCGAACGTCGCATC	Forward primer for amplification of the 753-bp 3' region of *bapA*, the entire *bapB* and the 5' region of *bapC*, specifying an *Xma*I site
JT6320	GGGCCCGAGCTCCCCGCCGATACGATGCCGAT	Reverse primer for amplification of the 753-bp 3' region of *bapA*, the entire *bapB* and the 5' region of *bapC*, specifying a *Sac*I site

*Underlined sequences indicate added restriction sites.

Table 2.2 Mutagenesis primers used to generate the K96243*ΔbapA*, K96243*ΔbapB*, K96243*ΔbapC* and K96243*ΔbapBC* strains (cont.).

Primer name	Sequence (5' – 3')*	Description
JT6179	TATTACGAGTCGGGGCTGAATCCGC GC	Forward primer for amplification of the 775-bp 3' downstream region of *bapC*, containing a native *Sal*I site
JT6180	GGGCCCGTCGACGGATCGGTGAATT CGTGGGGTTCTCG	Reverse primer for amplification of the 775-bp 3' downstream region of *bapC*, specifying a *Sal*I site
JT6177	GGGCCCGCATGC CGTCACATC GAACGT CG	Forward primer for amplification of the 448-bp 3' region of *bapA* and the 5' region of *bapB*, specifying an *Sph*I site
JT6074	CGATCGAATCGTTCCAGCCG	Reverse primer for amplification of the 448-bp 3' region of *bapA* and the 5' region of *bapB*, containing a native *Sph*I site
JT6279	CTTCTGTTTCTATCAGCTGTCCCT	Forward primer for amplification of the MCS of the pDM4 vector
JT6280	TGTGGAATTGTGAGCGGATAA	Reverse primer for amplification of the MCS of the pDM4 vector
MC3325	CGGCTTAGATCTAGGTCGAGGTGGC C	Forward primer at the 5' end of *tetA*(C) cassette derived from pUTminiTn*5*Tc
MC4629	TCCAACAGATCTATTTGCCGACTAC CTTGGTG	Reverse primer at the 3' end of *tetA*(C) cassette derived from pUTminiTn*5*Tc
NA5116	ATCAGGGACAGCTTCAAGGA	Primer for amplification out of the 3' end of *tetA*(C) cassette
NA5424	GCTGTCGGAATGGACGATAT	Primer for amplification out of the 5' end of *tetA*(C) cassette
JT6376	GGGCCCCCCGGGAACCTGCTCGAGC GCCTGGA	Forward primer for amplification of the 5' region of *bapA*, specifying an *Xma*I site
JT6073	ATGCGGGTGATGCGGGTGAT	Forward primer at the 3' end of *bapA*
JT6321	GGGCCCCCCGGGACGATGCCGATCG CGAACGC	Reverse primer at the 5' end of *bapC*, specifying an *Xma*I site
JT6640	GGGCCCAGATCTGATGGATTCGCTC GAGCTGA	Forward primer in the middle of *bapB*, specifying a *Bgl*II site

*Underlined sequences indicate added restriction sites.

Table 2.3 Primers used to generate complementation constructs in the *B. pseudomallei* plasmid pBHR1 and the site-specific transposon containing vector pUC18Tmini-Tn*7*T.

Primer name	Sequence (5' – 3')*	Description
JT6100	GGGCCCGGTACCACAGCTGATA GAAACAGAAGCCACT	Forward primer for amplification across the chloramphenicol acetyltransferase (*cat*) gene conferring chloramphenicol resistance, specifying a *Kpn*I site
JT6101	GGGCCCGGTACCATCACTTATTC AGGCGTAGCAACCA	Reverse primer for amplification across the chloramphenicol acetyltransferase (*cat*) gene conferring chloramphenicol resistance, specifying a *Kpn*I site
JT6102	GGGCCCCTGCAGGACGCTCACG GACACCGC	Forward primer for amplification of the full length *bapA* gene together with the predicted native promoter, specifying a *Pst*I site
JT6104	GGGCCCACTAGTGCGGCGTCGCT CAGATGC	Reverse primer for amplification of the full length *bapA* gene together with the predicted native promoter, specifying a *Spe*I site
JT6105	CTGCAGACGCTCACGGACACCG C	Forward primer for amplification of the full length *bapA*, *bapB* and *bapC*, specifying a *Pst*I site
JT6106	GGGCCCACTAGTCCTCGTCACCC GCTCAC	Reverse primer for amplification of the full length *bapA*, *bapB* and *bapC*, specifying a *Spe*I site
JT6071	CCGCCGTCCATTCACCGAACTT	Forward primer for amplification of a 634-bp section of the 5'end of *bapA*
JT6072	TGCGGTAACCCTTGTTGCCC	Reverse primer for amplification of a 634-bp section of the 5'end of *bapA*
JT6077	CGTTCGCGATCGGCATCGTA	Forward primer for amplification of a 478-bp section of *bapC*
JT6078	TCCTCGATCACGAGCCCCGG	Reverse primer for amplification of a 478-bp section of *bapC*
JT6183	TTGCTGAGGTCCGACGGCAT	Forward primer used for nucleotide sequencing of *bapA*
JT6184	TCGTTCCACTGGCGAGGCTT	Reverse primer used for nucleotide sequencing of *bapA*
JT6185	TCGTCAGGACCACCGAAGGT	Forward primer used for nucleotide sequencing of *bapA*
JT7065	GGGCCCGAATTCCCCCGATCCGA AGCAACCGACAAG	Forward primer used for amplification of the full length *bapA* including the predicted native promoter, specifying an *Eco*RI site
JT7066	GGGCCCAACGTTTCGCTTCGTGC CGTTGGCGATCGAATC	Reverse primer used for amplification of the full length *bapA* including the predicted native promoter, specifying an *Acl*I site

*Underlined sequences indicate added restriction sites.

Table 2.3 Primers used to generate complementation constructs in the *B. pseudomallei* plasmid pBHR1 and the site-specific transposon vector pUC18Tmini-Tn*7*T (cont.).

Primer name	Sequence (5' – 3')*	Description
JT7171	GGGCCCGAATTCCGGCACGAA GCGATGACGGCCGGCC	Forward primer used for amplification of the full length *bapB*, specifying an *Eco*RI site
JT7172	GGGCCCAACGTTTGCGCCTCCC GAATCGTCCG	Reverse primer used for amplification of the full length *bapB*, specifying an *Acl*I site
JT7173	GGGCCCGAATTCGGCCGCGCGC GCGGACGATTCGGGAGG	Forward primer used for amplification of the full length *bapC*, specifying an *Eco*RI site
JT7174	GGGCCCAACGTTCTGCACCGAC GCCTCCTCGATCACGAGCCC	Reverse primer used for amplification of the full length *bapC*, specifying an *Acl*I site
JT7080	GGGCCCATAACTGCCTTAAAAA AATTA	Forward primer for amplification of the chloramphenicol resistance gene of pBHR1
JT7081	GGGCCCGTATTTTTTGAGTTAT CGAGAT	Reverse primer for amplification of the chloramphenicol resistance gene of pBHR1
MC6028	GGGCCCAAGCTTCCTTGCGCGA GCGGGTTGAAATT	Forward primer upstream of the *glmS2* promoter of pUC18Tmini-Tn*7*T::*cat*::P_{glmS2}:: *bapA*, specifying a *Hin*dIII site
PA6067	AGTAGGACAAATCCGCCGCT	Forward primer outside of the pUC18Tmini-Tn*7*T MCS
PA6068	ATCTGGTTGGCCTGCAAGGC	Reverse primer outside of the pUC18Tmini-Tn*7*T MCS
PA6211	GAATGCGCGTCGAGCTTCAT	Forward primer for amplification of downstream region of *B. pseudomallei glmS2*
PA6212	CAGAACAGCGAGCCCGTGTT	Reverse primer for amplification of downstream region of *B. pseudomallei glmS2*
PA6271	GGGCTGCACTATCCGATCTC	Forward primer for amplification of downstream region of *B. pseudomallei glmS1*
PA6272	AGAGTGCGGTCAGCGAGAAC	Reverse primer for amplification of downstream region of *B. pseudomallei glmS1*
PA6273	GCTCGCGCTCGTGACGAATA	Forward primer for amplification of downstream region of *B. pseudomallei glmS3*
PA6274	CGATCACGCTGCTTTGGCTG	Reverse primer for amplification of downstream region of *B. pseudomallei glmS3*
PA6229	ATATCGTGCGAAAAAGGATGG ATAT	Forward primer for amplification of a section surrounding the mini-Tn*7 oriT*
PA6230	TGGTTTGTTTGCCGGATCAA	Reverse primer for amplification of a section surrounding the mini-Tn*7 oriT*

*Underlined sequences indicate added restriction sites.

Table 2.4 Primers used to generate constructs for FlAsH experiments.

Primer name	Sequence (5' – 3')*	Description
JT6929	GGGCCCCCCGGGGACCTCCTTCCCTTCAACCGA	Forward primer for amplification of *bopE*, specifying an *Xma*I site
JT6930	GGGCCCACTAGTCGCGCCGTCCGCCGCGTTCGT	Reverse primer for amplification of *bopE*, specifying an *Spe*I site
JT6931	CTAGTGCGGGCAGCTTCCTGAACTGCTGCCCGGGCTGCTGCATGGAGCCGGGCGGCCGCTAA	Forward primer for generating the TC motif, and for cloning at an *Spe*I site
JT6932	CTAGTTAGCGGCCGCCCGGCTCCATGCAGCAGCCCGGGCAGCAGTTCAGGAAGCTGCCCGCA	Reverse primer for generating the TC motif, and for cloning at an *Spe*I site
JT7063	GGGCCCAACGTTGACCTCCTTCCCTTCAACCGA	Forward primer for amplification of the full length *bopE*, specifying an *Acl*I site
JT7064	GGGCCCCCATGGCGCGCCGTCCGCCGCGTTCGT	Reverse primer for amplification of the full length *bopE*, specifying an *Nco*I site
MC6028	GGGCCCAAGCTTCCTTGCGCGAGCGGGTTGAAATT	Forward primer upstream of the *glmS2* promoter of pUC18Tmini-Tn*7*T::*tetA*(C):: P_{glmS2}::*bopE*, specifying a *Hin*dIII site
MC6029	GGGCCCGAATTCCGAACGCGATGGTAGAAT	Reverse primer upstream of the *glmS2* promoter of pUC18Tmini-Tn*7*T::*tetA*(C):: P_{glmS2}::*bopE*, specifying an *Eco*RI site
JT7125	GGGCCCAACGTTTAGCAATTTAACTGGTACCG	Forward primer for amplification of the fragment containing the *glmS2* promoter, *bopE* tagged with TC motif and two terminators, from the mini-Tn*7* construct, specifying an *Acl*I site
JT7126	GGGCCCCCATGGATCGATAAGCTAGCTTAATT	Reverse primer for amplification of the fragment containing the *glmS2* promoter, *bopE* tagged with TC motif and two terminators, from the mini-Tn*7* construct, specifying an *Nco*I site
JT7147	CGTTGCGGGCAGCTTCCTGAACTGCTGCCCGGGCTGCTGCATGGAGCCGGGCGGCCGCTAAAA	Forward primer for generating the TC tag, and for cloning at an *Acl*I site
JT7241	CGTTTTAGCGGCCGCCCGGCTCCATGCAGCAGCCCGGGCAGCAGTTCAGGAAGCTGCCCGCAA	Reverse primer for generating the TC tag, and for cloning at an *Acl*I site
JT6079	CGGTATGTGGCTTCGAGCGT	Forward primer for amplification of *bopE* fragment
JT6080	CGAAACGCTCGGGCAACTGT	Reverse primer for amplification of *bopE* fragment

*Underline indicates nucleotides specifying restriction sites.

Table 2.4 Primers used to generate constructs for FlAsH experiments (cont.).

Primer name	Sequence (5' – 3')*	Description
JT7472	TGACTTACAACCCGAGAATCG	Forward primer specific for amplification of *bopE* for real-time RT-PCR
JT7473	GATGCGCTTGATCTGTTGTG	Reverse primer specific for amplification of *bopE* for real-time RT-PCR
JT7474	CACGATTGCGAAGTCATCAA	Forward primer specific for amplification of *rpoA* for real-time RT-PCR
JT7475	GCCCTTTTCCACCTTGATCT	Reverse primer specific for amplification of *rpoA* for real-time RT-PCR

*Underline indicates nucleotides specifying restriction sites.

Chapter 3

Involvement of BapA, BapB and BapC in the *in vivo* growth and virulence of *B. pseudomallei*

Chapter 3: Involvement of BapA, BapB and BapC in the *in vivo* growth and virulence of *B. pseudomallei*

This chapter focuses on characterisation of the *B. pseudomallei* genes *bapA*, *bapB* and *bapC*, and analysis of their role in *B. pseudomallei* growth *in vivo* and virulence. The genes *bapA*, *bapB* and *bapC* are located in the TTSS3 (*bsa*TTSS) locus between *bopE* and *bipD*. The *bopE* and *bipD* genes encode the well-characterised TTSS3 effector and translocon proteins, respectively. Thus, the location of *bapA*, *bapB* and *bapC* strongly suggests a role in *B. pseudomallei* TTSS3 and therefore pathogenesis. Warawa and Woods (2005) reported an involvement of the TTSS3 in full virulence of *B. pseudomallei* strain 1026b. However, the predicted TTSS3 effector genes *bopA*, *bopE*, *bapA* and *bapC* did not contribute to bacterial virulence in the hamster melioidosis model. Stevens and colleagues (2004), nonetheless, demonstrated partial attenuation of a *B. pseudomallei bopA* mutant in the BALB/c mouse melioidosis model. Thus host-specific and/or strain-specific factors contribute to bacterial virulence and disease outcome (Forbes *et al.*, 2008; Gieseler *et al.*, 2005). Therefore it was decided to further characterise the function of the TTSS3 genes *bapA, bapB* and *bapC* with regard to the pathogenesis of *B. pseudomallei* in the mouse model and define their role as possible TTSS3 effectors.

3.1 Mutagenesis of *bapA*, *bapB* and *bapC* by double cross-over allelic exchange

In order to characterise *bapA*, *bapB* and *bapC*, each of the genes was disrupted using double cross-over allelic exchange. The *λ-pir* dependent vector pDM4, which contains the *sacB* gene for negative selection (Milton *et al.*, 1996), was used to generate the mutagenesis constructs in *E. coli* S17-1/λ*pir*. Genomic DNA from *B. pseudomallei* K96243 was amplified using specific primer pairs (*Chapter 2, Table 2.2*) to generate all DNA sections upstream and downstream of the target genes. For *bapA* mutagenesis, a 1,565-bp internal fragment, located from base pair 890 to 2409, was removed in the mutant and replaced by the *tetA*(C) gene. To generate the mutant construct, the primers MC5532 and MC5533 were used to amplify a 918-bp fragment from the 5' region of *bapA*, and MC5516 and MC5517 were used to amplify a 1,241-bp fragment encompassing the 3' region of *bapA* and the entire *bapB* and *bapC* genes. Both fragments were cloned into *Spe*I-/*Xba*I-digested pDM4. For selection, the tetracycline resistance gene *tetA*(C) was amplified from pUTminiTn*5*Tc using the primers MC3325 and NA4639 (*Chapter 2*, *Table 2.2*) and ligated into the *Bgl*II site between the *bapA* gene segments to generate the mutagenesis construct pDM4::*bapA*::*tetA*(C) (*Figure 3.1.1*). The mutagenesis construct was moved into

B. pseudomallei K96243 by conjugation, and tetracycline and sucrose resistant, and chloramphenicol sensitive colonies selected as potential double-crossover *bapA* mutants. Genetic verification of *bapA* mutagenesis was performed by PCR using three sets of primers (*Figure 3.1.2*). Two primer pairs JT6376/NA5424 and NA5116/JT6180 (*Chapter 2, Table 2.2*) were used to verify the insertion of *tetA*(C) within *bapA*. The first primer pair JT6376/NA5424 amplified the expected 1.8-kb fragment from the putative *bapA* mutant (*Figure 3.1.2C, lane 2*), but amplified no product from the wild-type strain (*Figure 3.1.2C, lane 3*). Similarly, the primers NA5116 and JT6180 produced the expected 1.6-kb fragment from the putative *bapA* mutant (*Figure 3.1.2C, lane 5*), but amplified no product from the wild-type strain (*Figure 3.1.2C, lane 6*) or the reaction with no DNA added (*Figure 3.1.2C, lane 7*). The deletion within *bapA* was confirmed using the primer pair JT6185/JT6104. PCR using these primers amplified the expected fragment from the wild-type strain (*Figure 3.1.2C, lane 10*), but not the putative *bapA* mutant (*Figure 3.1.2C, lane 9*). The identity of each of the amplified PCR products was confirmed by nucleotide sequencing (data not shown). Therefore, these analyses confirmed the presence of *tetA*(C) within *bapA* and this mutant strain was designated as K96243*ΔbapA* (*Chapter 2, Table 2.1*).

In a similar manner, *B. pseudomallei bapB* and *bapC* mutants were generated using double-crossover allelic exchange. For *bapB* mutagenesis (*Figure 3.1.3A*), the *tetA*(C) gene was inserted at base pair 132 of *bapB*. To generate the mutant construct, the primers JT6156 and JT6157 (*Chapter 2, Table 2.2*) were used to amplify an upstream 1,093-bp product, encompassing the 3' region of *bapA* and the 5' region of *bapB*. This upstream fragment, containing native *Sph*I sites, was ligated into *Sph*I-digested pDM4. Clones were screened for insertion of the upstream fragment by PCR and then confirmed by nucleotide sequencing using the primers JT6279 and JT6280 (*Chapter 2, Table 2.2*) specific for amplification of the MCS of pDM4 vector (data not shown). A downstream 662-bp fragment, containing the 3' region of *bapB* and the entire *bapC* gene, was amplified using the primers JT6175 and JT6176 (*Chapter 2, Table 2.2*) and subsequently ligated into *Spe*I-digested pDM4 containing the verified upstream fragment. Clones were screened and then verified for fragment insertion as described earlier (data not shown). For selection, as described in *bapA* mutagenesis, the *tetA*(C) gene was ligated into the central *Bgl*II site of pDM4 in order to generate pDM4::*bapB*::*tetA*(C) (*Chapter 2, Table 2.1*). This mutant construct was introduced by transformation into *E. coli* S17-1/λ*pir* (*Chapter 2.7*) and then into *B. pseudomallei* strain K96243 by conjugation (*Chapter 2.10*). To verify the disruption of *bapB*, tetracycline and sucrose resistant, and chloramphenicol sensitive transconjugants were selected

to perform PCR using two sets of primer pairs, JT6185/NA5116 and NA5424/JT6078 (*Chapter 2, Table 2.2* and *2.3*), which amplify from the middle of *bapA* to *tetA*(C) and from *tetA*(C) to the 3'end of *bapC* respectively. As expected, a fragment of 1.4-kb was amplified using genomic DNA of the *bapB* mutant with the primers JT6185/NA5116 (*Figure 3.1.4A, lane 2*), but not using genomic DNA of the wild-type strain (*Figure 3.1.4A, lane 3*) or from no DNA added control reaction (*Figure 3.1.4A, lane 4*). Similarly, a fragment of 977-bp was amplified with primers NA5424/JT6078 using the *bapB* mutant genomic DNA (*Figure 3.1.4A, lane 5*), but not using genomic DNA of the wild-type strain (*Figure 3.1.4A, lane 6*) or in the no DNA control (*Figure 3.1.4A, lane 7*). The minor products of 1.5-kb observed in both the *bapB* mutant and the wild-type strain were likely the result of non-specific amplification rather than contamination as there was no PCR product present in the no DNA control. The PCR products were verified by nucleotide sequencing (data not shown). Therefore, the *bapB* double cross-over mutant was confirmed and designated K96243*ΔbapB* (*Chapter 2, Table 2.1*).

For *bapC* mutagenesis (*Figure 3.1.3B*), the *tetA*(C) gene was inserted at base pair 90 of *bapC*. To generate the mutant construct, the primers JT6319 and JT6320 (*Chapter 2, Table 2.2*) were used to amplify an upstream 753-bp product, encompassing the 3' region of *bapA*, the entire *bapB* and the 5' region of *bapC*. This upstream fragment was then ligated into *Xma*I-/*Sac*I-digested pDM4. Clones were screened and then verified for fragment insertion as described above (data not shown). A downstream 775-bp fragment, containing native (5' end) and additional (3' end) *Sal*I sites, respectively, was amplified using the primers JT6179 and JT6180 (*Chapter 2, Table 2.2*) and subsequently ligated into *Sal*I-digested pDM4 containing the verified upstream fragment. Clones were screened and then verified for fragment insertion as described above (data not shown). The *tetA*(C) gene was subsequently ligated into the central *Bgl*II site in order to generate pDM4::*bapC*::*tetA*(C) (*Chapter 2, Table 2.1*). This mutant construct was introduced by transformation into *E. coli* S17-1/*λpir* (*Chapter 2.7*) and then into *B. pseudomallei* wild-type by conjugation (*Chapter 2.10*). Two sets of primer pairs, JT6185/NA5424 and NA5116/JT6080 (*Chapter 2, Table 2.2, 2.3* and *2.4*), were used for verifying the disruption of *bapC* in tetracycline and sucrose resistant, and chloramphenicol sensitive transconjugants. A fragment of 1.7-kb product was amplified from the middle of *bapA* to *tetA*(C) using genomic DNA of the *bapC* mutant with the primers JT6185/NA5424 (*Figure 3.1.4B, lane 2*), but not using genomic DNA of the wild-type strain (*Figure 3.1.4B, lane 3*) or in the no DNA control reaction (*Figure 3.1.4B, lane 4*). Similarly, a fragment of 1.6-kb was amplified from *tetA*(C) to downstream of *bapC* with primers NA5116/JT6080 using the *bapC* mutant genomic DNA (*Figure 3.1.4B, lane*

5), but not using genomic DNA of the wild-type strain (*Figure 3.1.4B, lane 6*) or in the no DNA control reaction (*Figure 3.1.4B, lane 7*). The PCR products were verified by nucleotide sequencing (data not shown). These PCR results also indicated that the *tetA*(C) gene orientation in this mutant was similar to the *tetA*(C) gene orientation in the K96243*ΔbapA*, but in an opposite direction to the K96243*ΔbapB* strain. The *bapC* double cross-over mutant was thus confirmed and designated K96243*ΔbapC* (*Chapter 2, Table 2.1*).

In addition to mutagenesis of *bapA*, *bapB* and *bapC*, a double *bapB*/*bapC* mutant was generated by double cross-over allelic exchange (*Figure 3.1.5*). The primers JT6177 and JT6074 (*Chapter 2, Table 2.2*) were used to amplify a 448-bp fragment encompassing the 3'end of *bapA* and the 5'end of *bapB*. This upstream fragment, containing additional (5' end) and native *Sph*I (3' end) sites, was ligated into *Sph*I-digested pDM4. Clones were screened and then verified for the presence of this fragment as described above (data not shown). The primers JT6179 and JT6180, containing native (5' end) and additional (3' end) *Sal*I sites, were used to generate a 775-bp downstream fragment containing the 3' end and downstream region of *bapC*. This fragment was subsequently cloned into *Sal*I-digested pDM4 containing the verified upstream fragment. Clones were screened and then verified for fragment insertion as described above (data not shown). The *tetA*(C) gene was subsequently ligated into the central *Bgl*II site in order to generate pDM4::*bapBC*::*tetA*(C) (*Chapter 2, Table 2.1*). This mutant construct was introduced into *E. coli* S17-1/λ*pir* and then into *B. pseudomallei* wild-type by conjugation (*Chapter 2.10*). Two sets of primer pairs, JT6185/NA5424 and NA5116/JT6080 (*Chapter 2, Table 2.2, 2.3* and *2.4*), were used for verifying the disruption of *bapB*/*bapC* in tetracycline and sucrose resistant, and chloramphenicol sensitive transconjugants (*Figure 3.1.6*). A 1.4-kb product was amplified from the middle of *bapA* to *tetA*(C) using genomic DNA of the *bapBC* mutant with the primers JT6185/NA5424 (*Figure 3.1.6, lane 2*), but not using genomic DNA of the wild-type strain (*Figure 3.1.6, lane 3*) or with the no DNA control (*Figure 3.1.6, lane 4*). Similarly, a fragment of 1.6-kb was amplified from *tetA*(C) to region downstream of *bapC* with the primers NA5116/ JT6080 using the *bapBC* mutant genomic DNA (*Figure 3.1.6, lane 5*), but not using genomic DNA of the wild-type strain (*Figure 3.1.6, lane 6*) or with the no DNA control (*Figure 3.1.6, lane 7*). The PCR products were verified by nucleotide sequencing (data not shown). Therefore, the double *bapBC* mutant was confirmed and designated K96243*ΔbapBC* (*Chapter 2, Table 2.1*).

3.2 The *in vitro* growth of the K96243*ΔbapA*, *ΔbapB*, *ΔbapC* and *ΔbapBC* strains was indistinguishable from the wild-type strain

To investigate whether disruption of the target genes had affected the growth of *B. pseudomallei*, the *in vitro* growth rate of the mutants and the wild-type strain was determined in LB broth. There was no significant difference between the growth of any of the mutants and the wild-type strain (*Figure 3.2.1*).

3.3 The K96243*ΔbapA*, *ΔbapB*, *ΔbapC* and *ΔbapBC* strains show reduced growth rate *in vivo* compared to the wild-type strain

To examine the importance of *bapA*, *bapB* and *bapC* for the *in vivo* growth of *B. pseudomallei*, competitive growth assays were conducted in the BALB/c mouse infection model (*Chapter 2.15*). In brief, an equal amount of each of the mutants was mixed with the wild-type strain before intranasal inoculation into mice. The infection was allowed to proceed for 20 h at which time the mice were euthanised and spleens removed and homogenised before plating on LB agar. The competitive index (CI) was defined as the ratio of mutant to wild-type strains as determined by patching recovered bacteria onto LB with or without 25 μg/mL tetracycline. An average CI of less than 0.5 indicates a role for the inactivated gene in growth *in vivo*. The CI of the K96243*ΔbapA* strain was 0.31 ± 0.13, indicating partial attenuation (*Figure 3.3.1*). Similarly, the CI values for the K96243*ΔbapB*, K96243*ΔbapC* and K96243*ΔbapBC* strains were 0.17 ± 0.05, 0.28 ± 0.03 and 0.38 ± 0.15, respectively. These data indicate that these genes play a role in *in vivo* growth of *B. pseudomallei*.

3.4 Virulence trials in the BALB/c mouse infection model

To further examine the role of *bapA*, *bapB* and *bapC* in regards to *B. pseudomallei* pathogenesis, virulence trials were carried out in female BALB/c mice (*Chapter 2.16*). All mice infected with 10^5 CFU of the wild-type *B. pseudomallei* were required to be euthanised within 80 h post infection (p.i.). In contrast, all but one of the seven mice infected with a similar dose of the K96243*ΔbapB* strain survived until the end of the experiment (240 h) (*Figure 3.4.1A*; $P < 0.0001$). Groups infected with the K96243*ΔbapA*, K96243*ΔbapC* and K96243*ΔbapBC* strains showed no difference in the total number of surviving mice ($P > 0.05$), but all showed a significant increase in time to death (*Figure 3.4.1A*; $P < 0.05$). Interestingly, the overall survival of mice infected with the K96243*ΔbapB* strain was significantly different from that of mice infected with the K96243*ΔbapC* or K96243*ΔbapBC* strains (*Figure 3.4.1A*; $P < 0.05$), whereas

there was no significant difference between survival of mice infected with the K96243*ΔbapC* and K96243*ΔbapBC* strains ($P > 0.05$), indicating phenotypic similarity of both mutants as observed in the *in vivo* competitive growth assay (*Figure 3.3.1*). PCR analyses of colonies recovered from the K96243*ΔbapA*-infected mice using the primer pairs JT6376/NA5424 and NA5116/JT6180 (*Figure 3.1.2*) confirmed that the recovered colonies still contained the *tetA*(C) insertion in *bapA* (*Figure 3.4.2A and Figure 3.4.2B*). Moreover, PCR amplification of the *bapA* deletion region in the K96243*ΔbapA* strain using the primer pair JT6185/JT6104 (*Figure 3.1.2*) confirmed the deletion within *bapA* (*Figure 3.4.2C, lane 11*). Therefore, the K96243*ΔbapA* strain was still able to cause disease in the BALB/c mouse model, although at a slower rate than the wild-type strain. Similarly, PCR analyses from output colonies recovered from mice infected with the K96243*ΔbapB* (*Figure 3.4.3*), K96243*ΔbapC* (*Figure 3.4.4*) and K96243*ΔbapBC* (*Figure 3.4.5*) strains using the primer pairs as illustrated in *Figure 3.1.4* and *Figure 3.1.6* confirmed the retention of the *tetA*(C) insertion in these strains.

A similar pattern was seen with the mice infected with 10^7 CFU of the wild-type or the mutant strains (*Figure 3.4.1B*). All mice infected with the wild-type strain at this dose were euthanised within 42 h p.i, whereas groups infected with the K96243*ΔbapA*, *ΔbapB*, *ΔbapC* and *ΔbapBC* strains showed a significant delay in time to death ($P < 0.05$). These data show that while each of the K96243*ΔbapA*, *ΔbapB* and *ΔbapC* strains can still cause disease, they do so less efficiently than the wild-type strain at either a medium (10^5 CFU) or high infectious dose (10^7 CFU). Furthermore, at a dose of 10^5 CFU the K96243*ΔbapB* strain showed significantly reduced lethality; the mutant also showed the lowest *in vivo* growth by competitive growth assay (*Figure 3.3.1*). Taken together, these data suggest that the TTSS3 genes *bapA, bapB* and *bapC* may play a minor role in *B. pseudomallei* virulence and *in vivo* survival.

3.5 Complementation of the *bap* mutant strains using pBHR1

To confirm that the reduced *in vivo* growth and attenuation of the K96243*ΔbapA, ΔbapB* and *ΔbapC* strains was due specifically to inactivation of the *bap* genes, each of the mutants was complemented with the full-length version of the appropriate gene cloned into the *B. pseudomallei* plasmid pBHR1 (Szpirer *et al.*, 2001). Each of the complemented strains was then tested for restoration of *in vivo* growth or virulence by performing competitive growth assays and/or direct virulence trials in the BALB/c mouse infection model.

To generate the complementation constructs, the primers JT7065/JT7066 (*bapA*), JT7171/ JT7172 (*bapB*) and JT7173/JT7174 (*bapC*) (*Chapter 2, Table 2.3*) were used to amplify fragments containing each of the full length wild-type genes from genomic DNA of the wild-type *B. pseudomallei*. KOD DNA polymerase was used for these PCRs (*Appendix 3, Table A3.3*). PCR products were digested with *Eco*RI/*Acl*I and cloned into *Eco*RI/*Acl*I-digested pBHR1, which are located in the *cat* gene of the pBHR1 (*Figure 3.5.1A*). Each of the *bap* genes was cloned with a native ribosomal binding site and are predicted to be transcribed from the *cat* promoter present in the vector. Correct constructs were identified by restriction digest analysis and confirmed by nucleotide sequencing (data not shown). Each of the complementation constructs was then transferred to the appropriate *B. pseudomallei* mutant strain by conjugation from *E. coli* S17-1/λ*pir*. Tetracycline and kanamycin resistant, and chloramphenicol sensitive colonies were analysed for the presence of the complementing plasmid using PCR with the primer pair JT7080/JT7081 (*Chapter 2, Table 2.3*). These primers are specific for the chloramphenicol resistance cassette in pBHR1 and would amplify fragments of 3,400-, 1,000- and 1,300-bp, respectively, from pBHR1 containing *bapA*, *bapB* and *bapC* (*Figure 3.5.1B*). Eleven K96243*ΔbapA* colonies contained the *bapA* complementation plasmid (*Figure 3.5.2, lane 2 to 12*) and the clone in lane 9, designated K96243*ΔbapA*[*bapA*] (*Chapter 2, Table 2.1*), was chosen for further characterisation. Ten K96243*ΔbapB* colonies contained the *bapB* complementation plasmid (*Figure 3.5.3, lane 2 to 11*) and the clone in lane 6, designated K96243*ΔbapB*[*bapB*] (*Chapter 2, Table 2.1*), was chosen for further characterisation. Ten K96243*ΔbapC* mutant colonies contained the *bapC* complementation plasmid (*Figure 3.5.4, lane 2 to 11*) and the clone in lane 6, designated K96243*ΔbapC*[*bapC*] (*Chapter 2, Table 2.1*), was chosen for further characterisation. As a control, the empty plasmid pBHR1 was also transferred into the K96243*ΔbapA*, *ΔbapB* and *ΔbapC* strains, and the wild-type strain by conjugation, and again all analysed colonies contained the empty pBHR1. The clones in lane 4 (*Figure 3.5.5*), 4 and 9 (*Figure 3.5.6*), and 2 (*Figure 3.5.7*) were chosen for further experiments. These strains were designated K96243*ΔbapA*[pBHR1], K96243*ΔbapB*[pBHR1], K96243*ΔbapC*[pBHR1], and K96243[pBHR1] (*Chapter 2, Table 2.1*), respectively.

3.6 *In vivo* growth of the complemented mutant strains

To examine the importance of *bapA*, *bapB* and *bapC* for the *in vivo* growth of *B. pseudomallei*, competitive growth assays were conducted in the BALB/c mouse infection model (*Chapter 2.15*). In brief, an equal amount of each of the mutants was mixed with the wild-type strain before intranasal inoculation into mice. The infection was allowed to proceed for 20 h at which

time the mice were euthanised and spleens removed and homogenised before plating on LB agar. The ratio of mutant to wild-type was determined by patching one hundred recovered colonies onto LB with or without 25 μg/mL tetracycline, and the CI was defined as the ratio of mutant to wild-type bacteria in the output pool divided by the ratio of mutant to wild-type bacteria in the input pool. A CI value of less than 1.0, indicates that the mutant has a reduced ability to survive or replicate *in vivo*, suggesting that inactivation of the gene affects *in vivo* growth of the bacteria. The CI of the K96243*ΔbapA* strain was 0.31 ± 0.13, and, similarly, the CI values for the K96243*ΔbapB*, *ΔbapC* and *ΔbapBC* strains were 0.17 ± 0.05, 0.28 ± 0.03 and 0.38 ± 0.15, respectively (*Figure 3.3.1*). These data indicate that these genes play a minor role in the *in vivo* growth of *B. pseudomallei*.

Of the four mutant strains, the K96243*ΔbapB* strain had shown the lowest CI, suggesting the highest degree of involvement in bacterial growth (*Chapter 3.3*). Thus, the K96243*ΔbapB*[*bapB*] strain was first used in a competitive growth assay with the wild-type strain versus the wild-type strain to determine whether the wild-type *in vivo* growth had been restored. The average CI of the K96243*ΔbapB* strain was 0.26 ± 0.07 (*Figure 3.6.1A*) which was not significantly different from the result obtained previously (0.17 ± 0.05; *Chapter 3.3*) ($P > 0.05$). The average CI of the K96243*ΔbapB*[pBHR1] strain was 0.41 ± 0.08 (*Figure 3.6.1A*), which was not statistically different from the original the K96243*ΔbapB* strain ($P > 0.05$). However, the average CI of the K96243*ΔbapB*[*bapB*] strain was 0.87 ± 0.22 (*Figure 3.6.1A*), indicating at least partial restoration of the wild-type phenotype. There was a significant difference between the CIs of the K96243*ΔbapB* strain and those of the K96243*ΔbapB*[*bapB*] strain ($P = 0.0088$). Although there was no significant difference between the CI of the K96243*ΔbapB*[pBHR1] strain and the K96243*ΔbapB*[*bapB*] strain ($P > 0.05$), these data suggest partial restoration of the wild-type phenotype. For the K96243*ΔbapC* strain, the average CIs of the K96243*ΔbapC*, K96243*ΔbapC*[pBHR1] and K96243*ΔbapC*[*bapC*] strains were 0.45 ± 0.08, 0.12 ± 0.03 and 0.40 ± 0.11, respectively (*Figure 3.6.1B*). Although the K96243*ΔbapC* strain showed no statistical difference from the K96243*ΔbapC*[*bapC*] strain ($P > 0.05$), there was a significant difference when comparing the K96243*ΔbapC*[pBHR1] to the K96243*ΔbapC*[*bapC*] strains ($P < 0.05$), indicating some level of wild-type phenotype restoration. In addition, the K96243*ΔbapC* strain showed a statistically significant difference from the K96243*ΔbapC*[pBHR1] strain which was opposite to what was found in the K96243*ΔbapB* strain. These *in vivo* growth data suggested that there may be some level of plasmid instability.

To determine whether the pBHR1 plasmid constructs used for complementation were stable, the level of plasmid loss was tested during growth *in vitro*. Overnight cultures of the *bap* mutants, the *bap* mutants harbouring pBHR1 and the complemented mutant strains were grown to an $O.D._{600}$ of 0.6. Each of the strains was then inoculated into fresh LB broth without antibiotics and incubated at 37^{o}C for 12 h and 20 h. At each time point, dilutions of the cultures were plated onto LB without antibiotics, and one hundred colonies were patched onto LB, LB containing 25 μg/mL tetracycline, and LB containing 25 μg/mL tetracycline and 1 mg/mL kanamycin. The percentage plasmid retention at each of the two different time points was calculated (*Figure 3.6.2*). For the K96243*ΔbapB*[pBHR1] strain, 64% of cells retained the plasmid after 12 h and 23% after 20 h. However, for the K96243*ΔbapB*[*bapB*] strain, only 9% of cells retained the plasmid after 20 h. The rate of plasmid retention for the K96243*ΔbapC*[*bapC*] and K96243*ΔbapA*[*bapA*] strains was even lower, with no retention of complementation plasmid at 20 h p.i. Therefore, these data suggest that the pBHR1-based plasmids are not stable in the absence of antibiotic selection, and plasmid loss would have negatively affected the *in vivo* competitive growth assays carried out with the K96243*ΔbapB*[*bapB*] and K96243*ΔbapC*[*bapC*] strains. Accordingly, the K96243*ΔbapA*[*bapA*] strain was not tested further. Moreover, low plasmid stability meant that these complemented strains could not be tested in virulence assays as these assays take up to 10 days. Complementation of the mutants with the integrative transposon vector pUC18Tmini-Tn*7* (Choi *et al.*, 2005) was therefore chosen as an alternative option (see *Chapter 3.7*).

3.7 Complementation of the *bap* mutants using the site-specific transposon vector pUC18Tmini-Tn*7*T

Due to the instability of pBHR1 in the absence of selection, the *bapA*, *bapB* and *bapC* genes were individually cloned into the site-specific transposon-containing vector pUC18Tmini-Tn*7*T as an alternative complementation approach (*Figure 3.7.1*). The mini-Tn*7* transposon is known to insert into the *B. pseudomallei* chromosome downstream of one of the three *glmS* genes (Choi & Kim, 2009; Choi *et al.*, 2006; Choi *et al.*, 2005; Choi *et al.*, 2008). The primer pairs JT6102/ JT6104 and JT6105/JT6106 (*Chapter 2*, *Table 2.3*) were used to amplify the full length *bapA* or a fragment containing the entire *bapA*, *bapB* and *bapC* genes, respectively from the *B. pseudomallei* wild-type strain K96243. To optimise amplification of these long gene fragments, DMSO and betaine were added to the PCR reactions (Frey *et al.*, 2008; Henke *et al.*, 1997; Jensen *et al.*, 2010). The optimum concentrations of DMSO and betaine were determined as 5% (v/v) and 2.5 M, respectively (data not shown). The amplified DNA fragments were then

ligated into a modified version of pUC18Tmini-Tn*7*T designated pUC18Tmini-Tn*7*T::P_{glmS2} (*Chapter 2, Table 2.1*). This modified pUC18Tmini-Tn*7*T contains a strong *B. pseudomallei* promoter, P_{glmS2}, upstream of the multiple cloning site (MCS). Positive transformants were identified by PCR using the primer pair JT6071/JT6072 (*Chapter 2, Table 2.3*) which should amplify a 634-bp fragment from the 5' end of *bapA*. A positive clone containing the *bapA* gene cloned in pUC18Tmini-Tn*7*T::P_{glmS2} was selected (*Figure 3.7.2, lane 17*), and the nucleotide sequence of the insert determined (data not shown). The nucleotide sequence of the fragment was identical to the wild-type *bapA* sequence. Similarly, the primer pair JT6077/JT6078 (*Chapter 2, Table 2.3*), amplifying a 478-bp fragment of *bapC*, was used to screen for recombinant plasmids containing the entire *bapA*, *bapB* and *bapC* fragment. A positive clone containing this DNA fragment was identified (*Figure 3.7.3, lane 20*), and the insert was confirmed by nucleotide sequencing (data not shown). For selection in *B. pseudomallei*, the chloramphenicol acetyl transferase (*cat*) gene derived from the plasmid pDM4 was inserted into each of the complementation constructs. The *cat* gene was amplified using the primers JT6100 and JT6101 (*Chapter 2, Table 2.3*) and ligated into *Kpn*I-digested pUC18Tmini-Tn*7*T::P_{glmS2}::*bapA* and pUC18Tmini-Tn*7*T::P_{glmS2}::*bapABC* (*Chapter 2, Table 2.1*). Colonies generated from this transformation were screened by patching onto LB agar containing 20 μg/mL chloramphenicol to verify their antibiotic resistance profiles. Chloramphenicol resistant colonies were confirmed as containing the chloramphenicol resistance gene by PCR using the primers JT6100/6101 (*Chapter 2, Table 2.3*). Plasmids which amplified the correct PCR product were selected (*Figure 3.7.4A and Figure 3.7.4B*) and then transferred into *E. coli* SM10/λ*pir*. The, *E. coli* SM10/λ*pir* strain and the *E. coli* SM10/λ*pir* containing the helper plasmid pTNS3 (*Chapter 2, Table 2.1*) were added together in a three way conjugation (*Chapter 2.10*). Each of the conjugation mixtures was spotted on LB agar and incubated at 30^{o}C for 2 days. The bacteria were then resuspended in 1 mL of sterile PBS, pH 7.4 and plated on LB agar containing 25 μg/mL tetracycline and 50 μg/mL chloramphenicol. However, in the first attempt, there was some bacterial growth on one of the negative control plates, so the minimum bactericidal concentration (MBC) for each antibiotic was determined using the broth microdilution technique (*Chapter 2.11*). The MBC for chloramphenicol against the wild-type *B. pseudomallei* was determined as 50 μg/mL; hence, the chloramphenicol selection was increased from 40 to 100 μg/mL. The conjugations were repeated, and transconjugants were selected on LB agar containing 25 μg/mL tetracycline and 100 μg/mL chloramphenicol. All transconjugants were patched to confirm their antibiotic resistance profile, and colonies with the correct profile. To verify the presence of the *cat* gene and confirm the integration of the mini-Tn*7* into the genome

of *B. pseudomallei*, transconjugants were first analysed by PCR using the primers JT6100/JT6101 (*Chapter 2, Table 2.3*). All of the potential K96243*ΔbapA-bapA* (*Chapter 2, Table 2.1*) transconjugants (*Figure 3.7.6, lane 2 to 12*) amplified PCR products identical to the positive control (*Figure 3.7.6, lane 15*), confirming the presence of the *cat* gene in *B. pseudomallei*. The miniTn*7* vector can insert downstream of any of the *glmS* genes, but we have observed that the most common integration site is downstream of *glmS2* (Alwis *et al.* unpublished data). Therefore, we screened for insertion downstream of *glmS2* using two sets of primer pairs PA6211/PA6212 and JT6185/PA6212 (*Chapter 2, Table 2.3*; *Figure 3.7.5*). However, PCR products from all transconjugants were identical to those amplified from the wild-type strain (*Figure 3.7.7*), indicating that there was no insertion downstream of *glmS2*. PCR using the primer pair JT6185/PA6212 (*Figure 3.7.5*), amplifying an approximately 2,400-bp fragment, was additionally performed, and again all transconjugants (*Figure 3.7.8, lane 2 to 12*) showed a similar result to the K96243*ΔbapA* strain (*Figure 3.7.8, lane 13*), confirming that there was no transposon integration after *glmS2*. The minor products of approximately 1,300- and 1,800-bp observed in both the potential K96243*ΔbapA-bapA* transoconjugants and the K96243*ΔbapA* strain were likely the result of non-specific amplification rather than contamination as there was no PCR product amplification in the *E. coli* SM10/λ*pir* strain harbouring the modified mini-Tn*7* construct (*Figure 3.7.8, lane 14*) or the no DNA control reaction (*Figure 3.7.8, lane 15*).

As *B. pseudomallei* contains three paralogous copies of *glmS*, names *glmS1*, *glmS2* and *glmS3*, the putative K96243*ΔbapA-bapA* transconjugants were analysed using the oligonucleotides PA6271/PA6272 and PA6273/PA6274 (*Chapter 2, Table 2.3; Figure 3.7.5A*) to identify if the mini-Tn*7* insertion had occurred downstream of *glmS1* (*Figure 3.7.9*) or *glmS3* (*Figure 3.7.10*), respectively. However, all of the transconjugants amplified PCR products identical to the wild-type and the K96243*ΔbapA* strain, indicating that there was no insertion after either *glmS1* or *glmS3*. To confirm integration in the bacterial genome, Southern blotting (*Chapter 2.26*) was used to assess the putative K96243*ΔbapA-bapA* transconjugants using a DIG-labelled probe specific for the deletion within *bapA*. The restriction endonuclease *Acl*I was used to digest genomic DNA from the potential transconjugants. If transposon integration into the genome had occurred, a single hybridising fragment larger than approximately 3.3 Kbp should be detected (*Figure 3.7.11A*). Alternatively, if free plasmid was present a single band of 4.5 Kbp should be observed (the size of the hybridising *Acl*I fragment in the pUC18Tmini-Tn*7*T::P_{glmS2}::*bapA* construct). However, all six tested clones demonstrated two hybridising bands of approximately

3,300- and 8,000-bp (*Figure 3.7.11B, lane 1 to 6*), which were absent in the K96243*ΔbapA* strain (*Figure 3.7.11B, lane 7*). These data clearly indicate that the transconjugants contained the complementing *bapA* fragment but the fragment sizes did not correlate precisely with either free plasmid or integrated transposon. Based on the sizes of the hybridising fragments, it is possible that the larger fragment corresponds to integrated transposon and the smaller fragment to either, a second site of genomic insertion or a free plasmid with a deletion in the hybridising *Acl*I fragment. However, there was no evidence for mini-Tn*7* insertion after *glmS1*, *glmS2* or *glmS3*, clearly showing that no integration of the transposon had taken place of at these sites. Taken together, these data suggested insertion of the complemented constructs into the genome but at sites other than those *glmS* downstream regions. Complementation of the K96243*ΔbapB*, K96243*ΔbapC* or K96243*ΔbapBC* strain using a mini-Tn*7* construct was also attempted. Based on the bioinformatic data (*Chapter 1, Figure 1.3.3*) and the reverse transcription PCR (data not shown), *bapA*, *bapB* and *bapC* are co-transcribed. Thus, it was decided to complement each of the mutant strains with the pUC18Tmini-Tn*7*T::*cat*::P_{glmS2}::*bapABC* construct (*Chapter 2, Table 2.1*) by conjugation as described earlier. All of the potential K96243*ΔbapB-bapABC*, K96243*ΔbapC-bapABC* and K96243*ΔbapBC-bapABC* transconjugants with the correct antibiotic profile were analysed by PCR using primers specific for the proposed regions of the mini-Tn*7* insertion following *glmS1*, *glmS2* and *glmS3*, previously for the putative K96243*ΔbapA-bapA* transconjugants. However, again all transconjugants amplified PCR fragments identical to the wild-type strain (data not shown), indicating that there was no insertion of the transposon after *glmS1*, *glmS2* or *glmS3* gene. However, PCR using the primer pair MC6229/MC6230 (*Chapter 2, Table 2.3*), which amplifies a section surrounding the pUC18Tmini-Tn*7*T *oriT*, amplified the correct sized product (*Figure 3.7.12*), indicating that the pUC18Tmini-Tn*7*T constructs were present in the *B. pseudomallei* recipient but possibly as non-integrated plasmids since *oriT* is generally not part of the transposon integration. Therefore, it was decided not to pursue any further attempts at complementation but rather to construct independent *bapA*, *bapB*, *bapC* and *bapBC* mutant strains and test their phenotypes *in vivo* (see *Chapter 3.8*).

3.8 Generation of independently derived *bap* mutant strains

Since complementation using either the replicating plasmid pBHR1 or the transposon vector pUC18Tmini-Tn*7*T was unsuccessful, it was decided to generate independently derived mutants and compare the phenotypes with the original mutants. Accordingly, mutants of *B. pseudomallei* were generated as described previously (*Chapter 3.1*). PCR analysis confirmed the independent

construction of double cross-over mutants (*Chapter 2, Table 2.2*). The primer pairs JT6376/ NA5424 and NA5116/JT6180 (*Figure 3.1.2A*) were used to verify the *tetA*(C) insertion within *bapA* (*Figure 3.8.1*). The primer pairs JT6185/NA5116 and NA5424/JT6078 (*Figure 3.1.4A*) were used to confirm the *tetA*(C) insertion within *bapB* (*Figure 3.8.2, left panel*) and the *tetA*(C) insertion within *bapC* was confirmed using the primer pairs, JT6185/NA5424 and NA5116/ JT6080 (*Figure 3.1.4B*; *Figure 3.8.2, right panel*). The independently derived K96243*ΔbapA*, K96243*ΔbapB* and K96243*ΔbapC* strains were designated K96243*ΔbapA*_2, K96243*ΔbapB*_2 and K96243*ΔbapC*_2 strains, respectively (*Chapter 2, Table 2.1*). The *in vivo* phenotypes of each of these mutants were then analysed using the BALB/c mouse infection model as described previously (*Chapter 3.4*).

All but one of the seven mice infected with 10^5 CFU of the wild-type strain were euthanised within 81 h p.i., which was consistent with the previous result (*Chapter 3.4*). Mice infected with 10^5 CFU of either the original K96243*ΔbapA* or K96243*ΔbapA*_2 strain showed a significant increase in time to death compared to the wild-type (*Figure 3.8.3A*; $P = 0.0011$). When comparing the survival of mice infected with the original K96243*ΔbapA* strain to mice infected with the K96243*ΔbapA*_2 strain, there was no significant difference ($P > 0.05$). PCR analyses from output colonies recovered from mice infected with either mutant using the primer pairs, as described earlier, revealed the retention of the *tetA*(C) insertion in these strains (data not shown). Therefore, these data strongly suggest that BapA plays a role in *B. pseudomallei* virulence but is not essential for virulence. Complementation is required to unequivocally confirm this.

In contrast, mice infected with 10^5 CFU of the K96243*ΔbapB* strain or K96243*ΔbapB*_2 strain exhibited no significant difference in survival time compared to the survival time of the wild-type infected mice (*Figure 3.8.3B*; $P > 0.05$). This result was different from the result obtained in the first animal trial with the K96243*ΔbapB* strain (*Chapter 3.4*). Colonies recovered from infected mice were analysed by PCR to determine whether there was any reversion of either mutant during the time course of the experiments. Two sets of primer pairs JT6185/NA5116 and NA5424/JT6078 (*Chapter 2, Table 2.2 and 2.3*) were used for PCR verification of the double cross-over mutagenesis, as described in *Chapter 3.1*, in the K96243*ΔbapB* and K96243*ΔbapB*_2 strains. All recovered colonies from mice infected with the K96243*ΔbapB*_2 (*Figure 3.8.5A*) or K96243*ΔbapB* (*Figure 3.8.5B*) still contained the *bapB* mutation since 1.4-kb products were amplified using the primers JT6185/NA5116. Similarly, 977-bp produts were amplified with

primers NA5424/JT6078 from colonies recovered from mice infected with the K96243*ΔbapB*_2 (*Figure 3.8.6A*) or K96243*ΔbapB* (*Figure 3.8.6B*) strain.

Similar to the data obtained from the K96243*ΔbapB* strain, the time to death of mice infected with 10^5 CFU of the K96243*ΔbapC* strain or K96243*ΔbapC*_2 strain exhibited no significant difference from that of mice infected with the wild-type (*Figure 3.8.3C*; $P > 0.05$). PCR analyses of colonies recovered from infected mice using the primer pairs JT6185/NA5424 (*Figure 3.8.7*) and NA5116/JT6080 (*Figure 3.8.8*) confirmed that these output colonies remained genetically identical to the original K96243*ΔbapC* strain.

A similar pattern was observed with the mice infected with 10^7 CFU of the wild-type or mutant strains (*Figure 3.8.4*). Although two mice infected with the wild-type showed a delay in the time to death, the median survival of wild-type infected mice was similar to the data obtained from the previous trials (see *Chapter 3.4*). Mice infected with either the original K96243*ΔbapA* or the K96243*ΔbapA*_2 strain showed a delay in the time to death compared to mice infected the wild-type (*Figure 3.8.4A*; $P = 0.0010$), confirming the partial attenuation observed in these strains was likely due to inactivation of *bapA* or downstream gene. The time to death of mice infected with the original K96243*ΔbapB* or the K96243*ΔbapB*_2, nonetheless, exhibited no difference compared to mice infected with the wild-type strain (*Figure 3.8.4B*; $P > 0.05$). Groups of mice infected with the original K96243*ΔbapC*, the K96243*ΔbapC*_2 or the wild-type strain showed no significant difference in time to death (*Figure 3.8.4C*; $P > 0.05$). Taken together, these data indicate that *bapA* plays a role in the virulence of *B. pseudomallei*. However, the virulence trials carried out with the K96243*ΔbapB* and K96243*ΔbapB*_2 strains and the K96243*ΔbapC* and K96243*ΔbapC*_2 strains indicate that BapB and BapC do not play a clear role in virulence. These data were not in accordance with the original virulence trials on the K96243*ΔbapB* and K96243*ΔbapC* strains (*Chapter 3.4*). However, the PCR amplification of the strains from these second virulence trials confirmed that all the mutants were genetically correct. These data suggest that BapB and BapC are unnecessary for bacterial virulence.

3.9 Discussion

The TTSS3 (*bsa*TTSS) of *B. pseudomallei* is known to be required for full virulence of the bacterium, but only a small number of effectors have been characterised in any detail and shown to play a role in bacterial pathogenesis. In this chapter, the genes *bapA*, *bapB* and *bapC*,

encoding putative effectors of the TTSS3, were inactivated by insertional mutagenesis using a double cross-over allelic exchange approach and characterised for their function with regard to bacterial *in vivo* growth and virulence. By employing a BALB/c mouse model of acute *B. pseudomallei* infection, it was observed that two independently-derived *bapA* mutants showed reduced virulence as mice infected with these strains showed a slightly increased time to death. Several attempts to complement the *bapA* mutant strain, using two different approaches, were unsuccessful, but the similar attenuation of both independently derived *bapA* mutants strongly suggests that BapA plays a minor role in virulence. However, given that the last four bp of the *bapA* gene overlap with the first four bp of the *bapB* gene, it is possible that these genes may be translationally coupled and that inactivation of *bapA* may have polar effects resulting in altered production of BapB and/or BapC. Therefore, to confirm the importance of BapA in virulence the absence of downstream effects on BapB and BapC should be confirmed.

In contrast to BapA, BapB and BapC appear to play a minor role in *B. pseudomallei* growth *in vivo*, but their role in bacterial virulence remains inconclusive. The original K96243*ΔbapB* and *ΔbapC* strains exhibited different levels of attenuation in different virulence trials. In addition, the independently derived K96243*ΔbapB*_2 and *ΔbapC*_2 strains showed no attenuation. It is unclear why the original and independently derived mutant strains exhibited different attenuation levels. Two possible explanations for this are that additional mutations occurred outside the regions subjected to mutagenesis and/or different susceptibility to *B. pseudomallei* infection of mice in each of the virulence trials. The first virulence trials displayed a clear role for BapA, BapB and BapC in bacterial virulence when either medium (10^5 CFU) or high (10^7 CFU) infectious doses were used. The independently derived K96243*ΔbapB*_2 and *ΔbapC*_2 strains showed no attenuation but still showed reduced *in vivo* competitive growth. This suggests that the different levels of attenuation observed between trials may have been due to different susceptibility of the BALB/c mice used. Alternatively, it is possible that the mutant strains contained different secondary mutations that affected their virulence phenotypes. The presence of secondary mutations should be assessed by whole genome sequencing in future work.

Thus, in this study, the K96243*ΔbapA*, K96243*ΔbapB* and K96243*ΔbapC* strains showed an involvement in the *in vivo* growth of *B. pseudomallei*, and only the K96243*ΔbapA* showed a minor role in bacterial virulence. The BapA attenuation supports the notion that susceptibility to *B. pseudomallei* infection is different between different route of infections (Liu *et al.*, 2002; Tan *et al.*, 2008; Titball *et al.*, 2008)

Several attempts were made to confirm that the altered virulence of the mutants was specifically due to inactivation of the specific *bap* genes; complementation was attempted using two different approaches. Although each of the plasmid-based complementation constructs was successfully generated, these complementation constructs were rapidly lost in the absence of antibiotic selection. Each of the mutants carrying an introduced intact gene was tested for *in vivo* growth in the BALB/c mouse model, and the K96243*ΔbapB*[*bapB*] and *ΔbapC*[*bapC*] strains showed some restoration of *in vivo* growth phenotype. However, the virulence of the strains could not be tested properly due to the high rate of plasmid loss. Previous successful complementation using this plasmid (D'Cruze *et al.*, 2011) has been restricted to *in vitro* studies, thus, allowing the maintenance of antibiotic selection. Complementation using the transposon integration vector pUC18Tmini-Tn*7*T was then attempted in order to overcome the instability of the pBHR1 constructs. However, despite being able to construct the complementation constructs within pUC18Tmini-Tn*7*T, the modified transposons did not integrate downstream of any of the three *B. pseudomallei glmS* genes as expected. Therefore, these studies were not pursued further.

BapB shares 36.84% identity to the acyl carrier protein AcpP from *Saccharopolyspora erythraea* (formerly known as *Streptomyces erythraeus*), a bacterium that produces erythromycin. Acp is an enzyme essential for transferring an acyl molecule during fatty acid biosynthesis (Byers & Gong, 2007; De Lay & Cronan, 2007). As fatty acids are essential components of lipopolysaccharide in Gram-negative bacteria, there may be an association of Acp with bacterial growth and membrane integrity. Thus, inactivation of Acp may affect growth and virulence of the bacteria. This could explain an association of *bapB* with the growth *in vivo*, and possibly virulence, of *B. pseudomallei*. In addition, BapB shares 33% identity to the TTSS acyl carrier protein IacP of *Salmonella enterica* serovar Typhimurium. IacP, encoded by *Salmonella* Pathogenicity Island 1 (SPI1), plays a role in bacterial virulence at least in part by modifying host actin for facilitating bacterial invasion during infection. Mice infected with the *iacP* mutant showed a delay in time to death, indicating a role of *iacP* in *S. enterica* serovar Typhimurium virulence (Kim *et al.*, 2011) and perhaps a role of the TTSS acyl carrier proteins in bacterial virulence.

BapC shares 42% identity to the *Salmonella typhi* invasion protein IagB and both contain a lytic transglycosylase (LT) domain. IagB has been experimentally shown to have peptidoglycanase activity through zymogram analyses, but is not required for virulence in *S. typhi* (Zahrl *et al.*, 2005). Specialised lytic transglycosylases (LTs) are known to have roles in promoting the

assembly of the needle-like apparatus of TTSS and the insertion through the bacterial peptidoglycan layer (Blackburn & Clarke, 2001; Yu *et al.*, 2010b). However, the specialised bacterial LTs are sometimes redundant; thus, inactivation of a single LT is unlikely to affect bacterial virulence.

Warawa and Woods (2005) reported an important role for the TTSS3 in the virulence of *B. pseudomallei*. They assessed several putative effector genes, including *bopA*, *bopE*, *bapA* and *bapC*, by generating deletion mutants and then conducting virulence trials using a Syrian golden hamster model. The hamsters were infected intraperitoneally, the infection was allowed to continue for 2 days, and the LD_{50} was then calculated. They found that none of the tested genes was required for bacterial virulence. However, Stevens *et al.* (2004) demonstrated an association of *bopA* with *B. pseudomallei* virulence using the BALB/c mouse model. Our previous study (Cullinane *et al.*, unpublished data) also supported the result of Stevens *et al.* (2004) that *bopA* can contribute to *B. pseudomallei* virulence in the BALB/c acute model. While there were some differences between the studies of Stevens *et al.* (2004) and Cullinane *et al.* (unpublished data), including the mutagenesis method, strains and infectious doses, the mutants from both studies exhibited similar degrees of attenuation. Therefore, there is precedence for different virulence levels between the Syrian golden hamster and BALB/c mouse melioidosis models. In addition, the outcome would clearly be affected by the route of infection. Intraperitoneal injection of the *bapA* mutant strain, as used by Warawa and Woods (2005), would bypass any interactions between the bacteria and the host mucosal surface, whereas the intranasal inoculation route used in this study does not. Thus, in this study, the two independently derived K96243*ΔbapA* strains showed reduced virulence in the BALB/c mouse model, supporting the notion that susceptibility to bacterial infection in each animal model and route of infection is different (Liu *et al.*, 2002; Tan *et al.*, 2008; Titball *et al.*, 2008). However, without complementation the possibility of secondary mutations in these *ΔbapA* strains cannot be entirely ruled out.

3.10 Conclusions

In this chapter, the *B. pseudomallei* genes *bapA*, *bapB* and *bapC* predicted to encode TTSS3 effector proteins were inactivated, and their roles in virulence and growth *in vivo* were assessed. Double cross-over allelic exchange was employed to generate mutants in each gene, and the mutants were then analysed by competitive growth assays and virulence trials in the BALB/c mouse infection model. In initial trials, all mutants showed an *in vivo* growth reduction and attenuation of virulence, indicating an involvement of the genes in both functions. Attempts were

made to complement each of the mutants; however, neither complementation using constructs in the replicating plasmid pBHR1 nor the transposon integration vector pUC18Tmini-Tn*7*T was successful. The pBHR1 constructs were unstable and were lost rapidly from the cells in the absence of antibiotic selection, while the mini-Tn*7* constructs did not integrate into the genome at the expected sites. Thus, independently derived mutants were generated and the virulence trials repeated. Both the K96243*ΔbapA* and *ΔbapA*_2 strains showed significant attenuation, strongly suggesting an involvement of BapA in bacterial virulence. However, both K96243*ΔbapB*_2 and K96243*ΔbapC*_2 strains behaved differently from the original mutants, suggesting the presence of other mutations in these mutants or variation in bacterial susceptibility of the BALB/c mice in the different virulence trials. Further experiments should be conducted in order to prove these hypotheses. Sequencing and analysis of the genomes of the original mutant compared to the independent-derived mutant strains could help to identify if there was any difference in the genotypes of the bacterial strains which may contribute to the attenuation of bacterial virulence. Regenerating independent-derived K96243*ΔbapB* and K96243*ΔbapC* strains and then conducting the virulence trial in comparison to the original and the second independent-derived mutant strains could additionally test the hypothesis.

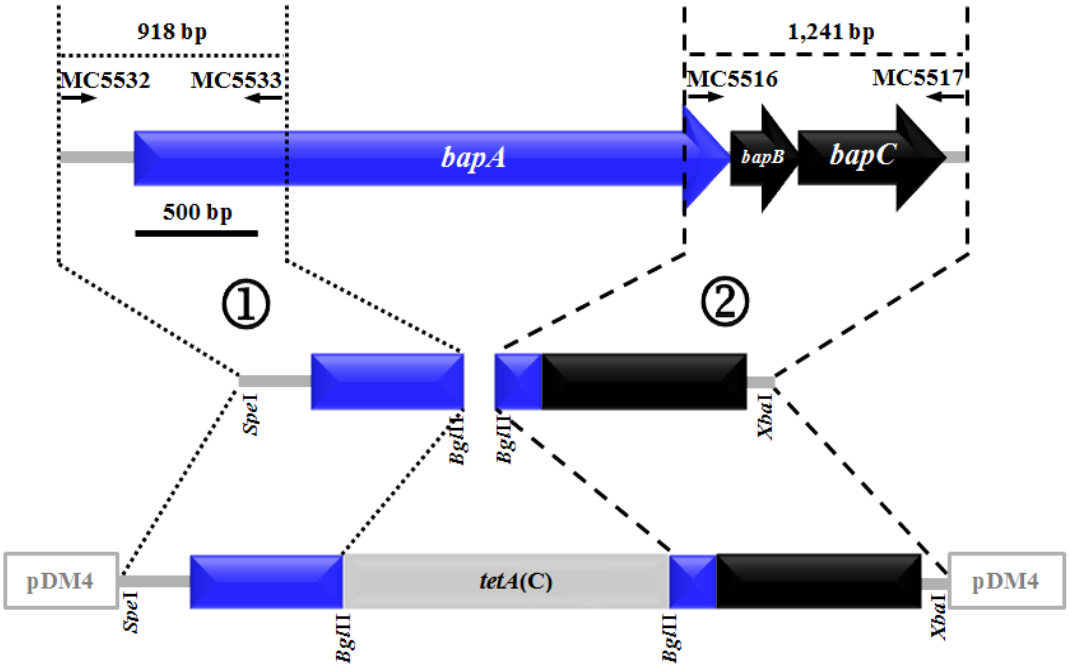

Figure 3.1.1 Generation of the *bapA* double-crossover mutagenesis construct in the suicide vector pDM4. The mutagenesis construct pDM4::*bapA*::*tetA*(C) was constructed by amplifying the upstream fragment (labelled ①) of *bapA* using the primer pair MC5532, containing a *Spe*I site, and MC5533, containing a *Bgl*II site. The downstream fragment encompassing the 3' region of *bapA* and the entire *bapB* and *bapC* (labelled ②) was amplified using the primer pair MC5516, containing a *Bgl*II site, and MC5533, containing an *Xba*I site. Both fragments were cloned into pDM4, and *tetA*(C) was then inserted at the central *Bgl*II site. The mutated *bapA* gene is highlighted in blue. Arrows indicate the orientation of the genes and primers. Arrows designating oligonucleotides are not shown to scale.

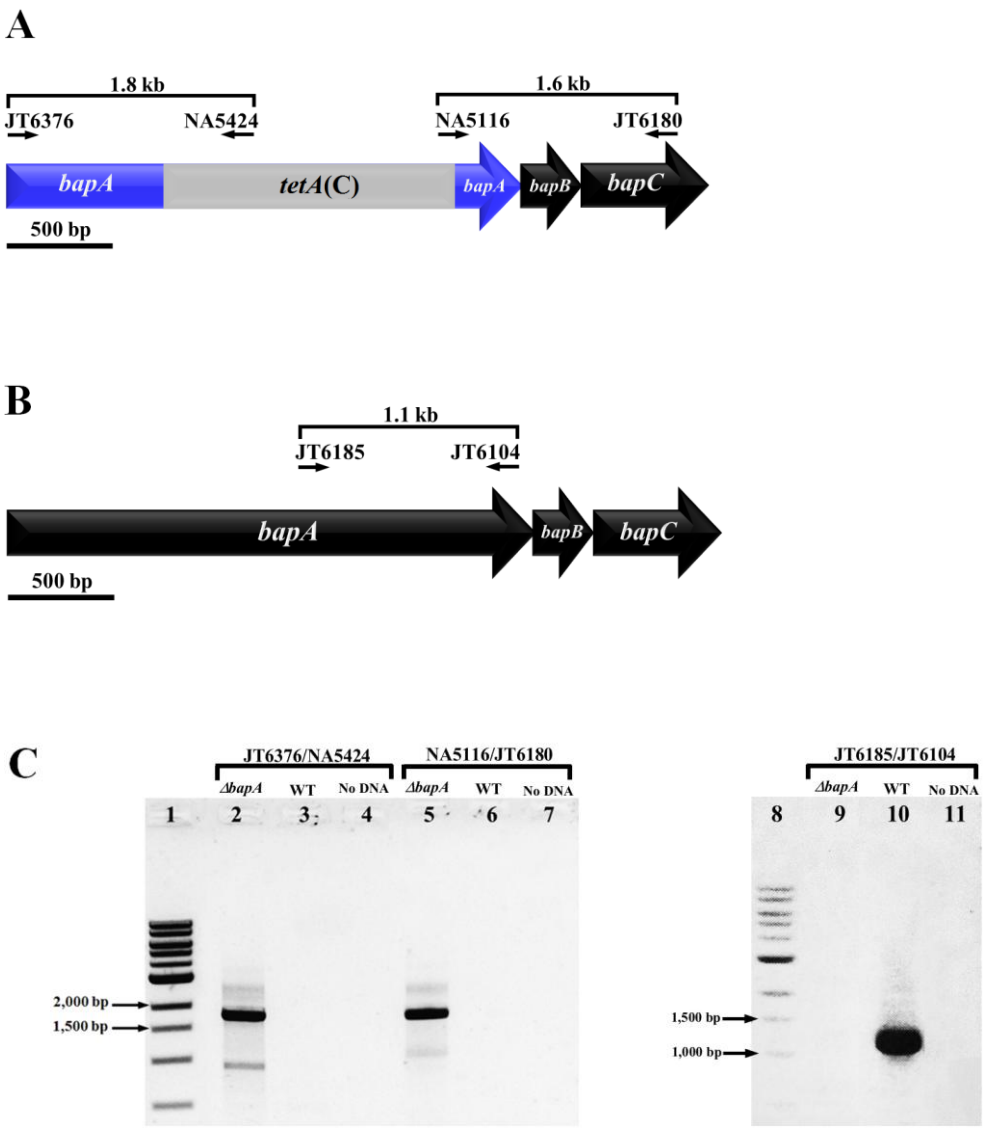

Figure 3.1.2 Genetic organisation of the *bapA*, *bapB* and *bapC* region in the K96243*ΔbapA* (A) and wild-type (B) strains, and PCR analysis of the K96243*ΔbapA* strain (C). Panel A; The position of the *tetA*(C) insertion is shown in *bapA* and the *tetA*(C)-specific primers (NA5424 and NA5116) and *bapA*-specific (JT6376) and *bapC*-specific (JT6180) primers are shown above the genes together with the predicted sizes of PCR products. Panel B; Arrows show the position and length of the genes *bapA*, *bapB* and *bapC*, and the *bapA*-specific primers JT6185 and JT6104 together with the predicted size of the PCR product shown above the gene. Panel C; Gel electrophoresis of PCR products amplified using either K96243*ΔbapA* genomic DNA, wild-type genomic DNA or no DNA as template. Two primer pairs JT6376/NA5424 and NA5116/JT6180 (right panel) were used to verify the insertion of *tetA*(C) within *bapA*, and the primers JT6185 and JT6104 (left panel) were used to confirm the deletion within *bapA*. The gel image has been cut between lanes 9 and 10 to remove unnecessary lanes. Lane 1 and 8, DNA size markers; lane 2, 5 and 9, PCR products generated using three primer pairs as indicated and the K96243*ΔbapA* genomic DNA; lane 3, 6 and 10, PCR amplification generated using three primer pairs as indicated and the wild-type genomic DNA; lane 4, 7 and 11, no DNA controls. The mutated *bapA* gene is highlighted in blue. Arrows indicate the orientation of the genes and primers. Arrows designating oligonucleotides are not shown to scale. Different features are indicated: *ΔbapA*, the K96243*ΔbapA* strain; WT, the wild-type strain.

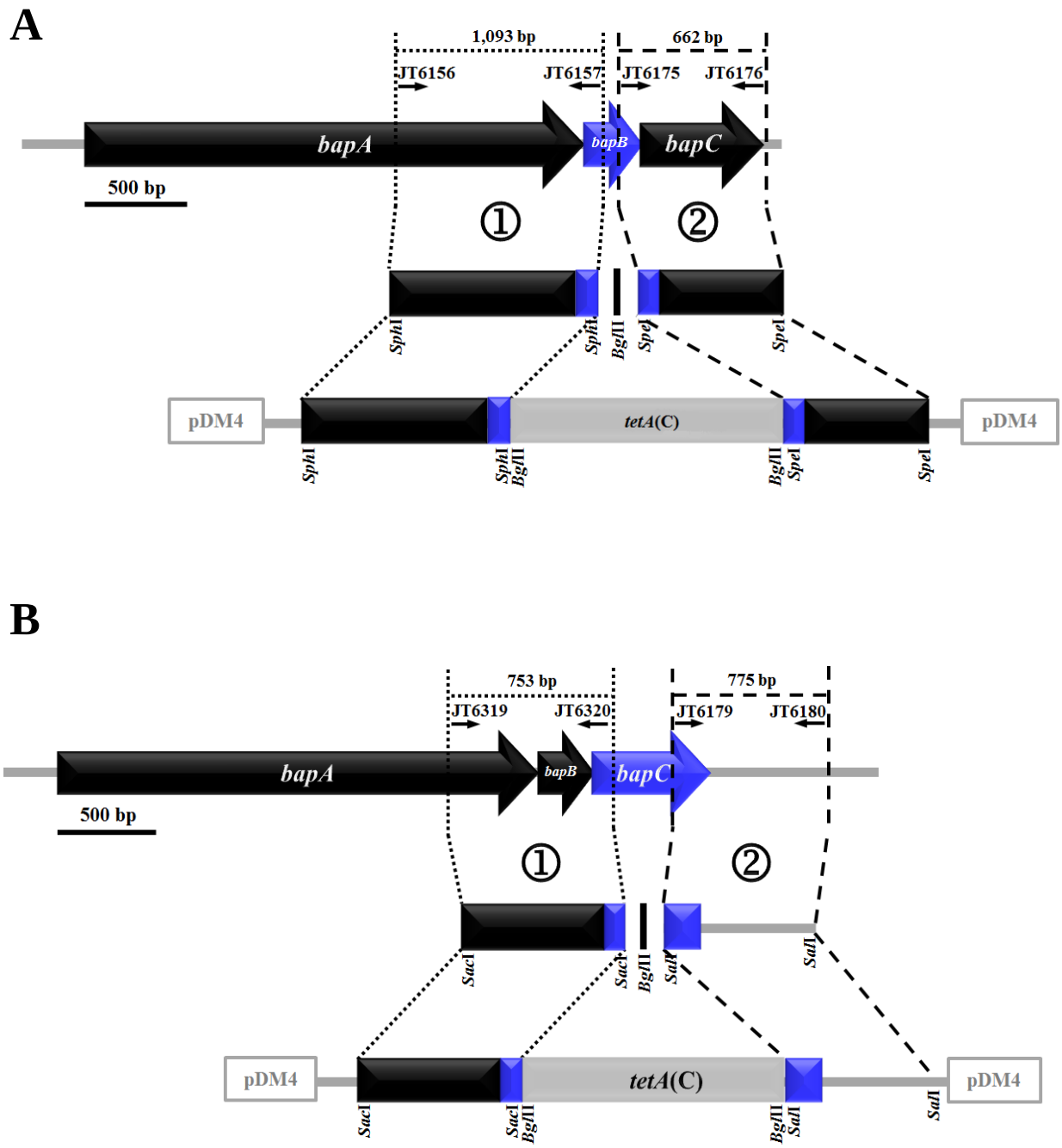

Figure 3.1.3 Generation of the *bapB* and *bapC* double-crossover mutagenesis constructs in the suicide vector pDM4. (A) The mutagenesis construct pDM4::*bapB*::*tetA*(C) was constructed by amplifying the upstream fragment (labelled ①) from the middle of *bapA* to the 5' region of *bapB* using the primer pair JT6156 and JT6157, both containing native *Sph*I sites. The downstream fragment encompassing the 3' region of *bapB* and the entire *bapC* (labelled ②) was amplified using the primer pair JT6175 and JT6176, both containing *Spe*I sites. (B) The mutagenesis construct pDM4::*bapC*::*tetA*(C) was constructed by amplifying the upstream fragment (labelled ①) from the 3' region of *bapA* encompassing the entire *bapB* and the 5' region of *bapC* using the primer pair JT6319 and JT6320, both containing *Sac*I sites. The downstream fragment (labelled ②) was amplified using the primer pair JT6179 and JT6180, containing native (5' end) and additional (3' end) *Sal*I site. Upstream and downstream fragments of each of the constructs were cloned into pDM4, and *tetA*(C) was then inserted at the central *Bgl*II site. Mutated genes are highlighted in blue. Arrows indicate the orientation of the genes and primers. Arrows designating oligonucleotides are not shown to scale.

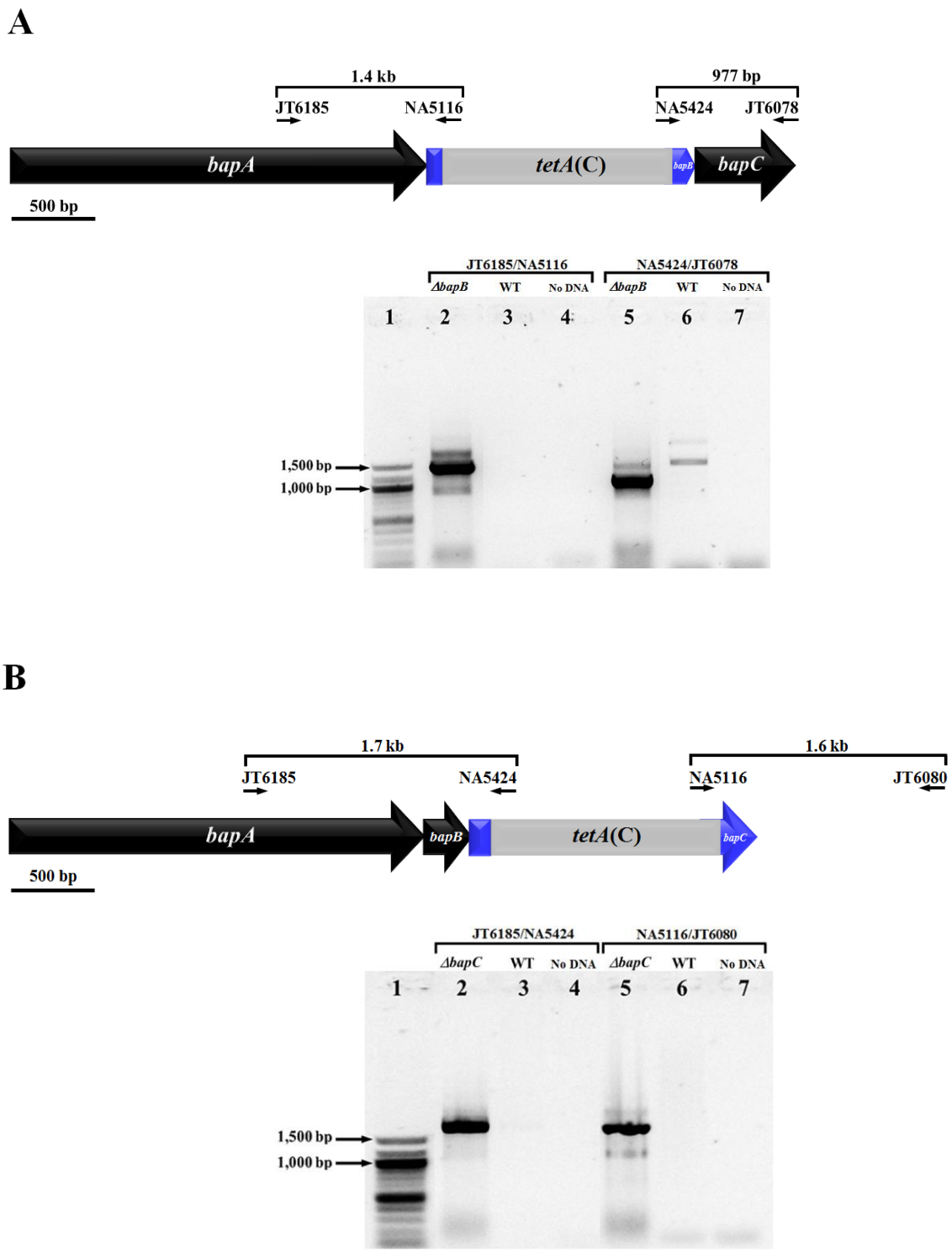

Figure 3.1.4 Genetic organisation of the *bapA*, *bapB* and *bapC* region in the K96243*ΔbapB* (A) and K96243*ΔbapC* (B) strains. The position of the *tetA*(C) insertion is shown and the *tetA*(C)-specific (NA5116 and NA5424), *bapA*-specific (JT6185), *bapC*-specific (JT6078) and *bapC* downstream-specific (JT6080) primers are shown above the genes together with the predicted sizes of PCR products. Gel electrophoresis of PCR products amplified using either K96243*ΔbapB*, K96243*ΔbapC* genomic DNA, wild-type genomic DNA or no DNA template. Lane 1, DNA size markers; lane 2 and 5, PCR products generated using the primer pairs as indicated and genomic DNA of both mutant strains; lane 3 and 6, PCR amplification generated using the primer pairs as indicated and the wild-type genomic DNA; lane 4 and 7, no DNA controls. Mutated genes are highlighted in blue. Arrows indicate the orientation of the genes and primers. Arrows designating oligonucleotides are not shown to scale. *ΔbapB* denotes the K96243*ΔbapB* strain; *ΔbapC* denotes the K96243*ΔbapC* strain and WT denotes the wild-type strain.

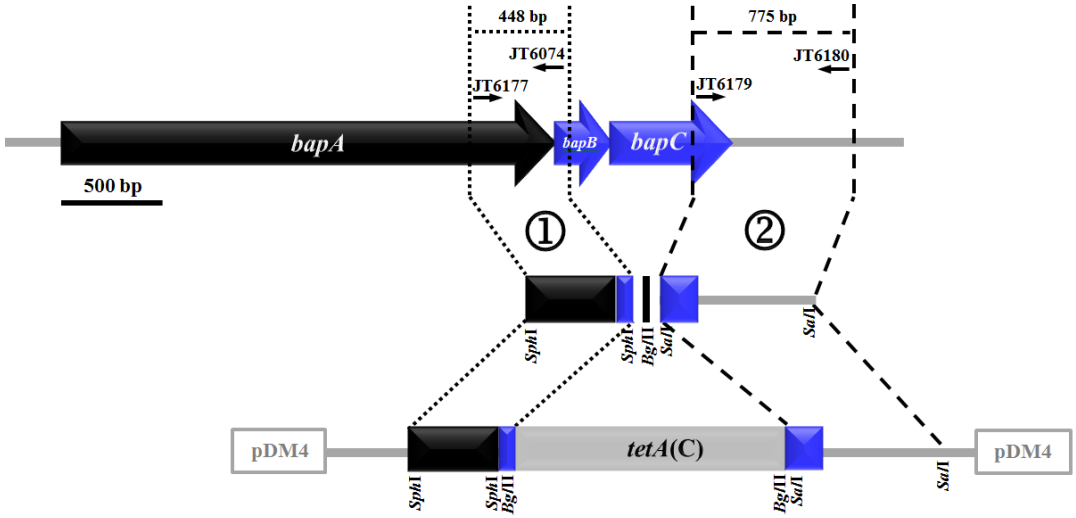

Figure 3.1.5 Generation of the double *bapBC* mutagenesis construct in the suicide vector pDM4. The mutagenesis construct pDM4::*bapBC*::*tetA*(C) was generated by amplifying the upstream fragment (labelled ①) from the middle of *bapA* to the 5' region of *bapB* using the primer pair JT6177 and JT6074, containing additional (5' end) and native (3' end) *Sph*I site. The downstream fragment (labelled ②) was amplified using the primer pair JT6179 and JT6180, containing native (5' end) and additional (3' end) *Sal*I site. Upstream and downstream fragments were cloned into pDM4, and *tetA*(C) was then inserted at the central *Bgl*II site. Mutated genes are highlighted in blue. Arrows indicate the orientation of the genes and primers. Arrows designating oligonucleotides are not shown to scale.

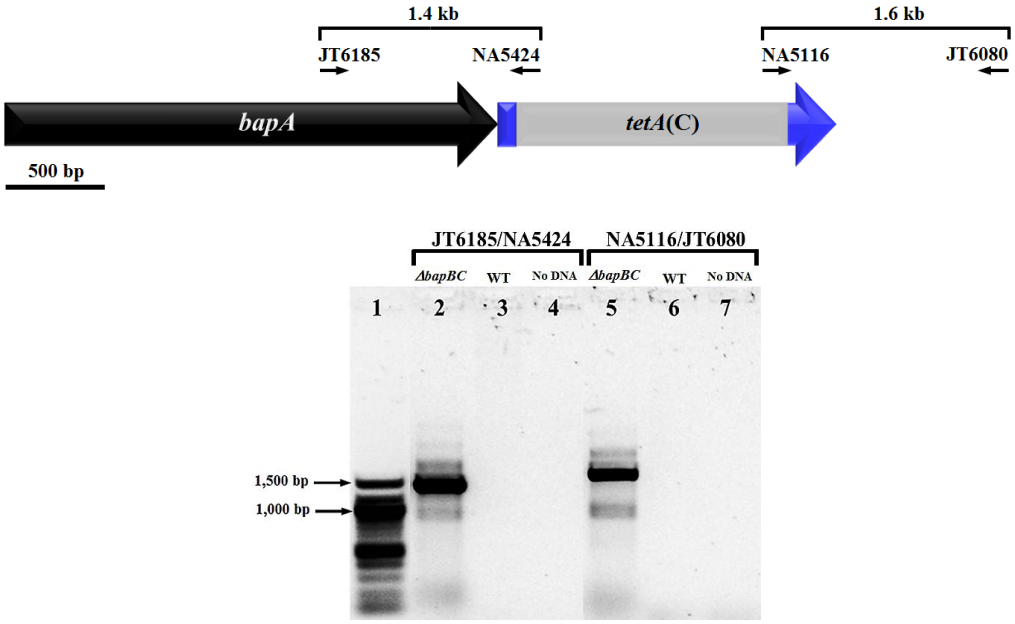

Figure 3.1.6 Genetic organisation of the *bapA*, *bapB* and *bapC* region in the K96243*ΔbapBC* strain. The position of the *tetA*(C) insertion is shown and the *tetA*(C)-specific (NA5116 and NA5424), *bapA*-specific (JT6185) and *bapC* downstream-specific (JT6080) primers are shown above the genes together with the predicted sizes of the PCR products. Gel electrophoresis of PCR products amplified using either K96243*ΔbapBC* genomic DNA, wild-type genomic DNA or no DNA control. Lane 1, DNA size markers; lane 2 and 5, PCR products generated using the primer pairs as indicated and genomic DNA of K96243*ΔbapBC*; lane 3 and 6, PCR amplification generated using the primer pairs as indicated and the wild-type genomic DNA; lane 4 and 7, no DNA controls. Mutated genes are highlighted in blue. Arrows indicate the orientation of the genes and primers. Arrows designating oligonucleotides are not shown to scale. *ΔbapBC* denotes the K96243*ΔbapBC* strain and WT denotes the wild-type strain.

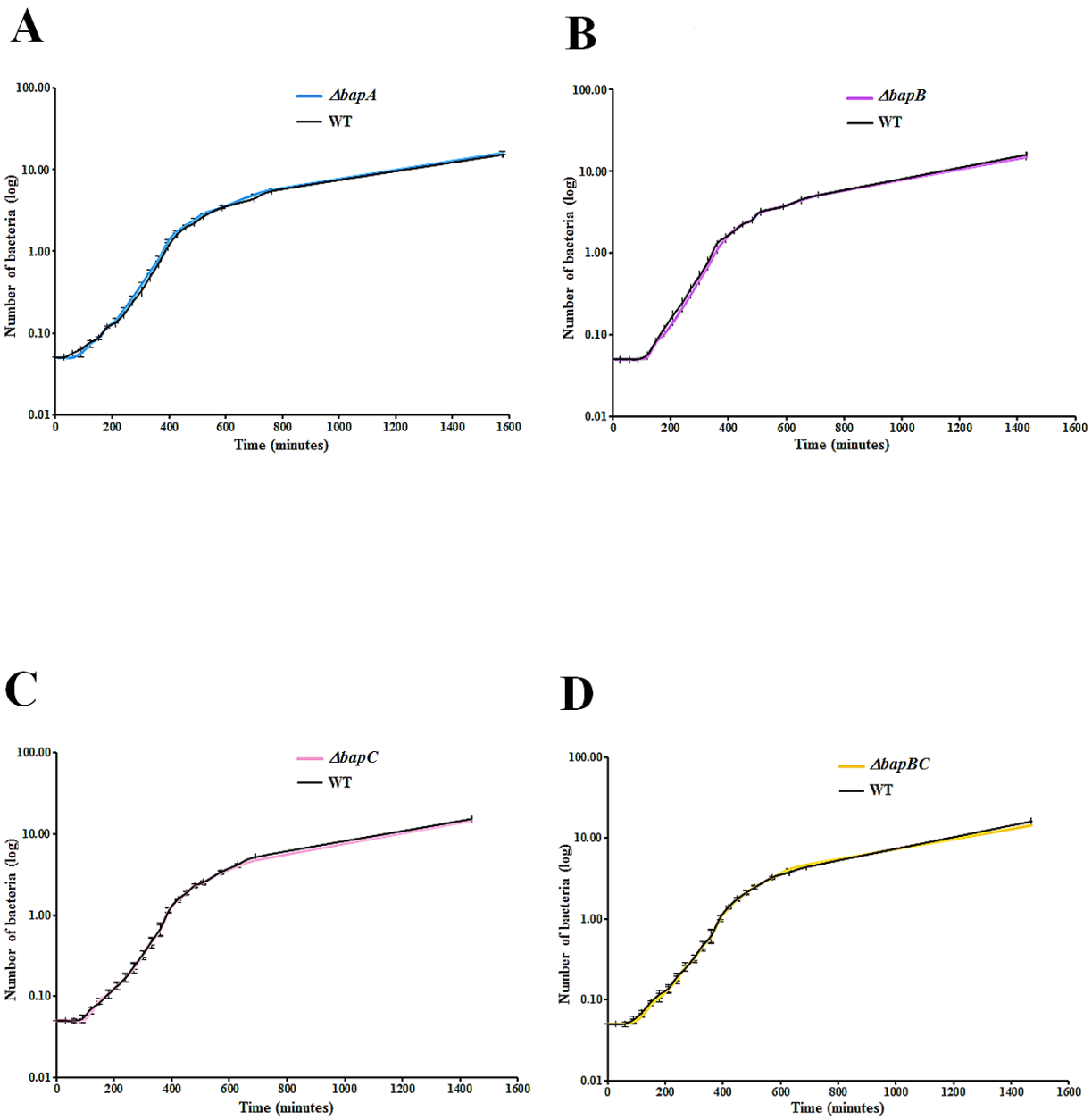

Figure 3.2.1 Growth curves for the K96243*ΔbapA* (A), *ΔbapB* (B), *ΔbapC* (C) and *ΔbapBC* (D) strains compared with the wild-type strain. Error bars represent the SEM from three independent experiments. *ΔbapA* denotes the K96243*ΔbapA* strain; *ΔbapB* denotes the K96243*ΔbapB* strain; *ΔbapC* denotes the K96243*ΔbapC* strain; *ΔbapBC* denotes the K96243*ΔbapBC* strain and WT denotes the wild-type strain.

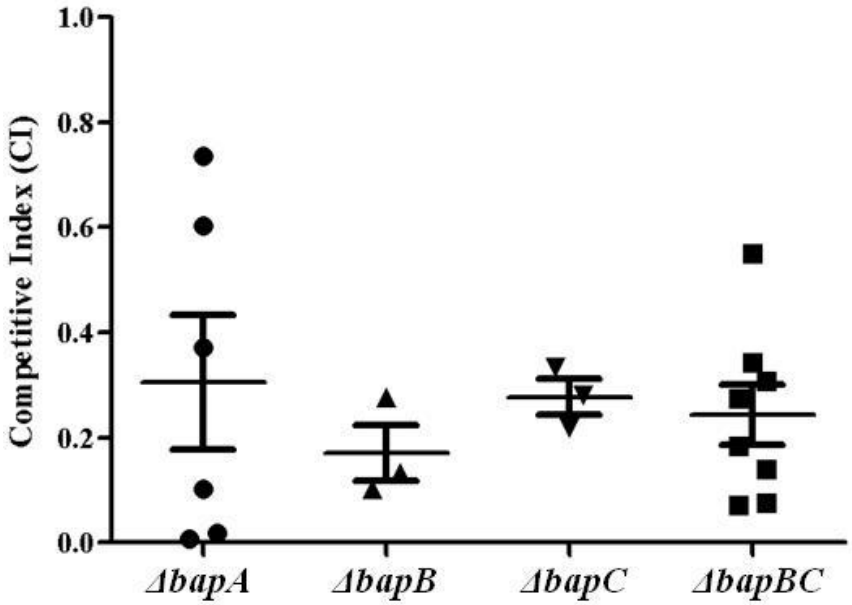

Figure 3.3.1 Competitive *in vivo* growth indices for each of the mutant strains. Groups of seven mice were intranasally infected with an equal amount of the mutant mixed with the wild-type strain, which served as the input pool. Spleens were removed for recovery of bacteria which served as the output pool. The ratio of the mutant to the wild-type strain in input and output pools was analysed and used to calculate the CI. Each point on the graph indicates the competitive index (CI) measured in a single mouse. The horizontal marks show the average CI ± 1 SEM. *ΔbapA* denotes the K96243*ΔbapA* strain; *ΔbapB* denotes the K96243*ΔbapB* strain; *ΔbapC* denotes the K96243*ΔbapC* strain and *ΔbapBC* denotes the K96243*ΔbapBC* strain.

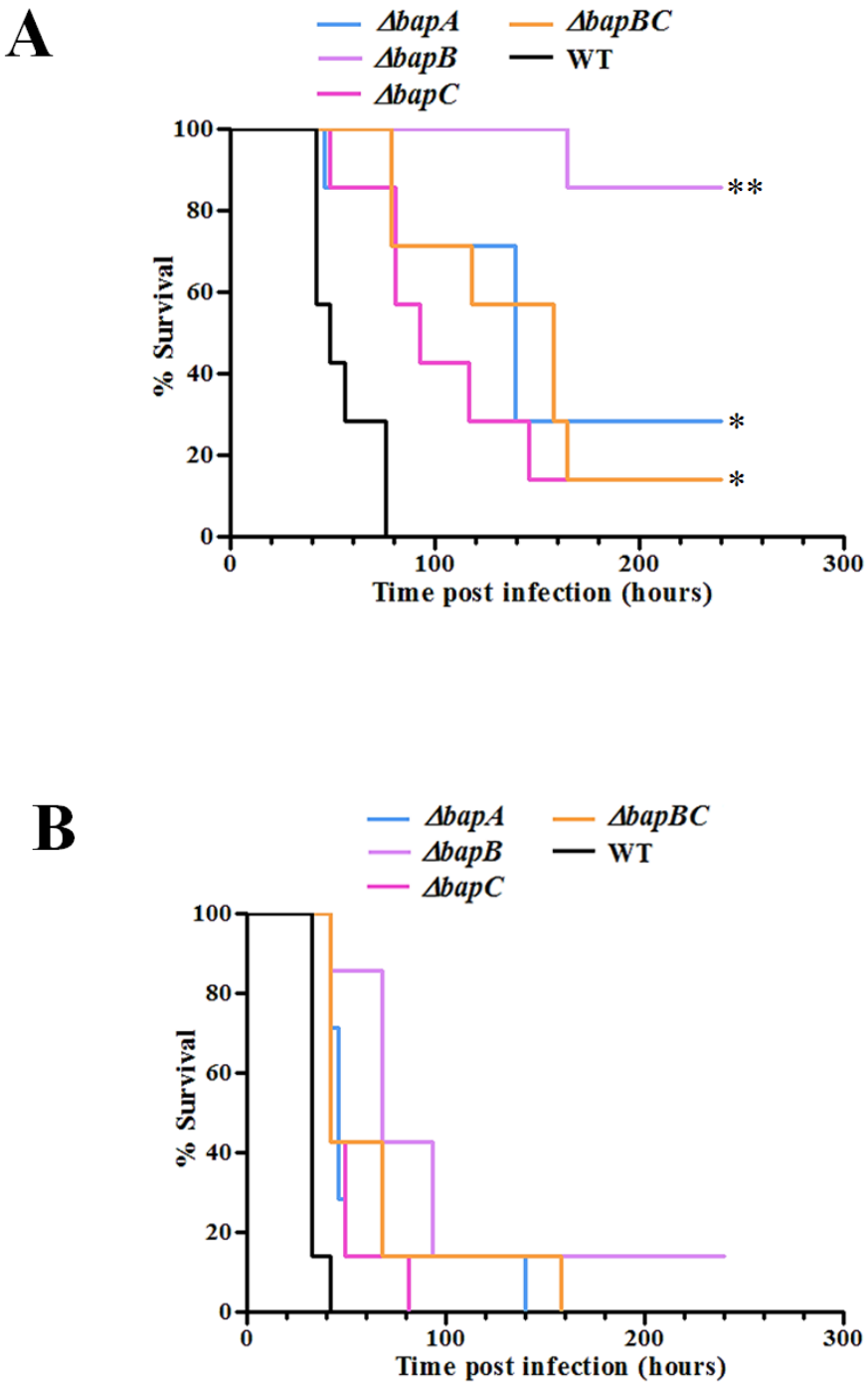

Figure 3.4.1 Kaplan-Meier survival curves of BALB/c mice infected intranasally with 10^5 CFU (A) or 10^7 CFU (B) of *B. pseudomallei* wild-type or each of the mutant strains. There was a significant difference in the time to death for mice infected with each of the mutant strains in comparison to the wild-type with either 10^5 or 10^7 CFU ($P < 0.05$). *$P < 0.05$, **$P < 0.001$. *ΔbapA* denotes the K96243*ΔbapA* strain; *ΔbapB* denotes the K96243*ΔbapB* strain; *ΔbapC* denotes the K96243*ΔbapC* strain; *ΔbapBC* denotes the K96243*ΔbapBC* strain and WT denotes the wild-type strain.

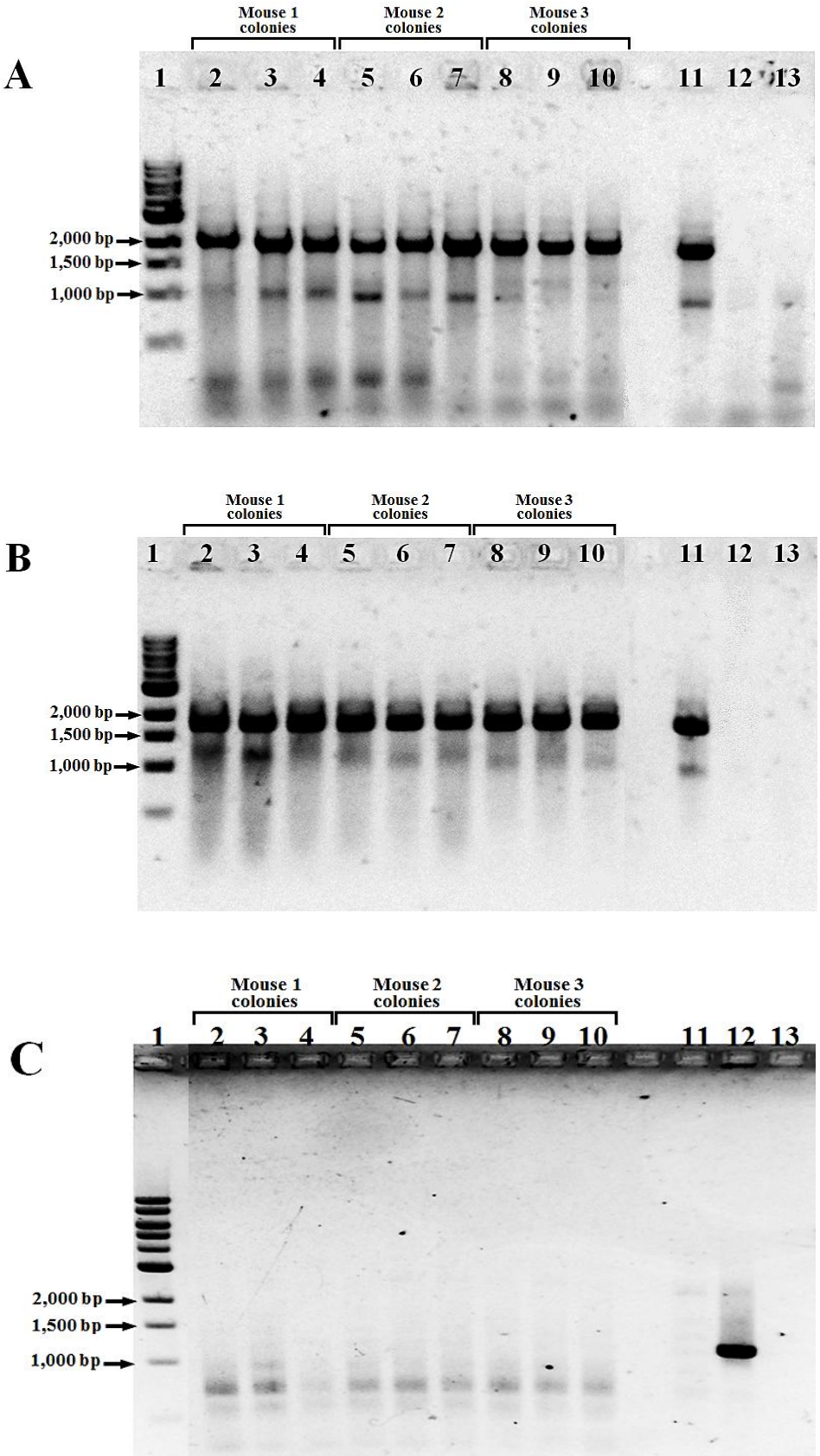

Figure 3.4.2 Representative PCR analyses of colonies recovered from mice infected with 10^5 CFU of the K96243*ΔbapA* strain using the primer pairs JT6376/NA5424 (A), NA5116/JT6180 (B) and JT6185/ JT6104 (C). Lane 1, DNA size markers (bp); lane 2 to 10, PCR using genomic DNA from colonies recovered from three mice (3 colonies per mouse); lane 11, K96243*ΔbapA* genomic DNA; lane 12, wild-type genomic DNA; lane 13, no DNA control.

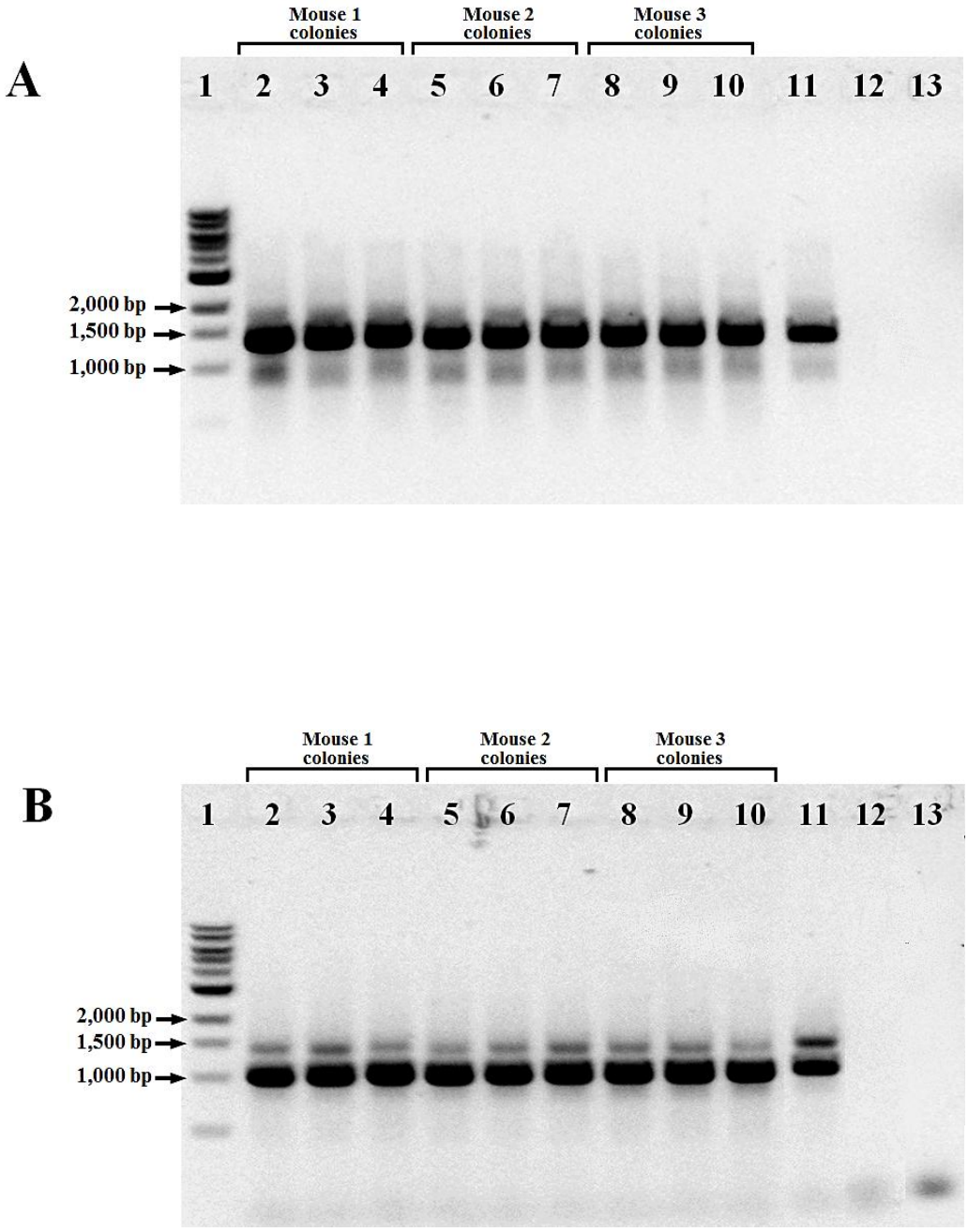

Figure 3.4.3 Representative PCR analyses of colonies recovered from mice infected with 10^5 CFU of the K96243*ΔbapB* strain using the primer pairs JT6185/NA5116 (A) and NA5424/JT6078 (B). Lane 1, DNA size markers (bp); lane 2 to 10, PCR using genomic DNA from colonies recovered from three mice (3 colonies per mouse); lane 11, K96243*ΔbapB* genomic DNA; lane 12, wild-type genomic DNA; lane 13, no DNA control.

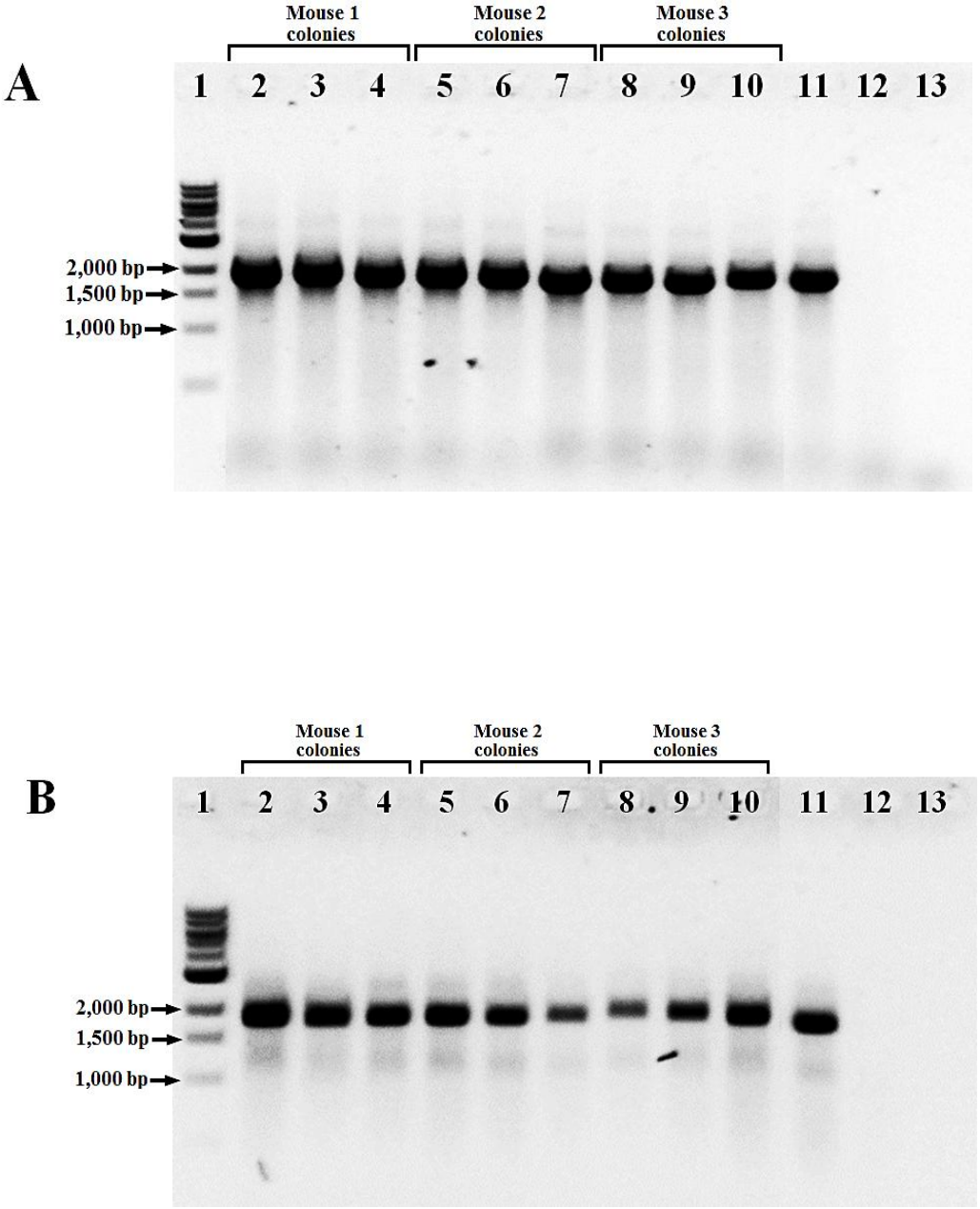

Figure 3.4.4 Representative PCR analyses of colonies recovered from mice infected with 10^5 CFU of the K96243*ΔbapC* strain using the primer pairs JT6185/NA5424 (A) and NA5116/JT6080 (B). Lane 1, DNA size markers (bp); lane 2 to 10, PCR using genomic DNA from colonies recovered from three mice (3 colonies per mouse); lane 11, K96243*ΔbapC* genomic DNA; lane 12, wild-type genomic DNA; lane 13, no DNA control.

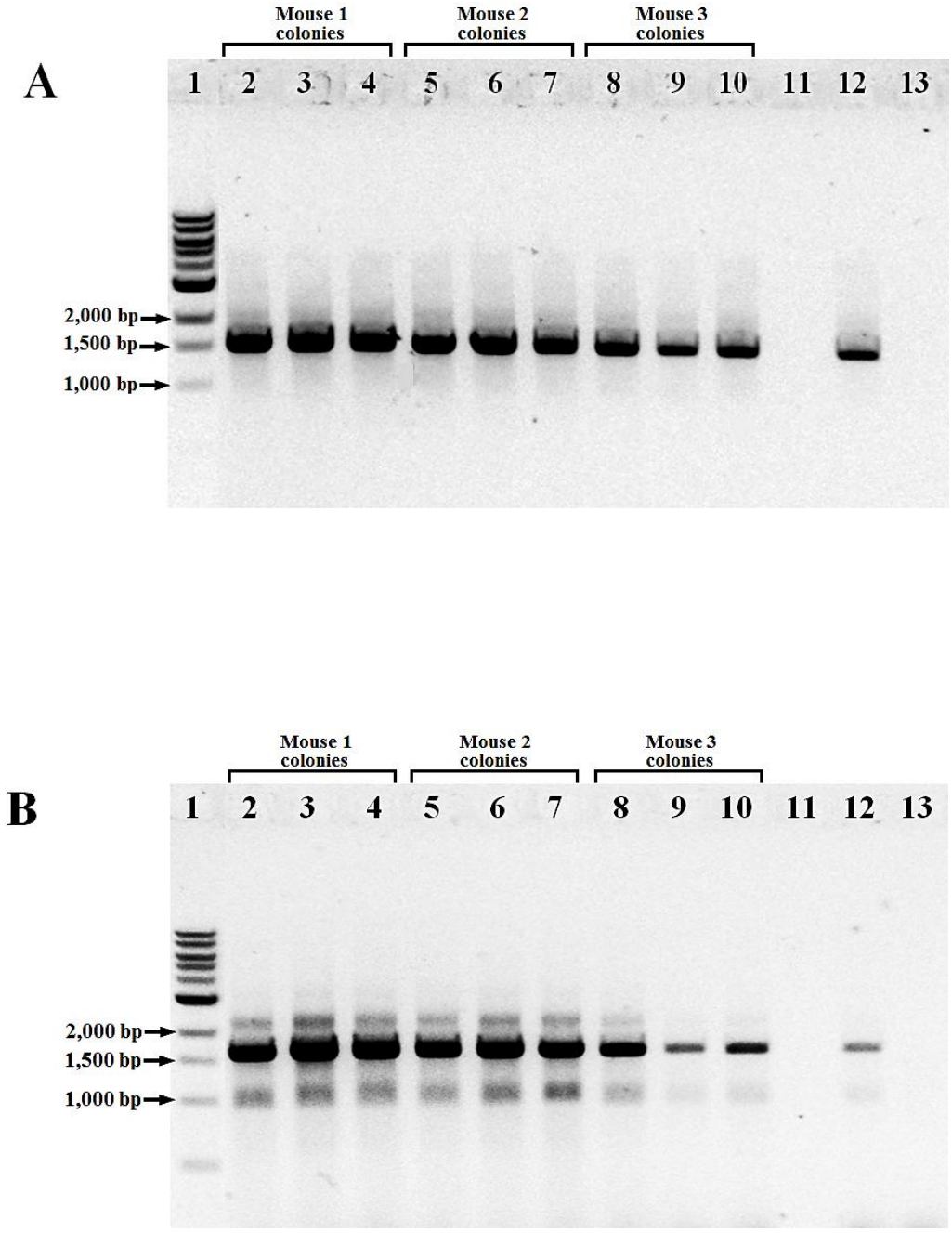

Figure 3.4.5 Representative PCR analyses of colonies recovered from mice infected with 10^5 CFU of the K96243*ΔbapBC* strain using the primer pairs JT6185/NA5424 (A) and NA5116/JT6080 (B). Lane 1, DNA size markers (bp); lane 2 to 10, PCR using genomic DNA from colonies recovered from three mice (3 colonies per mouse); lane 11, wild-type genomic DNA; lane 12, K96243*ΔbapBC* genomic DNA; lane 13, no DNA control.

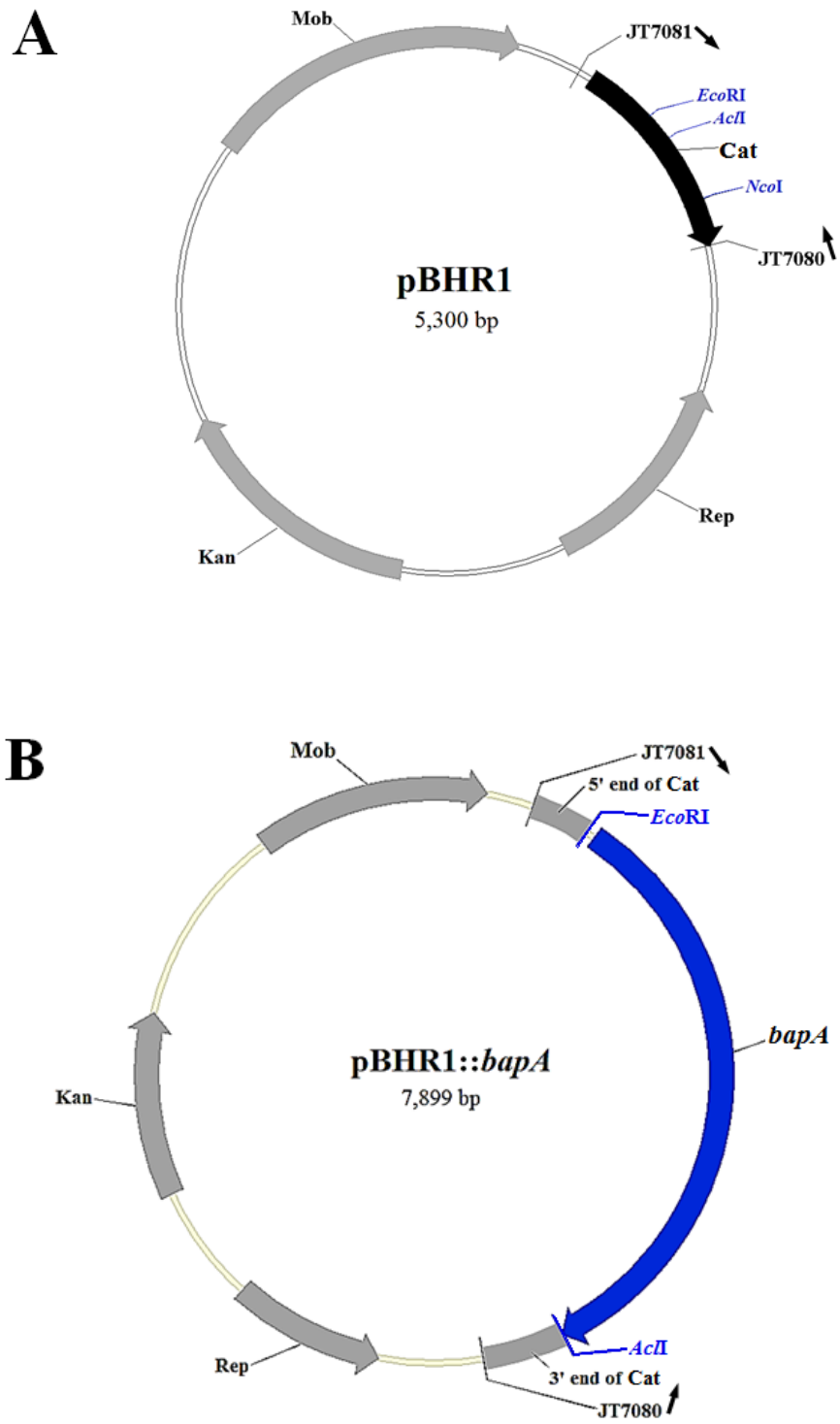

Figure 3.5.1 Plasmid maps illustrating the empty pBHR1 vector (A) and the K96243*ΔbapA*[*bapA*] strain (B). Full length *bapA*, derived from the *B. pseudomallei* wild-type strain, was cloned at the *Eco*RI (5') and *Acl*I (3') sites. The primers JT7080/JT7081 were used for verification of the cloning. Full length *bapB* or *bapC*, derived from the *B. pseudomallei* wild-type strain, were cloned into the same restriction sites in order to generate the K96243*ΔbapB*[*bapB*] or K96243*ΔbapC*[*bapC*] strains. Different features are indicated: Rep and Mob, *rep* and *mob* genes required for replication and mobilisation of pBHR1, respectively; Cat, chloramphenicol acetyl transferase gene; Kan, kanamycin resistance gene. Arrows indicate gene orientation.

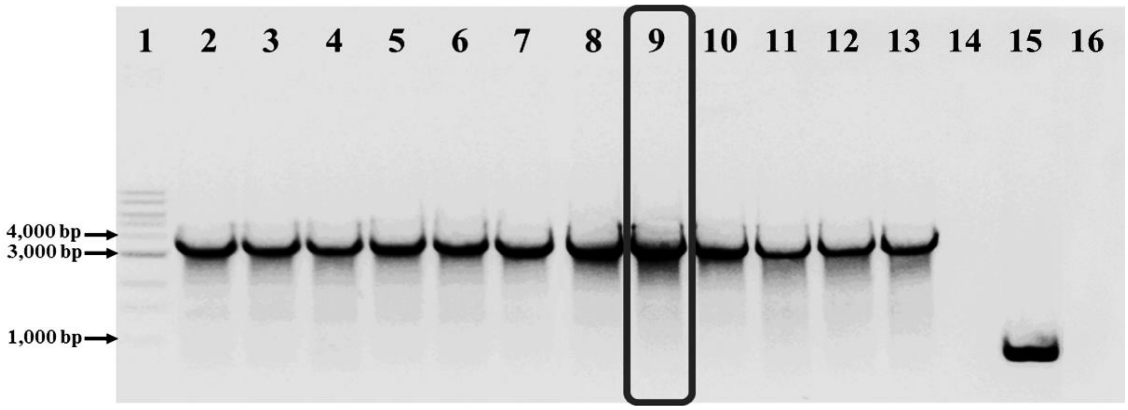

Figure 3.5.2 PCR screening of potential K96243*ΔbapA*[*bapA*] using the primer pair JT7080/JT7081 to amplify the region flanking the *Eco*RI/*Acl*I cloning sites of pBHR1. Lane 1, DNA size markers; lane 2 to 12, PCR products generated using genomic DNA of potential K96243*ΔbapA*[*bapA*] clones; lane 13, genomic DNA of *E. coli* S17-1/λ*pir* harbouring pBHR1::*bapA* as the positive control; lane 14, genomic DNA of the K96243*ΔbapA* strain; lane 15, genomic DNA of *E. coli* S17-1/λ*pir* harbouring empty pBHR1 vector; lane 16, no DNA control. The clone indicated by the black box in lane 9 was selected for further experiments.

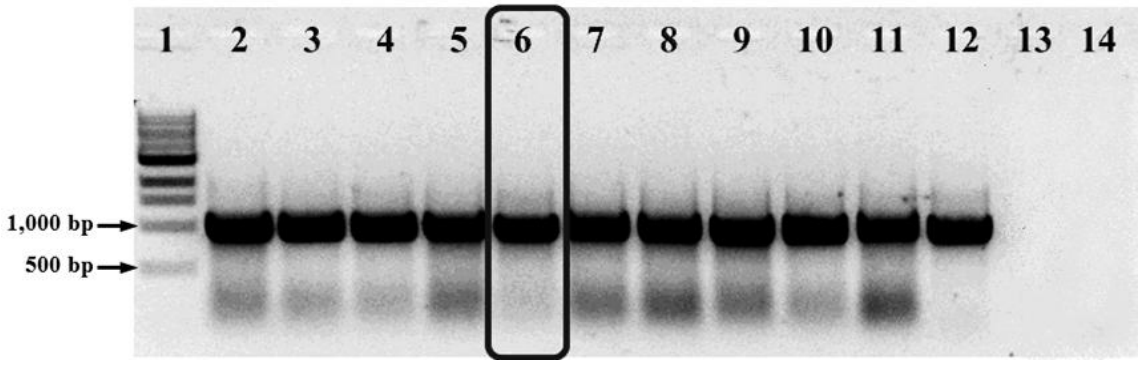

Figure 3.5.3 PCR screening of potential K96243*ΔbapB*[*bapB*] using the primer pair JT7080/JT7081 to amplify the region flanking the *Eco*RI/*Acl*I cloning sites of pBHR1. Lane 1, DNA size markers; lane 2 to 11, PCR products generated using genomic DNA of potential K96243*ΔbapB*[*bapB*] clones; lane 12, genomic DNA of *E. coli* S17-1/λ*pir* harbouring pBHR1::*bapB* as the positive control; lane 13, genomic DNA of the K96243*ΔbapB* strain; lane 14, no DNA control. The clone indicated by the black box in lane 6 was selected for further experiments.

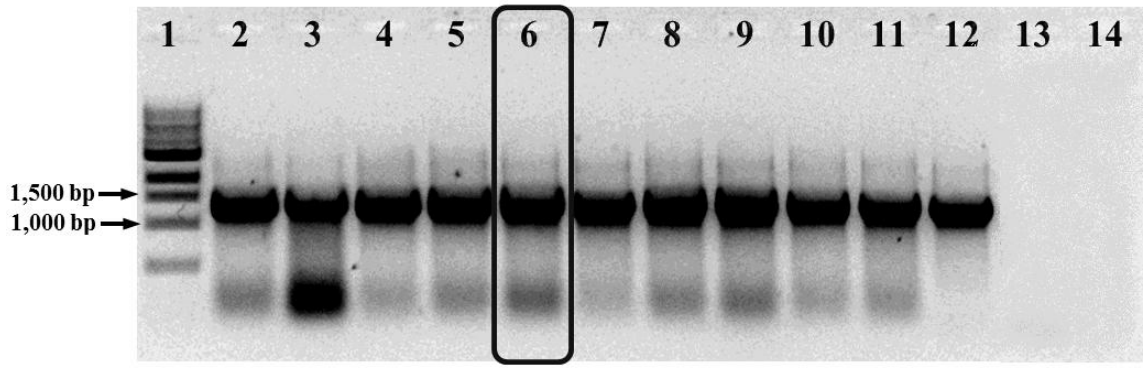

Figure 3.5.4 PCR screening of potential K96243*ΔbapC*[*bapC*] using the primer pair JT7080/JT7081 to amplify the region flanking the *Eco*RI/*Acl*I cloning sites of pBHR1. Lane 1, DNA size markers; lane 2 to 11, PCR products generated using genomic DNA of potential K96243*ΔbapC*[*bapC*] clones; lane 12, genomic DNA of *E. coli* S17-1/λ*pir* harbouring pBHR1::*bapC* as the positive control; lane 13, genomic DNA of the K96243*ΔbapC* strain; lane 14, no DNA control. The clone indicated by the black box in lane 6 was selected for further experiments.

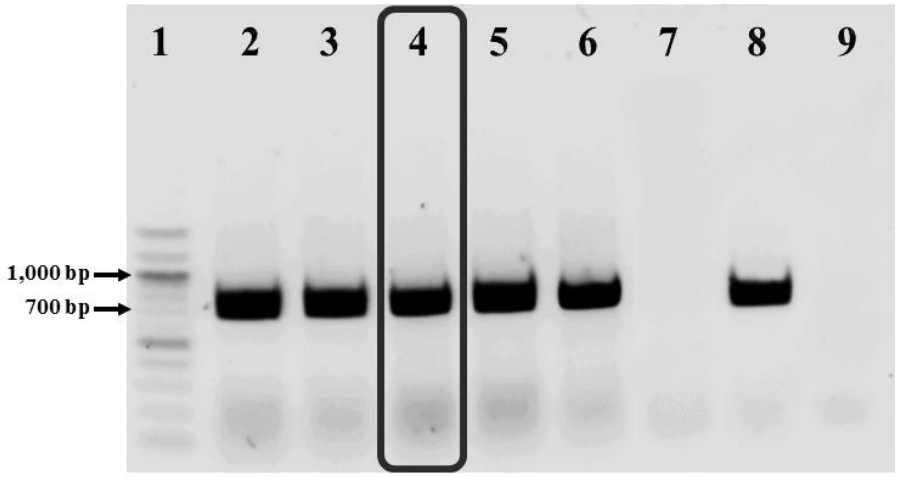

Figure 3.5.5 PCR screening of potential K96243*ΔbapA*[pBHR1] using the primer pair JT7080/JT7081 to amplify a 700-bp product of the chloramphenicol resistance cassette of pBHR1. Lane 1, DNA size markers; lane 2 to 6, PCR products generated using genomic DNA of putative K96243*ΔbapA*[pBHR1] clones; lane 7, genomic DNA of the K96243*ΔbapA* strain; lane 8, *E. coli* S17-1/λ*pir* containing pBHR1; lane 9, no DNA control. The clone indicated by the black box in lane 4 was selected for further experiments.

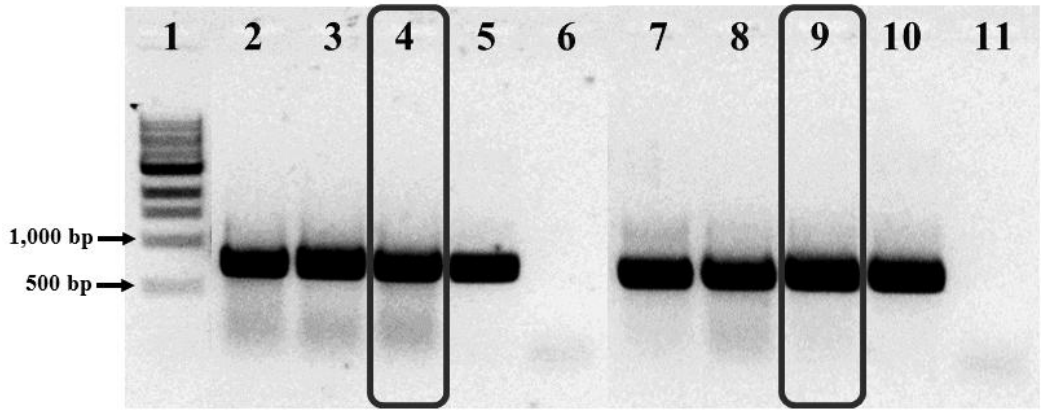

Figure 3.5.6 PCR screening of potential K96243*ΔbapB*[pBHR1] clones and K96243*ΔbapC*[pBHR1] clones using the primer pair JT7080/JT7081 to amplify a 700-bp product of the chloramphenicol resistance cassette of pBHR1. Lane 1, DNA size markers; lane 2 to 4 and 7 to 9, PCR products generated using genomic DNA of putative K96243*ΔbapB*[pBHR1] and K96243*ΔbapC*[pBHR1] clones, respectively; lane 5 and 10, *E. coli* S17-1/λ*pir* containing pBHR1; lane 6 and 11, genomic DNA of the K96243*ΔbapB* and K96243*ΔbapC* strains. The clones indicated by the black box in lane 4 and 9 were chosen for further experiments.

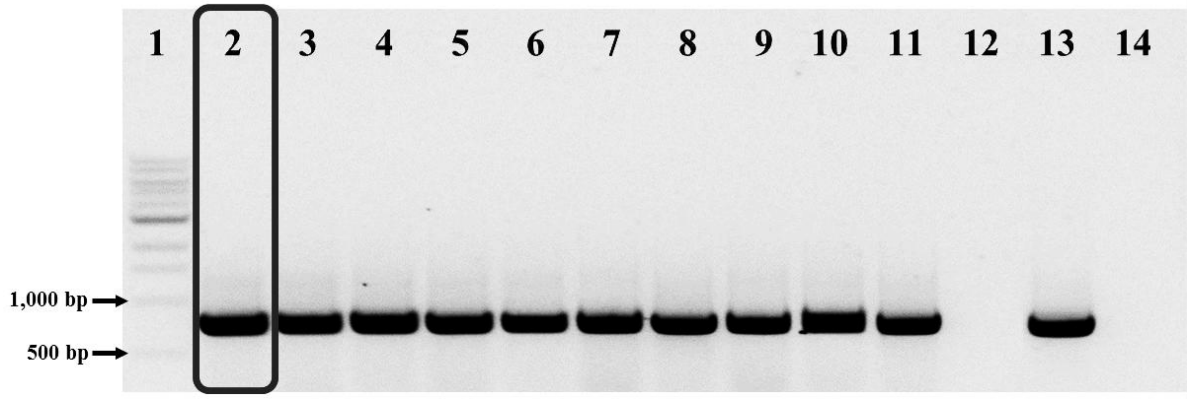

Figure 3.5.7 PCR screening of potential K96243[pBHR1] clones using the primer pair JT7080/JT7081 to amplify a 700-bp product of the chloramphenicol resistance cassette of pBHR1. Lane 1, DNA size markers; lane 2 to 11, PCR products generated using genomic DNA of the putative K96243[pBHR1] strains; lane 12, genomic DNA of the wild-type strain; lane 13, *E. coli* S17-1/λ*pir* containing pBHR1; lane 14, no DNA control. The clone indicated by the black box in lane 2 was selected for further experiments.

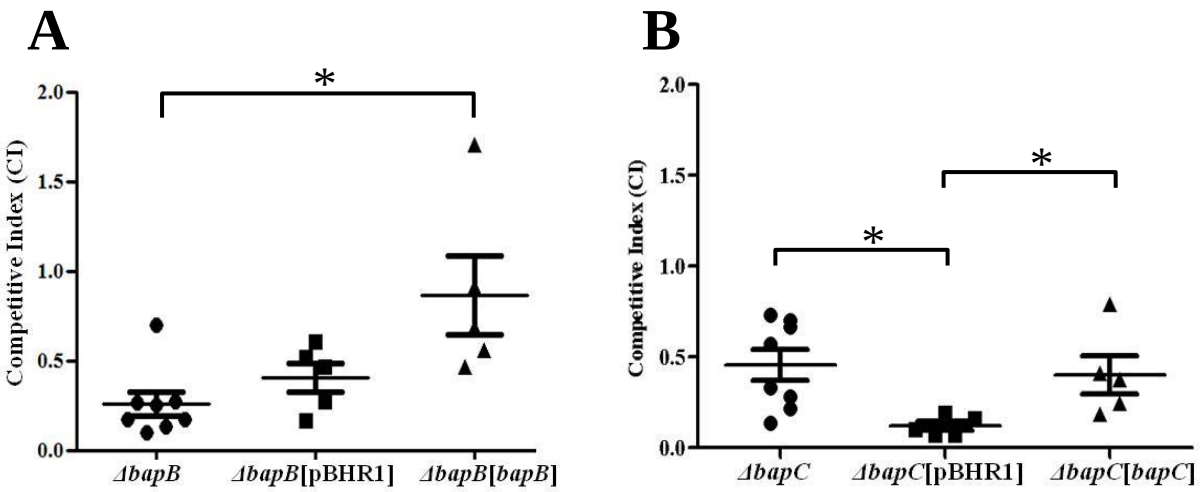

Figure 3.6.1 Competitive *in vivo* growth indices for the K96243*ΔbapB*[*bapB*] (A) and K96243*ΔbapC*[*bapC*] (B) mutants. Groups of seven mice were intranasally infected with an equal amount of the mutant mixed with the wild-type strain, which served as the input pool. Spleens were removed for recovery of bacteria which served as the output pool. The ratio of the mutant to the wild-type strain in input and output pools was analysed and used to calculate the CI. Each point on the graph indicates the competitive index (CI) measured in a single mouse. The horizontal marks show average CI ± 1 SEM. *$P < 0.05$. *ΔbapB* denotes the K96243*ΔbapB* strain; *ΔbapB*[pBHR1] denotes the K96243*ΔbapB*[pBHR1] strain; *ΔbapB*[*bapB*] denotes the K96243 *ΔbapB*[*bapB*] strain; *ΔbapC* denotes the K96243*ΔbapC* strain; *ΔbapC*[pBHR1] denotes the K96243 *ΔbapC*[pBHR1] strain; *ΔbapC*[*bapC*], the K96243*ΔbapC*[*bapC*] strain.

Strains	% Plasmid retention (12 h p.i.*)	% Plasmid retention (20 h p.i.*)
K96243*ΔbapA*[*bapA*]	0	0
K96243*ΔbapA*[pBHR1]	71	51
K96243*ΔbapB*[*bapB*]	56	9
K96243*ΔbapB*[pBHR1]	64	23
K96243*ΔbapC*[*bapC*]	13	0
K96243*ΔbapC*[pBHR1]	7	0

*p.i. = post inoculation.

Figure 3.6.2 %Plasmid retention at 12 and 20 hours post inoculation of the mutant strains containing appropriate complementation constructs or the empty plasmid pBHR1.

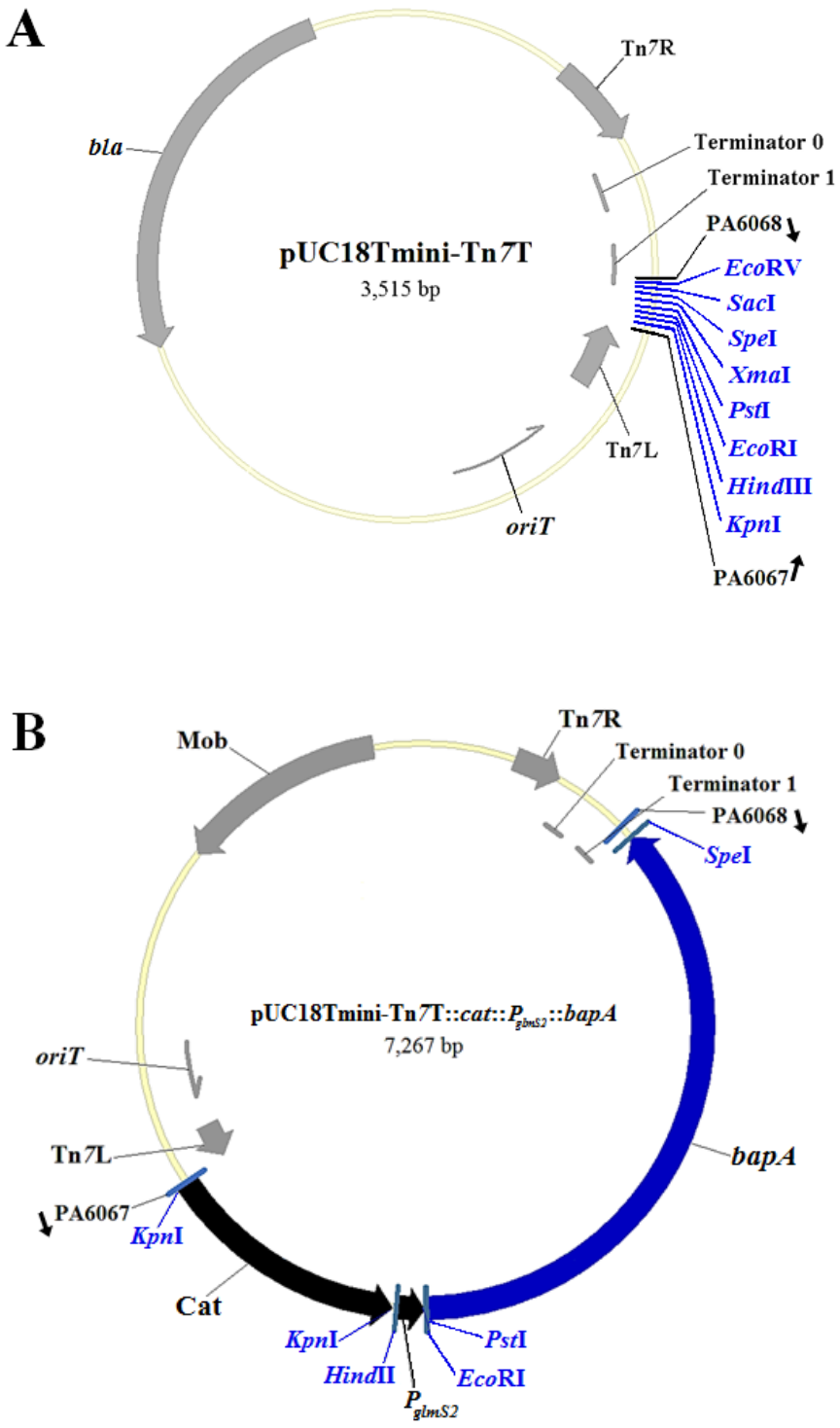

Figure 3.7.1 Plasmid maps illustrating the empty pUC18Tmini-Tn*7*T vector (A) and the complemented *bapA* mutant construct in pUC18Tmini-Tn*7*T (B). The primers PA6067/PA6068 amplifying the region flanking the cloning sites were used for screening and nucleotide sequencing. Different features are indicated: Tn*7*L and Tn*7*R, left and right end of Tn*7*; Cat, chloramphenicol acetyl transferase gene derived from pDM4 and cloned at the *Kpn*I site; P_{glmS2}, *glmS2* promoter derived from the wild-type *B. pseudomallei* strain and cloned at the *Hin*dIII (5') and *Eco*RI (3') sites; *bapA*, full length *bapA* derived from the wild-type strain and cloned at the *Pst*I (5') and *Spe*I (3') sites; *oriT*, origin of conjugative transfer; T_1T_0, transcriptional terminators T_1 and T_0 from bacteriophage λ and *E. coli rrnB* operon, respectively. Arrows indicate gene orientation.

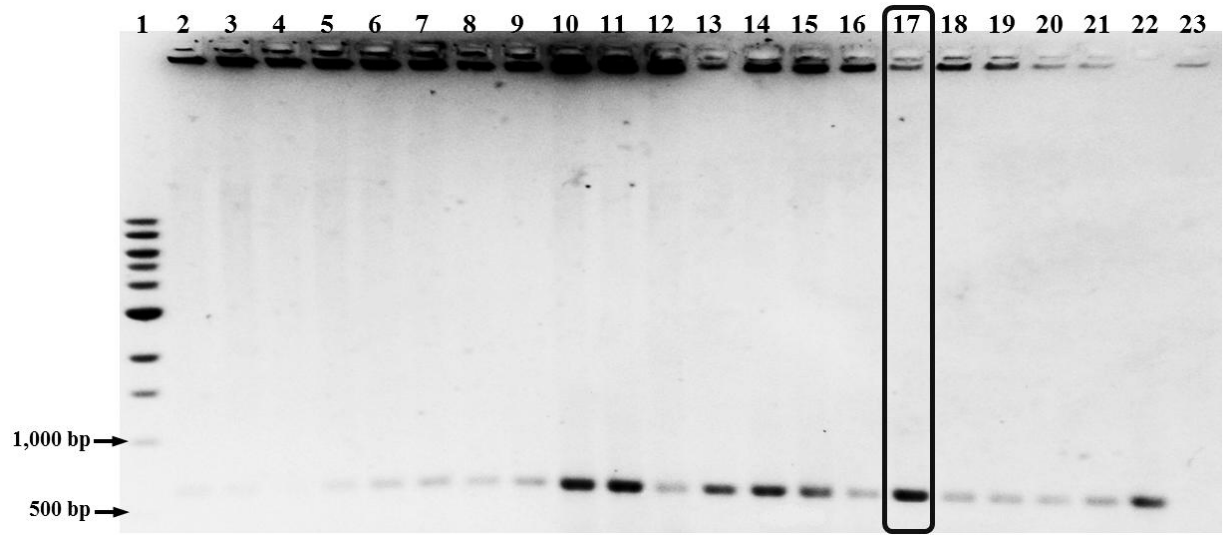

Figure 3.7.2 PCR screening for *E. coli* DH5α harbouring pUC18Tmini-Tn*7*T::P_{glmS2}::*bapA* using the primer pair JT6071/JT6072. Lane 1, DNA size markers (bp); lane 2 to 21, PCR products generated using the primers JT6071 and JT6072 and plasmid DNA of *E. coli* DH5α strains harbouring putative pUC18Tmini-Tn*7*T::*cat*::P_{glmS2}::*bapA* clones; lane 22, genomic DNA from wild-type *B. pseudomallei* as the positive control; lane 23, no DNA control. The clone indicated by the black box in lane 17 was selected for further experiments.

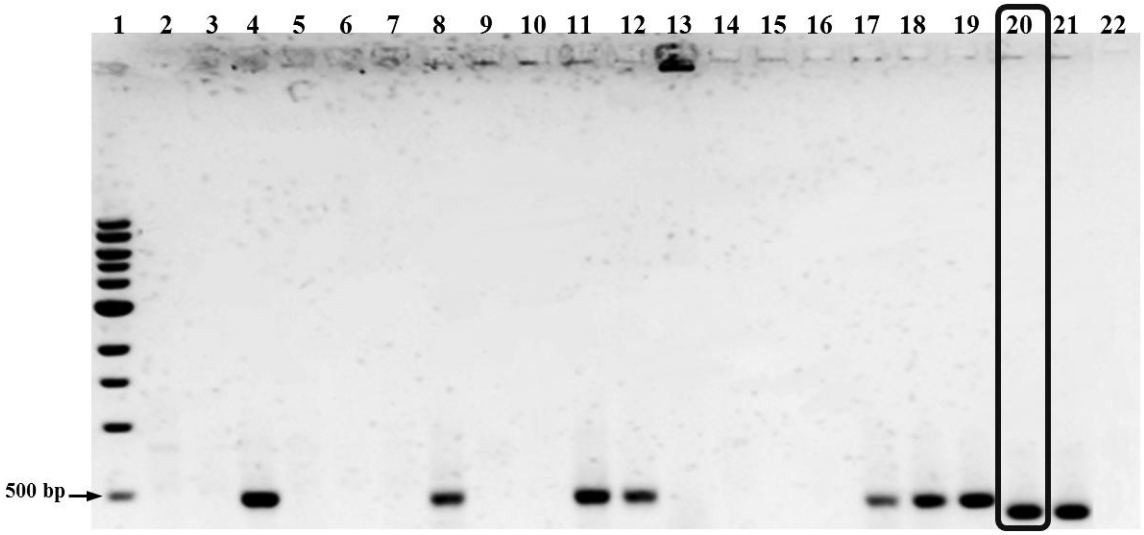

Figure 3.7.3 PCR screening for *E. coli* DH5α harbouring pUC18Tmini-Tn*7*T::P_{glmS2}::*bapABC* using the primer pair JT6077/JT6078. Lane 1, DNA size markers (bp); lane 2 to 20, PCR products generated using the primers JT6077 and JT6078 and plasmid DNA of *E. coli* DH5α strains harbouring pUC18T mini-Tn*7*T::*cat*::P_{glmS2}::*bapABC* clones; lane 21, genomic DNA from wild-type *B. pseudomallei* as the positive control; lane 22, no DNA control. The clone indicated by the black box in lane 20 was selected for further experiments.

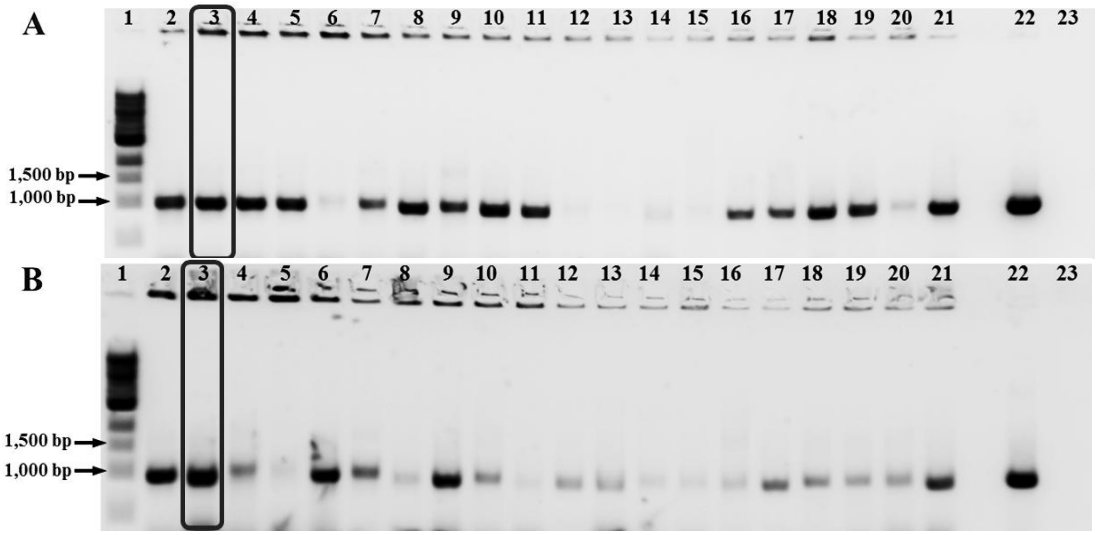

Figure 3.7.4 Gel electrophoresis of PCR products used to identify the insertion of the chloramphenicol acetyl transferase (*cat*) gene from pDM4 into the pUC18Tmini-Tn*7*T vector to generate the pUC18Tmini-Tn*7*T::*cat*::P_{glmS2}::*bapA* (A) and pUC18Tmini-Tn*7*T::*cat*::P_{glmS2}::*bapABC* (B). The primer pair JT6100/JT6101 was used for this screening. Lane 1: DNA size markers (bp); lane 2 to 21, PCR products generated using the primers JT6100/JT6101 and plasmid DNA from *E. coli* DH5α harbouring putative pUC18Tmini-Tn*7*T::*cat*::P_{glmS2}::*bapA* (A) or pUC18Tmini-Tn*7*T::*cat*::P_{glmS2}::*bapABC* (B) plasmids; lane 22, plasmid DNA of pDM4 as a positive control; lane 23, no DNA control. The clones indicated by the black box were selected for further experiments.

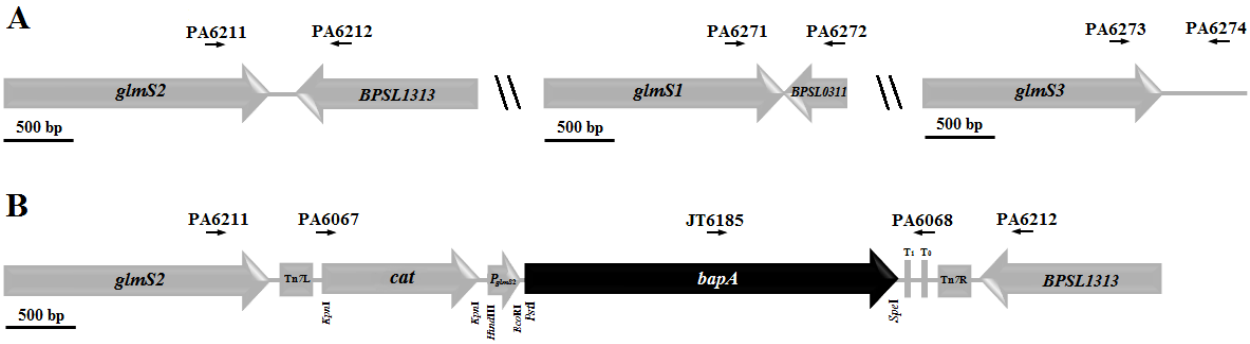

Figure 3.7.5 Primers used for identification of the position of the Tn*7* insertion in the putative K96243*ΔbapA-bapA* strain after conjugation. Tn*7* is proposed to insert following one of the *B. pseudomallei glmS* genes so primers downstream of each *glmS* gene were used. The primary site of insertions is generally following *glmS2* (Choi *et al.*, 2006). (A) Schematic representation of the wild-type gene *glmS2* (*BPSL1312*) and its adjacent gene *BPSL1313*, wild-type *glmS1* (*BPSL0312*) and its adjacent gene *BPSL0311*, and wild-type *glmS3*. The primer pairs PA6211/PA6212, PA6271/PA6272 and PA6273/6274 were used to identify if there was an insertion after *glmS2*, *glmS1* or *glmS3*, respectively. (B) Schematic representation of the expected integration of the pUC18Tmini-Tn*7*T::*cat*::P_{glmS2}::*bapA* construct into the bacterial chromosome after the *glmS2* gene. Different features are indicated: Tn*7*L and Tn*7*R, left and right end of Tn*7*; *cat*, the chloramphenicol acetyl transferase gene; P_{glmS2}, *glmS2* promoter derived from the wild-type strain and cloned at *Hin*dIII (5') and *Eco*RI (3') sites; *bapA*, the *bapA* gene derived from the wild-type strain and cloned at *Pst*I (5') and *Spe*I (3') sites; T_1T_0, transcriptional terminators T_1 and T_0 from bacteriophage λ and *E. coli rrnB* operon, respectively. Two sets of primer pairs (PA6211/PA6212 and JT6185/ PA6212) were used for screening the clones. Arrows indicate the orientation of primers. Arrows designating oligonucleotides are not shown to scale.

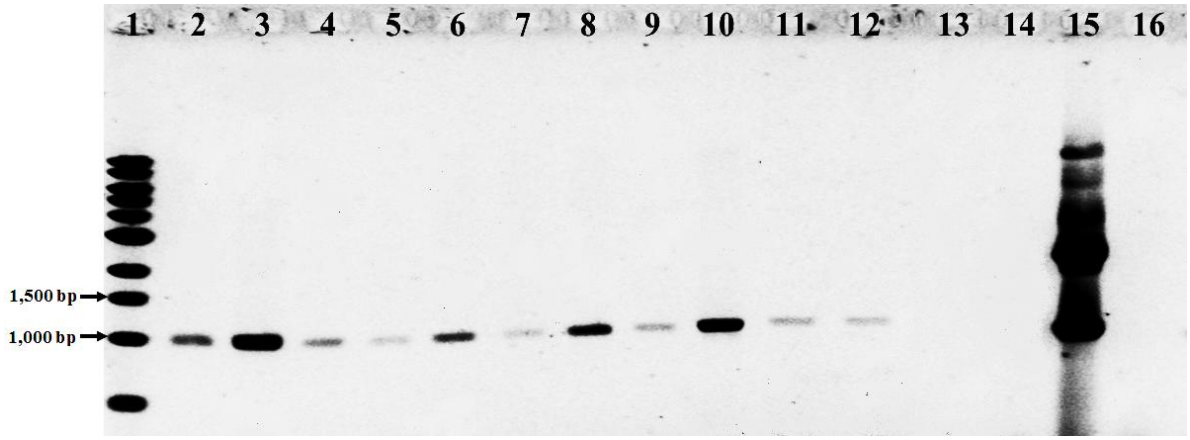

Figure 3.7.6 Gel electrophoresis of PCR products used to identify the presence of the chloramphenicol acetyl transferase (*cat*) gene in *B. pseudomallei* using the primer pair JT6100/JT6101. Lane 1: DNA size markers (bp); lane 2 to 12, PCR products using genomic DNA from the putative K96243*ΔbapA-bapA* transconjugants as template; lane 13, genomic DNA from the wild-type strain; lane 14, genomic DNA from the K96243*ΔbapA* strain; lane 15, genomic DNA from the *E. coli* SM10/λ*pir* strain harbouring the modified mini-Tn*7* construct as the positive control; lane 16, no DNA control.

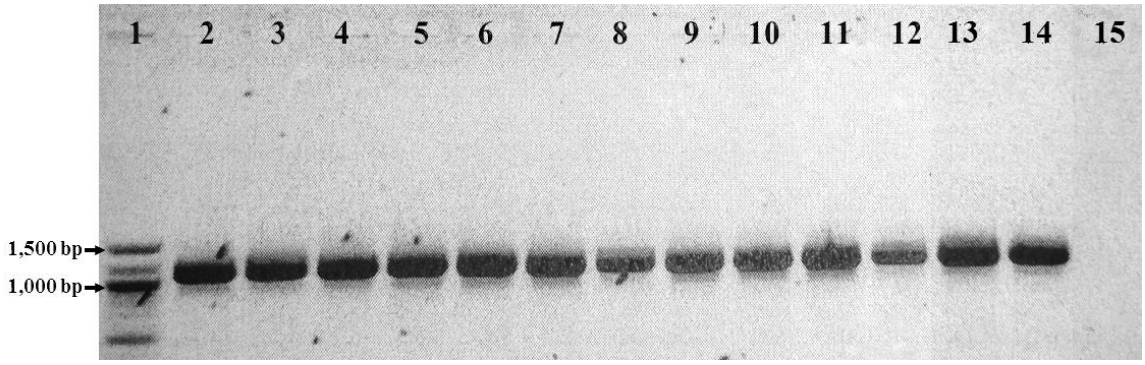

Figure 3.7.7 Gel electrophoresis of PCR products used to identify the presence of the pUC18Tmini-Tn*7*T::*cat*::P_{glmS2}::*bapA* insertion downstream of *glmS2*. The primers PA6211 and PA6212, amplifying a 1,100-bp fragment of the region between *glmS2* (*BPSL1312*) and *BPSL1313* genes, were used to determine if there was a transposon integration in that region. Lane 1: DNA size markers (bp); lane 2 to 12, PCR products using genomic DNA from the potential K96243*ΔbapA-bapA* transconjugants as template; lane 13, genomic DNA from the K96243*ΔbapA* strain; lane 14, genomic DNA from the wild-type strain; lane 15, no DNA control.

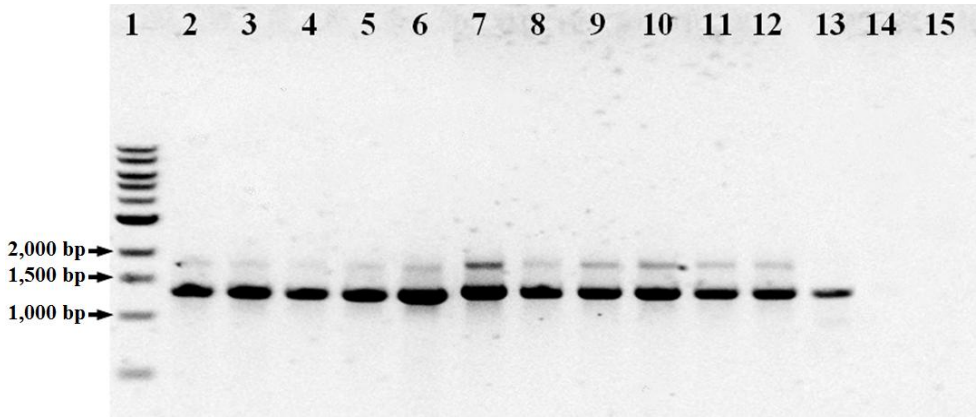

Figure 3.7.8 Gel electrophoresis of PCR products used to identify the presence of the pUC18Tmini-Tn*7*T::*cat*::P_{glmS2}::*bapA* insertion downstream of *glmS2*. The primers JT6185 and PA6212 were used to determine if there was a transposon integration in that region. Lane 1: DNA size markers (bp); lane 2 to 12, PCR products using genomic DNA from the potential K96243*ΔbapA-bapA* transconjugants as template; lane 13, genomic DNA from the K96243*ΔbapA* strain; lane 14, plasmid DNA from the *E. coli* SM10/λ*pir* strain harbouring the pUC18Tmini-Tn*7*T::*cat*::P_{glmS2}::*bapA* construct as the negative control; lane 15, no DNA control.

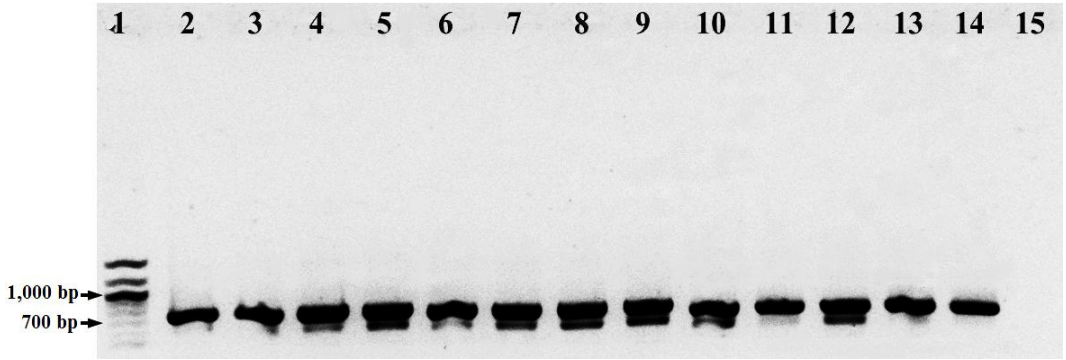

Figure 3.7.9 Gel electrophoresis of PCR products used to identify the presence of the pUC18Tmini-Tn*7*T::*cat*::P_{glmS2}::*bapA* insertion downstream of *glmS1*. The primers PA6271 and PA6272, amplifying an approximate 700-bp fragment of the region between *glmS1* (*BPSL0312*) and its adjacent gene *BPSL0311*, were used to determine if there was a transposon integration in that region. Lane 1: DNA size markers (bp); lane 2 to 12, PCR products using genomic DNA from the potential K96243*ΔbapA-bapA* transconjugants as template; lane 13, genomic DNA from the K96243*ΔbapA* strain; lane 14, genomic DNA from the wild-type strain; lane 15, no DNA control.

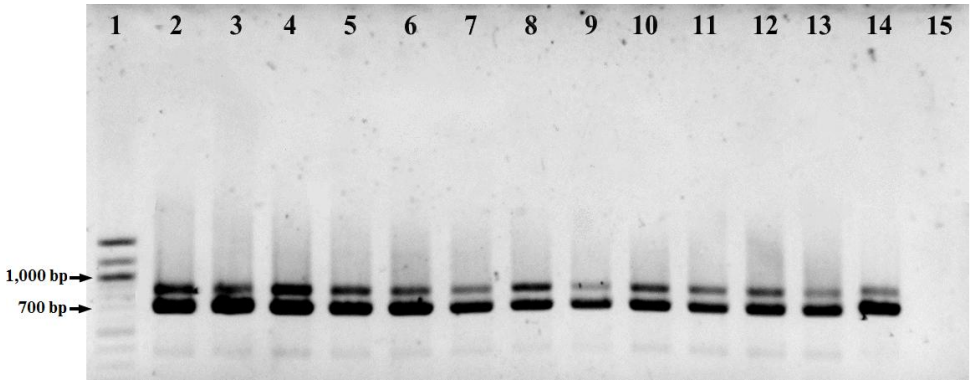

Figure 3.7.10 Gel electrophoresis of PCR products used to identify the presence of the pUC18Tmini-Tn*7*T::*cat*::P_{glmS2}::*bapA* insertion downstream of *glmS3*. The primers PA6273 and PA6274, amplifying an approximate 700-bp fragment, were used to determine if there was a transposon integration in that region. Lane 1: DNA size markers (bp); lane 2 to 12, PCR products using genomic DNA from the potential K96243*ΔbapA-bapA* transconjugants as template; lane 13, genomic DNA from the K96243*ΔbapA* strain; lane 14, genomic DNA from the wild-type strain; lane 15, no DNA control.

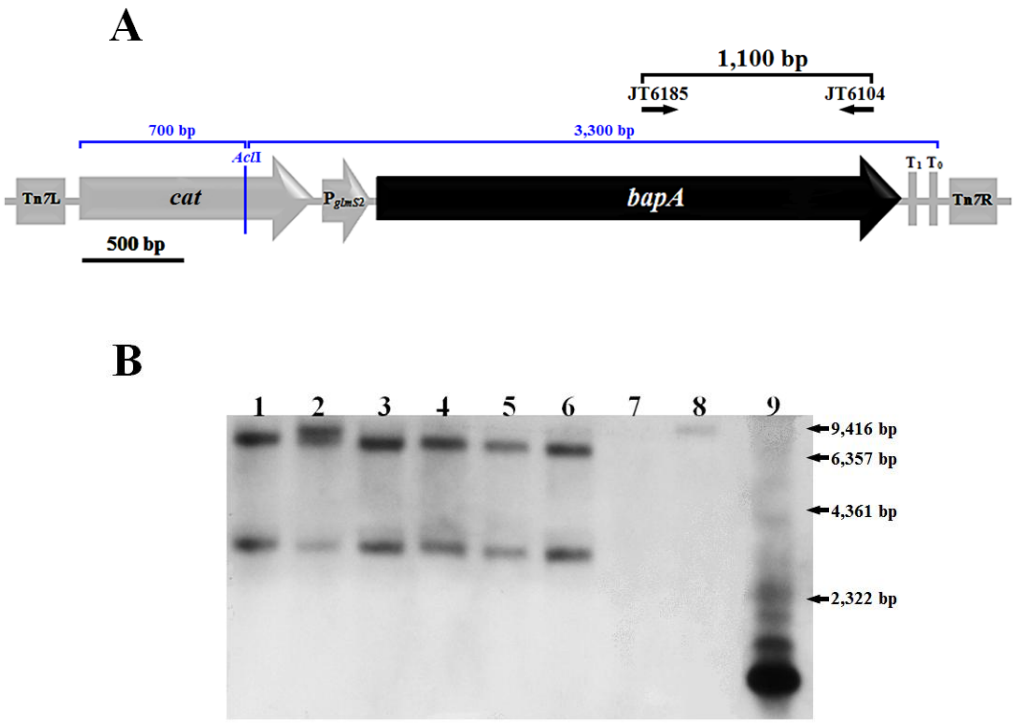

Figure 3.7.11 Southern blot analysis of the putative K96243*ΔbapA-bapA* transconjugants. The primer pair JT6185/JT6104 amplifying the deletion fragment within *bapA* was used to generate a DIG-labelled probe for hybridising with *Acl*I-digested genomic DNA from the potential transconjugants. (A) Schematic illustration showing where the deletion fragment is located in the K96243*ΔbapA* strain. The position of the DIG-labelled probe is shown above the *bapA* gene. (B) Southern blot. Lane 1 to 6, genomic DNA from the potential K96243*ΔbapA-bapA* transconjugants; lane 7, genomic DNA from the K96243*ΔbapA* strain as the negative control; lane 8, the DIG-labelled DNA size markers (bp); lane 9, DIG-labelled probe generated using the primers JT6185/JT6104 as the positive control. Arrows indicate the orientation of primers and genes. Arrows designating oligonucleotides are not shown to scale.

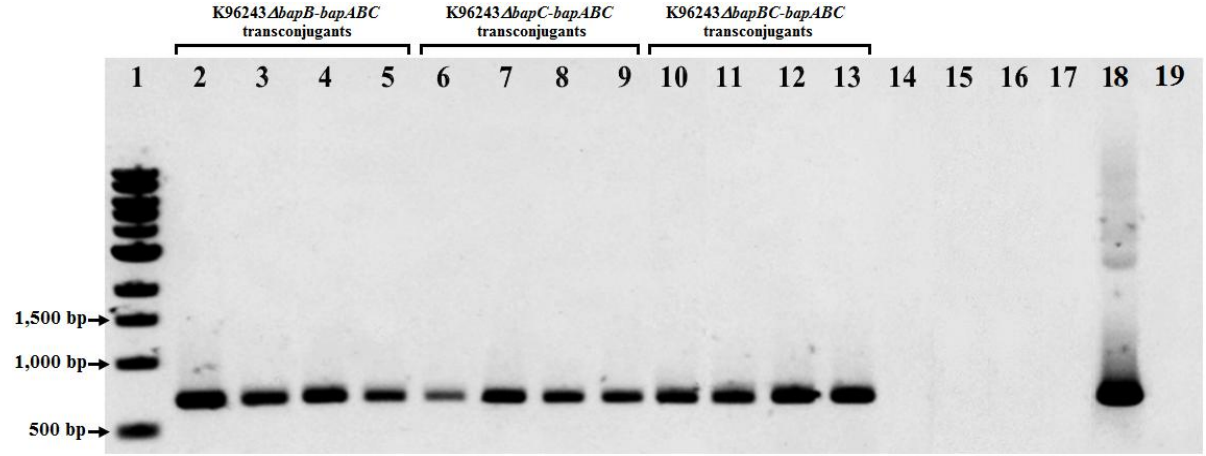

Figure 3.7.12 Gel electrophoresis of PCR products used to identify the presence of the *oriT* region of the pUC18Tmini-Tn*7*T::*cat*::P_{glmS2}::*bapA* construct using the primer pair MC6229/MC6230. Lane 1: DNA size markers (bp); lane 2 to 5, 6 to 9 and 10 to 13, PCR products using genomic DNA from the putative K96243*ΔbapB-bapABC*, *ΔbapC-bapABC* and *ΔbapBC-bapABC* transconjugants, respectively; lane 14, genomic DNA from the K96243*ΔbapB* strain; lane 15, genomic DNA from the K96243*ΔbapC* strain; lane 16, genomic DNA from the K96243*ΔbapBC* strain; lane 17, genomic DNA from the wild-type strain; lane 18, plasmid DNA from the *E. coli* SM10/λ*pir* strain harbouring the empty mini-Tn*7* vector as the positive control; lane 19, no DNA control.

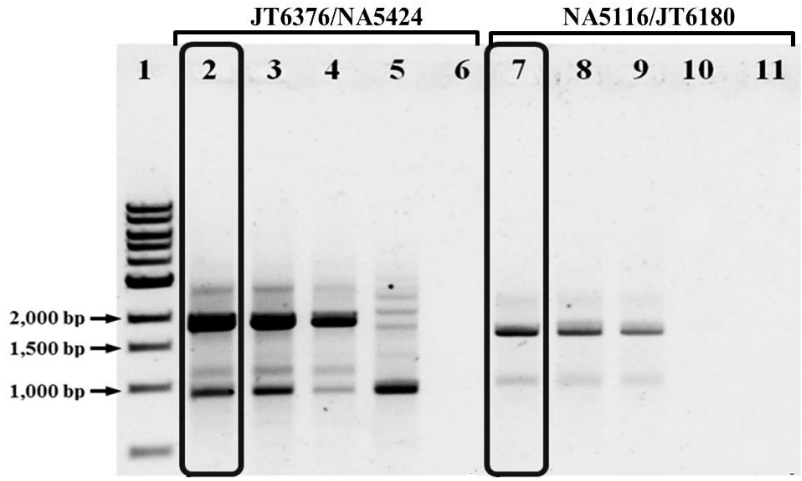

Figure 3.8.1 Electrophoretic separation of PCR analyses of the K96243*ΔbapA*_2 clones. The primer pairs JT6376/NA5424 (left) and NA5116/JT6180 (right) were used to verify the disruption of *bapA* by the insertion of the tetracycline resistance gene *tetA*(C). Lane 1, DNA size markers (bp); lane 2 to 3 and 7 to 8, genomic DNA from two potential K96243*ΔbapA*_2 clones; lane 4 and 9, genomic DNA from the original K96243*ΔbapA* strain; lane 5 and 10, genomic DNA from the wild-type strain; lane 6 and 11, no DNA controls. The clone indicated by the black boxes in lane 2 and 7 was selected for further experiments.

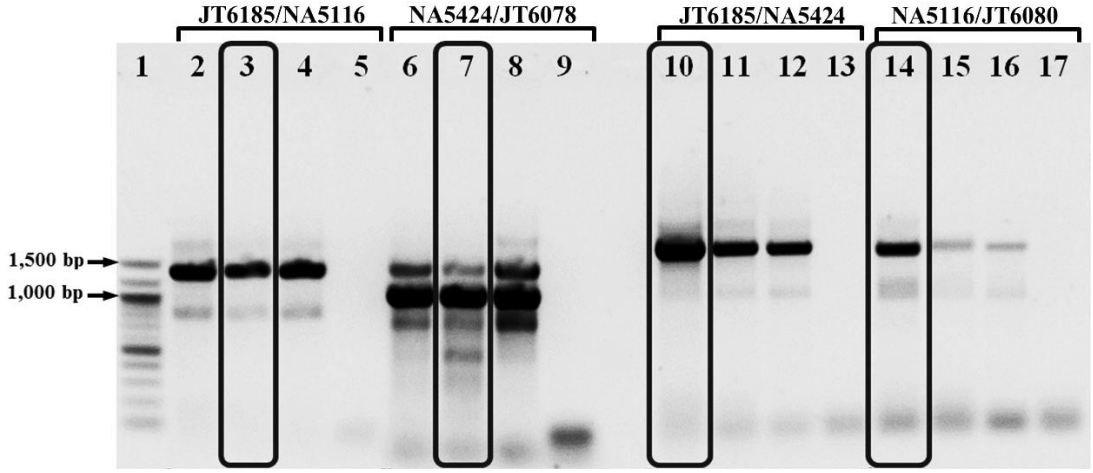

Figure 3.8.2 Electrophoretic separation of PCR analyses of the K96243*ΔbapB*_2 (lane 2 to 9) and *ΔbapC*_2 (lane 10 to 17) clones. The primers, as indicated, were used to verify the disruption of *bapB* and *bapC* by the insertion of the tetracycline resistance gene *tetA*(C). Lane 1, DNA size markers (bp); lane 2 to 3 and lane 6 to 7, genomic DNA from two potential K96243*ΔbapB*_2 clones; lane 4 and 8, genomic DNA from the original K96243*ΔbapB* strain; lane 5 and 9, genomic DNA from the wild-type strain; lane 10 to11 and lane 14 to 15, genomic DNA from two potential K96243*ΔbapC*_2 clones; lane 12 and 16, genomic DNA from the original K96243*ΔbapC* strain; lane 13 and 17, genomic DNA from the wild-type strain. The clones indicated by the black boxes in lane 3 and 7, and lane 10 and 14 were selected for further experiments.

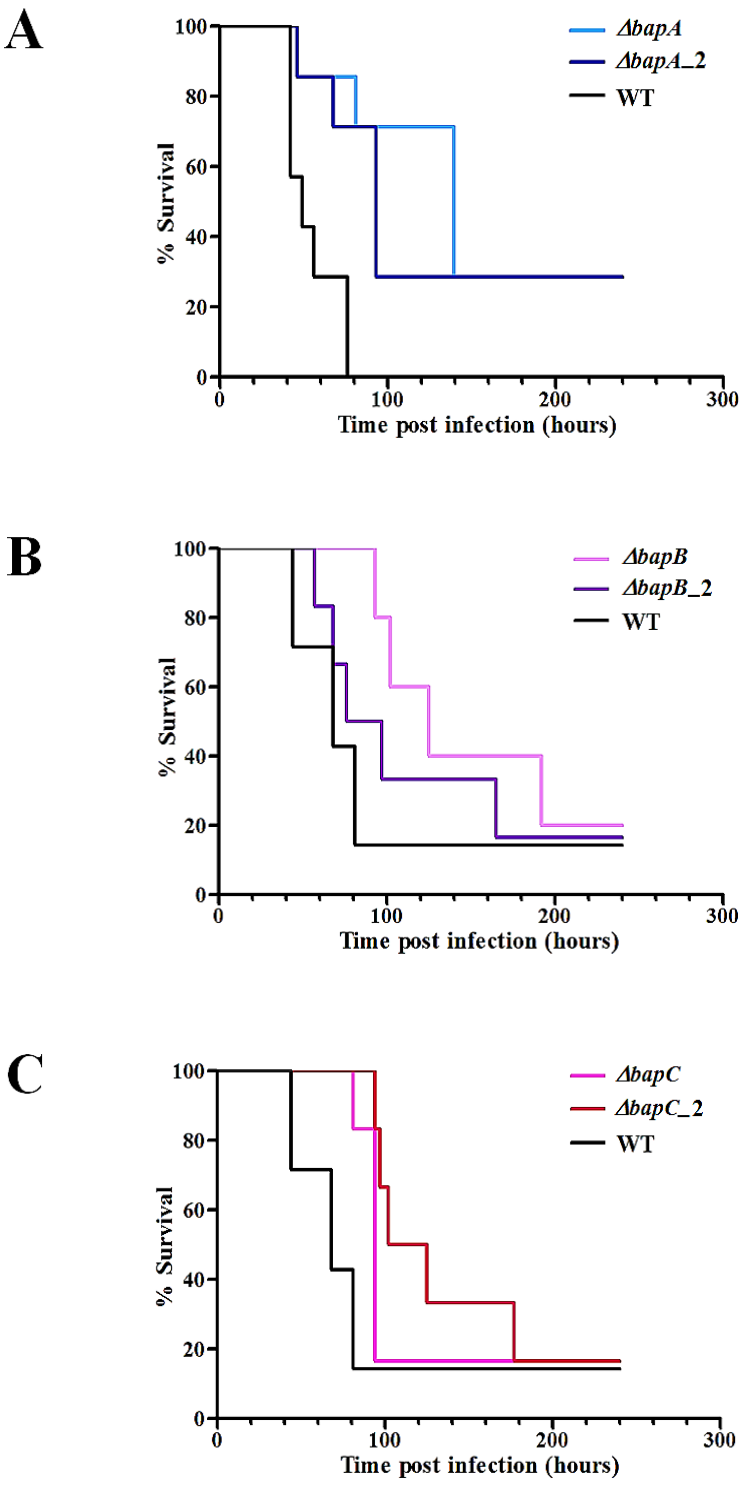

Figure 3.8.3 Kaplan-Meier survival curves of BALB/c mice infected intranasally with 10^5 CFU of the K96243*ΔbapA* (A), *ΔbapB* (B), *ΔbapC* (C) or the wild-type strain. There was a significant difference in the time to death for mice infected with the *bapA* mutant and the K96243*ΔbapA*_2 strains in comparison to the wild-type with ($P < 0.05$). Mice infected with other mutants showed no difference in the time to death compared to mice infected the wild-type ($P > 0.05$). *ΔbapA* denotes the K96243*ΔbapA* strain; *ΔbapA*_2 denotes the K96243*ΔbapA*_2 strain; *ΔbapB* denotes the K96243*ΔbapB* strain; *ΔbapB*_2 denotes the K96243*ΔbapB*_2 strain; *ΔbapC* denotes the K96243*ΔbapC* strain; *ΔbapC*_2 denotes the K96243*ΔbapC*_2 strain; WT denotes the wild-type strain.

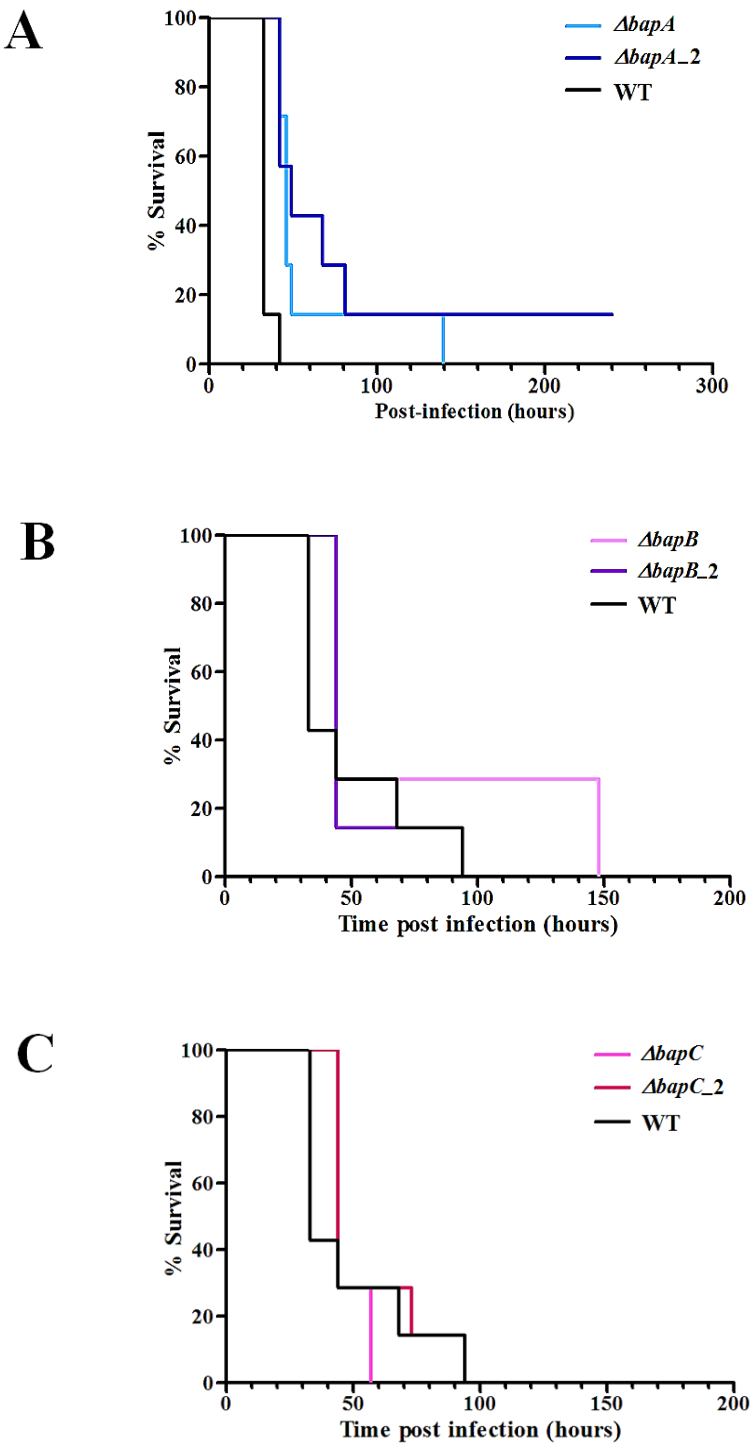

Figure 3.8.4 Kaplan-Meier survival curves of BALB/c mice infected intranasally with 10^7 CFU of the K96243*ΔbapA* (A), *ΔbapB* (B), *ΔbapC* (C) or the wild-type strain. There was a significant difference in the time to death for mice infected with the *bapA* mutant and the K96243*ΔbapA*_2 strains in comparison to the wild-type with ($P < 0.05$). Mice infected with other mutants showed no difference in the time to death compared to mice infected the wild-type ($P > 0.05$). *ΔbapA* denotes the K96243*ΔbapA* strain; *ΔbapA*_2 denotes the K96243*ΔbapA*_2 strain; *ΔbapB* denotes the K96243*ΔbapB* strain; *ΔbapB*_2 denotes the K96243*ΔbapB*_2 strain; *ΔbapC* denotes the K96243*ΔbapC* strain; *ΔbapC*_2 denotes the K96243*ΔbapC*_2 strain; WT denotes the wild-type strain.

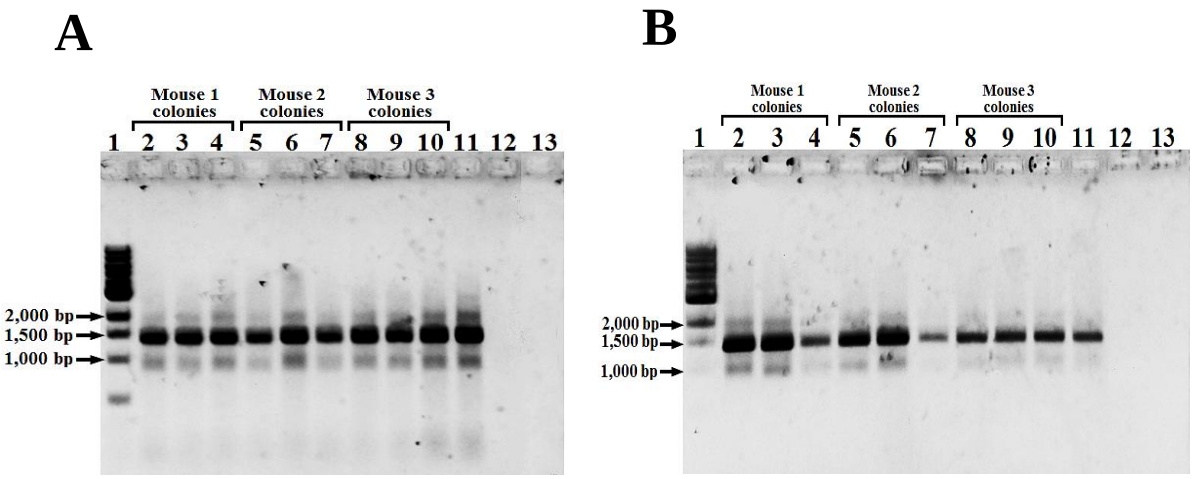

Figure 3.8.5 Electrophoretic separation of representative PCR analyses of colonies recovered from mice infected with 10^5 CFU of the K96243*ΔbapB*_2 strain (A) or the original K96243*ΔbapB* (B) strain using the primer pair JT6185/NA5116. Lane 1, DNA size markers (bp); lane 2 to 10, PCR using genomic DNA from colonies recovered from three mice (3 colonies per mouse); lane 11, the original K96243*ΔbapB* as the positive control; lane 12, the wild-type strain; lane 13, no DNA control.

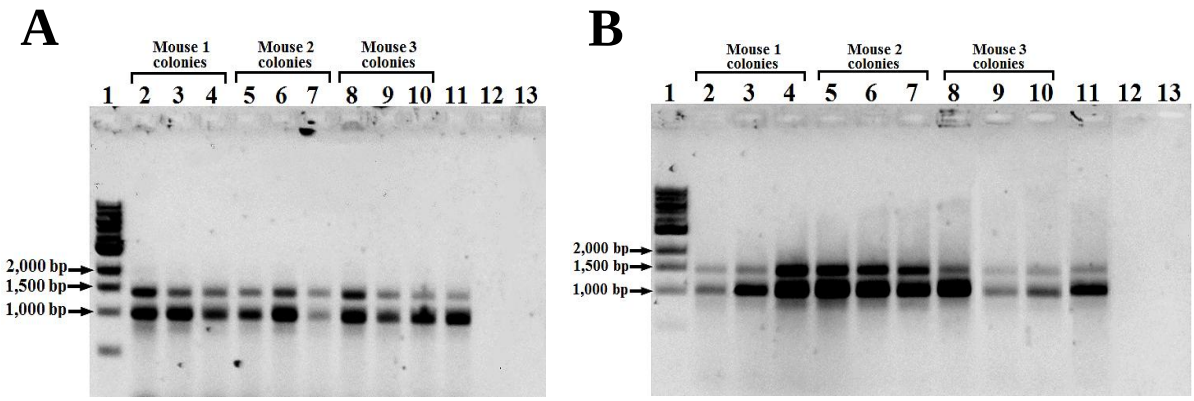

Figure 3.8.6 Electrophoretic separation of representative PCR analyses of colonies recovered from mice infected with 10^5 CFU of the K96243*ΔbapB*_2 strain (A) or the original K96243*ΔbapB* (B) strain using the primer pair NA5424/JT6078. Lane 1, DNA size markers (bp); lane 2 to 10, PCR using genomic DNA from colonies recovered from three mice (3 colonies per mouse); lane 11, the original K96243*ΔbapB* strain as the positive control; lane 12, the wild-type strain; lane 13, no DNA control.

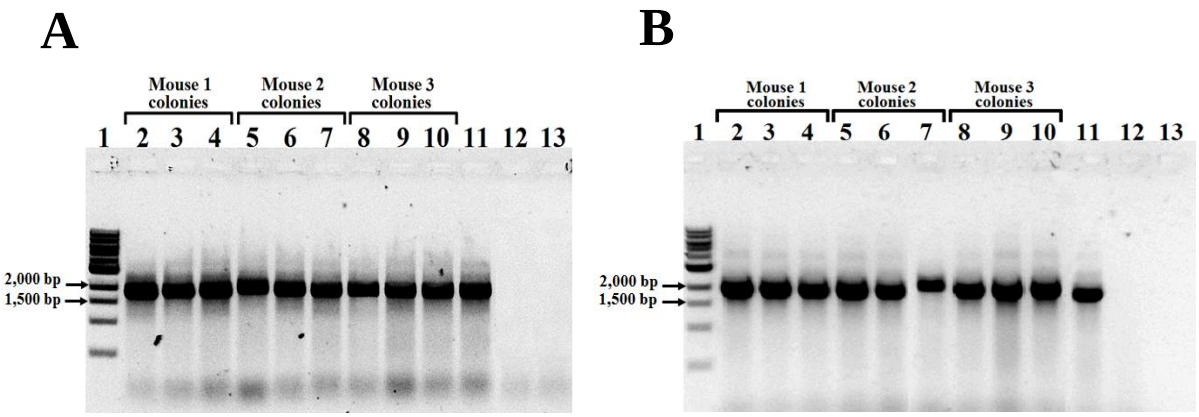

Figure 3.8.7 Electrophoretic separation of representative PCR analyses of colonies recovered from mice infected with 10^5 CFU of the K96243*ΔbapC*_2 strain (A) or the original K96243*ΔbapC* (B) strain using the primer pair JT6185/NA5424. Lane 1, DNA size markers (bp); lane 2 to 10, PCR using genomic DNA from colonies recovered from three mice (3 colonies per mouse); lane 11, the original K96243*ΔbapC* strain as the positive control; lane 12, the wild-type strain; lane 13, no DNA control.

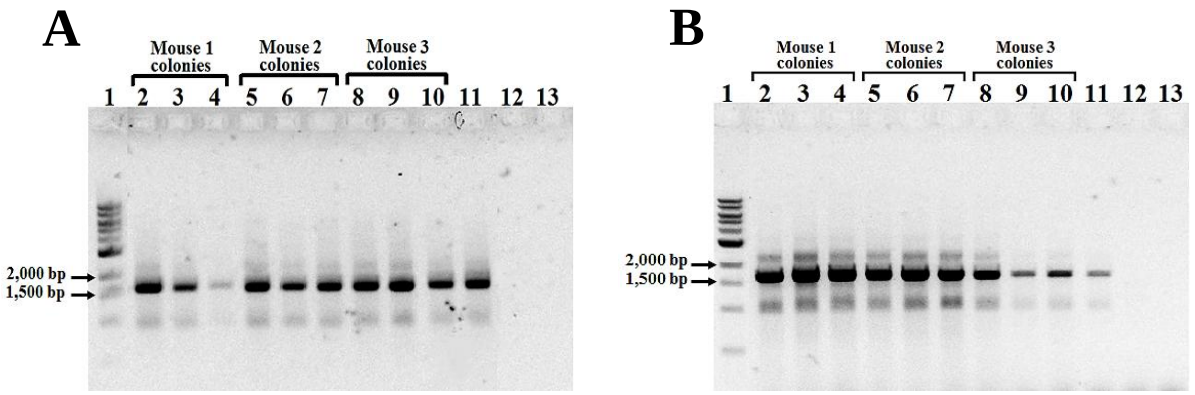

Figure 3.8.8 Electrophoretic separation of representative PCR analyses of colonies recovered from mice infected with 10^5 CFU of the K96243*ΔbapC*_2 strain (A) or the original K96243*ΔbapC* (B) strain using the primer pair NA5116/JT6080. Lane 1, DNA size markers (bp); lane 2 to 10, PCR using genomic DNA from colonies recovered from three mice (3 colonies per mouse); lane 11, the original K96243*ΔbapC* as the positive control; lane 12, the wild-type strain; lane 13, no DNA control.

Chapter 4

In vitro analyses of BapA, BapB and BapC

Chapter 4: *In vitro* analyses of BapA, BapB and BapC

The TTSS3 plays an important role in *B. pseudomallei* pathogenesis, specifically intracellular survival and replication, and escape from the host endosome/phagosome (French *et al.*, 2011). Upon activation of the TTSS3, the needle-like apparatus directly injects bacterial effector proteins into the host cell; these effectors modulate host cell function (Mota & Cornelis, 2005; Sun & Gan, 2010). So far, the proteins BopE, BopA and BopC are the only characterised effectors of *B. pseudomallei* and are known to play important roles in phagosome escape and intracellular survival (Cullinane *et al.*, 2008; Gong *et al.*, 2011; Muangman *et al.*, 2011). Given that *bapA*, *bapB* and *bapC* are located in the same locus as *bopE*, *bopA* and *bopC*, indeed *bapC* is adjacent to *bopE* (*Chapter 1, Figure 1.4.1*), *bapA*, *bapB* and *bapC* are likely to be associated with TTSS3 function and may encode novel effector proteins. In this chapter, the protein products of these three genes were characterised using a range of *in vitro* phenotypic assays, specific for previous known TTSS3 functions (Cullinane *et al.*, 2008; D'Cruze *et al.*, 2011; Gong *et al.*, 2011; Jones *et al.*, 1996; Kespichayawattana *et al.*, 2000; Muangsombut *et al.*, 2008; Stevens *et al.*, 2003; Stevens *et al.*, 2002). The experiments in this chapter were carried out with the original K96243*ΔbapA*, K96243*ΔbapB*, K96243*ΔbapC* and K96243*ΔbapBC* strains. The experiments were performed prior to generation of the independently derived mutant strains.

4.1 BapA, BapB and BapC are not essential for bacterial invasion of the human lung epithelial cell line A549

Inhalation is a major route of infection by *B. pseudomallei* and the bacterium is able to invade respiratory epithelial cells (Jones *et al.*, 1996; Muangman *et al.*, 2011; Muangsombut *et al.*, 2008; Stevens *et al.*, 2002; Suparak *et al.*, 2005). In addition, bioinformatic analysis of BapC indicated that it may function as a cell invasion protein. Thus, the lung epithelial cell line A549 was used to investigate the ability of the K96243*ΔbapA*, K96243*ΔbapB* and K96243*ΔbapC* strains to invade epithelial cells (*Chapter 2.17*). To ensure that the antibiotic combinations used for killing extracellular bacteria in all the *in vitro* assays were appropriate, the minimum bactericidal concentration (MBC) for each antibiotic was determined using the broth microdilution technique (*Chapter 2.11*). The MBC of kanamycin in combination with ceftazidime against all the mutants and the wild-type *B. pseudomallei* was 900 and 90 μg/mL, respectively (data not shown). Thus, this antibiotic combination was used for all further experiments.

The A549 monolayers were infected with each of the mutants, the wild-type strain or *E. coli* DH5α, as the negative control. After allowing the invasion to proceed for 2 h, extracellular bacteria were killed by antibiotic treatment and intracellular bacteria were liberated with Triton X-100 and enumerated. The average number of intracellular bacteria recovered from infection with the wild-type strain was 4.6 x 10^4 CFU/mL, whereas no bacterial colonies were recovered from the *E. coli* DH5α infected cells, indicating clearly that the wild-type *B. pseudomallei* can invade A549 cells (*Figure 4.1.1*; $P = 0.0029$). The average number of intracellular bacteria recovered from K96243*ΔbapA*, *ΔbapB*, *ΔbapC* and *ΔbapBC* strain-infected A549 monolayers was 1.7, 2.5, 3.0 and 2.6 x 10^4 CFU/mL, respectively. Among the four mutant strains, it is important to note that the K96243*ΔbapA* exhibited a 2.7-fold reduction of intracellular bacteria compared to the wild-type. However, due to the variability between experiments there was no statistical difference to that observed for the wild-type strain (*Figure 4.1.1*; $P > 0.05$). Thus, it is unlikely that the TTSS3 genes *bapB* and *bapC* play a role in invasion of non-phagocytic cells. However, *bapA* may play a minor role in this function and further intracellular survival experiments may be warranted to elaborate this possible role.

4.2 BapA, BapB and BapC are not required for intracellular survival and replication of *B. pseudomallei* in the murine macrophage-like cell line RAW264.7

Given that TTSS3 plays a role in the intracellular survival and replication of *B. pseudomallei* (Burtnick *et al.*, 2008; Stevens *et al.*, 2002), it was hypothesised that the *bap* genes might also be specifically involved in this function. To test this hypothesis, the wild-type and mutant strains were used to infect macrophage-like RAW264.7 cells for 2, 4 or 6 h. There was a significant increase in the number of wild-type, K96243*ΔbapB* and *ΔbapBC* bacteria recovered at 4 h p.i. compared to the number recovered at 2 h p.i. (*Figure 4.2.1;* $P < 0.05$). Similarly, the number of these strains recovered at 6 h p.i. was significantly greater than that observed at 2 h p.i. (*Figure 4.2.1;* $P < 0.05$). However, the K96243*ΔbapA* and *ΔbapC* strains did not show an increase in the number of intracellular bacteria either from 2 to 4 h p.i. or from 2 to 6 h p.i. (*Figure 4.2.1;* $P > 0.05$). Moreover, between 4 and 6 h p.i. the number of K96243*ΔbapA* and *ΔbapC* strains showed only a marginal increase whereas the K96243*ΔbapB* and *ΔbapBC* strains and the wild-type showed approximately a two-fold increase. Nevertheless, at 4 and 6 h p.i., there was no statistically significant difference in the number of intracellular bacteria recovered from the monolayers infected with the mutants compared to those infected with the wild-type. Therefore,

bapA, *bapB* and *bapC* do not appear to be required for intracellular survival, or *bapA* and *bapC* may indirectly be involved in this function.

4.3 BapA, BapB and BapC do not play a role in bacterial escape from host phagosome and actin-based motility

After internalisation, *B. pseudomallei* uses a variety of mechanisms to promote survival, including escape from host endosomal compartments into the host cytoplasm for replication, and polymerisation of host actin filaments for bacterial actin-mediated motility (Allwood *et al.*, 2011; Galyov *et al.*, 2010; Stevens *et al.*, 2006). In addition, *B. pseudomallei* induces host cell fusion and multinucleated giant cell (MNGC) formation, thereby facilitating cell-to-cell spread without triggering any host immune response (Kespichayawattana *et al.*, 2000). The TTSS3 is necessary for endosomal escape (Muangsombut *et al.*, 2008) and thus also necessary for actin tail formation and MNGC formation (Burtnick *et al.*, 2008; French *et al.*, 2011; Suparak *et al.*, 2005). The genes *bipD* and *bopA*, adjacent to *bapA*, *bapB* and *bapC*, have been shown to play a role in bacterial avoidance of killing by LC3-associated phagocytosis (LAP) and promoting bacterial escape from the phagosome (Cullinane *et al.*, 2008; Gong *et al.*, 2011). Furthermore, *B. pseudomallei bipD* and *bsaZ* mutants are unable to form host membrane protrusions and actin tails (Stevens *et al.*, 2002) although these phenotypes are likely due to reduced phagosomal escape and lack of access to the cytoplasm. Thus, it was hypothesised that the TTSS3 genes *bapA*, *bapB* and *bapC* might also be involved in these functions. To test this hypothesis, a role in bacterial avoidance of LAP and/or susceptibility to canonical autophagy was determined by measuring bacterial co-localisation with LC3-GFP, a marker specific for LC3-associated phagocytosis (LAP) and canonical autophagy. Murine macrophage-like RAW264.7 cells stably expressing LC3-GFP were infected with the K96243*ΔbapA*, *ΔbapB*, *ΔbapC*, *ΔbapBC* or the wild-type strain as described previously (*Chapter 2.19.1*). Infected monolayers were fixed, stained and analysed for co-localisation of the bacteria with LC3-GFP (*Figure 4.3.1A*). Over the 6 h of infection, the wild-type strain showed a decrease in percentage of bacterial co-localisation with LC3-GFP puncta from 8% at 2 h p.i. to 3% at 6 h p.i. (*Figure 4.3.1B*), confirming that the wild-type strain can escape host phagosomes/autophagosomes. Similar to the wild-type, each of the mutants exhibited a decrease in percentage of bacterial co-localisation with LC3-GFP from 2 to 6 h p.i. (*Figure 4.3.1B*), indicating that each of the mutants was able to escape into the host cytoplasm. Therefore, BapA, BapB and BapC do not appear to play a role in endosomal escape of avoidance of LAP or canonical autophagy. At 6 h p.i., MNGC formation was also observed in RAW264.7 cells infected with each of the mutants or the wild-type strain (*Figure 4.3.2*). This

indicates that *bapA*, *bapB* and *bapC* are not required for host cell fusion and MNGC formation by *B. pseudomallei*. To further investigate any association of BapA, BapB and BapC with bacterial actin-based motility, RAW264.7 cells were infected with each of the mutants or the wild-type strain for 2, 4 and 6 h, and actin filaments of infected cells labelled with Alexa Fluor® 647-conjugated phalloidin (*Chapter 2.19.2*). At 6 h p.i., each of the mutant strains was able to form actin tails similar to the wild-type strain (*Figure 4.3.3*). Thus, it was concluded that *bapA*, *bapB* and *bapC* do not play a role in actin-mediated motility of *B. pseudomallei*.

4.4 Influence of BapA, BapB and BapC on host innate immune response

B. pseudomallei possesses a number of strategies for altering host immune responses during infection, including suppression of nuclear factor-kappa B (NF-κB), a nuclear transcription factor controlling the expression of downstream molecules including cytokines and inducible nitric oxide synthase (iNOS) (Breitbach *et al.*, 2006; Ulett *et al.*, 2005; Wiersinga & van der Poll, 2009). The TTSS molecules of pathogenic bacteria have been shown to be both targets of and modulators of the host innate immune responses (Miao & Warren, 2010; Tan *et al.*, 2010). The *B. pseudomallei* TTSS3 has been suggested to function in regulating the secretion of TssM, which is an important virulence factor involved in NF-κB suppression (Tan *et al.*, 2010). It is important to note that the kinetics of IL-6 and TNF-α produced by RAW264.7 cells infected with *B. pseudomallei* has been previously shown to be *bsaZ*-independent (Burtnick *et al.*, 2008). Thus, in this study, *bapA*, *bapB* and *bapC* were investigated a possible role in modulating the host immune response. To test this hypothesis, the production of two essential cytokines, tumour necrosis factor-alpha (TNF-α) and interleukin-6 (IL-6), which are produced during early and late stage responses to *B. pseudomallei* infection (Ulett *et al.*, 2000), were analysed following infection of RAW264.7 cells with either the mutant or wild-type strains. The levels of each cytokine secreted from infected cells at 2, 4 and 6 h p.i. were determined by ELISA (*Figure 4.4.1*). At 2 h p.i., the amount of TNF-α secreted from cells infected with the K96243*ΔbapB* or K96243*ΔbapC* strain was increased approximately two-fold higher than that secreted from cells infected with the wild-type strain ($P < 0.05$). However, cells infected with the K96243*ΔbapA* strain showed no difference in TNF-α secretion from cells infected with the wild-type strain ($P > 0.05$). At 4 h p.i., only cells infected with the K96243*ΔbapBC* strain showed a significant decrease in TNF-α secretion (2-fold) compared to cells infected with the wild-type strain ($P < 0.05$), whereas cells infected with each of other mutant strains showed no significant difference ($P > 0.05$). Similar to the result observed at 4 h p.i., at 6 h p.i., cells infected with the K96243*ΔbapBC* strain again showed a decrease (2-fold) in TNF-α secretion compared to cells

infected with the wild-type strain ($P < 0.001$), whereas cells infected with each of the other mutant strains showed similar TNF-α secretion to cells infected with the wild-type strain ($P > 0.05$). These data indicate that BapA does not play a role in stimulation of TNF-α from RAW264.7 cells. However, they suggest that the combination of BapB and BapC may play a role early in infection and their combined loss results in decreased secretion levels at 4 and 6 h p.i.

The pattern of IL-6 secretion from cells infected with each of the mutants or the wild-type strain was also assessed (*Figure 4.4.2*). There was no difference in the amount of IL-6 secretion from cells infected with any of the mutant strains or uninfected cells at 2 h p.i. ($P > 0.05$). However, at 4 h p.i., cells infected with the K96243*ΔbapBC* strain exhibited an approximately two-fold lower decrease in IL-6 secretion than those infected with the wild-type strain ($P < 0.05$) whereas cells infected with each of the other mutants showed similar IL-6 secretion to cells infected with the wild-type strain ($P > 0.05$). At 6 h p.i., the amount of IL-6 secreted from cells infected with the K96243*ΔbapA*, *ΔbapB* or wild-type strain was similar ($P > 0.05$). However, cells infected with the K96243*ΔbapBC* strain again exhibited a decrease of approximately two-fold in IL-6 secretion compared to those infected with the wild-type strain ($P < 0.05$) and the K96243*ΔbapC* strain showed increased IL-6 production ($P < 0.05$). From 2 to 4 h p.i. ($P < 0.05$), a moderate increase of approximately five- to eight-fold was observed in the amount of IL-6 secreted from cells infected with the wild-type, K96243*ΔbapA*, *ΔbapB* or *ΔbapC* strain while cells infected with the K96243*ΔbapBC* strain showed a much smaller increase. However, a dramatic increase in IL-6 production was observed between 4 and 6 h p.i. ($P < 0.001$) in all cells infected with the mutants or wild-type strain. Uninfected cells, as the negative control, showed no significant difference in IL-6 production from 2 to 6 h p.i. ($P > 0.05$). Taken together, the alteration in secretion of both cytokines TNF-α and IL-6 observed in cells infected with the K96243*ΔbapB*, K96243*ΔbapC* or K96243*ΔbapBC* strain suggests that combined inactivation of *bapB* and *bapC* results in reduced stimulation of host innate immune response. The gene *bapA*, however, does not seem to play a major role in inducing host immune response as the cytokine secretion from cells infected with this mutant was indistinguishable from the wild-type strain at all time points.

4.5 Stimulation of RAW264.7 macrophage-like cell antibacterial activity with interferon-gamma (IFN-γ)

The pro-inflammatory cytokine IFN-γ is associated with enhancing phagocytic and bactericidal activity of macrophages (Ellis & Beaman, 2004; Herbst *et al.*, 2011; Schroder *et al.*, 2004). During the early stage of *B. pseudomallei* infection, this cytokine appears to play an important role in inhibiting bacterial growth and enhancing the bactericidal activity of macrophages (Breitbach *et al.*, 2006; Utaisincharoen *et al.*, 2003; Utaisincharoen *et al.*, 2004). IFN-γ can also stimulate autophagosome formation, thereby enhancing the ability to trap the bacteria within autophagosomal vacuoles during infection (Cullinane *et al.*, 2008). Thus, colocalisation of the K96243*ΔbapA*, K96243*ΔbapB*, K96243*ΔbapC* and K96243*ΔbapBC* strains, and the wild-type strain with LC3-GFP following IFN-γ stimulation was assessed. Three-hour IFN-γ treatment of RAW264.7 cells before infection resulted in the highest bactericidal activity (data not shown). Therefore, these conditions were used to activate mouse macrophage-like RAW264.7 cells.

4.5.1 Intracellular survival of the K96243*ΔbapA*, *ΔbapB*, *ΔbapC* and *ΔbapBC* strains within IFN-γ prestimulated RAW264.7 cells

IFN-γ prestimulated RAW264.7 macrophage-like cells were infected with each of the mutants or the wild-type strain. Intracellular bacteria were enumerated at 2, 4 and 6 h p.i as described previously. The infecting doses of the mutant and the wild-type strains were similar. Cells infected with the K96243*ΔbapC* strain at 2 h, 4 h and 6 h p.i. exhibited a decrease of approximately four-fold ($P < 0.05$), three-fold ($P < 0.05$) and eleven-fold ($P < 0.0001$) in the recovered CFU numbers compared to those infected with the wild-type strain (*Figure 4.5.1*). However, cells infected with each of other mutant strains showed no significant difference in the CFU numbers from those infected with the wild-type strain at all time points ($P > 0.05$). Although the number of wild-type bacteria continued to increase between 4 and 6 h p.i., while the mutant strains did not, except for the K96243*ΔbapC* strain, there was no statistical difference in the number of intracellular bacteria recovered from RAW264.7 cells infected with each of the mutants compared to those infected with the wild-type strain at all time points. These data suggest that BapC plays a role in intracellular survival and replication in IFN-γ stimulated cells while BapA and BapB are not required for this function.

4.5.2 Prestimulation of RAW264.7 cells with IFN-γ promotes an increase in bacterial co-localisation with LC3-GFP

The proinflammatory cytokine IFN-γ functions as an autophagy inducer by, at least in part, enhancing LC3 production, supporting an important role of this cytokine in eliminating intracellular bacteria (Alonso *et al.*, 2007; Cullinane *et al.*, 2008). Indeed, IFN-γ can stimulate

bacterial co-localisation with LC3-GFP (Cullinane *et al.*, 2008), and recent evidence suggests that this is due to LC3 recruitment to *B. pseudomallei*-containing phagosomes and plays an important role in killing of intracellular *B. pseudomallei* (Gong *et al.*, 2011). The TTSS3 proteins BipD and BopA have been demonstrated to delay this LAP process (Gong *et al.*, 2011). Thus, in this study, IFN-γ was used to enhance LC3-GFP formation in murine macrophage-like RAW264.7 cells. The IFN-γ-pretreated cells were infected with the wild-type or mutant strains, and the co-localisation of intracellular bacteria with LC3-GFP was then determined by confocal laser scanning microscopy. The localisation of bacteira with LC3 at all time points examined was higher than observed in RAW264.7 cells without IFN-γ prestimulation, confirming that IFN-γ induces increased bacterial localisation with LC3, probably through increased LAP (compare *Figure 4.5.2* with *Figure 4.3.1*). However, the level of bacterial co-localisation with GFP-LC3 at each of the time points was indistinguishable across all strains, indicating that these mutants retain the ability to evade host LAP and/or canonical autophagy, even under IFN-γ activation (*Figure 4.5.2*). Furthermore, supporting the previous results (see *Chapter 4.3, Figure 4.3.3*), all of the mutant and wild-type strains formed actin tails, confirming that they were able to escape from host phagosome and move by actin-mediated motility even in the IFN-γ-pretreated cells (data not shown). Finally, all strains were still able to form MNGCs by 6 h p.i., indicating that the mutants retain the ability to induce host cell fusion and cell-to-cell spread, even following IFN-γ stimulation (data not shown).

4.5.3 Cytokine secretion from IFN-γ pre-treated RAW264.7 macrophage-like cells following infection by the K96243*ΔbapA, ΔbapB, ΔbapC* or *ΔbapBC* strain

B. pseudomallei is capable of suppressing the host immune responses and therefore reducing the clearance of the bacteria. The proinflammatory cytokine IFN-γ, however, can activate bactericidal activity of phagocytic cells. Thus, to examine whether BapA, BapB or BapC were involved in the host immune suppression following IFN-γ stimulation, the production of TNF-α and IL-6 was analysed from IFN-γ-stimulated RAW264.7 cells that had been infected with the wild-type or mutant strains. The amounts of TNF-α (pg/mL) secreted at 2, 4 and 6 h p.i. were analysed by ELISA (*Figure 4.5.3*). All strains showed increased levels of TNF-α secretion, approximately 3- to 5-fold, at 4 h p.i. compared to 2 h p.i. ($P < 0.05$), but there was no difference in TNF-α secretion for any of the mutant strains in comparison with the wild-type strain ($P > 0.05$). At 4 h and 6 h p.i. again there was no difference in TNF-α secretion from cells infected

with any of the mutants or the wild-type strain ($P > 0.05$). These data may suggest that BapA, BapB and/or BapC do not have a role in TNF-α secretion following IFN-γ.

In contrast to TNF-α secretion, the expression of IL-6 revealed a different pattern (*Figure 4.5.4*). At 4 h p.i., the K96243*ΔbapA*, K96243*ΔbapC* and K96243*ΔbapBC* strain-infected, IFN-γ-stimulated, RAW264.7 cells displayed a slight decrease in IL-6 production compared to the cells infected with the wild type ($P < 0.05$). However, there was no difference in the level of IL-6 secretion from cells infected with the wild-type strain from that of cells infected with the K96243*ΔbapB* strain ($P > 0.05$). There was no significant difference in IL-6 secretion from IFN-γ-stimulated cells infected with any of the mutant or the wild-type strain at 6 h p.i. ($P > 0.05$). All strains showed a moderate increase in levels of IL-6 production (approximately 6- to 12-fold) at 4 h p.i. compared to 2 h p.i. ($P < 0.05$) and a more substantial increase in IL-6 secretion at 6 h p.i. compared to 4 h p.i. (approximately 10- to 20-fold; $P < 0.05$). When compared to the data at 4 h p.i. obtained from untreated RAW264.7 cells (*Chapter 4.4*), IFN-γ-stimulated RAW264.7 cells infected with the wild-type ($P < 0.001$), K96243*ΔbapA*, *ΔbapC* or *ΔbapBC* ($P < 0.05$) strain produced more IL-6, at least a two-fold increase, than non IFN-γ-prestimulated cells infected with any of these strains. However, there was no statistically significant difference between IFN-γ-pretreated and untreated cells infected with the K96243*ΔbapB* strain ($P > 0.05$).

4.6 Discussion

The TTSS3 of *B. pseudomallei* is essential for intracellular survival and persistence within the host. To understand the molecular mechanism(s) underlying the TTSS3 functions, it is essential to identify TTSS3 effector molecules and characterise their roles in modulation of host cell functions. In this chapter, the protein products of the TTSS3 genes *bapA*, *bapB* and *bapC* were investigated using several *in vitro* assays specific for known TTSS3 functions.

4.6.1 BapA, BapB or BapC are not involved in *B. pseudomallei* invasion of cultured A549 cells

To be able to cause infection, *B. pseudomallei* has evolved mechanisms for invading and surviving within many different host cell types (Jones *et al.*, 1996; Wiersinga *et al.*, 2006). The TTSS3 is a key mechanism required for full virulence of this bacterium as it plays a role in bacterial invasion, survival and replication within host cells, bacterial cell-to-cell spread and escape from host endosomes (Burtnick *et al.*, 2008; D'Cruze *et al.*, 2011; French *et al.*, 2011; Gong *et al.*, 2011; Muangman *et al.*, 2011; Suparak *et al.*, 2005). Two TTSS3 effectors BopE

and BipD of *B. pseudomallei* are involved in promoting bacterial internalisation, survival and replication within the host cells, and also bacterial escape into the host cytoplasm (Stevens *et al.*, 2002). Suparak *et al.* (2005) demonstrated a role for the TTSS3 translocon BipB in bacterial invasion of a human lung epithelial cell line A549. Recently, another *B. pseudomallei* TTSS3 effector molecule BopC, was shown to play a role in invasion of A549 cells (Muangman *et al.*, 2011). Furthermore, analysis of the gene expression profile of *B. pseudomallei* following infection of the human macrophage-like cell line U937 supported an involvement of the TTSS3 genes in early stages of the intracellular life cycle of this bacterium, including bacterial cell invasion (Chieng *et al.*, 2012). Thus, it was hypothesised that *bapA, bapB* and *bapC*, located in the TTSS3 locus, may be involved in cell invasion. To investigate this hypothesis, the K96243*ΔbapA*, *ΔbapB*, *ΔbapC* and *ΔbapBC* strains were assessed for their ability to invade A549 cells. However, the K96243*ΔbapB*, *ΔbapC* and *ΔbapBC* strains were still able to invade A549 cells as efficiently as the wild-type strain, whereas invasion of the K96243*ΔbapA* strain was approximately 40% of the level of the wild-type; however, this difference was not statistically significant. Further experiments may be warranted to confirm or exclude this effect of BapA. Previous studies done by Stevens *et al.* (2003) and Muangman *et al.* (2011) reported reduced bacterial invasion to some extent when *bipD* and *bsaQ*, respectively, have been inactivated. These findings are similar to what was observed in the K96243*ΔbapA* strain, suggesting a similar pattern of the TTSS3 genes with regard to bacterial invasion even though it is important to state that *bipD* and *bsaQ* encode TTSS3 translocon and structural components respectively, whereas *bapA* is predicted to encode a putative effector. This indicates that *bapB* and *bapC* are not required for bacterial invasion whereas *bapA* may play a minor role.

Given that the TTSS of Gram-negative pathogens, such as *Salmonella*, *Shigella* and *B. pseudomallei* share significant similarities (Büttner, 2012; Tampakaki *et al.*, 2004), the functions of individual components should be comparable. The *Salmonella* TTSS protein IagB shares approximately 37% identity with BapC of *B. pseudomallei* and both contain a lytic transglycosylase (LT) domain (Koraimann, 2003); thus, it is possible that they play a similar role. However, the *Salmonella iagB* mutant showed a significant reduction in invasion efficiency in cultured epithelial cells (Blackburn & Clarke, 2001; Koraimann, 2003; Miras *et al.*, 1995; Zahrl *et al.*, 2005), whereas the K96243*ΔbapC* strain retained the ability to invade non-phagocytic cells. Such differences may be due to different survival strategies after internalisation of *B. pseudomallei* and *Salmonella* (Hybiske & Stephens, 2008; Justice *et al.*, 2008). After being internalised, *B. pseudomallei* employs, at least in part, the TTSS3 for escaping from host

endosomal vacuoles into the host cytoplasm (Burtnick *et al.*, 2008; Gong *et al.*, 2011). *Salmonella*, in contrast, employs a second TTSS, named the *Salmonella* Pathogenicity Island 2 (SPI2), for biogenesis and maintenance of a modified host endosome called *Salmonella* Containing Vacuole (SCV) (Ibarra & Steele-Mortimer, 2009). In addition, *B. pseudomallei* can suppress host innate immunity by stimulating less host reactive oxygen and nitrogen species which consequently allows the bacteria to persist within the host (Utaisincharoen *et al.*, 2001). Similarly, the *Salmonella* SPI2 is required for suppression of host antimicrobial activity (Eriksson *et al.*, 2003; Ibarra & Steele-Mortimer, 2009). Therefore, the role of their TTSSs with regard to bacterial pathogenesis has some clear differences. Importantly, *B. pseudomallei* has a putative BapC paralogue BPSL0006 protein encoded on its genome, whereas *Salmonella* has only one. Thus, these BapC proteins may be functionally redundant, and inactivation of a single *bapC* may be insufficient to show a reduction in invasion phenotype. Another possibility arises from the recent report that bacterial invasion can occur independently of the TTSS3 activity (French *et al.*, 2011). This may support the data obtained in this study. BapC also shares 36% identity with the *S. flexneri* TTSS protein IpgF. As observed here following inactivation of the *B. pseudomallei bapC*, inactivation of the *S. flexneri ipgF* showed similar invasion efficiency to the wild-type strain (Allaoui *et al.*, 1993; Zahrl *et al.*, 2005), indicating that IpgF does not play a role in *S. flexneri* invasion. Indeed, *S. flexneri* and *B. pseudomallei* appear to have similar strategies for escaping from host endosomal vacuoles during infection (Hybiske & Stephens, 2008; Johnson *et al.*, 2007; Ray *et al.*, 2009). This also suggests a similarity in the TTSS mechanisms of both pathogens. As proteins with an LT domain are generally involved in cleavage of β-1,4-glycosidic bonds of bacterial peptidoglycan, further experiments should focus on determining the LT enzyme activity of *Salmonella* IagB, *S. flexneri* IpgF and *B. pseudomallei* BapC.

4.6.2 BapA, BapB or BapC do not play a role in survival or replication of *B. pseudomallei* in RAW264.7 cells

The TTSS3 of *B. pseudomallei* has been shown to play a role in survival and replication within phagocytic cells (Galyov *et al.*, 2010). A TTSS3 translocon BipD and a TTSS3 structural component BsaZ are required for bacterial survival and replication in macrophages during early stages of infection (Stevens *et al.*, 2002). BsaZ is likely to also be required for intracellular survival and replication during late stages of infection (Burtnick *et al.*, 2008). Given that each of the K96243*ΔbapA*, *ΔbapB*, *ΔbapC* and *ΔbapBC* strains showed reduce *in vivo* growth by competitive growth assay (*Chapter 3.3*), it was hypothesised that they may also be involved in

intracellular survival and replication. The K96243*ΔbapA*, *ΔbapB*, *ΔbapC* and *ΔbapBC* strains were assessed for their ability to survive and replicate within mouse macrophage-like RAW264.7 cells. As observed previously for *B. pseudomallei* (Burtnick *et al.*, 2008; Stevens *et al.*, 2002), the wild-type strain was able to survive and replicate over the 6 h infection period. All the mutants, however, retained the ability to replicate intracellularly, and no differences were observed in the final number of bacteria recovered at any of the time points analysed. Therefore, it appears that these genes do not influence intracellular survival and replication.

Hii *et al.* (2008) reported that a *B. pseudomallei bsaQ* mutant was also unimpaired for invasion and replication in cultured human embryonic kidney (HEK293T) cells. Although several factors need to be taken into consideration, including strain- and cultured cell line-specific events, and different functions of the TTSS3 components, the K96243*ΔbapA*, K96243*ΔbapB*, K96243*ΔbapC* and K96243*ΔbapBC* strains showed similar *in vitro* phenotypes to the *bsaQ* mutant, in contrast to the data obtained from previous studies (Pilatz *et al.*, 2006; Stevens *et al.*, 2003; Stevens *et al.*, 2002). Differences in bacterial growth conditions used to perform the infection may be another factor contributing to the discrepancy of these studies, since mid-log-phase bacteria were used in this study and the study of Hii *et al.* (2008), whereas stationary phase cultures were used in the previous three studies. Moreover, the use of different macrophage-like cell lines may be another factor. Stevens *et al.* (2002) showed that the *bipD* and *bsaZ* mutant strains were reduced for intracellular replication in a macrophage-like cell line J774.2 derived from a J774A.1 cell line. However, cultured RAW264.7 cells were used in this study. Indeed, a difference in the rate of *Bacillus anthracis* spore uptake between J774A.1 and RAW264.7 has been demonstrated (Stojkovic *et al.*, 2008). In addition, the signalling mechanisms responsible for ATP-induced release of pro-IL-1, a major contributor to the inflammatory response, is also different between these two cell lines (Pelegrin *et al.*, 2008). Future experiments should include analysis of the intracellular survival of the mutants in J774A.1 cells to determine if there are differences in the host response mechanisms. Moreover, repeating the assays using stationary phase cultures may help in determining whether these *in vitro* phenotypes are correlated with bacterial growth phases or not.

The proinflammatory cytokine IFN-γ is a potent macrophage activator, as it enhances the bactericidal activity of macrophages, by, at least in part, regulating growth and maturation of macrophages, and LC3 production leading to enhanced LAP (Cullinane *et al.*, 2008; Ellis & Beaman, 2004; Gordon *et al.*, 2005; Schroder *et al.*, 2004; Gong *et al.*, 2011). IFN-γ can

stimulate the production of nitric oxide (NO) and ROS (MacMicking *et al.*, 1997; Paludan, 2000). Thus, intracellular survival of the *B. pseudomallei* mutant strains following IFN-γ pre-treatment of the RAW264.7 cells was analysed. As expected, there was a slight decrease in the replication of the wild-type *B. pseudomallei* in IFN-γ stimulated cells up to 6 h p.i. compared to that of the wild-type strain in untreated RAW264.7 cells, suggesting that there was additional effect of IFN-γ on bactericidal activity against *B. pseudomallei*. However, the CFU numbers of the wild-type strain recovered from 2 h to 6 h p.i. continued to increase, indicating that the wild-type strain was still able to survive and replicate even following IFN-γ prestimulation. Interestingly, the K96243*ΔbapC* strain exhibited a dramatic decrease in the intracellular survival compared with the wild-type strain at all time points. The numbers of recovered K96243*ΔbapC* strain at all time points were almost identical, indicating that there was little replication of this mutant from 2 h to 6 h p.i. In addition to the K96243*ΔbapC* strain, the numbers of each of other mutant strains showed no significant increase from 4 h to 6 h p.i., indicating that IFN-γ may reduce the replication at these times. Taken together, these data suggest a direct role of BapC and indirect role of BapA and BapB in intracellular survival of this bacterium under IFN-γ stimulation but the mechanism(s) involved remains unresolved.

Given that *B. pseudomallei* can suppress the production of inducible nitric oxide synthase (iNOS), thereby facilitating bacterial survival and replication within macrophages (Utaisincharoen *et al.*, 2001; Utaisincharoen *et al.*, 2003), using IFN-γ as a single macrophage stimulant may be insufficient to effectively enhance the killing of intracellular *B. pseudomallei*. Several lines of evidence have previously demonstrated that IFN-γ alone was not capable of enhancing bacteriostatic and/or bactericidal activity against intracellular *Listeria monocytogenes* and *S. typhimurium* either *in vitro* or *in vivo* (Higginbotham *et al.*, 1992; Langermans *et al.*, 1990; Langermans *et al.*, 1991; van Dissel *et al.*, 1987). These findings support the observation that *B. pseudomallei* wild-type and most mutant strains, except for the K96243*ΔbapC* strain, can still replicate in IFN-γ pretreated macrophages. However, the difference in survival for the K96243*ΔbapC* strain indicates an involvement of the TTSS mechanism in defending against host immune responses in *B. pseudomallei* as has been observed in *L. monocytogenes* and *S. typhimurium*. Future experiments should further determine whether this decrease in survival of the K96243*ΔbapC* strain continues at later time points post infection, at other infectious doses and/or in the presence of other macrophage stimulants. A TNF receptor family member CD40L, for instance, enhances antimicrobial activity of human monocytes against intracellular

Mycobacterium tuberculosis, and this molecule appears to have a synergistic effect with IFN-γ with regard to antimicrobial activity (Klug-Micu *et al.*, 2013). Leukotriene, in addition, is associated with enhancing bactericidal activity of alveolar macrophages against *Klebsiella pneumoniae* (Bailie *et al.*, 1996; Serezani *et al.*, 2005). Myeloperoxidase has been also found to increase phagocytic and antimicrobial activity of mature macrophages against *E. coli* (Lincoln *et al.*, 1995). Given that the K96243*ΔbapC* strain showed a significant decrease in survival at all time points under IFN-γ pre-treatment, intracellular survival assay should be conducted to compare ability to survive and replicate in IFN-γ-pre-stimulated macrophages of the complemented strain K96243*ΔbapC*[*bapC*], the independently derived strain K96243*ΔbapC*_2, the original mutant and the wild-type strains.

4.6.3 Inactivation of *bapA*, *bapB* or *bapC* does not affect escape from host endosomes or actin polymerisation

After entering host cells, *B. pseudomallei* can modulate host actin polymerisation by expression of BimA resulting in actin-associated membrane protrusion, MNGC formation and intercellular spread (Jones *et al.*, 1996; Kespichayawattana *et al.*, 2000; Suparak *et al.*, 2005). This allows the bacteria to enter neighbouring cells without entering the extracellular environment and therefore without encountering extracellular host immune defence mechanisms (Stevens *et al.*, 2006; Stevens *et al.*, 2005a; Stevens *et al.*, 2005b). Several studies have proved that the TTSS3 plays an important role in host endosomal escape and this is a prerequisite for actin-mediated motility, MNGC formation and bacterial cell-to-cell spread (Attree & Attree, 2001; Burtnick *et al.*, 2008; French *et al.*, 2011; Pilatz *et al.*, 2006; Stevens *et al.*, 2003). In this study, endosomal escape and avoidance of LAP of the mutants was analysed through bacterial co-localisation with LC3-GFP. Furthermore, to see if there was an association of BapA, BapB or BapC with bacterial actin-mediated motility, fluorescence microscopy using Alexa Fluor® 647-labelled phalloidin was used. No differences were observed between mutant and the wild-type strains and each of the mutants was capable of polymerising host actin in order to form actin tails as efficiently as the wild-type strain. Therefore, BapA, BapB and BapC do not play a significant role in escape into the host cytoplasm and actin-mediated motility. A hallmark of *B. pseudomallei* infection is MNGC formation, and again each of the mutants was capable of inducing host cell fusion and cell-to-cell spread.

It has been shown that increased co-localisation of bacteria with LC3-GFP can be observed following IFN-γ stimulation of RAW246.7 cells (Cullinane *et al.*, 2008). Initially, this was

thought to be due to increased uptake of bacteria into autophagosomes. However, later work strongly suggests that *B. pseudomallei* is targeted by LAP and not canonical autophagy (Gong *et al.*, 2011). Thus, it is likely that IFN-γ treatment stimulates more rapid LC3 accumulation at the phagosome membrane or reduced escape of *B. pseudomallei* from the phagosome. It was therefore decided to analyse the co-localisation of LC3-GFP with the mutant strains in IFN-γ stimulated macrophage cells. As expected, IFN-γ stimulation resulted in an increase in LC3-GFP labelled structures. Moreover, the total number of wild-type bacteria observed to co-localise with GFP-LC3 was higher than that observed in untreated RAW246.7 cells. However, the level of co-localisation with LC3-GFP for the mutants was indistinguishable from that of the wild-type. Thus, it was concluded that the TTSS3 genes *bapA*, *bapB* and *bapC* do not play a significant role in *B. pseudomallei* avoidance of LAP and/or canonical autophagy.

4.6.4 BapA, BapB or BapC play a minor role in alteration of the host innate immune response to *B. pseudomallei* infection

During infection, *B. pseudomallei* uses a number of virulence factors to alter host immune responses for bacterial benefit (Wiersinga & van der Poll, 2009; Wiersinga *et al.*, 2006). One role of TTSS3 appears to be associated with alteration of the innate imune response. Burtnick *et al.* (2008) demonstrated a role for BsaZ, a TTSS3 structural protein, in inflammatory cytokine activation. They assessed the production of proinflammatory cytokines, including TNF-α and IL-6, from cells infected with the *bsaZ* mutant compared to those infected with the wild-type strain. They found that there was no significant difference in TNF-α and IL-6 secretion from cells infected with the *bsaZ* mutant compared to the wild-type strain. However, based on the differences in LD_{50} production and IL-1β secretion observed in cells infected with the mutant compared to the wild-type strain, they suggested that the mutant and the wild-type strains use different mechanisms to stimulate the host innate immune responses. Likewise, Miao *et al.* (2010) showed a role for BsaK, the minor subunit of the TTSS3 injectisome, in activation of the macrophage caspase 1 pathway via NLRC4, which is one of the host pattern recognition receptors (PRRs) responsible for detecting microbial components during infection. BsaQ, an export apparatus protein of the TTSS3 injectisome, and BsaU, a protein required for the TTSS3 injectisome assembly, play important roles in induction of IL-8, a key chemokine responsible for confronting bacterial invasion by recruiting phagocytes from the bloodstream into the tissue site (Hii *et al.*, 2008). Haque *et al.* (2006) demonstrated a role for BopE- and BipB-specific T-cells in host immunity to *B. pseudomallei* following immunisation with a live attenuated strain, again indicating an interaction of the TTSS3 and its effectors with the host immune system. Moreover,

Tan *et al.* (2010) demonstrated an involvement of the TTSS3 in transcriptional regulation of TssM (BPSS1512) expression, which is a virulence factor responsible for suppressing NF-κB and type I IFN mechanism by, at least in part, interfering with ubiquitination of molecules involved in these pathways. These data suggest an interaction of the TTSS3 molecules with the host innate immune response. Thus, the expression of two essential cytokines TNF-α and IL-6, markers of early and late stages of bacterial infection, from RAW264.7 cells infected with each of the mutants or the wild-type was analysed to determine whether *bapA*, *bapB* or *bapC* were involved in modulation of the innate immune response. In comparison to wild-type infected RAW264.7 cells, only RAW264.7 cells infected with the K96243*ΔbapBC* strain showed reduced expression of TNF-α at 4 h and at 6 h p.i. Similarly, only cells infected with the K96243*ΔbapBC* strain exhibited a significant reduction in IL-6 production at 4 h and 6 h p.i. When RAW264.7 cells were pre-stimulated with IFN-γ, cells infected with any of the mutants showed similar TNF-α production compared to the wild-type at all time points. IFN-γ-activated cells infected with the K96243*ΔbapA*, K96243*ΔbapC* or K96243*ΔbapBC* strain showed a significant decrease in IL-6 expression at 4 h p.i. compared to the wild-type strain while cells infected with any of the mutants at 2 h and 6 h p.i. showed no difference. These data suggest that, in untreated RAW264.7 cells, combined inactivation of BapB and BapC results in modulation of TNF-α and IL-6 secretion. Similarly, following IFN-γ pretrement of RAW264.7 cells at 4 h p.i., IL-6 expression from cells infected with the K96243*ΔbapA*, K96243*ΔbapC* or K96243*ΔbapBC* strain exhibited a significant decrease from the wild-type infected cells.

Although TNF-α and IL-6 are produced during infection, they seem to be triggered at different stages of infection; indeed, TNF-α requires IFN-γ activity in order to induce the production of IL-6 (Sanceau *et al.*, 1991). The IL-6 data obtained from this study suggest a combined involvement of BapB and BapC in modulation of host immune responses, and this is likely to be affected by IFN-γ. Inactivation of *bsaZ*, encoding a TTSS3 structural component, results in a delay in TNF-α stimulation at 12 h p.i., with no secretion of either IL-1α and IL-1β cytokines or the release of cytoplasmic enzyme lactate dehydrogenase (LDH_{50}) from 6 to 18 h p.i. (Burtnick *et al.*, 2008). Thus, future experiments at both early (30 min, 60 min and 90 min p.i.) and later (6, 12 and 18 h p.i.) time points should be conducted to assess the secretion of these cytokines from cells infected with each of the mutant or the wild-type strains. In addition, analysing other cytokines which could differentiate TNF-α from IL-6 secretion mechanisms, such as IL-8, IL-1β and IL-10 (Alciato *et al.*, 2010; Burtnick *et al.*, 2008; Smith *et al.*, 2011), could help in clarifying

the TNF-α and IL-6 data obtained from this study. Cytotoxicity assays, assessed by measuring the level of lactate dehydrogenase release (Smith *et al.*, 2011) should also be carried out along with *in vitro* infection assays in order to verify that there are no unintentional effects due to loss of cell integrity (Burtnick *et al.*, 2008). These experiments may also shed light on whether BapA, BapB and/or BapC play a role in host cell damage/death.

4.7 Conclusions

The TTSS3 is essential for pathogenesis of *B. pseudomallei* as it is required for bacterial survival and replication within the host cells and intercellular spread of this bacterium. In this chapter the potential roles of the TTSS3 proteins BapA, BapB and BapC were investigated with respect to their functions based on the previous TTSS3 studies. There was no statistically significant difference between any of the mutants and the wild-type strain in cell invasion, intracellular survival, actin-mediated motility and escape from host endosomal vacuoles. However, RAW264.7 cells infected with the K96243*ΔbapBC* strain showed altered expression of TNF-α and IL-6. Furthermore, in RAW264.7 cells pretreated with IFN-γ, there were minor changes in IL-6 secretion from the K96243*ΔbapA*, K96243*ΔbapC* and K96243*ΔbapBC* strain. Importantly, BapC was found to play a role in intracellular survival and replication of *B. pseudomallei* under IFN-γ stimulation. Taken together, it can be concluded that BapA, BapB and BapC do not play a role in bacterial invasion in non-phagocytic cells, escape from host phagosome, actin-mediated motility and formation of MNGCs. However, they may play a role in alteration of the host immune responses to *B. pseudomallei* and a minor role in bacterial survival and replication in phagocytic cells.

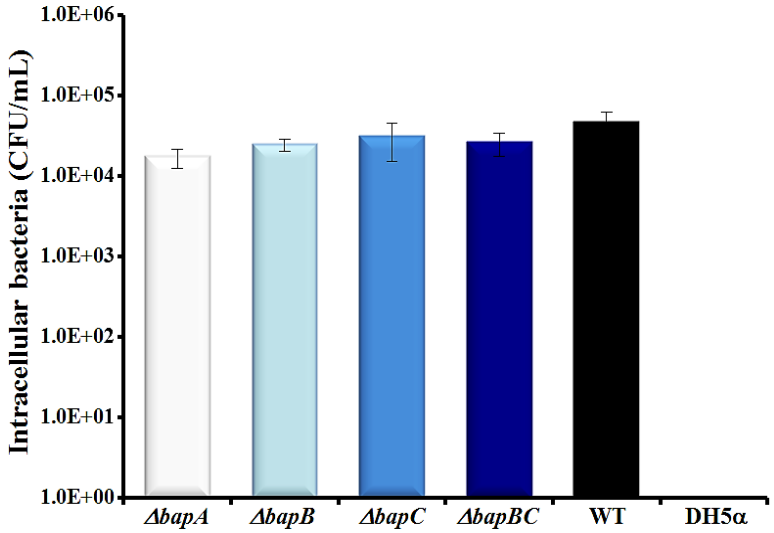

Figure 4.1.1 Ability of *B. pseudomallei* wild-type (WT) and the K96243*ΔbapA* (*ΔbapA*), K96243 *ΔbapB* (*ΔbapB*), K96243*ΔbapC* (*ΔbapC*) and K96243*ΔbapBC* (*ΔbapBC*) strains to invade the human lung epithelial cell line A549. *E. coli* DH5α (DH5α) was included as the negative control. The experiment was performed in biological triplicate, and each was performed in technical triplicate. Data are present as the mean ± SEM.

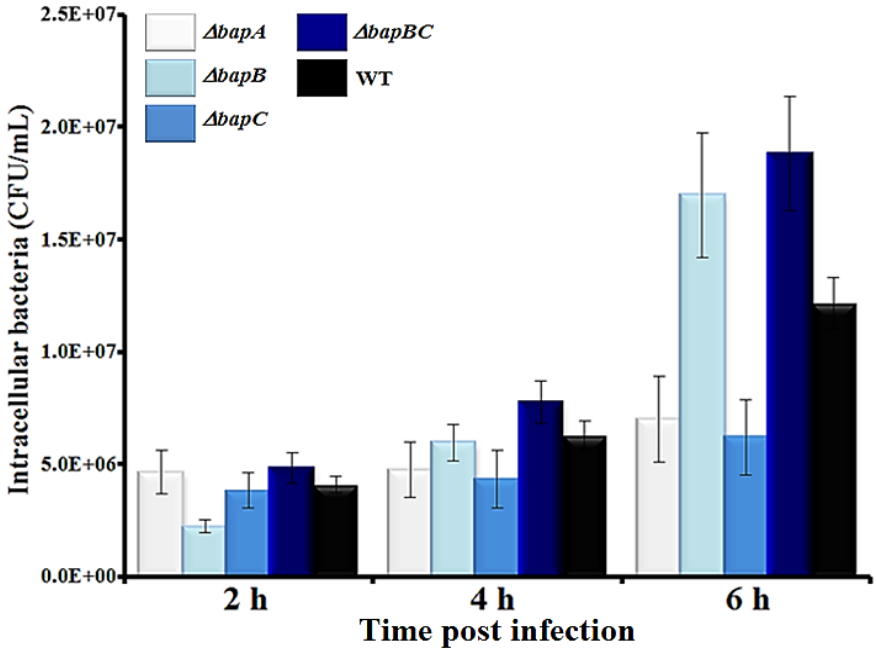

Figure 4.2.1 Recovery of *B. pseudomallei* strains from murine macrophage-like RAW264.7 cells at 2, 4 and 6 h p.i. Data are presented as the mean ± SEM of at least three biological replicates. The strains used were: *ΔbapA*, the K96243*ΔbapA* strain; *ΔbapB*, the K96243*ΔbapB* strain; *ΔbapC*, the K96243*ΔbapC* strain; *ΔbapBC*, the K96243*ΔbapBC* strain; WT, the wild-type strain.

A

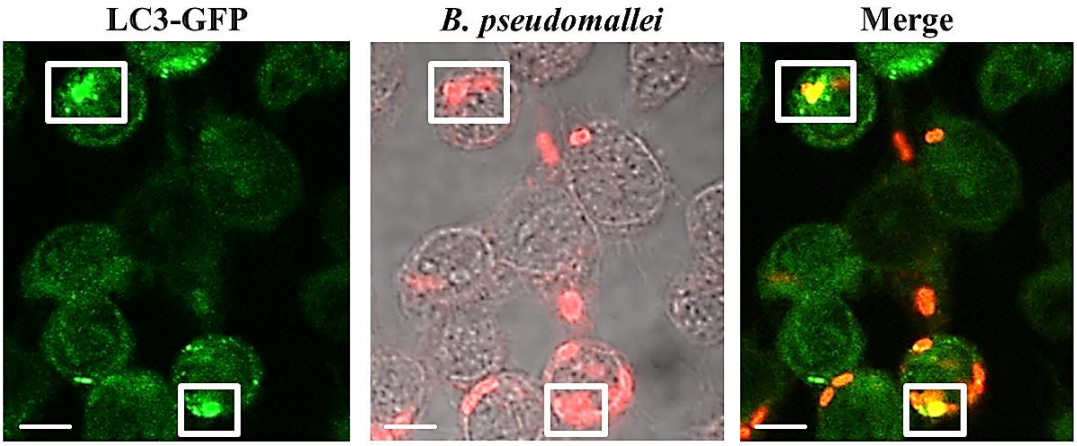

B

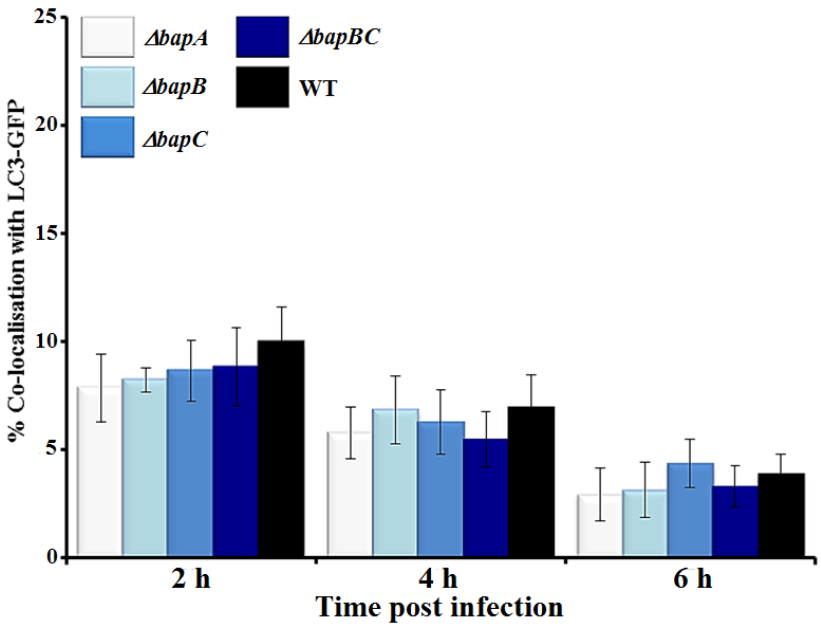

Figure 4.3.1 Bacterial co-localisation with LC3-GFP at 2, 4 and 6 h p.i. (A) Representative confocal micrographs with differential interference contrast (DIC) images of RAW264.7 cells stably expressing LC3-GFP (green) infected with *B. pseudomallei* (red) at 2 h p.i and the merged images of bacteria associated with LC3-GFP (yellow) as indicated by the white boxes. (B) Quantitative analysis of bacterial co-localisation with LC3-GFP at 2, 4 and 6 h p.i. Data are presented as the mean ± SEM of at least three biological replicates. The strains used were: *ΔbapA*, the K96243*ΔbapA* strain; *ΔbapB*, the K96243*ΔbapB* strain; *ΔbapC*, the K96243*ΔbapC* strain; *ΔbapBC*, the K96243*ΔbapBC* strain; WT, the wild-type strain. Scale bar = 5 μm.

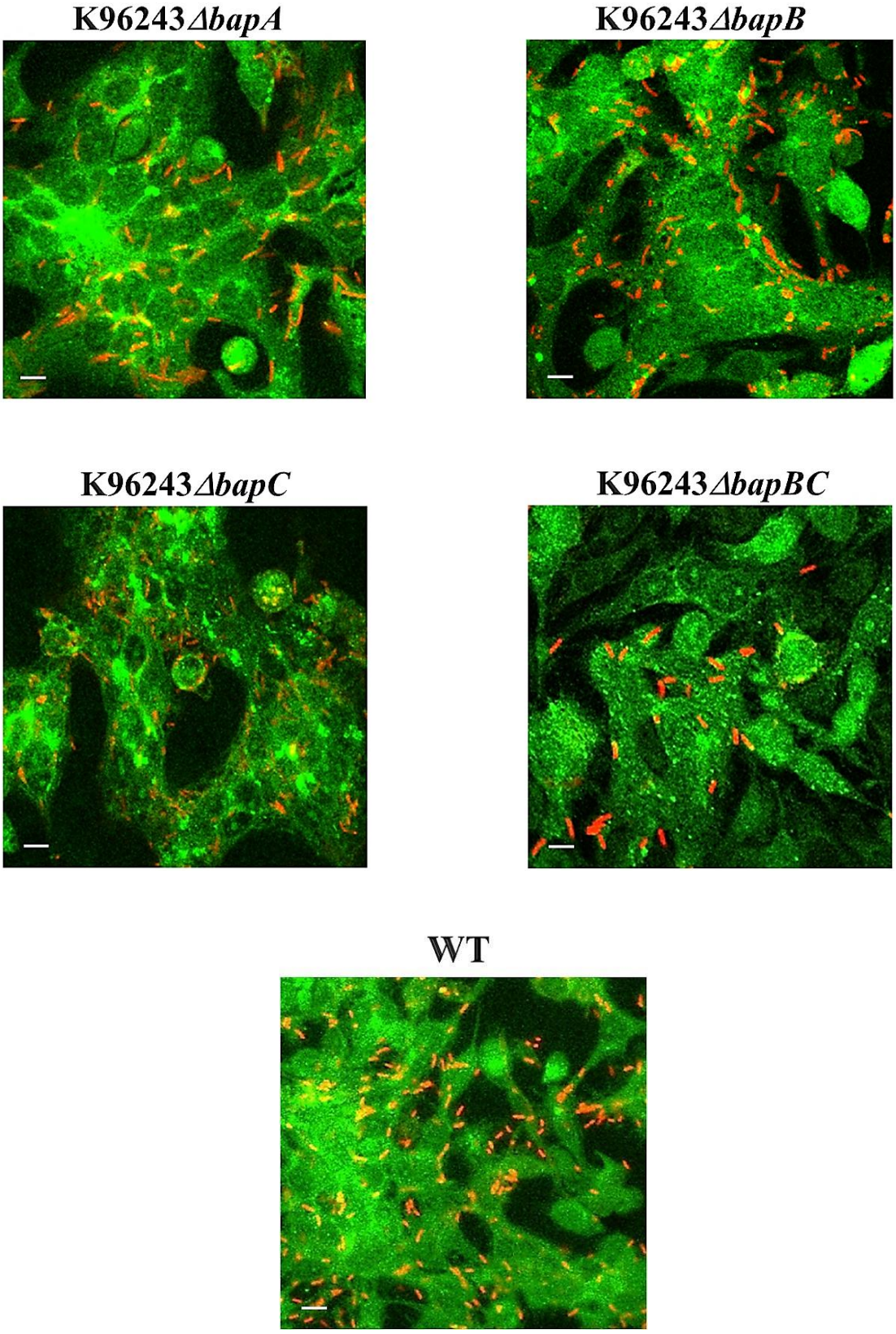

Figure 4.3.2 *B. pseudomallei*-associated host cell membrane protrusions and MNGC formation. Representative confocal micrographs illustrating MNGC formation of RAW264.7 cells stably expressing LC3-GFP (green) infected with the wild-type (WT) strain, the K96243*ΔbapA*, K96243*ΔbapB*, K96243*ΔbapC* or the K96243*ΔbapBC* strain at 6 h p.i. Bacteria were stained red. Scale bar = 5 µm.

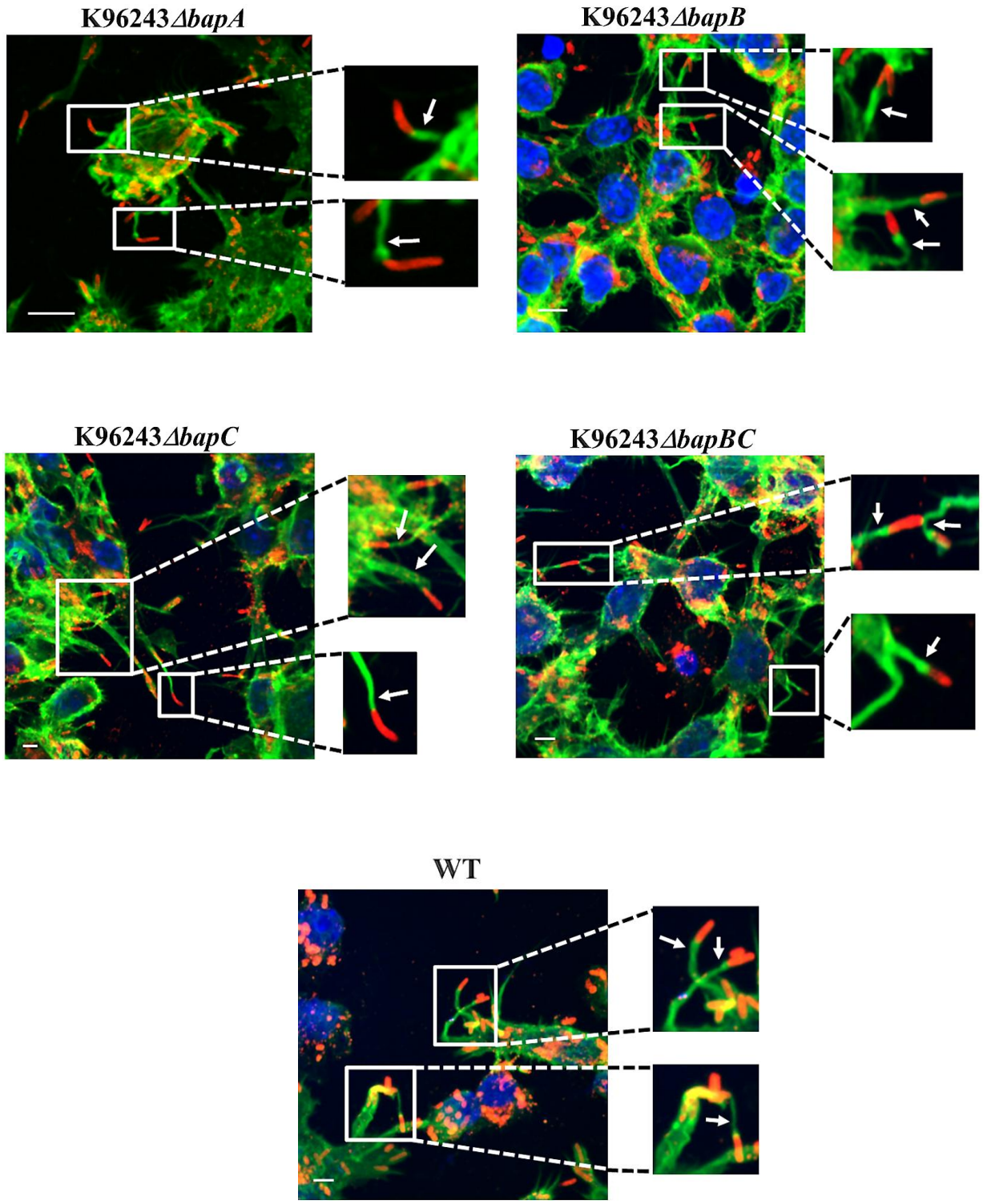

Figure 4.3.3 Ability of *B. pseudomallei* strains to form actin tails. Representative confocal micrographs of RAW264.7 cells stably expressing LC3-GFP infected with the K96243*ΔbapA*, K96243*ΔbapB*, K96243*ΔbapC*, or K96243*ΔbapBC*, or the wild-type (WT) strain for 6 h p.i. Bacteria were stained in red. Due to the similar spectral qualities of Alexa Fluor®-647-phalloidin and Texas Red®-X, the emitted fluorescence associated with actin tails was presented in green. Eukaryotic nuclei were stained in blue with DAPI. Bacteria have actin tails protruding at one pole. White arrows indicate clear evidence of actin tail formation. Scale bar = 5 μm.

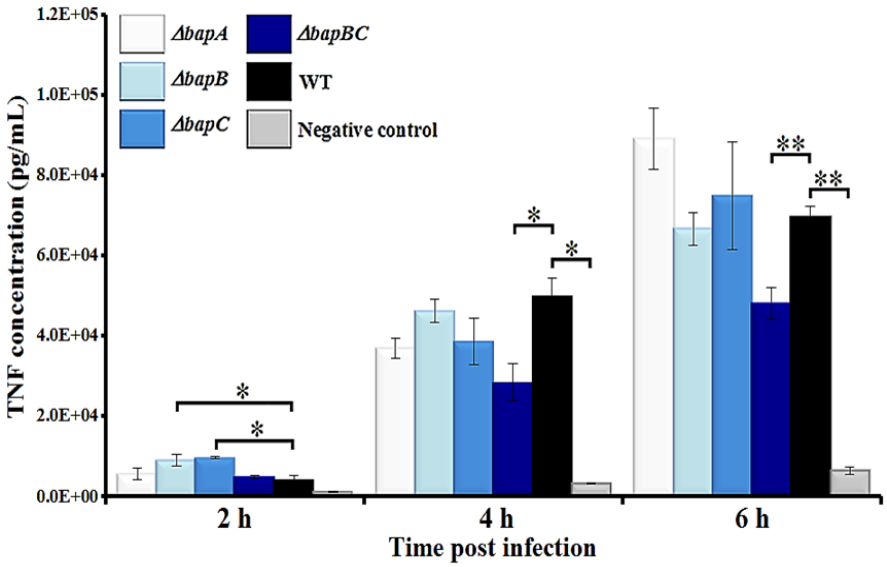

Figure 4.4.1 TNF-α secretion by RAW264.7 cells infected with each of the mutants or the wild-type strain. Supernatant samples collected from infected cells at 2, 4 and 6 h p.i. were analysed for the amount of TNF-α (pg/mL). Data are presented as the mean ± SEM of at least three biological replicates. The strains used were: *ΔbapA*, the K96243*ΔbapA* strain; *ΔbapB*, the K96243*ΔbapB* strain; *ΔbapC*, the K96243*ΔbapC* strain; *ΔbapBC*, the K96243*ΔbapBC* strain; WT, the wild-type strain. **P* < 0.05; ***P* < 0.001.

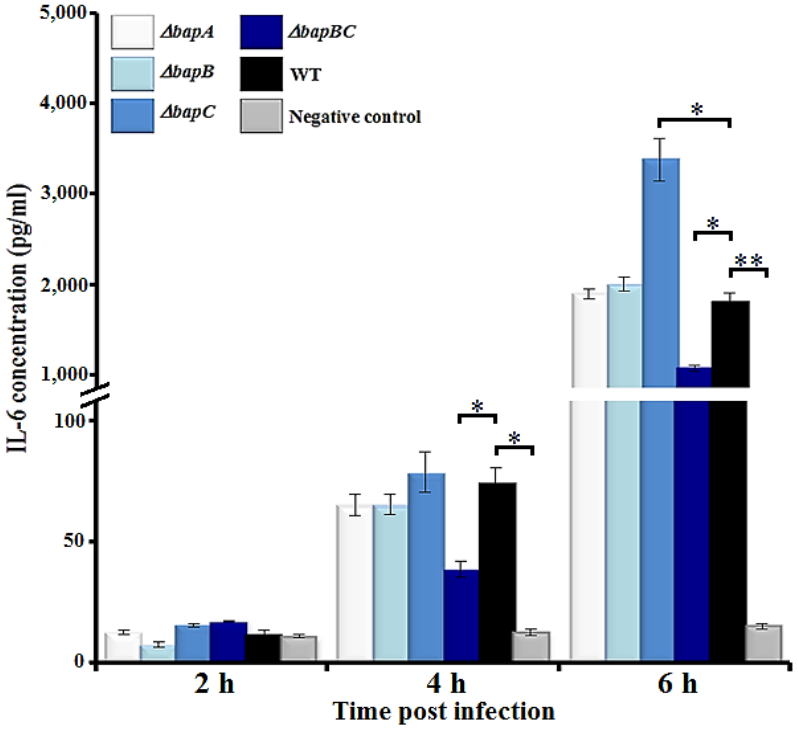

Figure 4.4.2 IL-6 secretion by RAW264.7 cells infected with each of the mutants or the wild-type strain. Supernatant samples collected from infected cells at 2, 4 and 6 h p.i. were analysed for the amount of IL-6 (pg/mL). Data are presented as the mean ± SEM of at least three biological replicates. The strains used were: *ΔbapA*, the K96243*ΔbapA* strain; *ΔbapB*, the K96243*ΔbapB* strain; *ΔbapC*, the K96243*ΔbapC* strain; *ΔbapBC*, the K96243*ΔbapBC* strain; WT, the wild-type strain. **P* < 0.05; ***P* < 0.001.

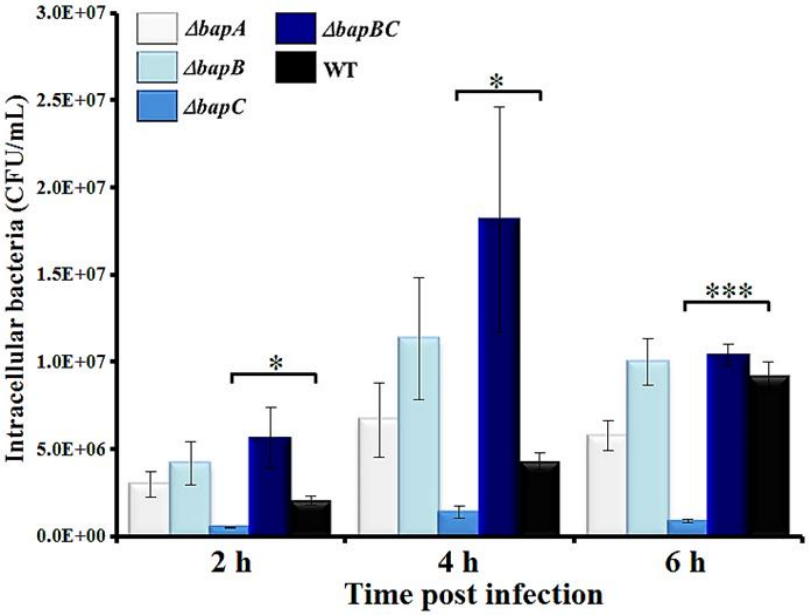

Figure 4.5.1 Recovery of *B. pseudomallei* wild-type and mutant strains from IFN-γ stimulated RAW264.7 cells at 2, 4 and 6 h p.i. Macrophage-like RAW264.7 cells were pretreated with IFN-γ before infection with *B. pseudomallei* strains. Data are presented as the mean ± SEM of at least three biological replicates. The strains used were: *ΔbapA*, the K96243*ΔbapA* strain; *ΔbapB*, the K96243*ΔbapB* strain; *ΔbapC*, the K96243*ΔbapC* strain; *ΔbapBC*, the K96243*ΔbapBC* strain; WT, the wild-type strain. **P* < 0.05; ****P* < 0.0001.

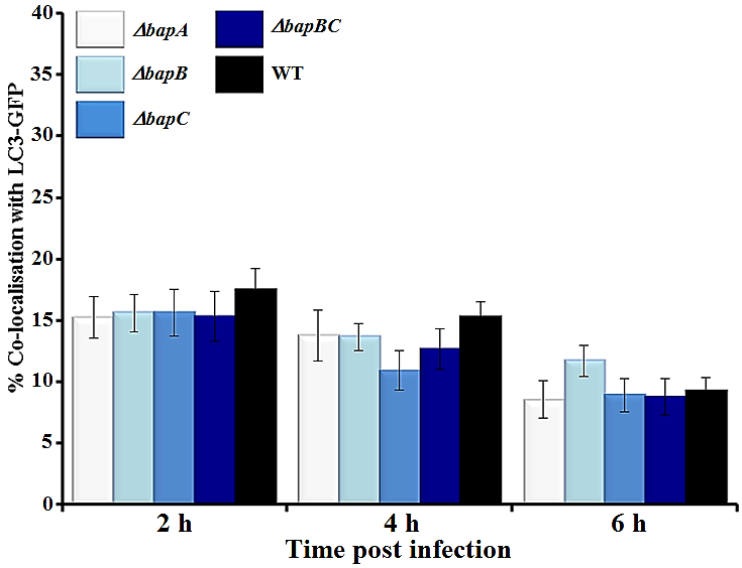

Figure 4.5.2 Bacterial co-localisation with LC3-GFP at 2, 4 and 6 h p.i. following IFN-γ prestimulation. RAW264.7 macrophage-like cells were pretreated with IFN-γ before infection with *B. pseudomallei* strains. Quantitative analysis of bacterial co-localisation with LC3-GFP of each of the mutants compared to the wild-type strain at 2, 4 and 6 h p.i. Data are presented as the mean ± SEM of at least three biological replicates. The strains used were: *ΔbapA*, the K96243*ΔbapA* strain; *ΔbapB*, the K96243*ΔbapB* strain; *ΔbapC*, the K96243*ΔbapC* strain; *ΔbapBC*, the K96243*ΔbapBC* strain; WT, the wild-type strain.

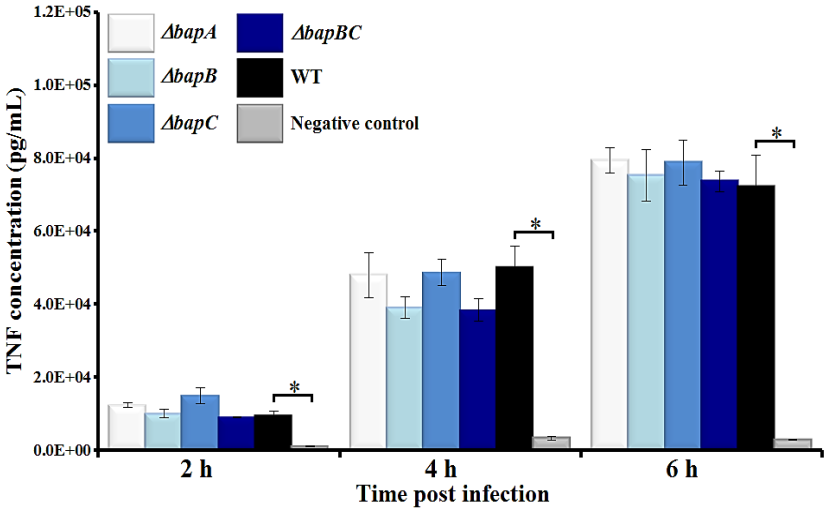

Figure 4.5.3 TNF-α secretion by IFN-γ-stimulated RAW264.7 cells infected with each of the mutants, or the wild-type strain. Macrophage-like RAW264.7 cells were pretreated with IFN-γ before infection with *B. pseudomallei* strains. Supernatant samples collected from infected cells at 2, 4 and 6 h p.i. were analysed for the amount of TNF-α (pg/mL). Data are presented as the mean ± SEM of three biological replicates. The strains used were: *ΔbapA*, the K96243*ΔbapA* strain; *ΔbapB*, the K96243*ΔbapB* strain; *ΔbapC*, the K96243*ΔbapC* strain; *ΔbapBC*, the K96243*ΔbapBC* strain; WT, denotes the wild-type strain. **P* < 0.05.

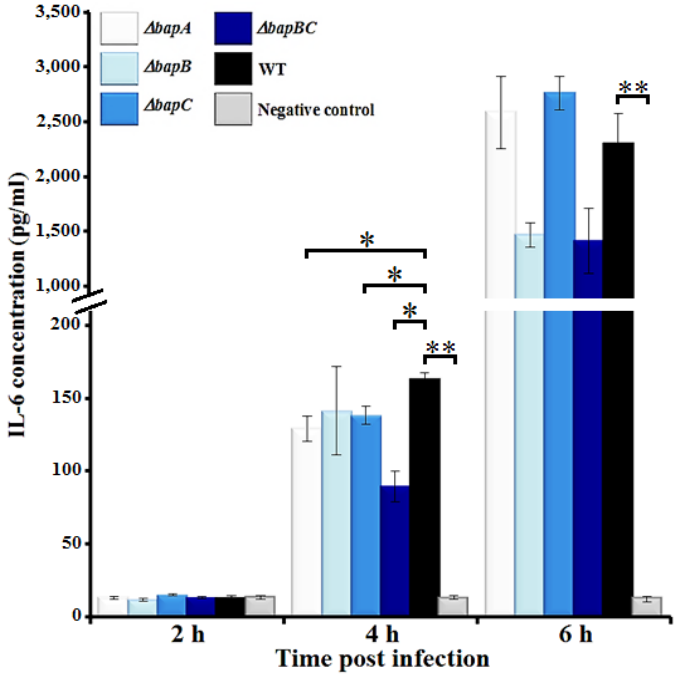

Figure 4.5.4 IL-6 secretion by IFN-γ-stimulated RAW264.7 cells infected with each of the mutants or the wild-type strain. Macrophage-like RAW264.7 cells were pretreated with IFN-γ before infection with *B. pseudomallei* strains. Supernatant samples collected from infected cells at 2, 4 and 6 h p.i. were analysed for the amount of IL-6 (pg/mL). Data are presented as the mean ± SEM of at least three biological replicates. The strains used were: *ΔbapA*, the K96243*ΔbapA* strain; *ΔbapB*, the K96243*ΔbapB* strain; *ΔbapC*, the K96243*ΔbapC* strain; *ΔbapBC*, the K96243*ΔbapBC* strain; WT, the wild-type strain. **P* < 0.05; ***P* < 0.001.

Chapter 5

Analysis of the secretion of BapA, BapB and BapC

Chapter 5: Analysis of the secretion of BapA, BapB and BapC

The type III secretion system (TTSS) is a key virulence factor of many Gram-negative pathogens and is responsible for subverting host signalling pathways, thereby, promoting bacterial survival within the host (Coburn *et al.*, 2007; Galan & Collmer, 1999). Of all the TTSS molecules, the effector proteins are the molecules directly delivered into host cells and are responsible for the modulation of host cell functions; these effectors are critical for bacterial pathogenesis (Dean, 2011; Haglund & Welch, 2011; Ham *et al.*, 2011). In this chapter, the putative TTSS3 effectors BapA, BapB and BapC were specifically characterised for their secretion. Each of the proteins BapA, BapB and BapC was expressed with the tetracysteine (TC) tag and their secretion assessed by using the TC-FlAsH^{TM} labelling technique (Hoffmann *et al.*, 2010; Machleidt *et al.*, 2006; Simpson *et al.*, 2010). Several conditions known to stimulate the TTSS of other Gram-negative bacteria (Bahrani *et al.*, 1997; Kane *et al.*, 2002; Pumirat *et al.*, 2010; Rietsch & Mekalanos, 2006; Walker & Miller, 2004) were tested to determine if they also affected the secretion of BapA, BapB or BapC. To further investigate any potential involvement of these proteins in TTSS3 assembly, the well-characterised TTSS3 effector BopE (Hii *et al.*, 2008; Stevens *et al.*, 2003) was used as the marker of the TTSS function to examine TTSS activity in the K96243*ΔbapA*, *ΔbapB*, *ΔbapC* and *ΔbapBC* strains compared to the wild-type and K96243*ΔbopE*::pDM4 strains. The transcription of *bopE* was also assessed in each of the strains to determine whether levels of *bopE* transcription were different in any of the mutant strains.

5.1 Investigation of the secretion of BapA, BapB and BapC using the TC-FlAsH^{TM}-based fluorescence labelling

In *Chapter 4*, the importance of BapA, BapB and BapC was assessed in a range of *in vitro* assays specific for known TTSS3 functions. Although BapA, BapB and BapC have been predicted as TTSS3 effectors, this has never been tested and only BopE and BopC have been experimentally shown to be secreted in a TTSS-dependent manner. In order to analyse the secretion, each of the proteins was fused with a tetracysteine (TC) tag at the C-terminal region, proteins or whole cells were directly labelled with the membrane-permeant 4',5'-bis(bis1,3,2-dithioarsolan-2-yl) fluorescein (FlAsH) (Adams *et al.*, 2002; Griffin *et al.*, 1998; Machleidt *et al.*, 2006) and then secretion measured by fluorescence. The binding between the biarsenical molecules of FlAsH and TC is a stable interaction via four covalent bonds; therefore, the fluorescent signal is stable

for detection by various techniques, including standard SDS-PAGE analysis (Adams *et al.*, 2002; Copeland *et al.*, 2010; Enninga *et al.*, 2005; Griffin *et al.*, 1998).

5.1.1 Generation of TC-tagged BopE

As the direct TC-FlAsH^{TM} labelling technique has never been used previously for labelling proteins in *B. pseudomallei*, optimisation of all steps was carried out using the characterised TTSS effector BopE prior to experimentation on BapA, BapB and BapC. Given that the transposon vector pUC18Tmini-Tn*7*T gives single site stable insertions in *B. pseudomallei* (Choi *et al.*, 2006; Choi *et al.*, 2005), a TC-tagged version of BopE was constructed in this vector (*Figure 5.1.1B*). The primers JT6929 and JT6930 (*Chapter 2, Table 2.4*) were used to amplify a 813-bp fragment of the full length *bopE* using KOD polymerase PCR (*Appendix 3, Table A3.3*). The amplified DNA fragments were ligated into *Xma*I-/*Spe*I-digested pUC18Tmini-Tn*7*T:: *tetA*(C)::P_{glmS2} (*Chapter 2, Table 2.1*) and introduced by transformation into *E. coli* DH5α (*Chapter 2.7*).

The primers PA6067 and PA6068 (*Chapter 2, Table 2.3*), amplifying the MCS of the mini-Tn*7* vector, were used to screen for recombinant clones with *bopE* insertions. These primers should generate a 2,000-bp product if there has been an insertion of *bopE* at the *Xma*I (5' end) and *Spe*I (3' end) sites of pUC18Tmini-Tn*7*T::*tetA*(C)::P_{glmS2} vector (*Figure 5.1.2, lane 4, 5, 7, 8 and 11*), but a 1,200-bp product if there has been no *bopE* insertion (*Figure 5.1.2, lane 3, 10, 13 and 15*). A clone with the correct sized insert (*Figure 5.1.2, lane 4*) was selected for further study and the nucleotide sequence of *bopE* in this clone verified (data not shown). The TC tag was then cloned in-frame at the 3' end of the *bopE* gene. The modified TC tag, encoding proline (CCG) and glycine (GGC) as spacers between four cysteine codons (TGC) (Simpson *et al.*, 2010) and a stop codon (TAA) (*Figure 5.1.3A*), was generated by annealing the primers JT6931 and JT6932 (*Chapter 2, Table 2.4*) and ligating the double-stranded product into *Spe*I-digested pUC18Tmini-Tn*7*T::*tetA*(C)::P_{glmS2}::*bopE* (*Chapter 2, Table 2.1*). Clones containing TC-tagged *bopE* were identified by nucleotide sequencing using the primer PA6068 (*Chapter 2, Table 2.3*). One clone containing the correct TC sequence at the 3' end of *bopE* (*Figure 5.1.3B*) was then introduced by transformation into *E. coli* SM10/λ*pir* (*Chapter 2.7*) and then by conjugation into the *B. pseudomallei* wild-type strain (*Chapter 2.10*). Transconjugants were selected on 25 μg/mL tetracycline and 8 μg/mL gentamicin and then patched to confirm the antibiotic profile prior to performing PCR analyses for verification of genomic integration of the pUC18Tmini-Tn*7*T:: *tetA*(C)::P_{glmS2}::*bopE*TC construct (*Chapter 2, Table 2.1*). The primers PA6211 and PA6212

(*Chapter 2, Table 2.3*) were first used to screen potential transconjugants for genomic integration downstream of *glmS2*, the most common insertion site of the mini-Tn*7* vector. PCR amplification of the wild-type *B. pseudomallei* DNA template with this primer pair should produce a 1,100-bp fragment (*Figure 5.1.4A*) while, following integration of the transposon after *glmS2*, these primers should generate an approximate 4,000-bp fragment (*Figure 5.1.4B*). PCR using DNA from all potential transconjugants (*Figure 5.1.5, lane 2 to 8*) yielded similar PCR products to that amplified when DNA from the wild-type strain was used (*Figure 5.1.5, lane 9*). Therefore, these data suggest that there was no integration of the mini-Tn*7* construct downstream of *glmS2*.

As these potential clones displayed the correct antibiotic profile, suggesting successful integration of the mini-Tn*7* construct into the bacterial genome, further analyses using the primer pair combinations PA6067/MC6029, MC6028/PA6068 and MC6028/PA6212 (*Figure 5.1.4B*) were conducted. These three primer combinations should produce an approximate 1,500-, 1,200- and 1,700-bp products, respectively, if the transposon is present. A 1,500-bp product was produced when DNA from almost all of the potential transconjugants was used as the template for PCR together with the primers PA6067 and MC6029 (*Figure 5.1.6A, lane 2 to 8*). This product was absent when DNA from the wild-type strain (*Figure 5.1.6A, lane 9*) was used or when no DNA was added (*Figure 5.1.6A, lane 11*). In addition, PCR using the primers MC6028 and PA6068 produced approximate 1,200-bp fragments when the transconjugant DNA was used as the template (*Figure 5.1.6B, lane 3 to 8*) and a 1,000-bp fragment when the positive control was used as the template (*Figure 5.1.6B, lane 10*). Again, no product was observed when DNA from the wild-type strain was used as the template (*Figure 5.1.6B, lane 9*). Therefore, these data confirmed the presence of the pUC18Tmini-Tn*7*T::*tetA*(C)::P_{glmS2}::*bopE*TC construct in *B. pseudomallei*. However, PCR using the primers MC6028 and PA6212 produced an approximately 2,500-bp fragment when DNA from the transconjugants (*Figure 5.1.6C, lane 2 to 8*) and DNA from the wild-type strain (*Figure 5.1.6C, lane 9*) was used, suggesting that the transposon integration did not occur after *glmS2*. More transconjugants were screened but all showed similar results to the clones described above (data not shown). Since *B. pseudomallei* contains three paralogous copies of *glmS*, it is possible that the mini-Tn*7* construct was integrated after any of these *glmS* even though the integration has been suggested to occur preferentially after *glmS2*. In *B. mallei*, the insertions of the mini-Tn*7* have been shown to occur after *glmS1*, *glmS2* or both *glmS1* and *glmS2* (Choi *et al.*, 2006). Therefore, PCR using the primer pairs amplifying the downstream regions of either *glmS1* (PA6271/PA6272) or *glmS3*

(PA6273/PA6274) (*Chapter 2, Table 2.3*) was carried out. However, PCR products using the potential conjugant DNA templates showed similar size to the wild-type (data not shown), indicating that there was no transposon integration after either *glmS1* or *glmS3*. PCR using the primer pair MC6229/MC6230 (*Chapter 2, Table 2.3*) for amplification of a section surrounding the mini-Tn*7 oriT* was also carried out, and it appears that there was freely replicating plasmid present in these potential transconjugants (*Figure 5.1.7, lane 2 to 8*). Taken together, these data indicate that the pUC18Tmini-Tn*7*T::*tetA*(C)::P_{glmS2}::*bopE*TC construct is present in *B. pseudomallei* but at it was not integrated in the genome. Freely replicating plasmid was also observed when using the mini-Tn*7* vector for complementation (see *Chapter 3.7*). However, the clone in lane 3 was designated K96243*bopE*TC (*Chapter 2, Table 2.1*) and used in further experiments.

An additional TC-tagged *bopE* was also generated in the replicating vector pBHR1. The *bopE* gene with 3' TC tag sequence was amplified from the sequence-verified pUC18Tmini-Tn*7*T:: *tetA*(C)::P_{glmS2}::*bopE*TC and cloned into the chloramphenicol resistance gene of pBHR1 (*Figure 5.1.8B*). The primers JT7125 and JT7126 (*Chapter 2, Table 2.4*) were used to amplify approximately a 1,200-bp fragment containing the *glmS2* promoter, *bopE*, the TC tag, and the two terminator sequences (T_1 and T_0) from the plasmid pUC18Tmini-Tn*7*T::*tetA*(C)::P_{glmS2}:: *bopE*TC. The PCR fragment was verified by nucleotide sequencing (data not shown) prior to cloning into *Acl*I-/*Nco*I-digested pBHR1, which are located in the *cat* gene of the pBHR1 (*Figure 3.5.1A*). The *bopE* gene was cloned with a native ribosomal binding site and is predicted to be transcribed from the *cat* promoter present in the vector. The ligation reaction was transformed into *E. coli* DH5α and putative transformants screened by patching onto LB agar containing either 50 µg/mL kanamycin or 20 µg/mL chloramphenicol. Only kanamycin resistance and chloramphenicol sensitive clones were selected for further characterisation. Plasmid DNA was analysed by *Acl*I/*Nco*I restriction digestion. Digestion of a correctly assembled construct should give a 1,500-bp fragment containing the P_{glmS2}::*bopE*TC DNA and a 5,000-bp vector fragment (*Figure 5.1.9, lane 3 to 5*). The nucleotide sequencing of one clone showing the appropriate profile (*Figure 5.1.9, lane 3*) was determined and the correct sequence confirmed (data not shown). The recombinant plasmid was used to transform *E. coli* S17-1/λ*pir* and then moved into the *B. pseudomallei* wild-type strain by conjugation. Transconjugants were selected on LB agar containing 8 µg/mL gentamicin and 1 mg/mL kanamycin and verified for the presence of the pBHR1::P_{glmS2}::*bopE*TC plasmid by PCR using the primers JT7080/JT7081 (*Chapter 2, Table 2.3*). PCR using these primers should amplify a 1,400-bp fragment containing

the chloramphenicol resistance cassette of pBHR1 and the cloned P_{glmS2}::*bopE*TC fragment. PCR from a number of the potential transconjugants (*Figure 5.1.10, lane 2, 4, and 5*) amplified fragments of the expected size (1,400-bp), indicating the presence of the pBHR1::P_{glmS2}::*bopE*TC plasmid. Furthermore, PCR using DNA from the strains containing the empty vector pBHR1 produced an 800-bp PCR fragment (*Figure 5.1.10, lane 9*) as expected, and no PCR product was observed when genomic DNA from the wild-type strain was used (*Figure 5.1.10, lane 8*). One clone containing the correct plasmid (*Figure 5.1.10, lane 2*) was designated K96243[*bopE*TC] (*Chapter 2, Table 2.1*) and used for further experiments.

In order to show that any secretion of TC tagged BopE was TTSS-dependent, the pBHR1::P_{glmS2}::*bopE*TC construct was also transferred into a *B. pseudomallei bsaS* mutant (Gong *et al.*, manuscript in preparation), designated K96243*ΔbsaS* (*Chapter 2, Table 2.1*), by conjugation. BsaS encodes the TTSS3 ATPase and is essential for TTSS function, and loss-of-function of BsaS has been found to affect the secretion of BopE (Gong *et al.*, manuscript in preparation). Transconjugants were selected on LB agar containing 25 µg/mL tetracycline and 1 mg/mL kanamycin and clones were screened for the presence of the pBHR1::P_{glmS2}::*bopE*TC by PCR using the primers JT7080/JT7081 (*Chapter 2, Table 2.3*). As described above, PCR using these primers should amplify a 1,400-bp fragment from the pBHR1::P_{glmS2}::*bopE*TC plasmid. All clones tested showed the presence of the correct fragment (*Figure 5.1.11, lane 2 to 4*) and, as expected, no PCR product was observed when DNA from the K96243*ΔbsaS* strain was used as the template (*Figure 5.1.11, lane 6*). One clone (*Figure 5.1.11, lane 3*) was designated K96243*ΔbsaS*[*bopE*TC] (*Chapter 2, Table 2.1*) and selected for further experiments.

5.1.2 Generation of the TC-tagged BapA, BapB and BapC

Following generation of the TC-tagged *bopE* constructs, further constructs expressing TC-tagged BapA, BapB and BapC were generated. As the genomic insertion site of the TC-tagged *bopE* construct in mini-Tn*7* could not be identified, it was decided to generate the TC-tagged BapA, BapB and BapC in pBHR1. Since pBHR1 constructs containing the full-length *bapA*, *bapB* and *bapC* had already been generated and nucleotide-sequence confirmed during complementation (see *Chapter 3.5*), the TC encoding sequence was cloned separately into each of these constructs. In each case, the TC tag was generated by annealing the primers JT7147 and JT7241 (*Chapter 2, Table 2.4*) prior to ligation into *Acl*I-digested pBHR1::*bapA* (*Figure 5.1.12A*), pBHR1::*bapB* (*Figure 5.1.12B*) or pBHR1::*bapC* (*Figure 5.1.12C*). Potential pBHR1::*bapA*TC, pBHR1::*bapB*TC and pBHR1::*bapC*TC (*Chapter 2, Table 2.1*) recombinant plasmids were screened for

the presence of the TC motif by nucleotide sequencing using the primer JT7080 (data not shown). A single correct plasmid representing each construct was then transformed into *E. coli* S17-1/λ*pir* and introduced into the *B. pseudomallei* wild-type strain by conjugation. Colonies were selected on LB agar containing 8 µg/mL gentamicin and 1 mg/mL kanamycin and putative transconjugants were screened for the presence of the TC-tagged *bapA*, *bapB* and *bapC* sequences by PCR using the primers JT7080 and JT7081. PCR using this primer pair should amplify a 3,400-, 1,000- or 1,300-bp fragment in correct pBHR1::*bapA*TC, pBHR1::*bapB*TC or pBHR1::*bapC*TC constructs, respectively. Single pBHR1::*bapA*TC (*Figure 5.1.13A, lane 2*), pBHR1::*bapB*TC (*Figure 5.1.13B, lane 4*) and pBHR1::*bapC*TC (*Figure 5.1.13C, lane 2*) containing strains were identified and designated K96243[*bapA*TC], K96243[*bapB*TC] and K96243[*bapC*TC], respectively (*Chapter 2, Table 2.1*). The pBHR1::*bapA*TC, pBHR1::*bapB*TC and pBHR1::*bapC*TC constructs were also introduced into the K96243*ΔbsaS* strain by conjugation. Transconjugants that grew on LB agar containing 25 µg/mL tetracycline and 1 mg/mL kanamycin were screened for the presence of the pBHR1 constructs by PCR using the primers JT7080 and JT7081 as described previously. PCR using genomic DNA from strains putatively containing pBHR1::*bapA*TC (*Figure 5.1.14A, lane 2*), pBHR1::*bapB*TC (*Figure 5.1.14B, lane 4*) and pBHR1::*bapC*TC (*Figure 5.1.14C, lane 4*) generated the expected fragments of 3,400-, 1,000- and 1,300-bp, respectively. Thus, three clones were designated K96243*ΔbsaS*[*bapA*TC], K96243*ΔbsaS*[*bapB*TC] and K96243*ΔbsaS*[*bapC*TC] (*Chapter 2, Table 2.1*), respectively, and selected for further experiments.

5.1.3 Optimisation of the TC-FlAsH™-based fluorescence labelling

5.1.3.1 Visualisation of TC-tagged BopE and TC-tagged GspD

The arsenic molecules of the membrane-permeant fluorophore FlAsH can form covalent bonds with a TC motif and produce the fluorescent FlAsH-peptide complex (Adams *et al.*, 2002; Griffin *et al.*, 1998; Madani *et al.*, 2009). Following generation of the TC-tagged BopE, BapA, BapB and BapC constructs in *B. pseudomallei*, the TC-tagged BopE expressed constructs, both from the mini-Tn*7* (K96243*bopE*TC) and pBHR1 (K96243[*bopE*TC]), were tested first as a positive control to allow optimisation of the FlAsH labelling and to identify whether the arsenic molecules of FlAsH were able to access and bind to the TC tag. As another positive control for FlAsH labelling, an *E. coli* GspD tagged with TC, designated DH5α[pJP117] (*Chapter 2, Table 2.1*), was used since this had been characterised previously for FlAsH labelling (Dunstan *et al.*, 2013). Indeed, the TC-tagged GspD had been confirmed to fluoresce in the presence of FlAsH both following SDS-PAGE analysis and TCA/methanol precipitation (Dunstan *et al.*, 2013).

The strains DH5α[pJP117], K96243*bopE*TC and K96243[*bopE*TC] were grown in LB and cells were harvested at early- (OD_{600} = 0.3), mid- (OD_{600} = 0.6) and late- (OD_{600} = 1.0) exponential growth phase. Expression of TC-tagged GspD in the DH5α[pJP117] strain was induced by addition of arabinose as described previously (*Chapter 2.22*). Total proteins from each culture were precipitated with DOC/TCA (*Chapter 2.21*). Each of the protein samples (40-60 μg) was labelled with FlAsH (*Chapter 2.22*), the proteins were separated using SDS-PAGE (*Chapter 2.23*) and then the fluorescence measured immediately at 520 nm with an excitation at 488 nm with the GE Typhoon Trio™ imager (GE Healthcare, NSW, Australia). In addition, unlabelled samples were run on a separate gel for Coomassie Brilliant Blue staining (*Chapter 2.25*) in order to visualise and compare the amount of total protein on the gels. As expected, total protein samples recovered from the DH5α[pJP117] cultures, harvested at mid- (*Figure 5.1.15A, lane 3*) or late-exponential (*Figure 5.1.15A, lane 4*) phase, showed a strongly fluorescent protein of approximately 75-kDa, corresponding to the expected size of GspD. Therefore, sample preparation and FlAsH labelling conditions were appropriate for visualisation of TC-labelled GspD. However, a fluorescent signal at the expected size of the TC-tagged BopE was only detected in protein samples derived from cultures of the K96243[*bopE*TC] strain (*Figure 5.1.15E, lane 3 and 4*), but not protein samples derived from the K96243*bopE*TC strain (*Figure 5.1.15C, lane 3 and 4*). Putative TC-tagged BopE was observed in whole protein samples derived from both mid- (*Figure 5.1.15E, lane 3*) and late- (*Figure 5.1.15E, lane 4*) exponential phase cultures, but not early-exponential phase culture (*Figure 5.1.15E, lane 2*). Therefore, the TC-tagged BopE expressed from the replicating pBHR1 vector was accessible for formation of a fluorescent complex with the FlAsH compound. A non-specific fluorescent signal of an approximate 30-kDa was also observed in the positive control DH5α[pJP117] (*Figure 5.1.15A, lane 2 to 4*), K96243*bopE*TC (*Figure 5.1.15C, lane 2 to 4*) and K96243[*bopE*TC] (*Figure 5.1.15E, lane to 4*) strains.

To confirm that this fluorescent protein (~ 33-kDa) was indeed TC-tagged BopE, protein samples from the K96243[*bopE*TC] cultures were compared with proteins from the *E. coli* S17-1/λ*pir*[pBHR1::P_{glmS2}::*bopE*TC] cultures (*Chapter 2, Table 2.1*). DOC/TCA was used to precipitate total proteins from mid log phase cultures of each strain and these proteins labelled with the FlAsH compound and separated by SDS-PAGE. A fluorescent protein of an approximate 75-kDa was observed in the positive control DH5α[pJP117] strain (*Figure 5.1.16A, lane 7*). Both the K96243[*bopE*TC] and *E. coli* S17-1/λ*pir*[pBHR1::P_{glmS2}::*bopE*TC] total

protein samples contained a fluorescent protein of an approximate 33-kDa as expected for TC-tagged BopE (*Figure 5.1.16A, lane 2 and 5*, respectively). Importantly, FlAsH labelling of total protein samples from the K96243[pBHR1] and wild-type K96243 strains (*Figure 5.1.16A, lane 3 and 4*, respectively), did not identify any fluorescent proteins at 33 kDa, indicating that the TC-tagged BopE could form a fluorescent complex with FlAsH but the endogenous BopE (with no TC motif) could not. However, fluorescent proteins of approximated 22 (*Figure 5.1.16A, lane 2 to 5*), 30 (*Figure 5.1.16A, lane 2, 4, 5, 6 and 7*), 45 (*Figure 5.1.16A, lane 5 and 6*) and 51 (*Figure 5.1.16A, lane 5*) kDa were observed indicating that some native proteins could form a fluorescent complex with the FlAsH compound.

5.1.3.2 Labelling conditions using a range of reducing agents

In order to optimise the labelling of TC-tagged BopE, a range of different reducing agents (Enninga *et al.*, 2005; Getz *et al.*, 1999; Hearps *et al.*, 2007; Hoffmann *et al.*, 2010; Langhorst *et al.*, 2006; Stroffekova *et al.*, 2001) were tested to improve the signal-to-noise ratio of the TC-tagged BopE-FlAsH complex. Two commonly-used reducing agents tris(2-carboxyethyl) phosphine (TCEP) and 2,3-dimercapto-1-propanol (BAL) were compared with β-mercaptoethanol (BME). DOC/TCA precipitated total protein samples were prepared from the K96243*bopE*TC, K96243[*bopE*TC], K96243[pBHR1] and DH5α[pJP117] cultures as described previously. Each of the samples was resuspended in 1X sample buffer containing either BME (14.4 mM final concentration), TCEP (10 mM final concentration) or BAL (0.25 mM final concentration), prior to heating at 99^{o}C for 10 min and FlAsH labelling as described previously. Labelled samples were subjected to SDS-PAGE and the fluorescent signal visualised. The amount of protein loaded in each lane was evaluated by SDS-PAGE analysis of unlabelled samples and visualisation using Coomassie Brilliant Blue staining. As expected, the fluorescent signal from TC-tagged BopE derived from the K96243[*bopE*TC] strain (*Figure 5.1.17A, lane 5*) was stronger than the signal from the K96243*bopE*TC strain (*Figure 5.1.17A, lane 2*), confirming the previous results. This is likely due to the increased copy number of the pBHR1 construct compared to the mini-Tn*7* construct. Comparison of the effectiveness of the three reducing agents showed that resuspension in sample buffer containing TCEP (*Figure 5.1.17A, lane 3 and 6*) or BAL (*Figure 5.1.17A, lane 4 and 7*) gave no fluorescent signal from the TC-tagged BopE-FlAsH complex in either the mini-Tn*7* (*Figure 5.1.17A, lane 3 and 4*) or pBHR1 (*Figure 5.1.17A, lane 6 and 7*) constructs, suggesting that both reducing agents were incompatible with the FlAsH labelling conditions used in this study. Simultaneously, fluorescence from TC-tagged GspD was not observed when BAL was used as the reducing agent

(*Figure 5.1.17C, lane 7*), and a stronger non-specific fluorescent fragment was observed when TCEP was used (*Figure 5.1.17C, lane 6*). The BME-treated sample gave a strong GspD fluorescent signal and low non-specific fluorescence (*Figure 5.1.17C, lane 5*). Almost no fluorescence was observed in the negative control K96243[pBHR1] samples when the DOC/TCA precipitated proteins were labelled with either BME, TCEP or BAL (*Figure 5.1.17C, lane 2, 3 or 4*, respectively). Taken together, it was decided that BME be used as the reducing agent for all further FlAsH labelling experiments.

Given that BopE is a known TTSS3 effector that is secreted *in vitro* (Stevens *et al.*, 2003), following FlAsH labelling optimisation, the *in vitro* secretion of BopE was assessed. The K96243[*bopE*TC] and K96243[pBHR1] strains were grown to mid exponential phase. Total culture and supernatant samples were precipitated with DOC/TCA and labelled with FlAsH using BME as the reducing agent. Samples were separated by SDS-PAGE and the fluorescence measured. The separated proteins were also transferred to PVDF membrane and used in Western immunoblotting experiments with BopE-specific antiserum (*Chapter 2.24*). Protein samples were also assessed for total proteins by SDS-PAGE and Coomassie Brilliant Blue staining. A fluorescently labelled protein of the expected size of the TC-tagged BopE was observed on total proteins derived from either whole culture or supernatant of the K96243[*bopE*TC] (*Figure 5.1.18A, lane 2 or 3*, respectively). This was confirmed by the presence of an extra BopE-specific protein identified by Western immunoblotting (*Figure 5.1.18B, lanes 2 and 3*) in the K96243[*bopE*TC] strain, one corresponding to the wild-type BopE and one corresponding to the TC-tagged version expressed from the pBHR1::P_{glmS2}::*bopE*TC construct, indicating both wild-type and TC-tagged BopE were secreted. However, only a single BopE-specific band was observed in supernatant samples derived from the K96243[pBHR1] strain (*Figure 5.1.18B, lane 5*), indicating normal secretion of the chromosomally encoded BopE in the presence of pBHR1. Thus, the presence of TC-tagged BopE does not interfere with normal TTSS function and FlAsH can be used to assess effector protein secretion.

5.1.3.3 Optimisation of the TC-FlAsH^{TM}-based fluorescence labelling inside live bacterial cells

In addition to the use of FlAsH-labelling of DOC/TCA precipitated protein samples, the FlAsH labelling technique can be used to label TC-tagged proteins inside live bacterial cells (Enninga *et al.*, 2005). In an attempt to verify the secretion of TC-tagged BopE from the pBHR1 construct, live cell labelling was conducted. Mid exponential phase cultures of the K96243[*bopE*TC],

K96243[pBHR1] and DH5α[pJP117] strains were incubated with the FlAsH compound, and then proteins separated by SDS-PAGE. Three commonly-used reducing agents for live FlAsH labelling (DTT, TCEP and Lumio™ Gel Sample Buffer) were tested to optimise the signal-to-noise ratio of the fluorescent signal since no TC-tagged BopE protein was detected when BME was used as the reducing agent (data not shown). Lumio™ Gel Sample Buffer (1X), taken from the Lumio™ Green Detection Kit (catalogue number T34561, Life Technologies™, USA), was also tested as this buffer was specifically designed for FlAsH labelling. Interestingly, the best labelling was observed when DTT was used as the reducing agent as the labelling of TC-tagged BopE (*Figure 5.1.19A, lane 2*) and GspD (*Figure 5.1.19A, lane 8*) was most specific and sensitive in the presence of DTT. As expected, no fluorescent signal was observed in the K96243[pBHR1] samples (*Figure 5.1.19A, lane 5 to 7*). Thus, live cell labelling followed by denaturation in DTT-containing sample buffer was used for further experiments on the TC-tagged BapA, BapB and BapC.

5.1.4 Investigation of the TC-FlAsH™-based fluorescence labelling of TC-tagged BapA, BapB and BapC constructs

5.1.4.1 Live bacterial samples of TC-tagged BapA and BapC

Following optimisation of FlAsH labelling conditions, TC-tagged BopE could be detected following the labelling of either live bacterial cells or DOC/TCA precipitated proteins. Therefore, TC-tagged BapA, BapB and BapC constructs were generated in both the *B. pseudomallei* wild-type strain and the TTSS-defective *bsaS* mutant (see *Chapter 5.1.2*). Live cell labelling was first used to verify the ability of the TC-tagged BapA, BapB and BapC to associate with the FlAsH compound and to form a fluorescent complex. Mid exponential growth phase cultures of the K96243[*bapA*TC], K96243[*bapC*TC], K96243[*bopE*TC] and K96243[pBHR1] were labelled with FlAsH (*Chapter 2.22*) and the fluorescent complex detected following SDS-PAGE (*Chapter 2.23*). As expected, a fluorescent position of 33 kDa corresponding to TC-tagged BopE was observed in the K96243[*bopE*TC] samples (*Figure 5.1.20A, lane 4*) but not in the K96243[pBHR1] samples (*Figure 5.1.20A, lane 5*). In samples derived from the K96243[*bapA*TC], a strongly fluorescent signal at approximately 120 kDa was observed (*Figure 5.1.20A, lane 2*). This 120 kDa band was predicted to be TC-tagged BapA. The size of BapA is predicted to be 88 kDa, but no fluorescent proteins were observed in the K96243[pBHR1] negative control, indicating that there may be some protein-protein interactions of BapA with another protein, possibly a chaperone. In samples derived from the K96243[*bapC*TC] strain, a fluorescent protein of approximately 23 kDa was observed; this is at

the predicted size for BapC (*Figure 5.1.20A, lane 3*). Therefore, both TC-tagged BapA and BapC were able to form a fluorescent complex with the FlAsH reagent.

5.1.4.2 Precipitated protein samples of TC-tagged BapA and BapC

As BapA and BapC are located in the same putative operon as BopE (*Chapter 1.3.8, Figure 1.3.3*), it was hypothesised that both BapA and BapC should be expressed during *in vitro* growth of *B. pseudomallei* and may be secreted in a similar manner to BopE. To prove both hypotheses, the K96243[*bapA*TC] and K96243[*bapC*TC] strains were investigated for secretion of TC-tagged BapA and BapC using FlAsH labelling. As done previously for TC-tagged BopE, strains were grown to mid exponential phase, supernatant samples collected, proteins precipitated with DOC/TCA and then labelled with the FlAsH reagent. As expected, a fluorescent signal corresponding to TC-tagged BopE was detected in the DOC/TCA precipitated proteins from the supernatant of the K96243[*bopE*TC] strain (*Figure 5.1.21A, lane 6*) but no fluorescent proteins identified in the supernatant samples from K96243[pBHR1] cultures (*Figure 5.1.21A, lane 8*), confirming *in vitro* secretion of BopE. In the DOC/TCA precipitated supernatant samples of the K96243[*bapA*TC] strain (*Figure 5.1.21A, lane 2*), a fluorescent protein of approximately 120 kDa was observed. This is the same size as identified previously for TC-tagged BapA (see *Figure 5.1.20A, lane 2*). Therefore, BapA is secreted during *in vitro* growth of *B. pseudomallei*. Similarly, in the supernatant samples derived from the DOC/TCA precipitated supernatant samples of the K96243[*bapC*TC] strain (*Figure 5.1.21A, lane 4*), a strongly fluorescent band of 23 kDa was observed which corresponds to TC-tagged BapC, as identified previously (see *Figure 5.1.20A, lane 3*). Thus, TC-tagged BapC is also secreted by *B. pseudomallei* during *in vitro* growth.

As hypothesised both TC-tagged BapA and BapC exhibited *in vitro* secretion. In order to show that BapA and BapC are secreted in a TTSS3-dependent manner, as is the use for BopE, the supernatant samples from the K96243*ΔbsaS*[*bapA*TC] and K96243*ΔbsaS*[*bapC*TC] strains (*Chapter 2, Table 2.1*) were analysed for the secretion of TC-tagged BapA and BapC, respectively. Proteins in supernatant samples from mid exponential growth phase cultures of the K96243*ΔbsaS*[*bapA*TC], K96243*ΔbsaS*[*bapC*TC], K96243*ΔbsaS*[*bopE*TC] and K96243*ΔbsaS*[pBHR1] strains were precipitated with DOC/TCA, labelled with the FlAsH reagent, separated by SDS-PAGE and then fluorescence measured. Importantly, no fluorescent bands corresponding to BapA (120 kDa) or BapC (23 kDa) were observed in the supernatant samples derived from the appropriate K96243*ΔbsaS* strains (*Figure 5.1.21A, lane 3 and 5*,

respectively). Similarly, as observed previously, no fluorescent band corresponding to BopE was observed in the K96243*ΔbsaS*[*bopE*TC] strain supernatant samples. Therefore, TC-tagged BapA and BapC are secreted during *in vitro* growth in a TTSS3-dependent manner and are likely TTSS3 effectors.

5.1.4.3 The TC-FlAsH™-based fluorescence labelling of TC-tagged BapB

Following the demonstration that BapA and BapC are secreted in a TTSS3-dependent manner using the TC-FlAsH™-based labelling technique, BapB was also analysed in order to determine whether it is secreted in a similar manner. The TC-tagged BapB construct was mobilised into both the *B. pseudomallei* wild-type K96243 and the K96243*ΔbsaS* strains as described in *Chapter 5.1.2*. Proteins in both supernatant and total cultures from mid exponential phase cultures of either the K96243[*bapB*TC], K96243[pBHR1], K96243*ΔbsaS*[*bapB*TC] or K96243*ΔbsaS*[pBHR1] strain were precipitated by DOC/TCA precipitation, labelled with the FlAsH reagent, separated by SDS-PAGE and fluorescence measured as described previously. No fluorescent proteins were identified either in the DOC/TCA precipitated supernatant samples (*Figure 5.1.22A, lane 2*) or in total culture samples (*Figure 5.1.22A, lane 6*), suggesting that there was no formation of the TC-tagged BapB-FlAsH complex. Several attempts were conducted to optimise the BapB visualisation, including Tris-glycine and Tris-Tricine gradient SDS-PAGE, however no fluorescent signals corresponding to BapB were detected. Further analysis of BapB was not pursued.

5.1.5 Effect of sodium chloride (NaCl) and congo red on secretion of TTSS3 effectors

Pumirat *et al.* (2010) demonstrated an effect of high salt concentration on the *B. pseudomallei* TTSS3 effector genes. Indeed, a significant increase in both transcription and translation of BopE was observed when bacteria were cultured in 320 mM NaCl for 3 h. Given that the TTSS3 genes *bapA*, *bapB* and *bapC* are located downstream of *bopE*, and BapA and BapC are secreted effectors (see *Chapter 5.1.4*), it was hypothesised that expression of BapA, BapB and/or BapC would be increased when bacteria were grown in high salt concentrations (Pumirat *et al.*, 2010). Firstly, BopE expression was analysed in the K96243[*bopE*TC] and K96243[pBHR1] strains grown under high (320 mM) and normal (85.6 mM) NaCl conditions using both FlAsH labelling and Western blotting. Both bacterial strains were grown overnight in LB without additional NaCl. Strains were then subcultured in LB supplemented with either 85.6 mM or 320 mM NaCl

for 3 ½ to 4 h to mid exponential growth phase. Total cultures (1 mL) and filtered supernatant samples were collected. Total proteins in each sample were precipitated with DOC/TCA, FlAsH labelled and separated by SDS-PAGE. After measuring the fluorescent signal, proteins were transferred to PVDF membranes in order to perform Western blotting with BopE-specific antiserum. Total proteins were also visualised by SDS-PAGE followed by Coomassie Brilliant Blue staining. Although, to our knowledge, the effect of high NaCl concentration on the expression of *E. coli* type II secretion system molecules has never been reported, it was decided to additionally test the effect of growth in high salt conditions on the secretion of GspD from the DH5α[pJP117] strain.

DOC/TCA precipitated proteins from total culture and supernatant samples of the K96243[*bopE*TC] grown in normal LB exhibited a fluorescent TC-tagged BopE-FlAsH band (*Figure 5.1.23A, lane 2 and 3*, respectively), and showed two BopE-specific proteins when probed with the BopE-specific antiserum (*Figure 5.1.23B, lane 2 and 3*, respectively). No fluorescent signal was detected in any of DOC/TCA precipitated total culture and supernatant samples of the negative control K96243[pBHR1] (*Figure 5.1.23A, lane 6 to 9*) but a single wild-type BopE band was observed (*Figure 5.1.23B, lane 6 to 9*). The fluorescent signal corresponding to TC-tagged GspD (75 kDa) from the FlAsH positive control DH5α[pJP117] showed no substantial increase when the strain was cultured in media containing 320 mM NaCl (*Figure 5.1.24A, lane 3*) comparred with 85.6 mM NaCl (*Figure 5.1.24A, lane 2*), suggesting that high NaCl does not stimulate GspD expression in *E. coli*. The level of BopE expression and secretion after 3 h of incubation in media containing 320 mM NaCl, measured by either FlAsH labelling (*Figure 5.1.23A, lane 4 and 5*, respectively) or Western blotting (*Figure 5.1.23B and Figure 5.1.23C, lane 4 and 5*, respectively) was increased slightly from growth in normal media, measured by FlAsH labelling (*Figure 5.1.23A, lane 2 and 3*, respectively) or Western blotting (*Figure 5.1.23B and Figure 5.1.23C, lane 2 and 3*, respectively). However, the level of BopE expression and secretion following 3 h growth in 320 mM NaCl for the K96243[pBHR1] strain showed an increase of approximately two-fold (*Figure 5.1.23C, lane 8*; $P < 0.05$) and three-fold (*Figure 5.1.23C, lane 9*; $P < 0.05$), respectively, compared with the strain grown in media with normal levels of NaCl (*Figure 5.1.23C, lane 6 and 7*, respectively). These data indicate and confirm that 3 h incubation of 320 mM NaCl can enhance BopE expression and secretion.

In addition to high NaCl as a stimulating condition for the TTSS3 expression, congo red has been widely used as an inducer of *Shigella* TTSS effector secretion (Bahrani *et al.*, 1997;

Enninga *et al.*, 2005; Firdausi Qadri *et al.*, 1988; Simpson *et al.*, 2010). Given that there is significant similarity between some of the TTSS effectors of *Shigella* and *B. pseudomallei* (Sun & Gan, 2010), it was hypothesised that the expression of the *B. pseudomallei* TTSS effectors might also be upregulated by treating the bacteria with congo red. To examine this hypothesis, the level of BopE expression in the K96243[*bopE*TC] and K96243[pBHR1] strains was tested after congo red stimulation. In a similar manner to high salt concentration experiment, the FlAsH positive control DH5α[pJP117] was also tested even though, to our knowledge, the effect of congo red on the stimulation of *E. coli* type II secretion system has never been reported. In addition, sucrose was added to the congo red solution to analyse whether it enhanced the effect of congo red as sucrose (5% w/v) has been reported to enhance uptake of congo red in *Staphylococcus* spp. (Freeman *et al.*, 1989). In brief, overnight cultures were subcultured into either LB, LB supplemented with 5% (w/v) sucrose, LB supplemented with 0.08% (w/v) congo red or LB supplemented with 5% (w/v) sucrose and 0.08% (w/v) congo red, and grown to mid exponential growth phase. Live bacterial cultures were incubated with the FlAsH reagent and proteins separated by SDS-PAGE analysis. Analysis of the levels of fluorescent BopE indicated no significant difference in BopE expression from cells grown in the presence of sucrose (5% w/v) and/or congo red (0.08% w/v) (*Figure 5.1.25*). Similarly, there was no difference in the levels of GspD expression from the DH5α[pJP117] under any of the conditions tested (data not shown). Interestingly, growth of *B. pseudomallei* cultures in the presence of congo red caused significant obstruction of the fluorescent signal of the TC-tagged BopE (*Figure 5.1.25A, lane 4 and 5*), but not that of the GspD-FlAsH (data not shown), suggesting that *B. pseudomallei* can bind or take up the congo red dye. Extra rounds of cell washing before SDS-PAGE failed to remove this congo red from *B. pseudomallei* (data not shown). Thus, BopE secretion in the presence of congo red was assessed by Western immunoblotting. Strains were grown to mid exponential phase in either LB or LB supplemented with 0.08% (w/v) congo red. Proteins from either total cultures or supernatants were precipitated by DOC/TCA, labelled with the FlAsH reagent and separated by SDS-PAGE. The fluorescence was measured and proteins transferred to PVDF membranes for Western immunoblotting using BopE-specific antiserum. A fluorescent band corresponding to TC-tagged BopE was observed in protein samples derived from total culture and supernatant of the K96243[*bopE*TC] strain grown in the absence of congo red (*Figure 5.1.26A, lane 2 and 3*, respectively), but not in the presence of congo red, due to obstruction of the fluorescent signal, and as expected no signal was observed in any of the K96243[pBHR1] samples (*Figure 5.1.26A, lane 6 to 9*). However, Western blot analysis indicated that BopE expression was indistinguishable in the presence or absence of congo red

(*Figure 5.1.27*). Similarly, there was no difference in BopE secretion and expression for the K96243[pBHR1] strain grown with or without congo red (*Figure 5.1.27*). These data indicate that it is unlikely that congo red functions as an inducer of *B. pseudomallei* TTSS effector secretion.

5.2 Role of BapA, BapB or BapC in regulation of the TTSS3 function

The TTSS is a highly complex secretion system and the expression of structural and effector proteins must be tightly regulated (Cornelis & Van Gijsegem, 2000; Deane *et al.*, 2010; Ham *et al.*, 2011). Following host cell contact, the tip complex proteins of the needle-like apparatus form a pore through the host cell membrane, allowing the secretion of appropriate effectors into the host (Deane *et al.*, 2006; Matteï *et al.*, 2011; Mueller *et al.*, 2008) although in *B. pseudomallei* secretion of BopE, BapA and BapC also occur *in vitro*. To determine whether BapA, BapB or BapC play a role in regulating TTSS expression and/or function, the *in vitro* secretion of BopE was assessed in each of the K96243*ΔbapA*, K96243*ΔbapB*, K96243*ΔbapC* and K96243*ΔbapBC* strains. Furthermore, the transcription of *bopE* in each of the mutants was additionally evaluated using reverse transcription PCR (RT-PCR).

5.2.1 BopE secretion and expression is increased in the K96243*ΔbapB* strain

To analyse the secretion of BopE in each of the mutant strains, Western immunoblotting using BopE-specific antiserum was conducted on culture supernatants. As a negative control, a *bopE* single-crossover mutant was constructed by allelic exchange using the pDM4::*bopE* mutagenesis vector constructed by Stevens *et al.* (2002). This construct was mobilised into *B. pseudomallei* by conjugation (*Chapter 2.9*) and transconjugants selected on LB agar containing 8 µg/mL of gentamicin and 40 µg/mL of chloramphenicol. Putative single-crossover mutants were screened by PCR using the primer pair JT6100/JT6101 (*Chapter 2, Table 2.3*) specific for the chloramphenicol acety transferase (*cat*) gene of pDM4 (*Figure 5.2.1A*). Seven clones (*Figure 5.2.1B, lane 2 to 8*) displayed the appropriate size of PCR product compared to the positive control (*Figure 5.2.1B, lane 9*), indicating the presence of the *bopE* single-crossover mutant construct. Following PCR screening, three potential K96243*ΔbopE*::pDM4 strains (*Figure 5.2.1B, lane 4 to 6*) were selected for Western immunoblotting using the BopE-specific antiserum. Protein samples from supernatant (*Figure 5.2.2A, lane 6*) or total culture (*Figure 5.2.2C, lane 6*) of the wild-type strain showed a BopE-specific band at 33 kDa. This band was also observed in protein samples from supernatant (*Figure 5.2.2A, lane 2*) or total culture (*Figure 5.2.2C, lane 2*) of the K96243*ΔbapC* strain. However, no BopE-specific band was

observed in supernatant or total culture samples derived from the putative single-crossover mutants. Therefore, the K96243*ΔbopE*::pDM4 (*Chapter 2, Table 2.1*) shown in *Figure 5.2.2, lane 4* was used for further experiments.

Following generation of the K96243*ΔbopE*::pDM4 strain, the *in vitro* secretion and expression of BopE was investigated in each of the K96243*ΔbapA*, K96243*ΔbapB*, K96243*ΔbapC* and K96243*ΔbapBC* strains. Furthermore, BopE secretion was analysed at three distinct growth phases (early, mid and late exponential) for each of the bacterial strains. Both total culture and supernatant samples were used for assessing the BopE expression and secretion, respectively, and the same cultures were used for RNA extraction for transcriptional analyses (see *Chapter 5.2.2*). Protein samples were normalised using 2-D Quant Kit (GE Healthcare, Australia) according to the manufacturer's instruction prior to SDS-PAGE (*Chapter 2.21*).

In early-exponential phase culture supernatants (*Figure 5.2.3*), as expected, the K96243*ΔbopE*::pDM4 strain showed no expression of full length BopE although a truncated BopE was observed. The wild-type, K96243*ΔbapA* and K96243*ΔbapC* strains showed similar levels of secreted BopE, but the K96243*ΔbapB* strain showed a substantial increase of approximately 30-fold compared to the wild-type ($P < 0.05$). The K96243*ΔbapBC* strain also exhibited a 7-fold increase in secreted BopE ($P < 0.05$). A significant increase of approximately 30-fold ($P < 0.05$) and 10-fold ($P < 0.05$) in BopE production was also observed in total culture samples derived from the K96243*ΔbapB* and K96243*ΔbapC* strains, respectively (*Figure 5.2.3D and F*). However, total culture samples derived from the K96243*ΔbapA*, K96243*ΔbapBC* and K96243*ΔbopE*::pDM4 strains exhibited no significant difference in BopE production compared to the wild-type strain. Analysis of BopE secretion from mid-exponential phase cultures (*Figure 5.2.4A and C*) indicated that only the K96243*ΔbapB* strain exhibited a statistically significant increase of approximately 2-fold ($P < 0.05$) in secreted BopE, whereas the K96243*ΔbapA* strain showed a slight decrease of approximately 1.5-fold ($P < 0.05$) in secreted BopE. The K96243*ΔbapC* and K96243*ΔbapBC* strains showed a similar level of BopE production to that of the wild-type strain. A slight decrease of approximately 2-fold ($P < 0.05$) in BopE production was also observed in total culture samples derived from the K96243*ΔbapA* strain (*Figure 5.2.4D and F*). In late-exponential phase culture supernatants (*Figure 5.2.5A and C*), the K96243*ΔbapB* strain again showed a significant increase in secreted BopE (4-fold, $P < 0.05$). The K96243*ΔbapA* strain also exhibited a slight increase of approximately 2-fold ($P < 0.05$) in

secreted BopE while there was no difference in BopE secretion observed in the K96243*ΔbapC* and K96243*ΔbapBC* strains. Surprisingly, in late exponential phase total culture samples there was no difference in BopE production observed in the K96243*ΔbapA*, K96243*ΔbapB*, K96243*ΔbapC* or K96243*ΔbapBC* strains compared to the wild-type strain (*Figure 5.2.5D and F*).

5.2.2 The transcription of *bopE* is increased in the K96243*ΔbapB* strain

Given the substantial increase in both BopE secretion observed in the K96243*ΔbapB* strain, it was decided to further investigate whether there was altered transcription of *bopE* in any of the mutant strains using reverse transcription PCR (RT-PCR). Total RNA was harvested from each of the mutant strains and cDNA generated as described (*Chapter 2.12*). The transcription of *bopE* was first assessed by semi-quantitative RT-PCR (*Chapter 2.12*) using cDNA samples derived from the K96243*ΔbapA*, *ΔbapB*, *ΔbapC* and *ΔbapBC* strains together with the primers JT6079 and JT6080 (*Chapter 2, Table 2.4; Figure 5.2.6*). A PCR product corresponding to the *bopE* transcript was observed using cDNA derived from all of the strains and no products were observed in the RT- negative controls (*Figure 5.2.7A*). A weak *bopE*-specific PCR product was observed when cDNA from the K96243*ΔbapA*, *ΔbapC* and *ΔbapBC* and wild-type strains was used, whereas significantly more product was amplified when cDNA from the K96243*ΔbapB* strain was used as the template (*Figure 5.2.7A, lane 4*). These data suggest that transcription of *bopE* was increased in the K96243*ΔbapB* strain. This result was verified by using quantitative real-time RT-PCR (*Chapter 2.13*).

The primers JT7472 and JT7473 (*Chapter 2, Table 2.4; Figure 5.2.6*) were specifically designed for amplification of *bopE* for real-time RT-PCR. For normalisation of the real-time RT-PCR data, the oligonucleotide primers JT7474 and JT7475 (*Chapter 2, Table 2.4; Figure 5.2.6*) were specifically designed to amplify a portion of the housekeeping gene *rpoA*. The *rpoA* gene was chosen as the normaliser based on the high stability of *rpoA* transcription under various conditions (Lipscomb & Schell, 2011; Ritz *et al.*, 2009). The transcription of *bopE* was assessed in early-, mid- and late-exponential phase cultures of the K96243*ΔbapA* and *ΔbapB* strains in comparison to that of the wild-type strain. At early-exponential growth phase, the transcription of *bopE* in the wild-type and K96243*ΔbapA* strains was indistinguishable but *bopE* transcription in the K96243*ΔbapB* strain was approximately 5-fold ($P < 0.05$) higher than that in the wild-type strain (*Figure 5.2.7B*). At mid-exponential growth phase (*Figure 5.2.8A*), *bopE* transcription was significantly increased (3-fold; $P < 0.0001$) in the K96243*ΔbapB* strain whereas the transcription

of *bopE* was decreased in the K96243*ΔbapA* strain (3-fold; $P < 0.001$). Interestingly, for late exponential growth phase samples (*Figure 5.2.8B*), *bopE* transcription was also increased approximately 3-fold in the K96243*ΔbapB* strain compared to the wild-type strain ($P < 0.0001$) but there was a 3-fold decrease in transcription in the K96243*ΔbapA* strain ($P < 0.001$). Therefore, *bopE* transcription was increased between 3- and 5-fold in the K96243*ΔbapB* strain during all three exponential growth phases (early, mid and late).

5.3 Discussion

Following the characterisation of the role of the putative TTSS3 effectors BapA, BapB and BapC in *B. pseudomallei* virulence and in a range of *in vitro* assays (see *Chapters 3 and 4*), fluorescent-labelling of the proteins BapA, BapB and BapC were used to determine whether they were truly TTSS3-dependent secreted effectors.

5.3.1 BapA and BapC are secreted by the TTSS3

The TTSS is a special structure produced by many Gram-negative pathogens that allows the direct transfer of bacterial effector proteins from the bacteria to host cells (Coburn *et al.*, 2007; Deane *et al.*, 2006; Galan & Collmer, 1999). These bacterial effectors are essentially responsible for interacting with and modulating host cell functions (Dean, 2011). However, only two *B. pseudomallei* proteins, namely BopE and BopC, are known to be specifically secreted by the TTSS3. In order to identify novel effector proteins, fluorescent-tagging of putative effectors has been widely used in other species (Enninga & Rosenshine, 2009; Giepmans *et al.*, 2006). In this study, the putative effectors BapA, BapB and BapC were fused with a TC tag and the location of the fusion proteins assessed by FlAsH labelling. This technique has been successfully used to investigate secretion of TTSS effectors in *S. flexneri*, Enteropathogenic *E. coli* (EPEC) and *S. enterica* serovar Typhimurium (Enninga *et al.*, 2005; Simpson *et al.*, 2010; VanEngelenburg & Palmer, 2008). Stevens *et al.* (2003) first proved that BopE was secreted in a TTSS3-dependent manner, by Western blot analysis using BopE-specific antiserum, and also characterised the major role of this effector in facilitating bacterial invasion by modifying host actin. Thus, this well-characterised TTSS3 effector was chosen as the test protein for optimisation of FlAsH labelling conditions. The TC-tagged BopE was first constructed in the mini-Tn*7* vector and used for integration into the bacterial genome (Choi *et al.*, 2006; Choi *et al.*, 2005). As had been observed previously for complementation of the various *bap* mutants (see *Chapter 3.7*), the location of transposon integration in the bacterial genome could not be determined. In addition, when labelled with the FlAsH compound, the TC-tagged BopE

fluorescent signal in the mini-Tn*7* construct was undetectable whereas there was a detectable signal from the BopE-pBHR1 construct. Therefore, TC-tagged BapA, BapB and BapC were generated only in the pBHR1 vector. After several rounds of optimisation, BME and DTT were chosen as the best reducing agents for FlAsH labelling in DOC/TCA precipitated samples and live bacterial cells, respectively, since the signal-to-noise ratio was highest. When using the optimum labelling conditions to investigate the *in vitro* secretion of the TC-tagged BapA, BapB and BapC, BapA and BapC were clearly shown to be secreted in a TTSS3-dependent manner since the expected bands of the BapA and BapC fluorescent complex were detected only in the K96243[*bapA*TC] and the K96243[*bapC*TC] strains, but were absent in the K96243*ΔbsaS*[*bapA*TC] and K96243*ΔbsaS*[*bapC*TC] strains. To our knowledge, this is the first time FlAsH labelling has been used to investigate the secretion of *B. pseudomallei* TTSS molecules and the first direct demonstration that BapA and BapC as TTSS3-secreted effectors.

In contrast to what was observed for BapA and BapC, the labelling of the TC-tagged BapB could not be demonstrated either in total cultures or supernatants using the optimum FlAsH labelling conditions even when high percentage polyacrylamide gels were used for protein separation. Identification of the labelled TC-tagged BapB was attempted under a range of conditions specific for small proteins, including 4-20% gradient Tris-glycine or Tris-Tricine SDS-PAGE gels (data not shown). Nonetheless, we were unable to measure any fluorescent signal even in the total culture samples. The possible explanations for this could be that, firstly, the localisation of the TC tag, in the BapB structure, was not accessible for the FlAsH compound to bind. Secondly, based on the bioinformatic data of BapB, it is possible that this small, acidic pI protein functions as a TTSS3 chaperone. The predicted functional domain of BapB is a 4'-phosphopantetheine prosthetic group which generally functions as a 'swinging arm' for transferring an acyl molecule during fatty acid biosynthesis (Byers & Gong, 2007; Chan & Vogel, 2010). This suggests a high conformational flexibility of BapB in order to properly transfer the acyl protein from one molecule to another. Given that the distance between the two pairs of cysteines in the TC fused protein has to be properly matched to the spacing of the bi-arsenic molecules of the FlAsH compound (Griffin *et al.*, 1998), such conformational flexibility may inhibit the TC-FlAsH interaction (Hoffmann *et al.*, 2010; Machleidt *et al.*, 2006). Thirdly, the TC-tag at the C-terminal end of BapB may alter the conformation and/or function of the protein resulting in the formation of a non-functional BapB which is rapidly degraded within the cell. Fourthly, the expression level of BapB could possibly be too low to be measured by the FlAsH labelling technique. Finally, given that the K96243*ΔbapB* strain showed a significant decrease in *in vivo* growth (see

Chapter 3.3), it is possible that BapB is only maximally expressed *in vivo*. This specificity for expression in the host has been demonstrated for some effectors secreted by the SPI2 of *Salmonella*, with expression only triggered after internalisation of the bacteria (Geddes *et al.*, 2007). In addition, secretion of the *Bordetella* TTSS effector Bsp22 can only be detected in clinical samples and not from cells grown in *in vitro* culture medium (Fennelly *et al.*, 2008; Gaillard *et al.*, 2011). Thus, it is possible that BapB, unlike BapA, BapC and BopE, is not secreted under normal *in vitro* growth conditions. Investigation of BapB expression in sera from *B. pseudomallei*-infected mice and/or from melioidosis patients should be further conducted to prove this hypothesis. Nevertheless, given the current data, it is not possible to determine whether BapB is a TTSS3 effector.

5.3.2 The *B. pseudomallei* TTSS3 is not stimulated by congo red but is altered by high salt conditions

Upon contact of the bacteria with the host cell, the TTSS3 would be activated, and the appropriate effectors subsequently secreted (Hayes *et al.*, 2010). This suggests that TTSS3 secretion will be regulated by host conditions, such as the temperature and/or cholesterol in plasma membrane. However, in other bacterial species e.g. *Shigella*, *Salmonella* and *P. aeruginosa*, several artificial conditions have been used to trigger TTSS activities, including congo red (Bahrani *et al.*, 1997; Qadri *et al.*, 1988), acidic conditions (Markham *et al.*, 2008; Rappl *et al.*, 2003), calcium depletion (Kim *et al.*, 2005) and reduced oxygen (O'Callaghan *et al.*, 2011; Sturm *et al.*, 2011) conditions. In this study, two possible TTSS stimulation conditions were tested.

Growth of *B. pseudomallei* in *in vitro* culture medium supplemented with 320 mM NaCl has been demonstrated to increase production and secretion of BipD and BopE after 3 and 6 h incubation (Pumirat *et al.*, 2010). Similarly, in this study, a small increase in expression and secretion of BopE was observed when the K96243[pBHR1] strain was grown in LB supplemented with 320 mM NaCl for 3 h. In adidition, Pumirat *et al.* (2010) additionally stated that the upregulation of several TTSS3 genes occurred in a time-dependent manner as the level of gene expression was greater in the cultures treated with high salt condition for 6 h as compared with those treated for 3 h. They also showed that the expression of BipD and BopE was increased only at 6 h of incubation using Western blot analysis. This could explain why we observed only a marginal increase in BopE secretion in cells grown in high salt for 3 h. In contrast to the K96243[pBHR1] strain, the fluorescent signal corresponding to TC-tagged BopE

in the K96243[*bopE*TC] strain showed no difference when bacteria was grown in LB supplemented with 320 mM NaCl for 3 h. One possible explanation for this is that such high NaCl condition only stimulates native BopE in the bacterial genome. In addition, the *bopE* gene in the K96243[*bopE*TC] strain contained 30 bp upstream of the ATG translation start codon, which almost certainly does not contain the native promoter; hence, the TC-tagged BopE in a replicating plasmid pBHR1 would be highly unlikely to respond to any environmental signals. A more detailed time-course experiment of BopE expression in high salt incubation, for instance, 3, 6 and 9 h time points, should be further conducted in order to prove this hypothesis. Moreover, the TC-tagged BopE, BapA and BapC constructs with a native *B. pseudomallei* TTSS3 promoter should be generated and used to compare the fluorescent signal in the strains grown under high NaCl condition to the signal under normal condition.

Congo red has been widely used as a stimulant of *Shigella* TTSS activity (Bahrani *et al.*, 1997; Enninga *et al.*, 2005; Simpson *et al.*, 2010). Although the mechanism by which this dye functions with regard to TTSS stimulation has not yet been described, there appears to be a direct correlation between congo red uptake and pathogenicity (Qadri *et al.*, 1988). In this study, the same congo red treatment conditions known to stimulate the TTSS secretion in *Shigella* (Enninga *et al.*, 2005; Freeman *et al.*, 1989) were analysed for their effect on TTSS3 function in *B. pseudomallei*. In contrast to the high salt concentration conditions tested, there was no substantial increase observed in either the expression or secretion of BopE, suggesting that congo red does not stimulate the TTSS3 in *B. pseudomallei*. The survival mechanisms of different Gram-negative pathogens following host cell internalisation are different and it is likely that different factors stimulate the TTSS (Allwood *et al.*, 2011; Galyov *et al.*, 2010; Schroeder & Hilbi, 2008). This may explain the specificity of certain TTSS stimulants, which only activate TTSS function in particular pathogenic bacteria, for example, acidic conditions (Rappl *et al.*, 2003) or a low-calcium environment (Kim *et al.*, 2005) activate the *Salmonella* or *P. aeruginosa* TTSSs, respectively. Nonetheless, it remains possible that further optimisation of congo red stimulation conditions, including different concentrations and longer incubation times, could identify a condition that would stimulate *B. pseudomallei* TTSS3 activity.

5.3.3 An involvement of BapA, BapB and/or BapC in the *B. pseudomallei* TTSS3 secretion

While BapA and BapC are clearly secreted in a TTSS3-dependent manner, indicating their role as TTSS3 effectors, it is also possible that both proteins, and perhaps BapB, may play a role in

the TTSS3 secretion process. Therefore, to test whether loss of BapA, BapB or BapC affected the activity of the TTSS3, expression of the effector BopE, as the marker of the TTSS activity, was analysed in the K96243*ΔbapA*, *ΔbapB*, *ΔbapC*, *ΔbapBC* strains in comparison to the wild-type strain, at early, mid and late exponential growth phase. BopE secretion in the K96243*ΔbapA* strain was similar to that of the wild-type strain at early exponential growth phase, but showed a slight decrease and then increase at mid and late exponential growth phase, respectively. Surprisingly, transcription of *bopE* in the K96243*ΔbapA* strain was decreased at both mid and late growth phase. These data clearly indicate that BapA is not required for TTSS3 secretion, but indicate that loss of BapA may play a minor or indirect role in regulation of TTSS activity.

The level of BopE secretion was significantly increased in the K96243*ΔbapB* strain at all three-growth phases tested. The total production of BopE was also significantly higher in the K96243*ΔbapB* strain at early, but not mid and late growth phase. Furthermore, there was significantly increased transcription of the *bopE* gene in the K96243*ΔbapB* strain at all growth phases. These data suggest that BapB negatively regulates the transcription of *bopE* either directly or indirectly. Based on the bioinformatic analysis, the only functional domain of BapB is a predicted phosphopantetheine (pantetheine 4' phosphate; PP) group of acyl carrier protein (ACP). The BapB protein displays most similarity to the TTSS acyl carrier protein IacP of *S. enterica* serovar Typhimurium (approximately 33%; *Figure 5.3.1*). The *Salmonella* IacP is involved in invasion of *S. enterica* serovar Typhimurium into non-phagocytic cells and modulation of host actin. A *S. enterica* serovar Typhimurium *iacP* mutant demonstrated a significant decrease in the *in vitro* secretion of some effector proteins (Kim *et al.*, 2011). However, on the contrary, the K96243*ΔbapB* strain showed increased effector secretion. Furthermore, BapB does not appear to play a role in invasion, at least of A549 cells, thus both proteins are unlikely to have identical functions.

While the protein with the highest amino acid identity is IacP, other features of BapB, such as acidic pI and the size, suggest it may function as a TTSS3 chaperone. In general, TTSS chaperones are essential not only for preventing the degradation and/or misfolding of bacterial effectors prior to secretion into the host, but they also play important roles in preventing undesirable interactions of the effectors with other TTSS components (Büttner & He, 2009; Dasgupta *et al.*, 2004; Francis *et al.*, 2001; Yip *et al.*, 2005). Moreover, some TTSS chaperones have exhibited a role in regulation of TTSS gene transcription under TTSS activation, resulting in transcription of a set of genes encoding effectors (Büttner, 2012; Parsot *et al.*, 2003). In *Salmonella*, for instance, a TTSS chaperone SicA, in association with InvF, regulates

transcription of several TTSS genes encoding effectors (Darwin & Miller, 1999). These correlate with and support what had been observed in the K96243*ΔbapB* strain. TTSS chaperones can broadly be divided into different groups (class IA, IB, II and III; *Figure 5.3.2*) according to their substrate specificities (Parsot *et al.*, 2003). Class IA and IB chaperones are discriminated on the number of effector interaction (one for IA; several for IB) and the location of the chaperone and effector substrate genes on the chromosome (adjacent for IA; disseminated for IB). However, class II and III chaperones are those that interact with translocons and flagellar-related TTSS molecules, respectively (Costa *et al.*, 2012; Parsot *et al.*, 2003). Alignment of the BapB amino acid sequence with representative TTSS chaperone classes from *Yersinia*, *Shigella* and *Salmonella* spp. showed no significant identities to class IA, IB and II (*Figure 5.3.2*). However, BapB showed significant similarities to the class III chaperones (22% identity; *Figure 5.3.3*). Among the class III chaperones, FliS functions as a negative regulator of the flagellar biosynthesis operon of *Salmonella* (Chilcott & Hughes, 2000; Fraser *et al.*, 2003). Thus, this perhaps suggests a possible function of BapB as a TTSS3 chaperone with a negative regulatory function.

Bioinformatic analysis of BapC indicated that it contains a TTSS-associated lytic transglycosylase (LT) domain. LTs generally function by cleaving the β-1,4 glycosidic bond between *N*-acetylmuramoyl and *N*-acetylglucosaminyl residues of bacterial peptidoglycan (PG) for the recycling of PG, cell division and insertion of either flagellar or secretion systems including the TTSS (Blackburn & Clarke, 2001; Koraimann, 2003; Scheurwater *et al.*, 2008; Scheurwater & Burrows, 2011). Alignment of the amino acid sequence of BapC with other TTSS proteins that contain LT domains (Blackburn & Clarke, 2001; Koraimann, 2003) indicated that the two TTSS-associated LTs HpaH and Hpa2 from plant pathogens *Xanthomonas campestris* pv. vesicatoria and *X. oryzae* pv. oryzae, respectively displayed the highest identity (approximately 39%; *Figure 5.3.4*). HpaH plays a role in promoting TTSS assembly and secretion of other TTSS proteins by, at least in part, remodelling bacterial peptidoglycan (Noël *et al.*, 2002). However, the secretion of HpaH, as a TTSS effector, has not been yet verified. The *X. oryzae* Hpa2 is likely to function as a translocon by interacting and forming the translocon complex with another translocon HrpF in order to bind to host cell membrane, promoting pathogenicity of this plant pathogen (Zhu *et al.*, 2000). Based on the BapC data in this study, BapC may function differently from HpaH and Hpa2 even though these three proteins shared three conserved motifs of the LT domains (*Figure 5.3.5A*). Alignment of the amino acid of BapC with other putative TTSS effectors indicated that the *Salmonella* IagB and the *Shigella* effector

IpgF showed the highest identity (approximately 36%). Although both putative effectors IagB and IpgF shared the three conserved motifs of the LT domains with BapC (*Figure 5.3.5B*), they play a role in bacterial invasion but not in virulence. In addition, IagB and IpgF have been shown to cleave bacterial peptidoglycan, indicating a proof for their function as LT containing proteins (Bernadsky *et al.*, 1994; Koraimann, 2003; Zahrl *et al.*, 2005). This should be further tested for BapC in order to confirm and verify its LT function. Since the end product of PG digestion by LT enzymes is a non-reducible 1,6-anhydro-*N*-acetylmuramyl residue, this could be assayed using this specific end product as a marker (Blackburn & Clarke, 2000). Furthermore, the region from 50 to 90 amino acid sequence of BapC displayed approximately 59% identity (*Figure 5.3.6*) to amino acid residues involved in the conformational stability and folding of human lysozyme. Lysozyme in humans is generally abundant in a number of secretions, such as mucous and saliva, and is also present in cytoplasmic granules of neutrophils. This amino acid identity may suggest a possible role of BapC in interaction with host immune responses (see *Chapter 4.4*).

Several lines of evidence have shown similarities in the structure and function of TTSSs and flagella in several Gram-negative bacteria (Abby & Rocha, 2012; Blocker *et al.*, 2003; Gophna *et al.*, 2003; Pallen *et al.*, 2005; Saier, 2004). Indeed, comparison of TTSS proteins with flagella components may be an alternative approach for defining the possible function of uncharacterised TTSS proteins (Galan & Collmer, 1999; Galan & Wolf-Watz, 2006; Soscia *et al.*, 2007). Both flagellar and TTSS components must be expressed in a regulated manner for appropriate action of secreted proteins since, at least in part, the expression of both virulence factors can be disadvantageous to bacterial growth and survival under some circumstances (Pallen & Gophna, 2007; Sturm *et al.*, 2011). The regulation of flagellar gene expression is controlled by three major operons, designated early, middle and late, based on the order of gene transcription during the flagellar assembly (McCarter, 2006). The middle operon encodes several essential proteins required for biosynthesis and assembly of the flagellar hook-basal body, including the muramidase proteins that facilitate the protrusion and expansion of the flagellar structure through the bacterial PG layer (Chilcott & Hughes, 2000; Nambu *et al.*, 1999). Moreover, this operon contains the negative regulatory protein complex that regulates transcription factors required for the late operon, preventing premature transcription (Aldridge *et al.*, 2006; Yokoseki *et al.*, 1996). The results in this Chapter strongly suggest that BapA and BapC are secreted, and that BapB may play a role in controlling the transcription of BopE and perhaps other TTSS genes. These proteins may act in concert during the assembly of the TTSS3 injectisome; BapC could be

secreted first and facilitate injectisome protrusion and expansion through the bacterial peptidoglycan, BapB may act both as a chaperone and a negative regulator that prevents premature secretion of the TTSS3 effectors. However, neither BapB nor BapC is absolutely required for TTSS function as the K96243*ΔbapB* and K96243*ΔbapC* strains are still capable of BopE secretion.

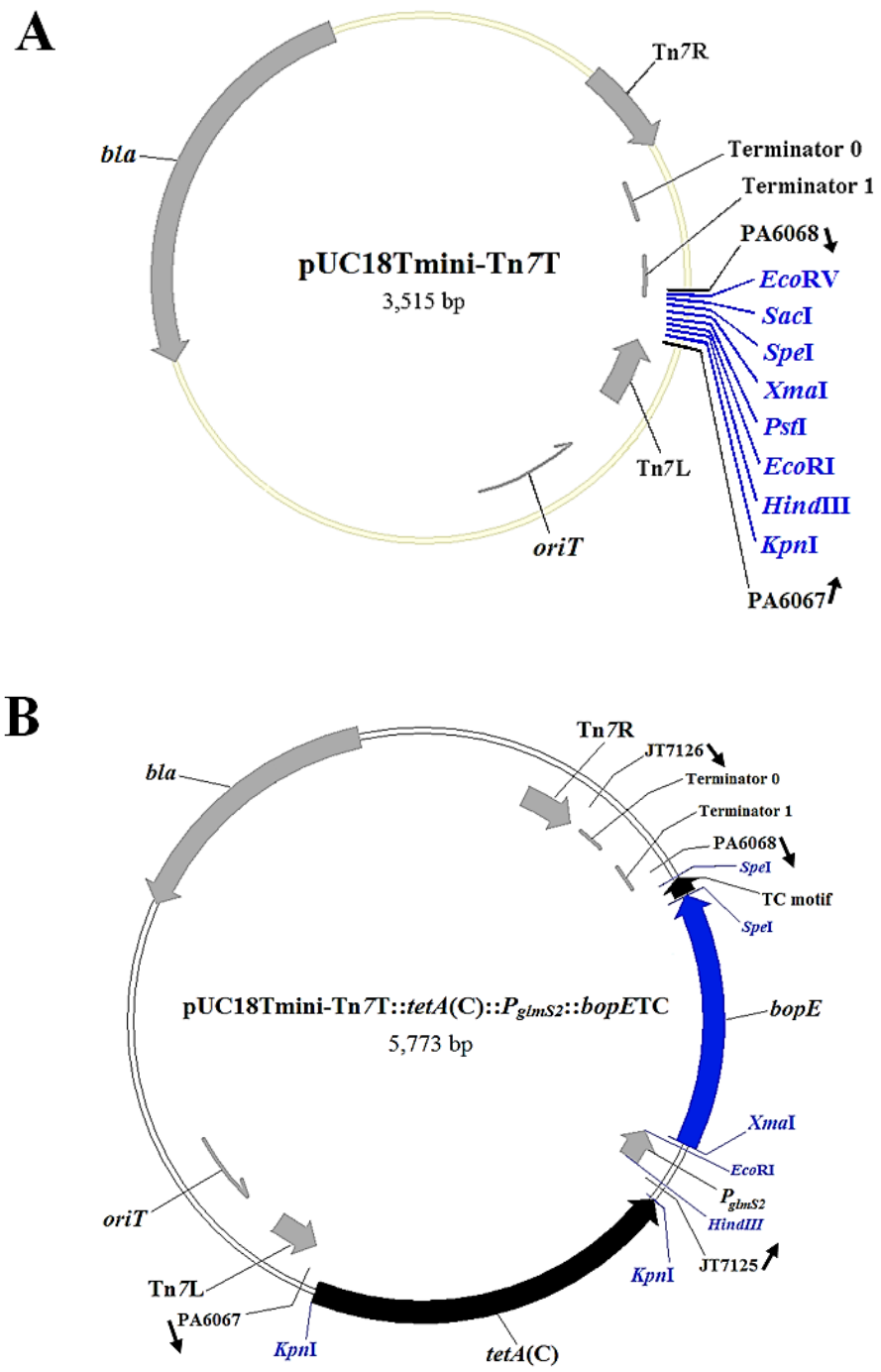

Figure 5.1.1 Plasmid maps of the empty pUC18T-miniTn*7*T vector (A) and the TC-tagged *bopE* construct in pUC18T-miniTn*7*T (B). The primer pair PA6067 and PA6068, amplifying a fragment containing the MCS of the plasmid, was used for verification of gene insertion and nucleotide sequencing. The following features are indicated: Tn*7*L and Tn*7*R, left and right end of Tn*7*, respectively; *tetA*(C), tetracycline resistance cassette derived from pUTminiTn*5*Tc vector and cloned into the *Kpn*I site; P_{glmS2}, *glmS2* promoter derived from the wild-type strain and cloned at the *Hin*dIII (5') and *Eco*RI (3') sites; *bopE*, full length *bopE* derived from the wild-type K96243 strain and cloned at the *Xma*I (5') and *Spe*I (3') sites; TC motif, tetracysteine motif cloned at a *Spe*I site; *oriT*, origin of conjugative transfer; T_1T_0, transcriptional terminators T_1 and T_0 from bacteriophage λ and *E. coli rrnB* operon, respectively. Arrows indicate gene orientation.

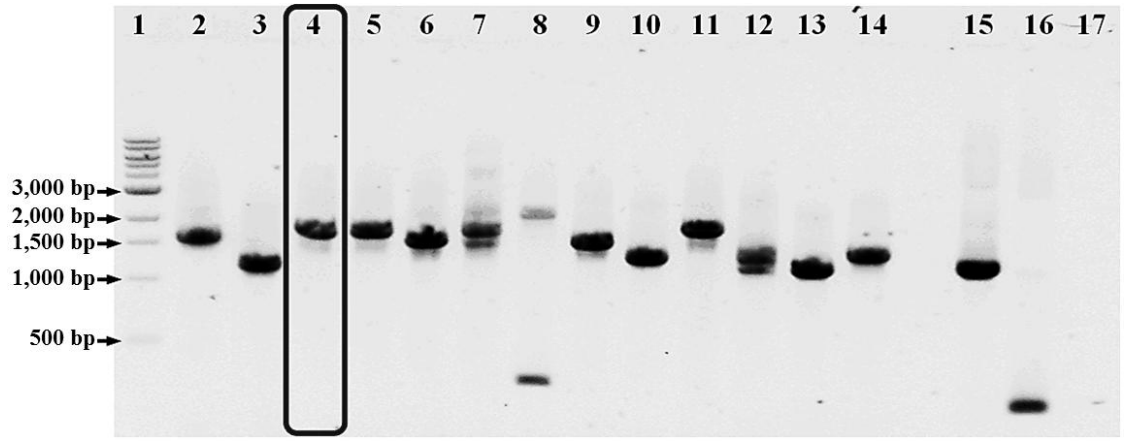

Figure 5.1.2 PCR analysis of potential *E. coli* SM10/λ*pir* clones harbouring pUC18Tmini-Tn*7*T:: *tetA*(C)::P_{glmS2}::*bopE*TC using the primer pair PA6067/PA6068. Lane 1, DNA size markers; lane 2 to 14, PCR products using plasmid DNA of potential *E. coli* SM10/λ*pir* clones; lane 15, PCR product using pUC18Tmini-Tn*7*T::*tetA*(C)::P_{glmS2} plasmid DNA; lane 16, PCR product using pUC18Tmini-Tn*7*T plasmid DNA; lane 17, no DNA control. The clone indicated by the black box in lane 4 was selected for further experiments.

A

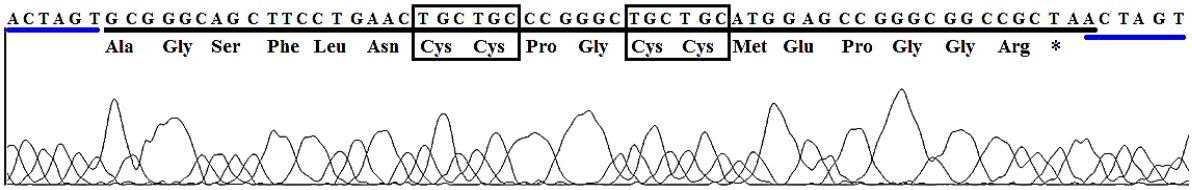

B

```
CAA GAC GCG TCG CGC GAC GAG AAG GGC GCG ACG
Gln Asp Ala Ser Arg Asp Glu Lys Gly Ala Thr

        ← bopE (3' end)
AAC GCG GCG GAC GGC GCG ACT AGT GCG GGC AGC
Asn Ala Ala Asp Gly Ala Thr Ser Ala Gly Ser

TTC CTG AAC TGC TGC CCG GGC TGC TGC ATG GAG
Phe Leu Asn Cys Cys Pro Gly Cys Cys Met Glu

CCG GGC GGC CGC TAA
Pro Gly Gly Arg *
```

Figure 5.1.3 Nucleotide and deduced amino acid sequence of the modified TC tag with proline (Pro) and glycine (Gly), as spacers, and the stop codon TAA (*) (A). The modified TC tag (black underline) was cloned at a *Spe*I site (blue underline) and inserted at the 3' region of *bopE* of the pUC18Tmini-Tn*7*T::*tetA*(C)::P_{glmS2}::*bopE* construct (B). The core TC tag is indicated by black boxes.

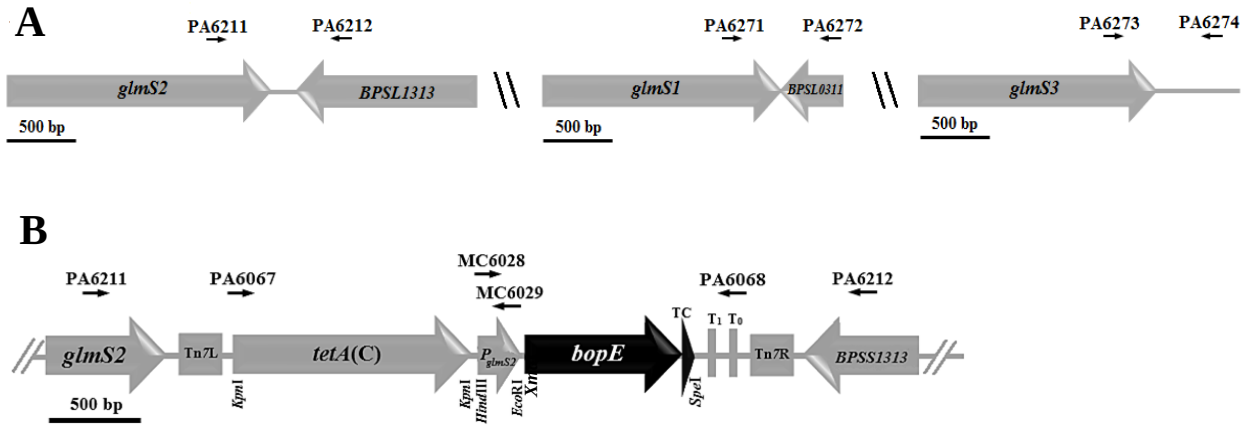

Figure 5.1.4 Primers used for confirmation of the site of genomic integration of pUC18Tmini-Tn*7*T:: *tetA*(C)::P_{glmS2}::*bopE*TC. (A) Schematic representation of the wild-type gene *glmS2* (*BPSL1312*) and its adjacent gene *BPSL1313*, *glmS1* (*BPSL0312*) and its adjacent gene *BPSL0311*, and *glmS3*. The primer pairs PA6211/PA6212, PA6271/PA6272 and PA6273/6274 were used to identify if there was an insertion after *glmS2*, *glmS1* and *glmS3*, respectively. (B) Schematic representation of the wild-type *glmS2* and *BPSL1313* after the expected integration of pUC18Tmini-Tn*7*T::*tetA*(C)::P_{glmS2}::*bopE*TC construct into the chromosome. The primer pair combinations PA6067/MC6029, MC6028/PA6068 and MC6028/ PA6212 were used for further analyses. The following features are indicated: Tn*7*L and Tn*7*R, left and right end of Tn*7*; *tetA*(C), tetracycline resistance cassette cloned at the *Kpn*I site; P_{glmS2}, *glmS2* promoter derived from the wild-type strain and cloned at *Hin*dIII (5') and *Eco*RI (3'); *bopE*, full length *bopE* derived from the wild-type strain and cloned at *Xma*I (5') and *Spe*I (3') sites; TC, tetracysteine tag cloned at the *Spe*I site; T_1T_0, transcriptional terminators T_1 and T_0 from bacteriophage λ and *E. coli rrnB* operon, respectively. Arrows indicate the orientation of primers. Arrows designating oligonucleotides are not shown to scale.

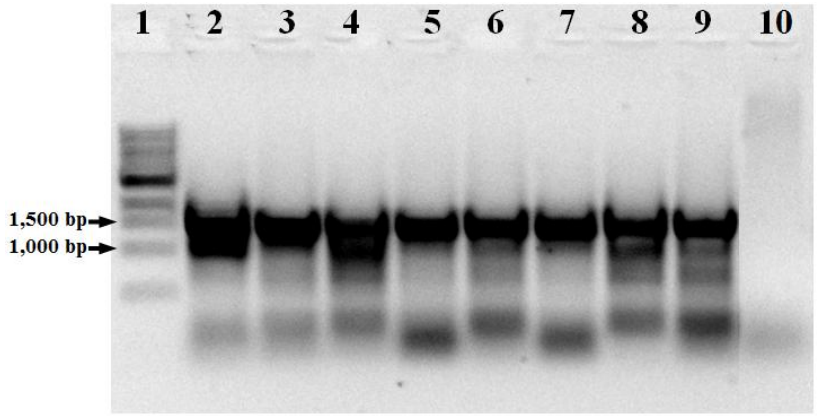

Figure 5.1.5 PCR screening of potential transconjugants for integration of the pUC18Tmini-Tn*7*T:: *tetA*(C)::P_{glmS2}::*bopE*TC. The primers PA6211 and PA6212, which amplify the section between *glmS2* (*BPSL1312*) and its adjacent gene *BPSL1313*, were used for verification of transposon integration. Lane 1, DNA size markers; lane 2 to 8, PCR products derived from transconjugant DNA templates; lane 9, genomic DNA of the wild-type as the negative control; lane 10, no DNA control.

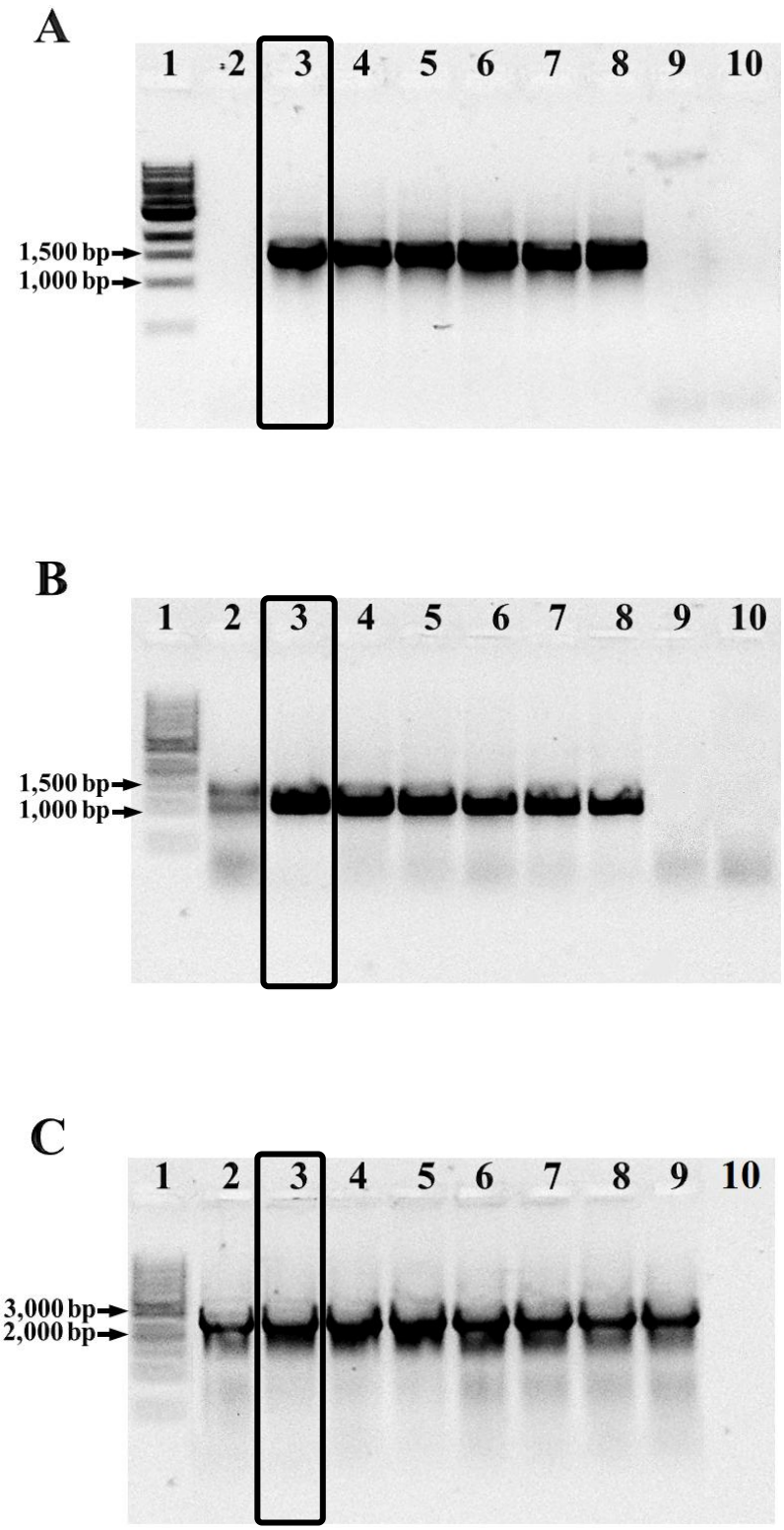

Figure 5.1.6 PCR screening of potential *B. pseudomallei* transconjugants for integration of pUC18T mini-Tn*7*T::*tetA*(C)::P_{glmS2}::*bopE*TC. Three sets of primer combinations, PA6067/MC6029 (A), MC6028/ PA6068 (B) and MC6028/PA6212 (C), were used for verification of the mini-Tn*7* integration downstream of *glmS2*. Lane 1, DNA size markers; lane 2 to 8, PCR products derived from transconjugant DNA templates; lane 9, genomic DNA of the wild-type as the negative control; lane 10, no DNA control. The clone indicated by the black box in lane 3 was selected for further experiments.

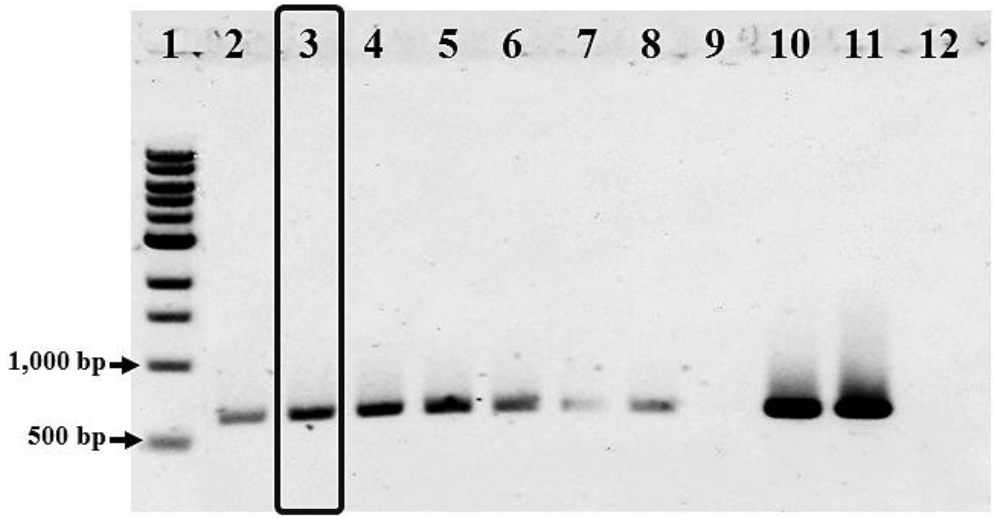

Figure 5.1.7 PCR screening of potential *B. pseudomallei* transconjugants for integration of pUC18T mini-Tn*7*T::*tetA*(C)::P_{glmS2}::*bopE*TC. The primers MC6229 and MC6230 were used to examine if there was free replicating construct presence in the transconjugants. Lane 1, DNA size markers; lane 2 to 8, PCR products derived from transconjugant DNA templates; lane 9, genomic DNA of the wild-type as the negative control; lane 10, PCR product derived from plasmid DNA of *E. coli* DH5α harbouring pUC18T mini-Tn*7*T::*tetA*(C)::P_{glmS2}::*bopE*TC, as a positive control; lane 11, PCR product derived from plasmid DNA of *E. coli* DH5α harbouring pUC18Tmini-Tn*7*T, as another positive control; lane 12, no DNA control. The clone indicated by the black box in lane 3 was selected for further experiments.

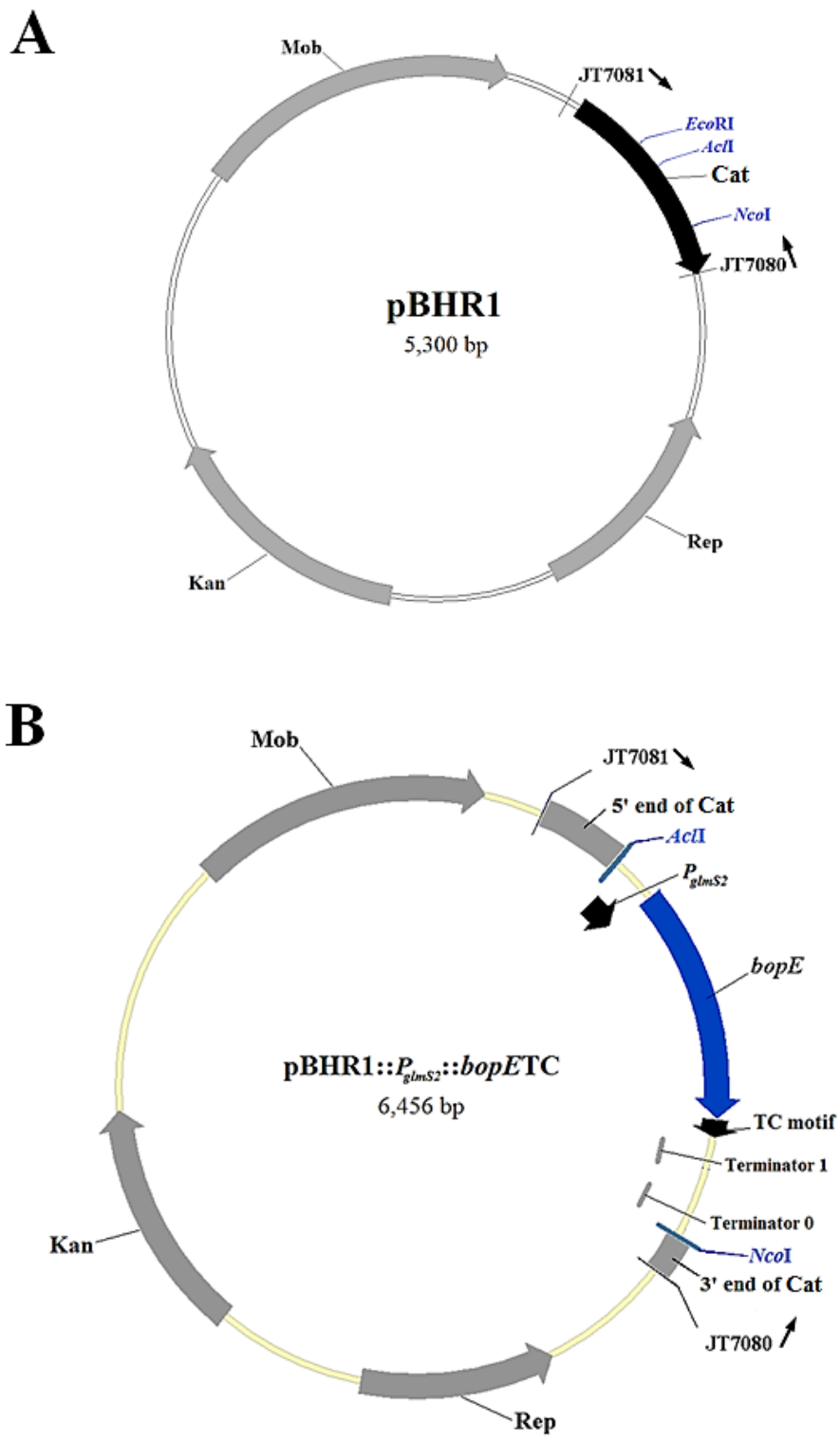

Figure 5.1.8 Schematic representation of the plasmid pBHR1 (A) and pBHR1::P_{glmS2}::*bopE*TC, containing the P_{glmS2}::*bopE*TC fragment cloned into the *Acl*I/*Nco*I sites of pBHR1 (B). Features are indicated as follows: Rep and Mob, *rep* and *mob* genes required for replication and mobilisation of pBHR1 respectively; Cat, chloramphenicol acetyl transferase gene; Kan, kanamycin resistance gene; P_{glmS2}, *glmS2* promoter; *bopE*, full length *bopE*; TC motif, tetracysteine motif; T_1T_0, transcriptional terminators T_1 and T_0 from bacteriophage λ and *E. coli rrnB* operon, respectively. Arrows indicate gene orientation. JT7080 and JT7081 are primers used for PCR screening of recombinant clones and nucleotide sequencing, and are denoted by arrows.

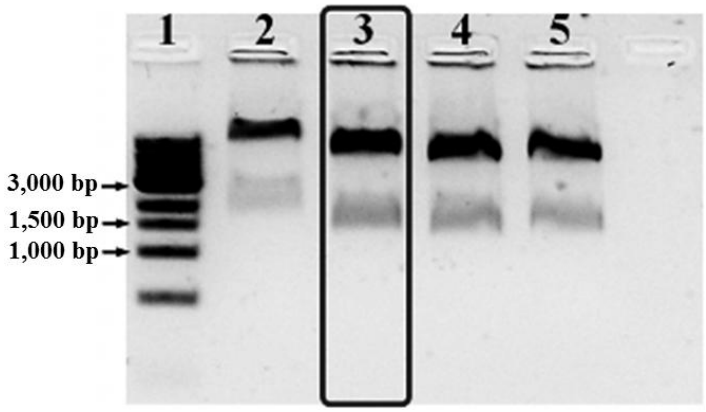

Figure 5.1.9 Electrophoretic separation of restriction enzyme digests of plasmid DNA isolated from putative *E. coli* DH5α harbouring pBHR1::P_{glmS2}::*bopE*TC clones. Lane 1, DNA size markers; lane 2 to 5, plasmid DNA from putative recombinant clones digested with *Acl*I and *Nco*I. The recombinant plasmid indicated by the black box in lane 3 was selected for further experiments.

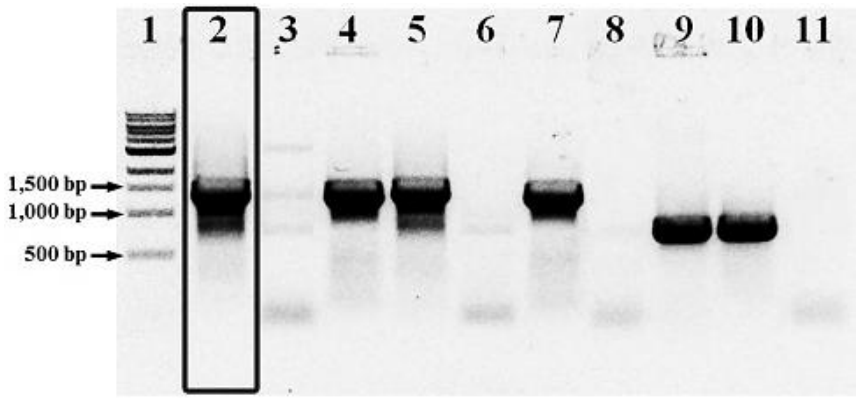

Figure 5.1.10 Electrophoretic separation of PCR fragments generated from putative *B. pseudomallei* transconjugants containing pBHR1::P_{glmS2}::*bopE*TC. The primer pair JT7080/JT7081 was used to verify the presence of the pBHR1::P_{glmS2}::*bopE*TC construct. Lane 1, DNA size markers; lane 2 to 6, genomic DNA from putative transconjugants as template PCR; lane 7, plasmid DNA derived from *E. coli* DH5α harbouring pBHR1::P_{glmS2}::*bopE*TC as the positive control; lane 8, genomic DNA from the wild-type strain as the negative control; lane 9, genomic DNA from the wild-type strain harbouring empty pBHR1 vector; lane 10, genomic DNA of *E. coli* DH5α harbouring empty pBHR1 vector; lane 11, no DNA control. The clone indicated by the black box in lane 2 was selected for further experiments.

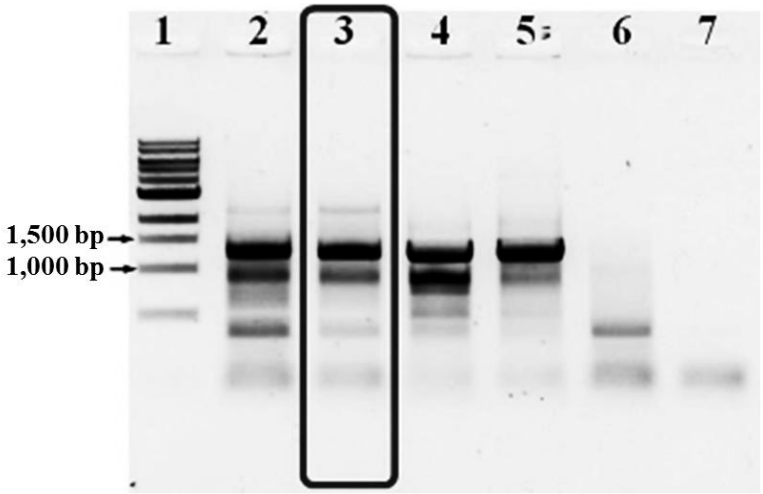

Figure 5.1.11 Electrophoretic separation of PCR fragments generated from genomic DNA of potential K96243*ΔbsaS* transconjugants following introduction of pBHR1::P_{glmS2}::*bopE*TC. The primer pair JT7080/JT7081 was used to verify the presence of the pBHR1::P_{glmS2}::*bopE*TC construct. Lane 1, DNA size markers; Lane 2 to 4, PCR products derived from transconjugant DNA templates; lane 5, PCR product derived from plasmid DNA of *E. coli* S17-1/λ*pir* harbouring the pBHR1::P_{glmS2}::*bopE*TC construct as a positive control; lane 6, genomic DNA from the K96243*ΔbsaS* strain as the negative control; lane 7, no DNA control. The clone indicated by the black box in lane 3 was selected for further experiments.

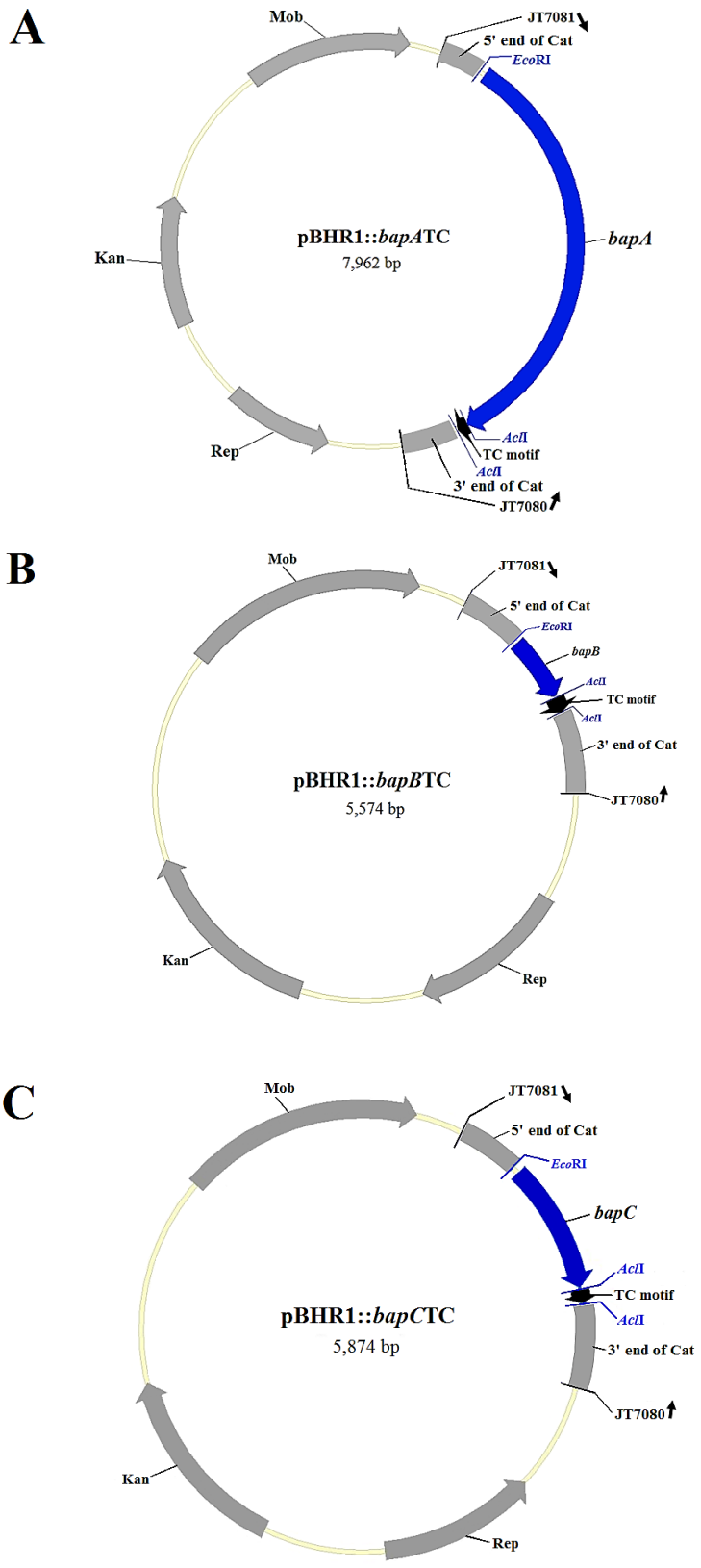

Figure 5.1.12 Schematic representation of the pBHR1 construct containing *bapA* (A), *bapB* (B) and *bapC* (C) tagged with the TC motif. Different features are indicated as follows: Rep and Mob, *rep* and *mob* genes required for replication and mobilisation of pBHR1 respectively; Cat, chloramphenicol acetyl transferase gene; Kan, kanamycin resistance gene; TC motif, tetracysteine motif. Arrows indicate gene orientation. The primers JT7080 and JT7081 are denoted by arrows.

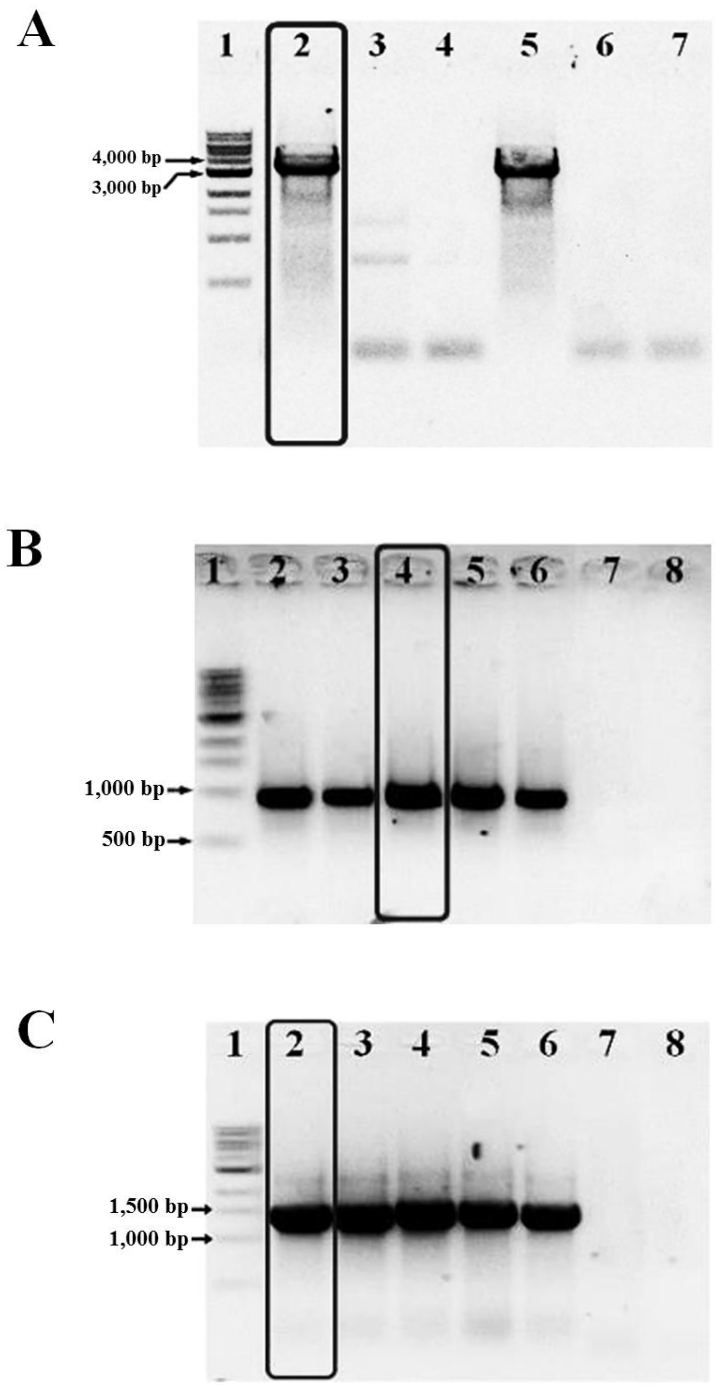

Figure 5.1.13 Electrophoretic separation of PCR fragments generated from putative *B. pseudomallei* transconjugants containing pBHR1::*bapA*TC (A), pBHR1::*bapB*TC (B) or pBHR1::*bapC*TC (C). The primer pair JT7080/JT7081 was used to verify the presence of the pBHR1::*bapA*TC, pBHR1::*bapB*TC or pBHR1::*bapC*TC constructs, respectively. Lane 1, DNA size markers; lane 2 to 4 (A), 2 to 5 (B), and 2 to 5 (C), genomic DNA from putative transconjugants as template PCR; lane 5 (A), 6 (B), and 6 (C), plasmid DNA derived from *E. coli* DH5α harbouring pBHR1::*bapA*TC, pBHR1::*bapB*TC, and pBHR1::*bapC*TC, respectively, as the positive controls; lane 6 (A), 7 (B) and 7 (C), genomic DNA from the wild-type as the negative control; lane 7 (A), 8 (B) and 8 (C), no DNA control. The clones indicated by the black boxes in lane 2 (A), 4 (B) and 2 (C) were selected for further experiments.

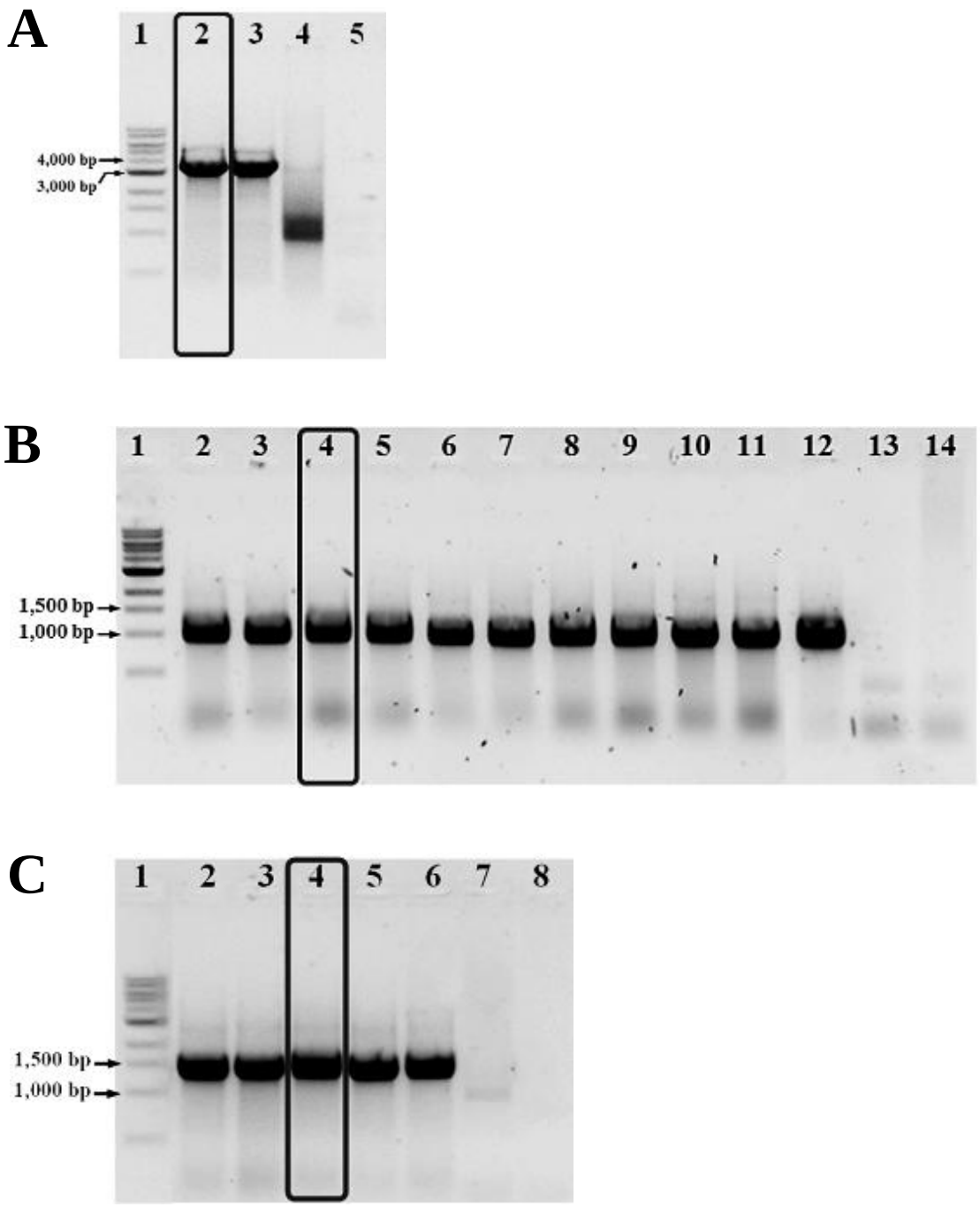

Figure 5.1.14 Electrophoretic separation of PCR fragments generated from putative K96243*ΔbsaS* transconjugants containing pBHR1::*bapA*TC (A), pBHR1::*bapB*TC (B) or pBHR1::*bapC*TC (C). The primer pair JT7080/JT7081 was used to verify the presence of the pBHR1::*bapA*TC, pBHR1::*bapB*TC or pBHR1::*bapC*TC constructs, respectively. Lane 1, DNA size markers; lane 2 (A), 2 to 11 (B), and 2 to 5 (C), genomic DNA from putative transconjugants as template PCR; lane 3 (A), 12 (B), and 6 (C), plasmid DNA derived from *E. coli* DH5α harbouring pBHR1::*bapA*TC, pBHR1::*bapB*TC, and pBHR1::*bapC*TC, respectively, as the positive controls; lane 4 (A), 13 (B) and 7 (C), genomic DNA from the K96243*ΔbsaS* strain as the negative control; lane 5 (A), 14 (B) and 8 (C), no DNA control. The clones indicated by the black boxes in lane 2 (A), 4 (B) and 4 (C) were selected for further experiments.

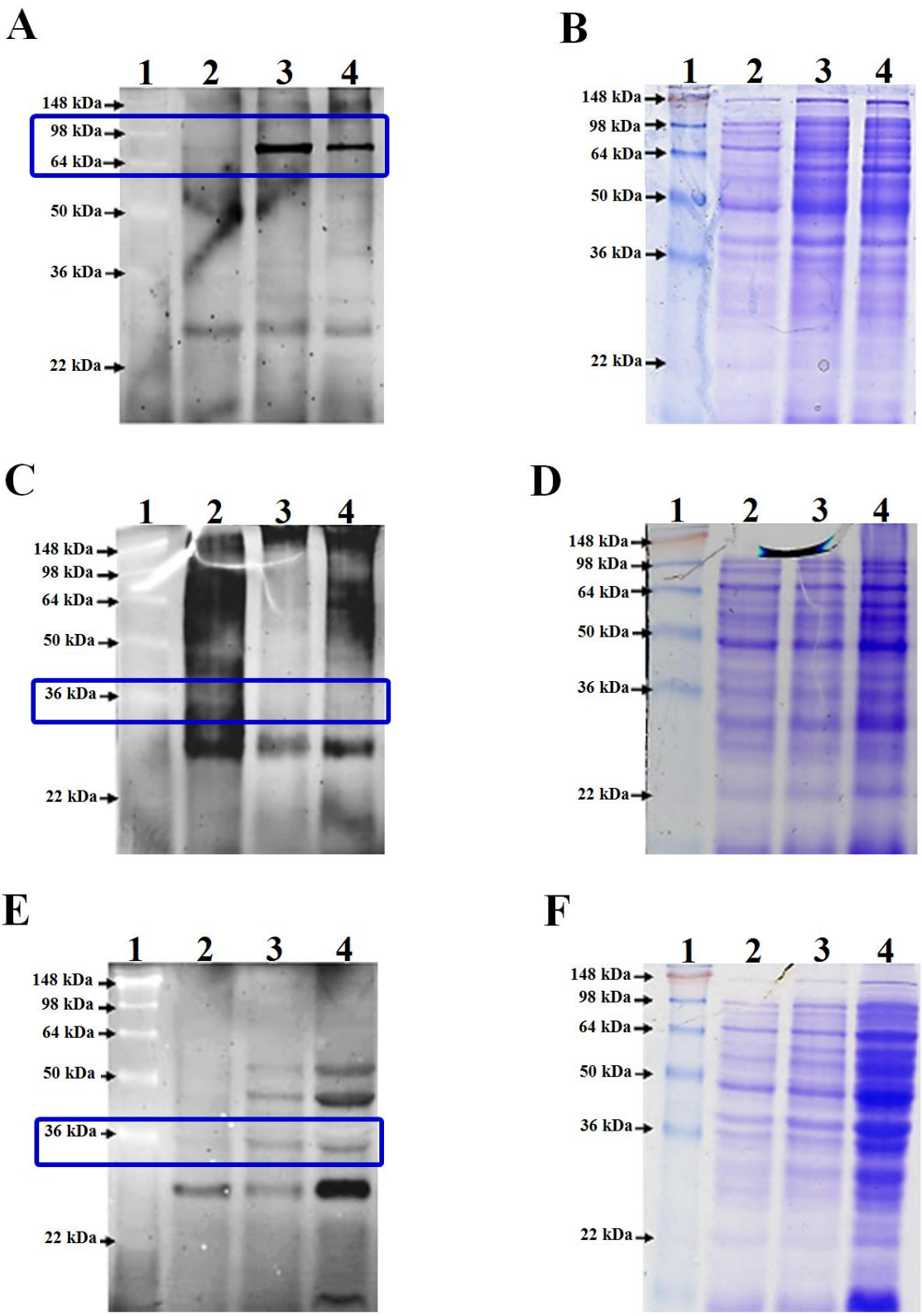

Figure 5.1.15 FlAsH labelling and Coomassie Brilliant Blue staining of DOC/TCA precipitated total protein samples taken at three growth phases (early-, mid- and late-exponential) of the DH5α[pJP117] (A and B), K96243*bopE*TC (C and D) and K96243[*bopE*TC] (E and F) strains. Lane 1: SeeBlue® Plus2 pre-stained protein markers (Life Technologies™, USA); lane 2, total proteins from early exponential phase culture; lane 3, total proteins from mid exponential phase culture; lane 4, total proteins from late exponential phase culture. The expected size of TC-tagged GspD (75 kDa, A) and BopE (33 kDa, C and E) is indicated by the blue boxes.

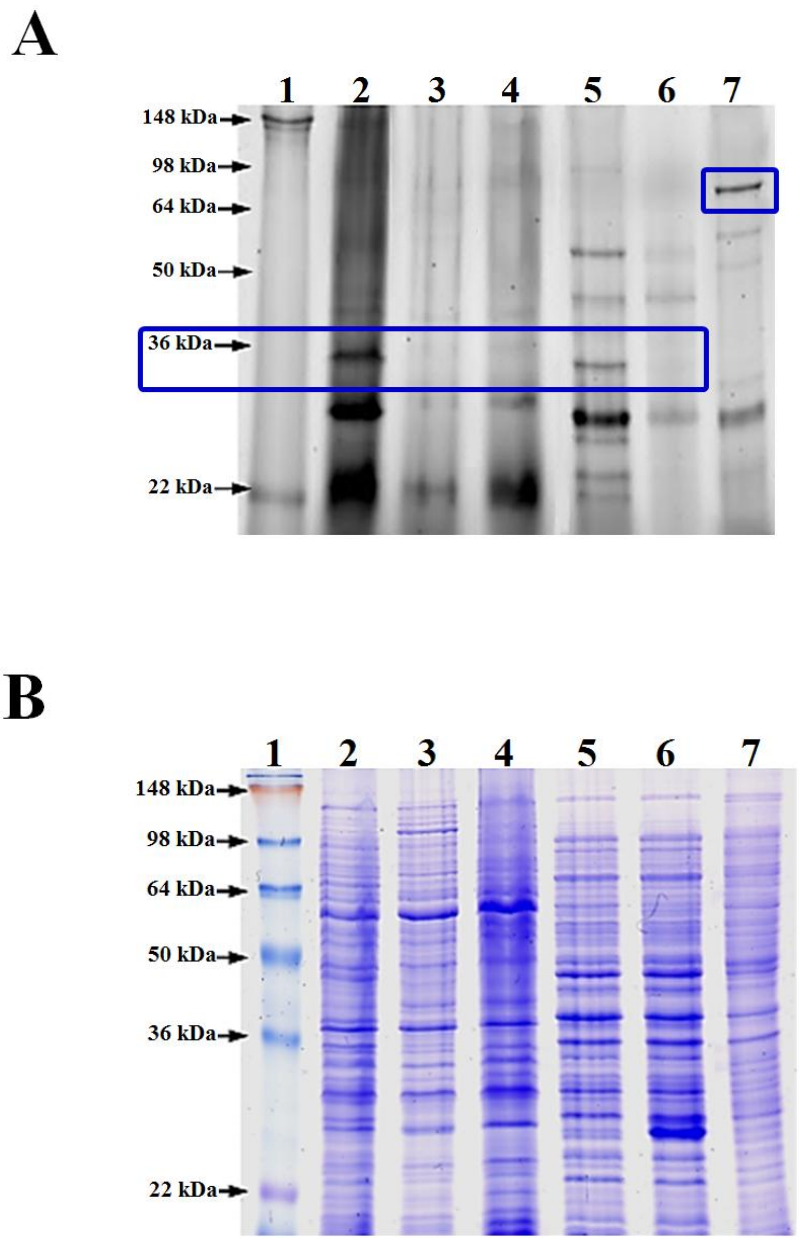

Figure 5.1.16 SDS-PAGE separation of total proteins from *E. coli* and *B. pseudomallei* strains. Proteins were visualised by (A) FlAsH-labelling or (B) Coomassie Brilliant Blue staining. Proteins in mid exponential phase cultures were precipitated with DOC/TCA and labelled with FlAsH reagent (A) or left untreated (B). Lane 1: SeeBlue® Plus2 pre-stained protein markers; lane 2, total proteins from the K96243[*bopE*TC] strain; lane 3, total proteins from the K96243[pBHR1] strain; lane 4, total proteins from *B. pseudomallei* K96243 strain; lane 5, total proteins from *E. coli* S17-1/λ*pir*[pBHR1::P_{glmS2}::*bopE*TC]; lane 6, total proteins from *E. coli* S17-1/λ*pir*[pBHR1]; lane 7, total proteins from the DH5α[pJP117] strain. The expected size of TC-tagged GspD (75 kDa, lane 7) and BopE (33 kDa, lane 2 and 5) is indicated by the blue boxes.

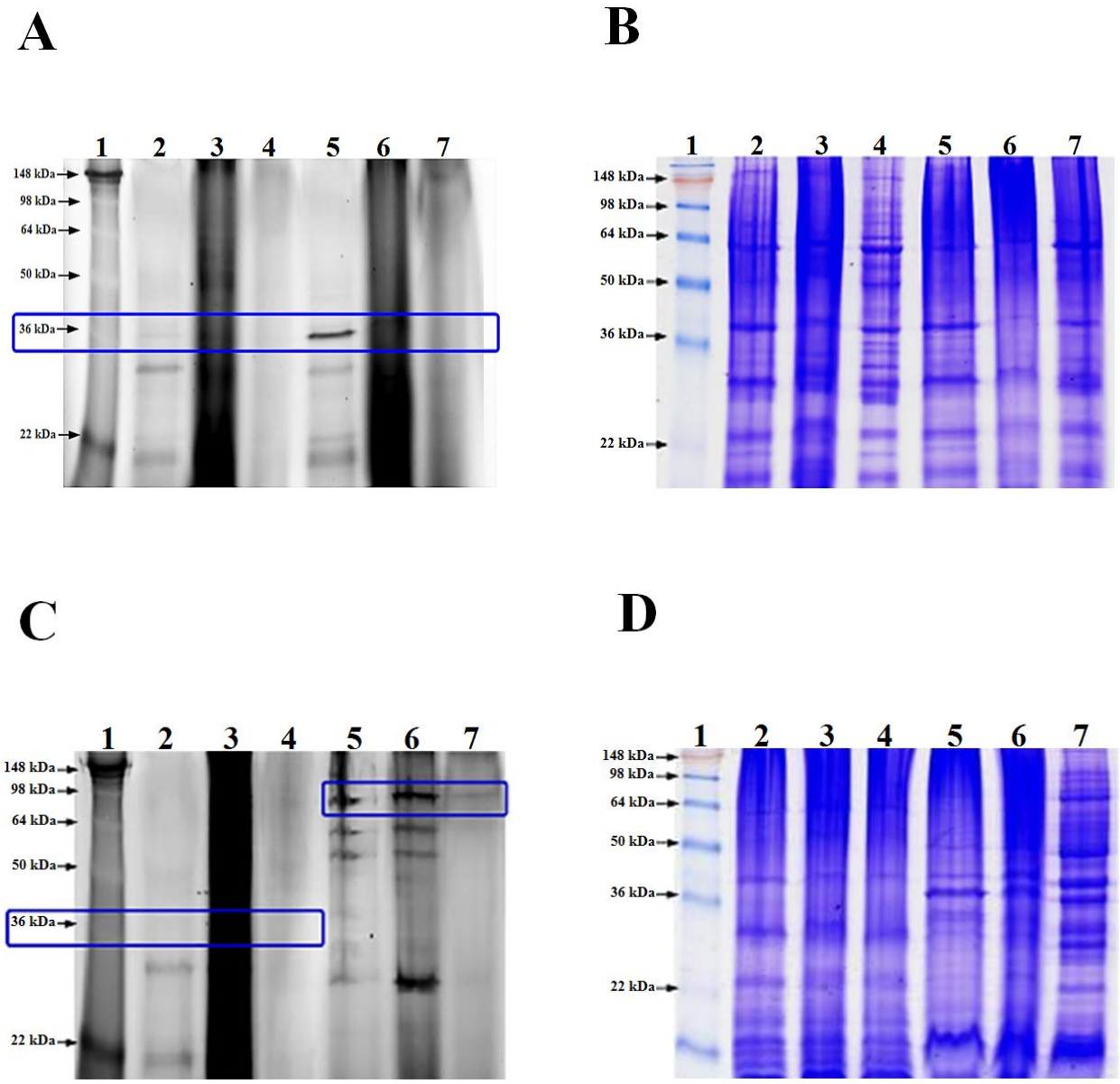

Figure 5.1.17 Effect of reducing agents on FlAsH labelling of DOC/TCA precipitated proteins from the K96243*bopE*TC (lanes 2A to 4A), K96243[*bopE*TC] (lanes 5A to 7A), K96243[pBHR1] (lanes 2C to 4C) and DH5α[pJP117] (lanes 5C to 7C). Total cultures were harvested at mid exponential growth phase, protein precipitated with DOC/TCA and then labelled with FlAsH compound using three different thiol reducing agents: β-mercaptoethanol (BME; lane 2A, 5A, 2C and 5C), tris(2-carboxyethyl) phosphine (TCEP; lane 3A, 6A, 3C and 6C) and 2,3-dimercapto-1-propanol (BAL; lane 4A, 7A, 4C and 7C). Labelled samples were separated using SDS-PAGE and the fluorescence measured. Unlabelled samples were separated by SDS-PAGE and visualised with Coomassie Brilliant Blue staining (B and D). Lane 1: SeeBlue® Plus2 pre-stained protein markers. The expected size of TC-tagged BopE (33 kDa) and GspD (75 kDa) is indicated by the blue boxes.

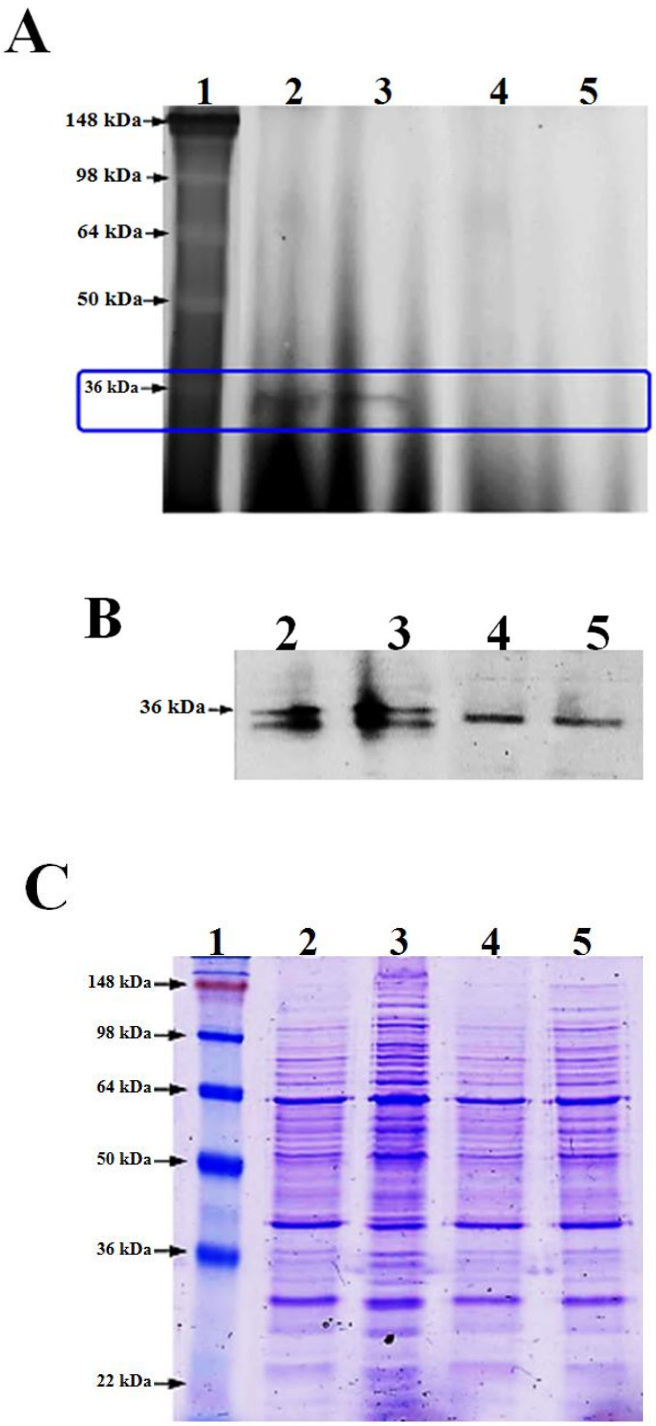

Figure 5.1.18 Analysis of the *in vitro* secretion of BopE using the FlAsH labelling technique. Total culture and supernatant protein samples from the K96243[*bopE*TC] (lane 2 and 3) and K96243[pBHR1] (lane 4 and 5) strains were precipitated with DOC/TCA and labelled with FlAsH using BME as the reducing agent. Labelled samples were separated using SDS-PAGE and fluorescence measured (A). Proteins were transferred to PVDF membranes and used in Western immunoblotting using BopE-specific antiserum (B). Unlabelled samples were separated by SDS-PAGE and visualised by Coomassie Brilliant Blue staining (C). Lane 1: SeeBlue® Plus2 pre-stained protein markers; lane 2 and 3, total culture and supernatant, respectively, proteins from the K96243[*bopE*TC] strain; lane 4 and 5, total culture and supernatant, respectively, proteins from the K96243[pBHR1] strain. The expected size of TC-tagged BopE (33 kDa) is indicated by the blue box.

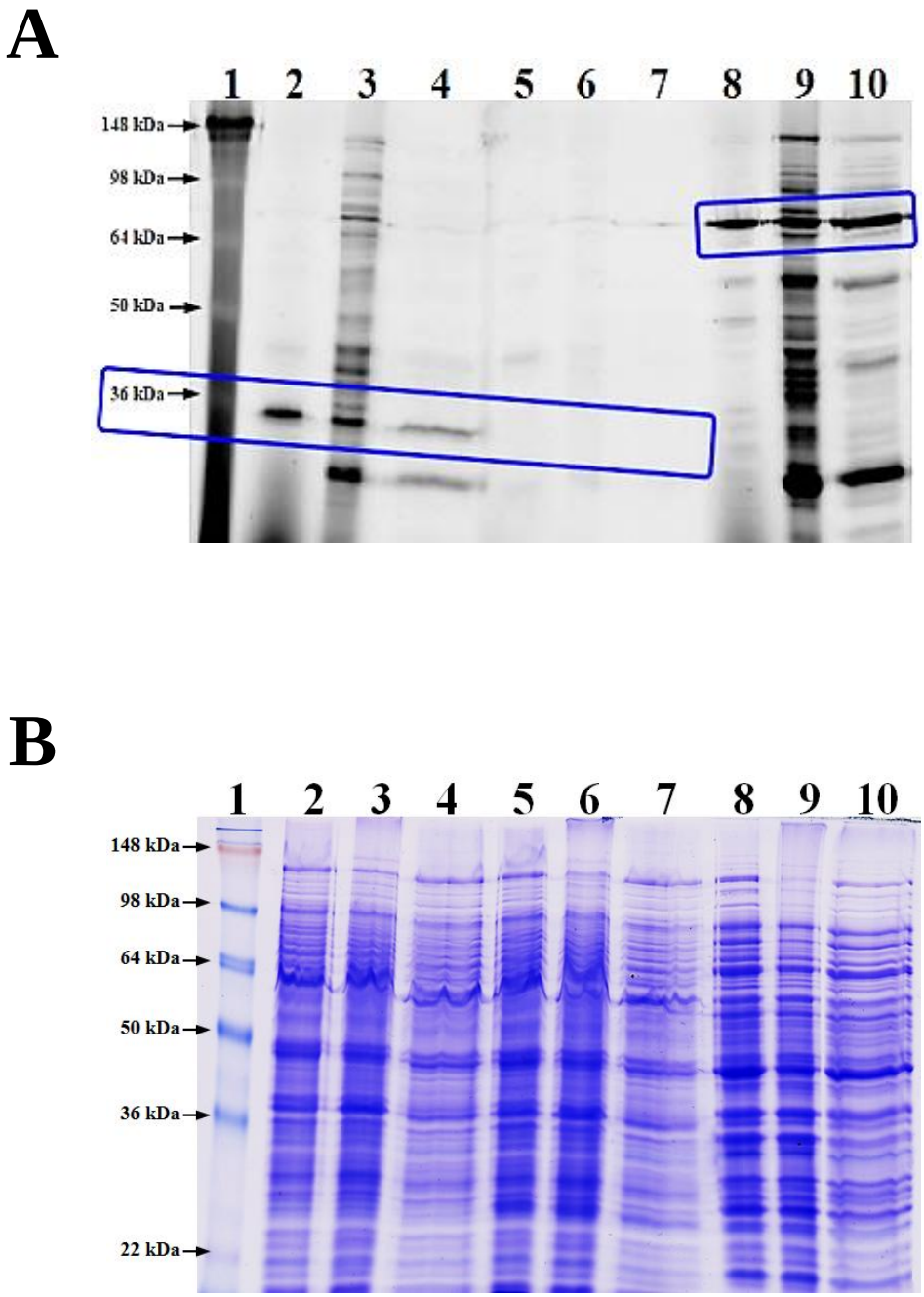

Figure 5.1.19 Efficacy of different reducing agents on FlAsH labelling of live cells expressing TC-tagged proteins. Live bacterial cells were incubated with FlAsH compound prior to denaturation in 1X sample buffer containing either dithiothreitol (DTT; lane 2, 5 and 8), TCEP (lane 3, 6 and 9), or Lumio™ Gel Sample Buffer (lane 4, 7 and 10). Labelled samples were separated by SDS-PAGE and the fluorescence measured (A). Unlabelled samples were separated by SDS-PAGE and visualised by Coomassie Brilliant Blue staining (B). Lane 1: SeeBlue® Plus2 pre-stained protein markers; lane 2 to 4, the K96243[*bopE*TC] strain; lane 5 to 7, the K96243[pBHR1] strain; lane 8 to 10, the DH5α[pJP117] strain. The expected size of TC-tagged BopE (33 kDa) and GspD (75 kDa) is indicated by the blue boxes.

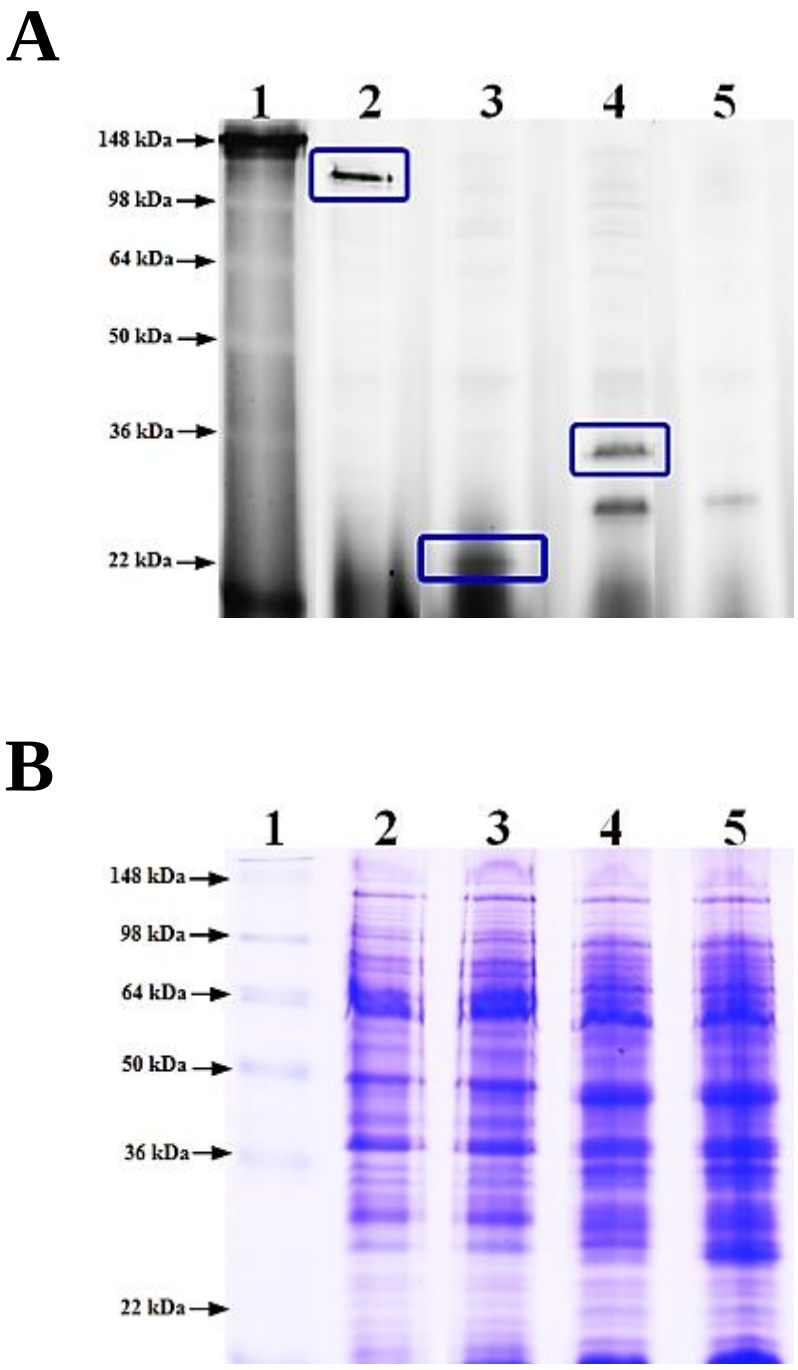

Figure 5.1.20 Identification of TC-tagged BapA and BapC by FlAsH labelling of live *B. pseudomallei*. Bacterial cells were incubated with the FlAsH reagent prior to killing and protein denaturation using 1X sample buffer containing dithiothreitol (DTT). Labelled samples were separated by 10% SDS-PAGE and fluorescence measured (A). Unlabelled samples were separated by SDS-PAGE and visualised with Coomassie Brilliant Blue staining (B). Lane 1: SeeBlue® Plus2 pre-stained protein markers; lane 2, the K96243[*bapA*TC] strain; lane 3, the K96243[*bapC*TC] strain; lane 4, the K96243[*bopE*TC] strain; lane 5, the K96243[pBHR1] strain. Protein bands at or near the expected size of TC-tagged BapA (120 kDa), BapC (23 kDa) and BopE (33 kDa) are indicated by the blue boxes.

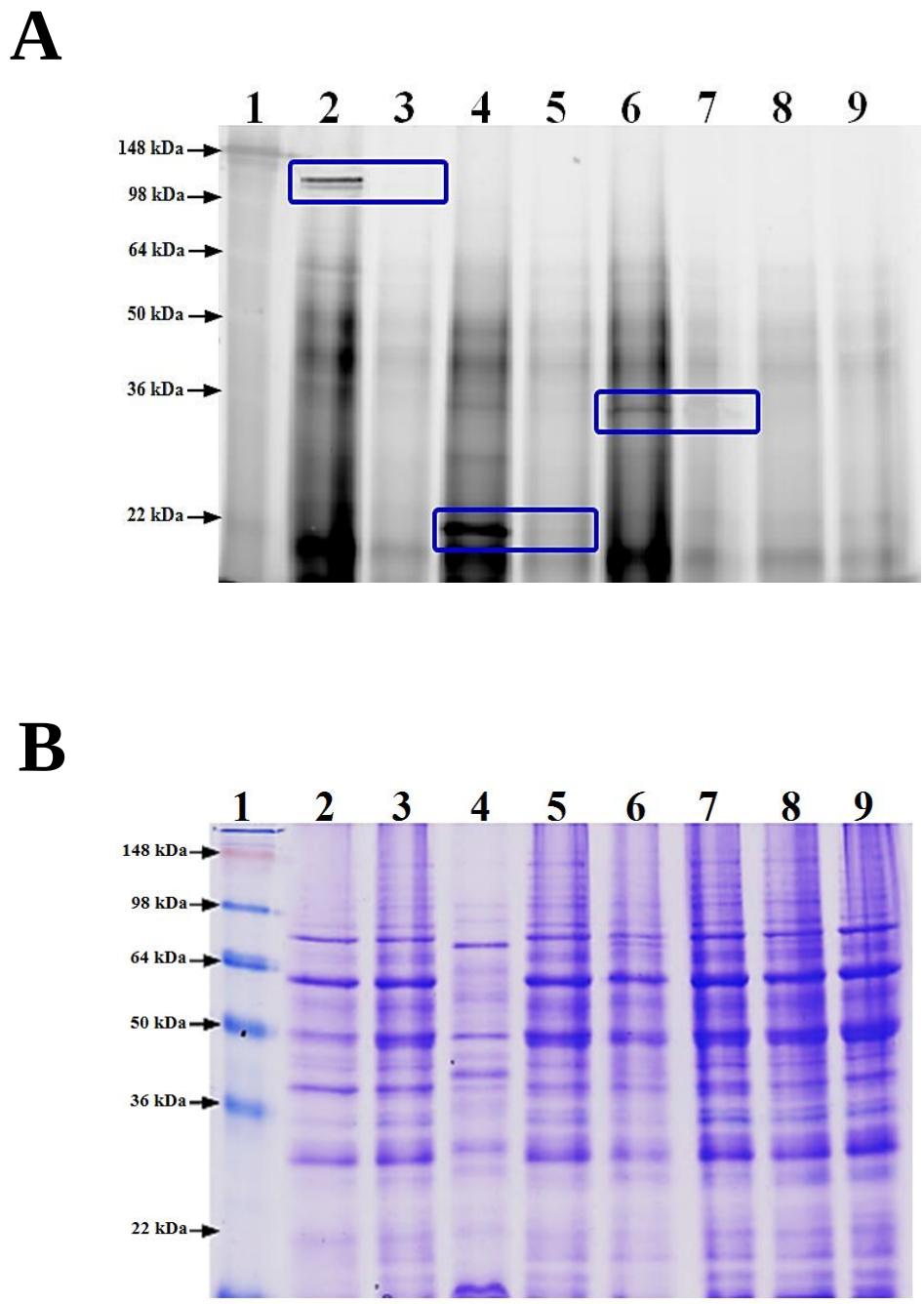

Figure 5.1.21 BapA and BapC are secreted in a TTSS3-dependent manner. Proteins in supernatant samples from mid exponential growth phase cultures of *B. pseudomallei* wild-type or the K96243*ΔbsaS* strain were precipitated using DOC/TCA and labeled with the FlAsH reagent using BME as the reducing agent. Labelled samples were separated by 10% SDS-PAGE and the fluorescence measured (A). Unlabelled samples were separated by SDS-PAGE and visualised with Coomassie Brilliant Blue staining (B). Lane 1: SeeBlue® Plus2 pre-stained protein markers; lane 2, the K96243[*bapA*TC] strain; lane 3, the K96243*ΔbsaS*[*bapA*TC] strain, lane 4, the K96243[*bapC*TC]; lane 5, the K96243*ΔbsaS*[*bapC*TC] strain; lane 6, the K96243[*bopE*TC]; lane 7, the K96243*ΔbsaS*[*bopE*TC] strain; lane 8, the K96243[pBHR1]; lane 9, the K96243*ΔbsaS*[pBHR1] strain. Protein bands at or near the expected size of TC-tagged BapA (120 kDa), BapC (23 kDa) and BopE (33 kDa) are indicated by the blue boxes.

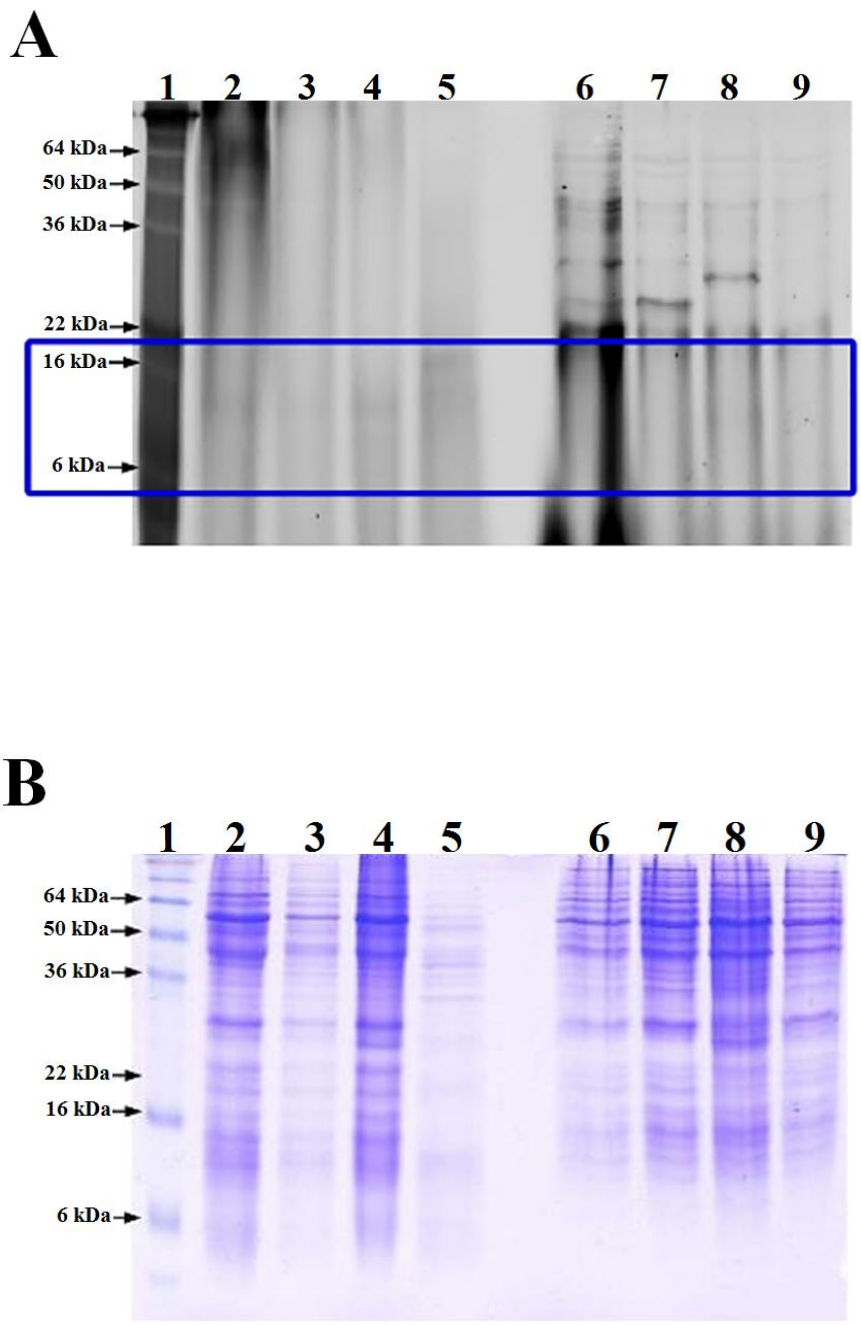

Figure 5.1.22 Analysis of *in vitro* secretion of BapB using the FlAsH labelling technique. Total proteins from supernatant (lane 2 to 5) or total culture (lane 6 to 9) samples of mid exponential growth phase *B. pseudomallei* strains were precipitated with DOC/TCA and labeled with FlAsH using BME as the reducing agent. Labelled samples were separated by 16% SDS-PAGE and the fluorescence measured (A). Unlabelled samples were separated by SDS-PAGE and visualised with Coomassie Brilliant Blue staining (B). Lane 1: SeeBlue® Plus2 pre-stained protein markers; lane 2 and 6, the K96243[*bapB*TC] strain; lane 3 and 7, the K96243*ΔbsaS*[*bapB*TC] strain; lane 4 and 8, the K96243[pBHR1] strain; lane 5 and 9, the K96243*ΔbsaS*[pBHR1] strain. The expected size of TC-tagged BapB (10 kDa) is indicated by the blue box.

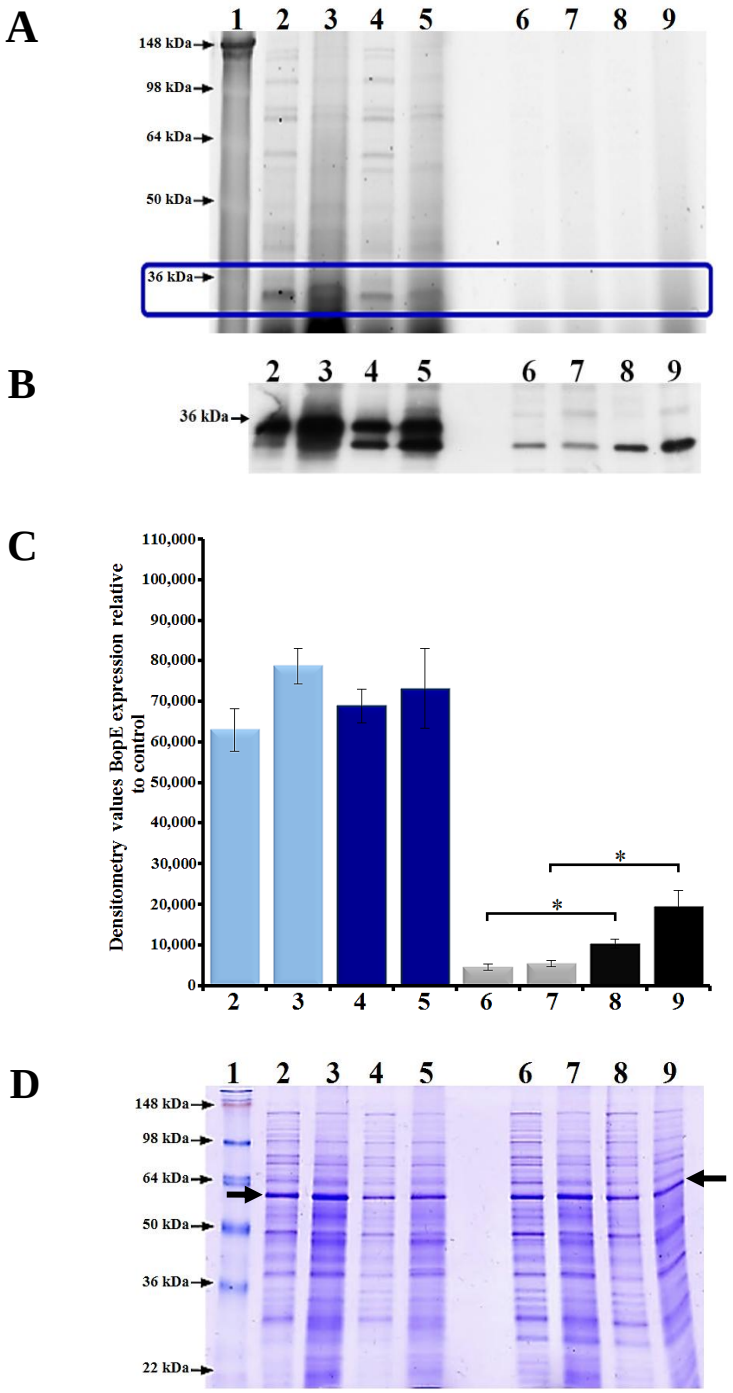

Figure 5.1.23 Effect of salt concentration on secretion and expression of BopE. Total proteins from cultures or filtered supernatants from mid exponential growth phase cultures of *B. pseudomallei* grown in LB supplemented with high salt (320 mM NaCl, lane 4, 5, 8 and 9) or normal salt (85.6 mM NaCl, lane 2, 3, 6 and 7) concentration were precipitated with DOC/TCA, labelled with the FlAsH reagent using BME as the reducing agent. Labelled samples were separated using SDS-PAGE and the fluorescence measured (A). Western blot analysis using BopE-specific antiserum was subsequently conducted (B). Intensities of protein bands corresponding to BopE were measured (C) and normalised to the 60 kDa bands, indicated by black arrows, on the Coomassie Brilliant Blue stained gel (D). Data are presented as the mean ± SEM of three biological replicates. **P* < 0.05. Lane 1: SeeBlue® Plus2 pre-stained protein markers; lane 2 and 4, total culture proteins from the K96243[*bopE*TC] strain; lane 3 and 5, supernatant proteins from the K96243[*bopE*TC] strain; lane 6 and 8, total culture proteins from the K96243[pBHR1]; lane 7 and 9, supernatant proteins from the K96243[pBHR1] strain. The expected size of TC-tagged BopE (33 kDa) is indicated by the blue box.

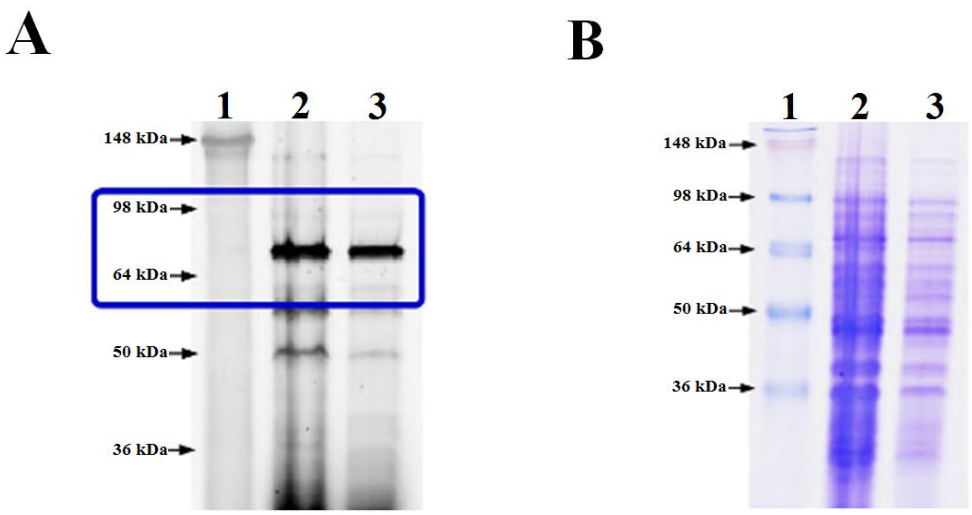

Figure 5.1.24 *E. coli* GspD expression during growth in medium supplemented with high (320 mM) or normal (85.6 mM) NaCl levels. Total proteins from mid exponential growth phase cultures of the DH5α[pJP117] strain were precipitated with DOC/TCA and labelled with the FlAsH compound using BME as the reducing agent. Labelled samples were separated using SDS-PAGE and the fluorescence measured (A). Unlabelled samples were separated by SDS-PAGE and visualised by Coomassie Brilliant Blue staining (C). Lane 1: SeeBlue® Plus2 pre-stained protein markers; lane 2, total proteins from the DH5α[pJP117] strain after growth in LB supplemented with 85.6 mM NaCl for 3 h; lane 3, total proteins from the DH5α[pJP117] strain after growth in LB supplemented with 320 mM NaCl for 3 h. The expected size of TC-tagged GspD (75 kDa) is indicated by the blue box.

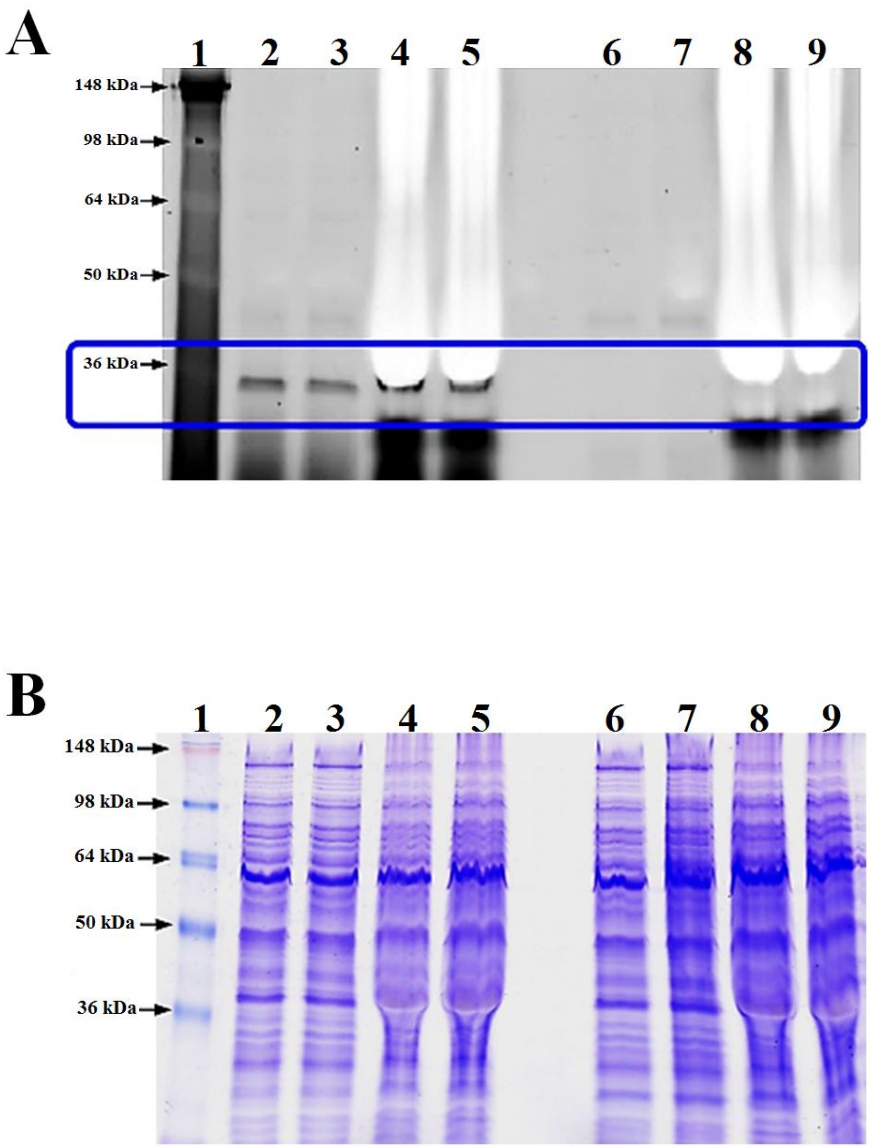

Figure 5.1.25 Effect of congo red treatment on BopE expression. The K96243[*bopE*TC] and K96243 [pBHR1] strains were cultured in either LB (lane 2 and 6), LB supplemented with 5% (w/v) sucrose (lane 3 and 7), LB supplemented with 0.08% (w/v) congo red (lane 4 and 8) or LB supplemented with 5% (w/v) sucrose and 0.08% (w/v) congo red (lane 5 and 9) and grown to mid exponential growth phase. Live bacterial cells were incubated with FlAsH prior to denaturation with 1X sample buffer containing dithiothreitol (DTT) as the reducing agent for live cell labelling. Labelled samples were separated using SDS-PAGE and the fluorescence measured (A). Unlabelled samples were separated by SDS-PAGE and visualised with Coomassie Brilliant Blue staining (B). Lane 1: SeeBlue® Plus2 pre-stained protein markers; lanes 2 to 5, the K96243[*bopE*TC] strain; lanes 6 to 9, the K96243[pBHR1] strain. The expected size of TC-tagged BopE (33 kDa) is indicated by the blue box.

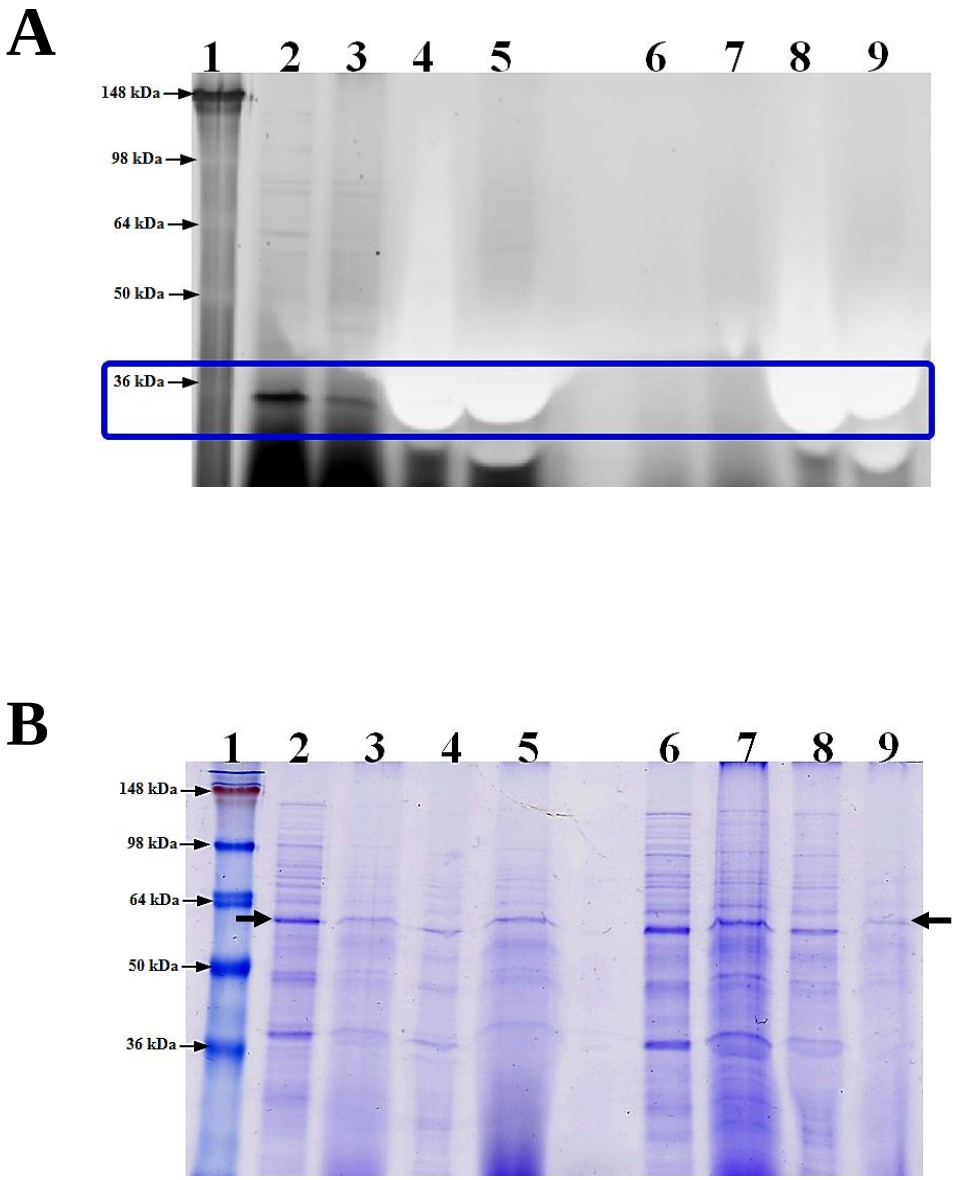

Figure 5.1.26 Effect of Congo Red treatment on secretion and expression of BopE. The K96243[*bopE*TC] and K96243 [pBHR1] strains were cultured in either LB (lane 2, 3, 6 and 7) or LB supplemented with 0.08% (w/v) congo red (lane 4, 5, 8 and 9) and grown to mid exponential growth phase. Total proteins from cultures or filtered supernatants from mid exponential growth phase cultures were precipitated with DOC/TCA and labelled with the FlAsH reagent using BME as the reducing agent. Labelled samples were separated using SDS-PAGE and the fluorescence measured (A). Unlabelled samples were separated by SDS-PAGE and visualised by Coomassie Brilliant Blue staining (B). Lane 1: SeeBlue® Plus2 pre-stained protein markers; lanes 2 and 4, total culture proteins from the K96243[*bopE*TC] strain; lanes 3 and 5, supernatant proteins from the K96243[*bopE*TC] strain; lanes 6 and 8, total culture proteins from the K96243[pBHR1] strain; lanes 7 and 9, supernatant proteins from the K96243[pBHR1] strain. The expected size of TC-tagged BopE (33 kDa) is indicated by the blue box.

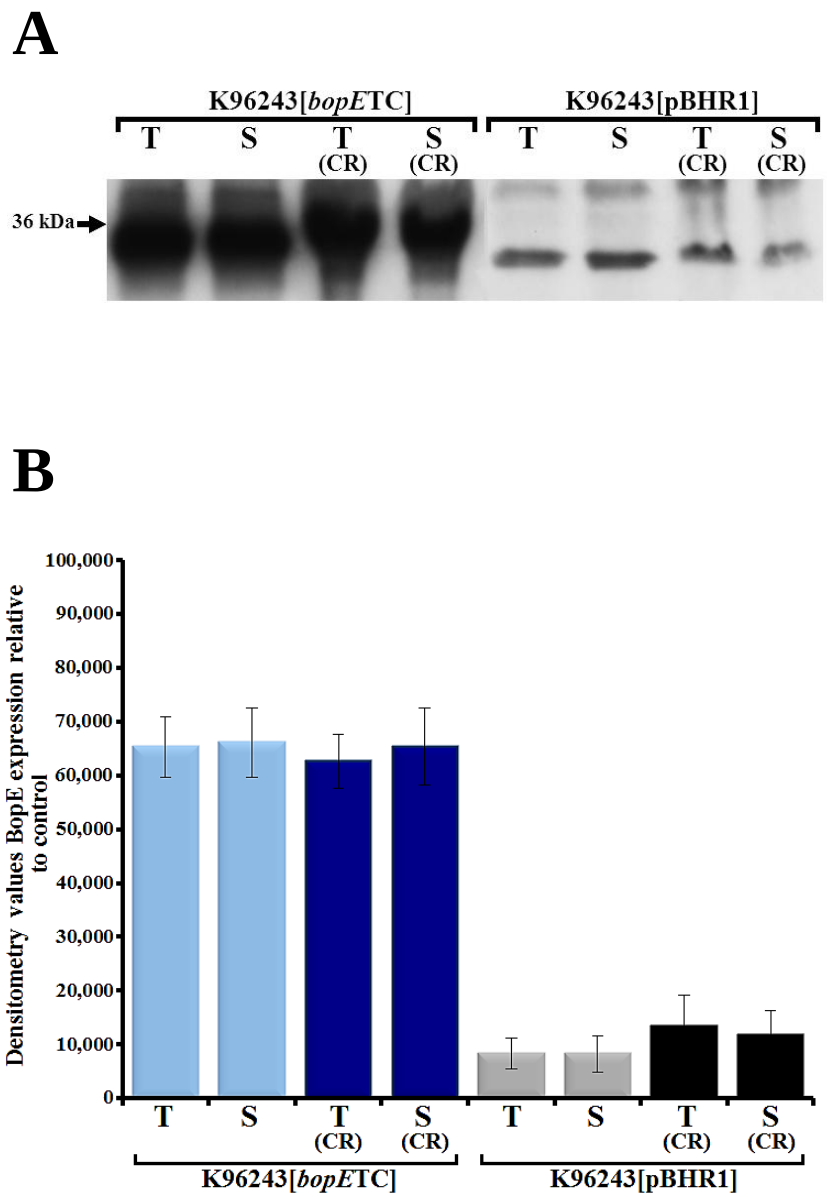

Figure 5.1.27 Effect of congo red treatment on secretion and expression of BopE. (A) After measuring the fluorescent signal (see *Figure 5.1.26*), proteins were transferred to PVDF membranes in order to perform Western immunoblotting with BopE-specific antiserum. (B) Intensities of protein bands corresponding to BopE were measured and normalised to the 60 kDa bands, indicated by black arrows, on the Coomassie Brilliant Blue stained gel in *Figure 5.1.26B*. Data are presented as the mean ± SEM of three biological replicates. T, total culture; S, supernatant; CR, congo red stimulation condition.

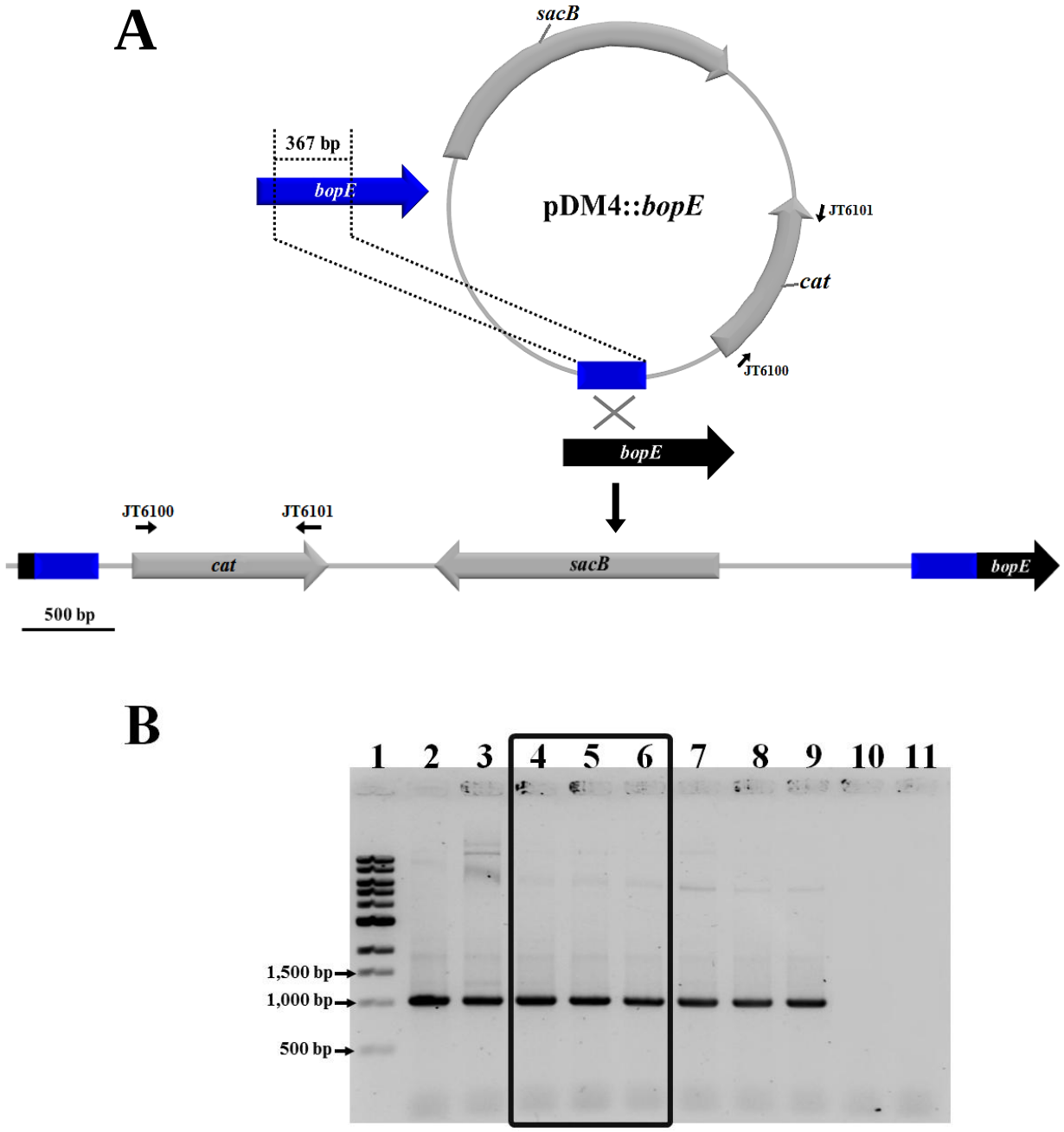

Figure 5.2.1 Construct for *bopE* single-crossover mutagenesis using the suicide vector pDM4. (A) The mutagenesis construct pDM4::*bopE* was constructed by amplifying a 367-bp internal fragment of *bopE* (highlighted in blue) and cloning into *Bgl*II-/*Xho*I-cut pDM4 as described previously (Stevens *et al.*, 2002). The wild-type *bopE* gene is highlighted in black and the putative final genomic organisation is shown. The primer pair JT6100/JT6101 amplifying the chloramphenicol acetyl transferase (*cat*) gene was used for screening potential transconjugants. Arrows indicate the orientation of genes and primers. Arrows designating oligonucleotides are not shown to scale. (B) PCR screening of potential K96243*ΔbopE*::pDM4 strains using the primer pair JT6100/JT6101. Lane 1, DNA size markers; lanes 2 to 8, PCR products derived from potential K96243*ΔbopE*::pDM4 genomic DNA templates; lane 9, genomic DNA of *E. coli* S17-1/λ*pir* harbouring pDM4::*bopE* as the positive control; lane 10, genomic DNA of the wild-type strain; lane 11, no DNA control. Clones indicated by the black box were selected for further experiments.

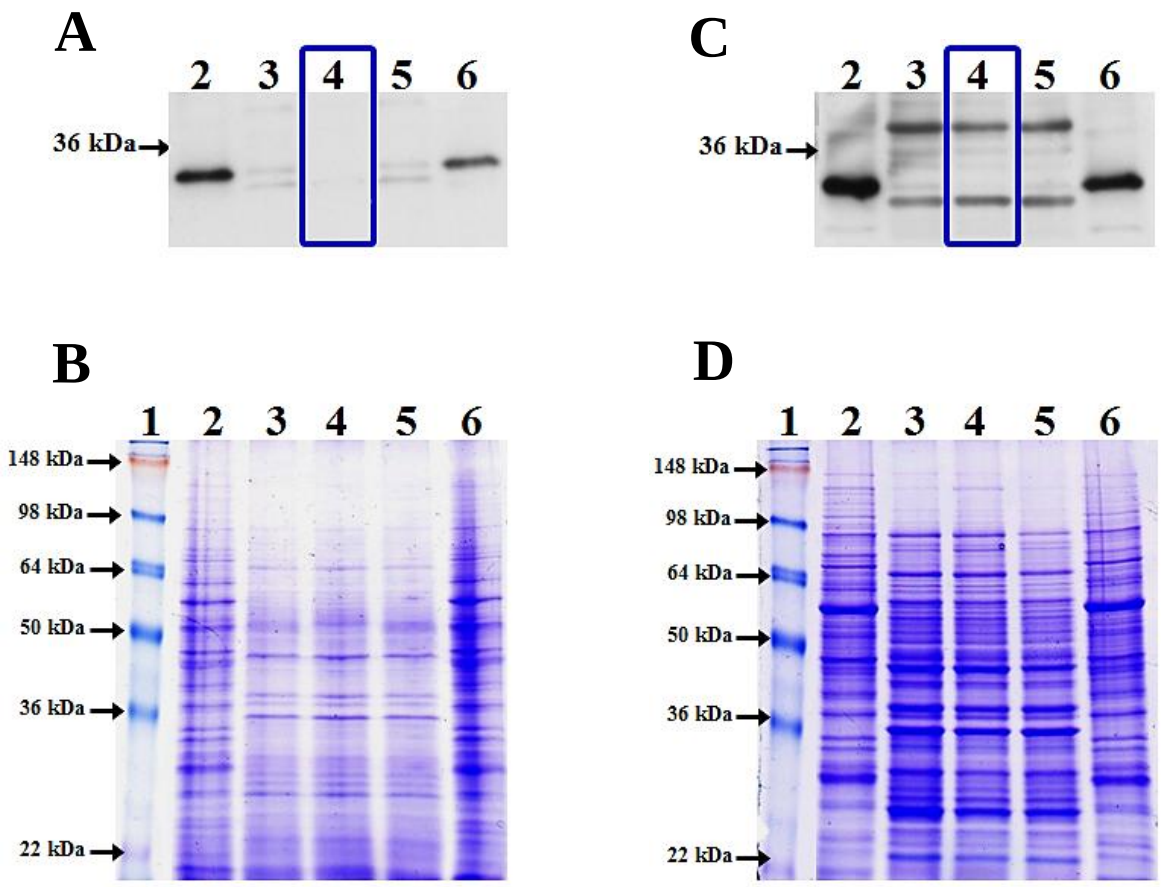

Figure 5.2.2 BopE secretion and expression from putative K96243*ΔbopE*::pDM4 strains. Total proteins (C, D) from cultures or filtered supernatants (A, B) from mid exponential growth phase cultures were precipitated with DOC/TCA, separated by SDS-PAGE and Western immunoblotting using BopE-specific antiserum was subsequently conducted (A, C). DOC/TCA precipitated supernatant (B) and total culture (D) samples were separated by SDS-PAGE and visualised by Coomassie Brilliant Blue staining. Lane 1: SeeBlue® Plus2 pre-stained protein markers; lane 2, the *K96243ΔbapC* strain; lanes 3 and 5, putative K96243*ΔbopE*::pDM4 strains; lane 6, the wild-type strain. The clone in lane 4 as indicated by the blue box was selected for further experiments.

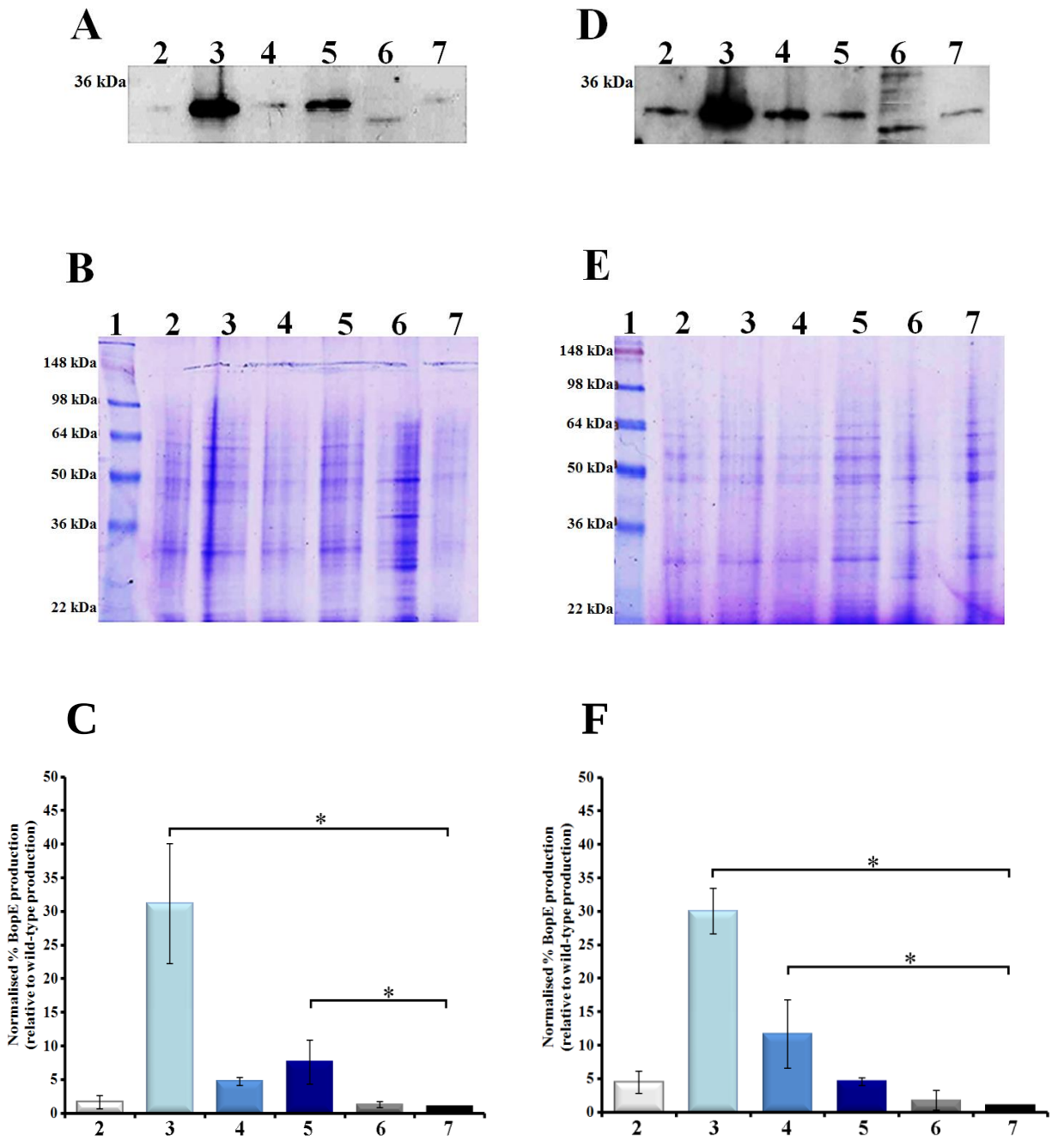

Figure 5.2.3 BopE secretion is increased in the K96243*ΔbapB* and K96243*ΔbapBC* strains during early-exponential growth phase. Proteins from supernatant samples (A, B and C) and total cultures (D, E and F) were precipitated using DOC/TCA, separated by SDS-PAGE and either transferred to PVDF membranes for Western immunoblotting using BopE-specific antiserum (A, D) or visualised directly by Coomassie Brilliant Blue staining (B, E). BopE-specific bands in the Western immunoblots were quantified by densitometry using ImageJ (http://rsbweb.nih.gov/ij/). The relative secretion levels, normalised against the wild-type secretion, were presented as the mean ± SEM of three biological replicates (C, F). Lane 1: SeeBlue® Plus2 pre-stained protein markers; lane 2, the K96243*ΔbapA* strain; lane 3, the K96243*ΔbapB* strain; lane 4, the K96243*ΔbapC* strain; lane 5, the K96243*ΔbapBC* strain; lane 6, the K96243*ΔbopE*::pDM4 strain; lane 7, the wild-type strain. *$P < 0.05$.

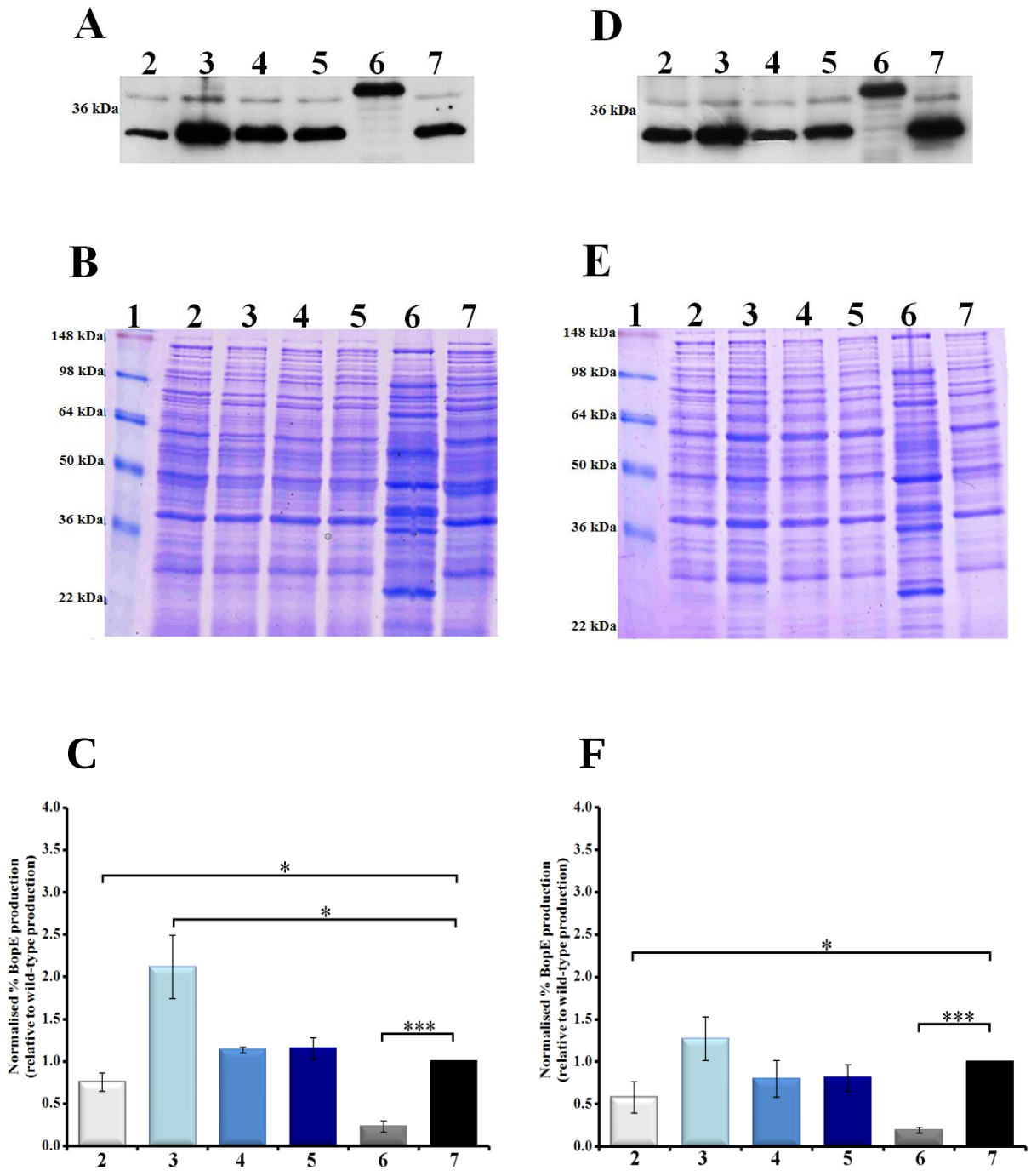

Figure 5.2.4 BopE secretion is increased in the K96243*ΔbapB* strain during mid-exponential growth phase. Proteins from supernatant samples (A, B and C) and total cultures (D, E and F) were precipitated using DOC/TCA, separated by SDS-PAGE and either transferred to PVDF membranes for Western immunoblotting using BopE-specific antiserum (A, D) or visualised directly by Coomassie Brilliant Blue staining (B, E). BopE-specific bands in the Western immunoblots were quantified by densitometry using ImageJ. The relative secretion levels, normalised against the wild-type secretion, were presented as the mean ± SEM of three biological replicates (C, F). Lane 1: SeeBlue® Plus2 pre-stained protein markers; lane 2, the K96243*ΔbapA* strain; lane 3, the K96243*ΔbapB* strain; lane 4, the K96243*ΔbapC* strain; lane 5, the K96243*ΔbapBC* strain; lane 6, the K96243*ΔbopE*::pDM4 strain; lane 7, the wild-type strain. *P < 0.05, ***P < 0.0001.

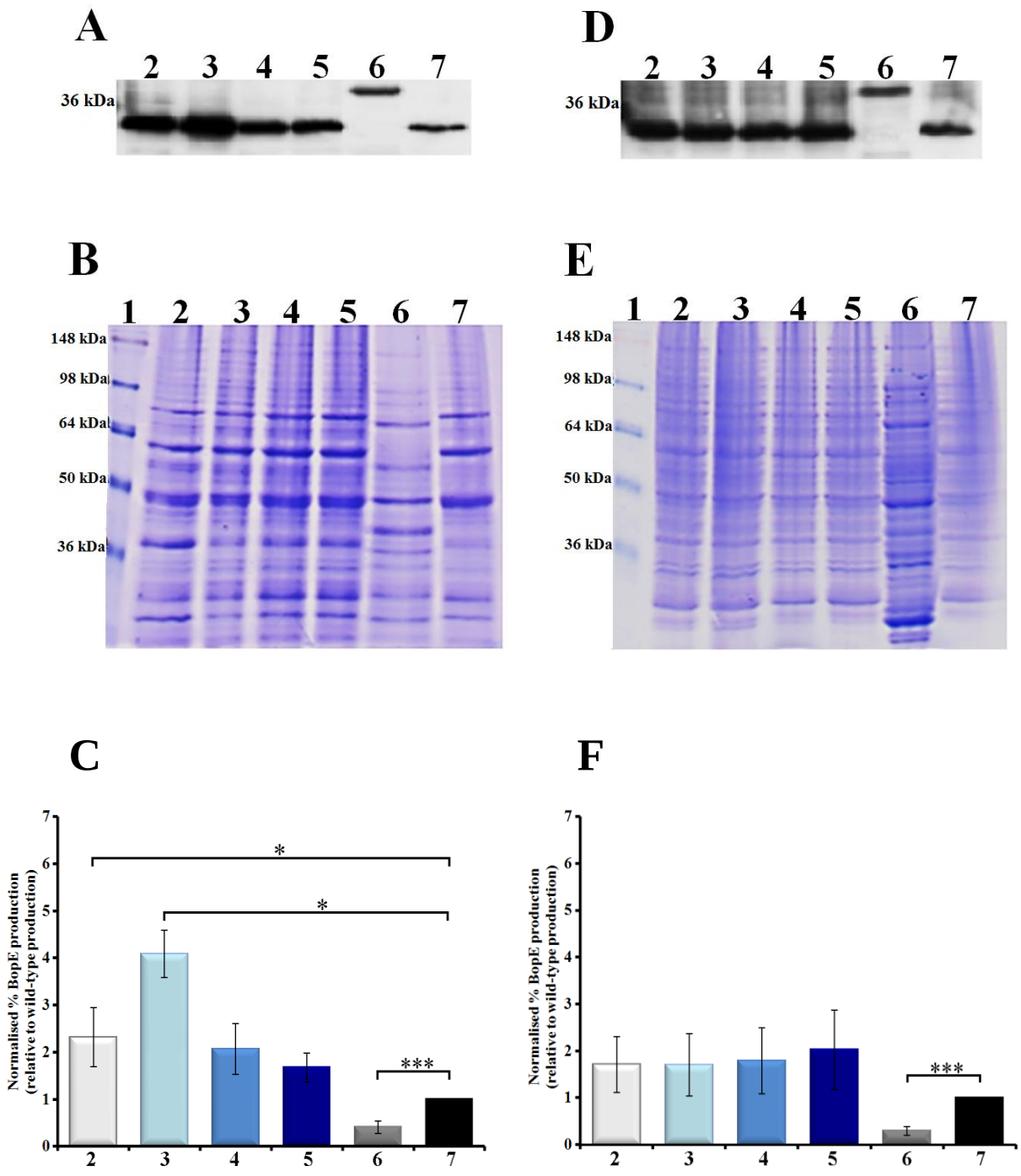

Figure 5.2.5 BopE expression is increased in the K96243*ΔbapA* and K96243*ΔbapB* strains during late-exponential growth phase. Proteins from supernatant samples (A, B and C) and total cultures (D, E and F) were precipitated using DOC/TCA, separated by SDS-PAGE and either transferred to PVDF membranes for Western immunoblotting using BopE-specific antiserum (A, D) or visualised directly by Coomassie Brilliant Blue staining (B, E). BopE-specific bands in the Western immunoblots were quantified by densitometry using ImageJ. The relative expression levels, normalised against the wild-type expression, were presented as the mean ± SEM of three biological replicates (C, F). Lane 1: SeeBlue® Plus2 pre-stained protein markers; lane 2, the K96243*ΔbapA* strain; lane 3, the K96243*ΔbapB* strain; lane 4, the K96243*ΔbapC* strain; lane 5, the K96243*ΔbapBC* strain; lane 6, the K96243*ΔbopE*::pDM4 strain; lane 7, the wild-type strain. *$P < 0.05$, ***$P < 0.0001$.

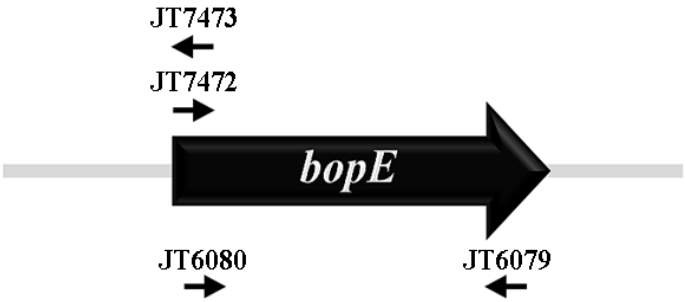

Figure 5.2.6 Location of oligonucleotide primers used for analysis of *bopE* gene expression by RT-PCR. Arrows indicate the orientation of primers and *bopE*. Arrows designating oligonucleotides and *bopE* are not shown to scale.

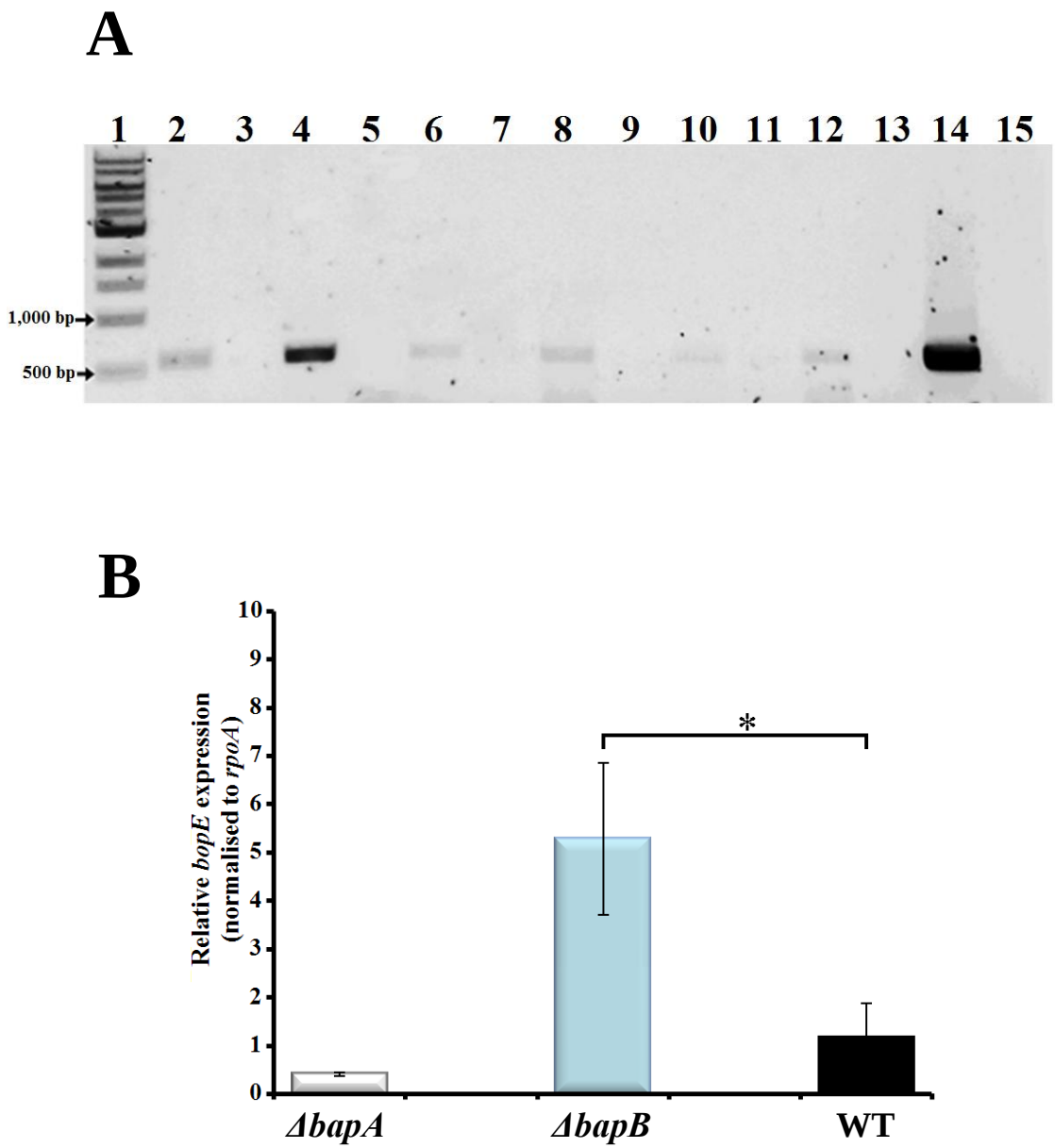

Figure 5.2.7 Transcription of *bopE* is increased in the K96243*ΔbapB* strain during early exponential growth phase. Total RNA from *B. pseudomallei* strains was extracted and used for reverse transcription PCR (RT-PCR). RT-PCR was carried out using the primer pair JT6079/JT6080 for amplification of *bopE* (A). Lane 1, DNA size markers; lane 2 and 3, RT+ and RT-, respectively, of the K96243*ΔbapA* strain; lane 4 and 5, RT+ and RT- of the K96243*ΔbapB* strain; lane 6 and 7, RT+ and RT- of the K96243*ΔbapC* strain; lane 8 and 9, RT+ and RT- of the K96243*ΔbapBC* strain; lane 10 and 11, RT+ and RT- of the K96243*ΔbopE*::pDM4 strain; lane 12 and 13, RT+ and RT- of the wild-type strain; lane 14, genomic DNA of the wild-type strain as the positive control; lane 15, no DNA control. Quantitative real-time RT-PCR was subsequently conducted on cDNA from the K96243*ΔbapA* (*ΔbapA*), K96243*ΔbapB* (*ΔbapB*) strains and the wild-type (WT) strain (B). The level of *bopE* transcription in each sample was normalised to the housekeeping gene *rpoA* expression. Data are expressed as mean ± SEM. Error bars represent the SEM from three technical replicates of biological duplicates (n = 2). **P* < 0.05.

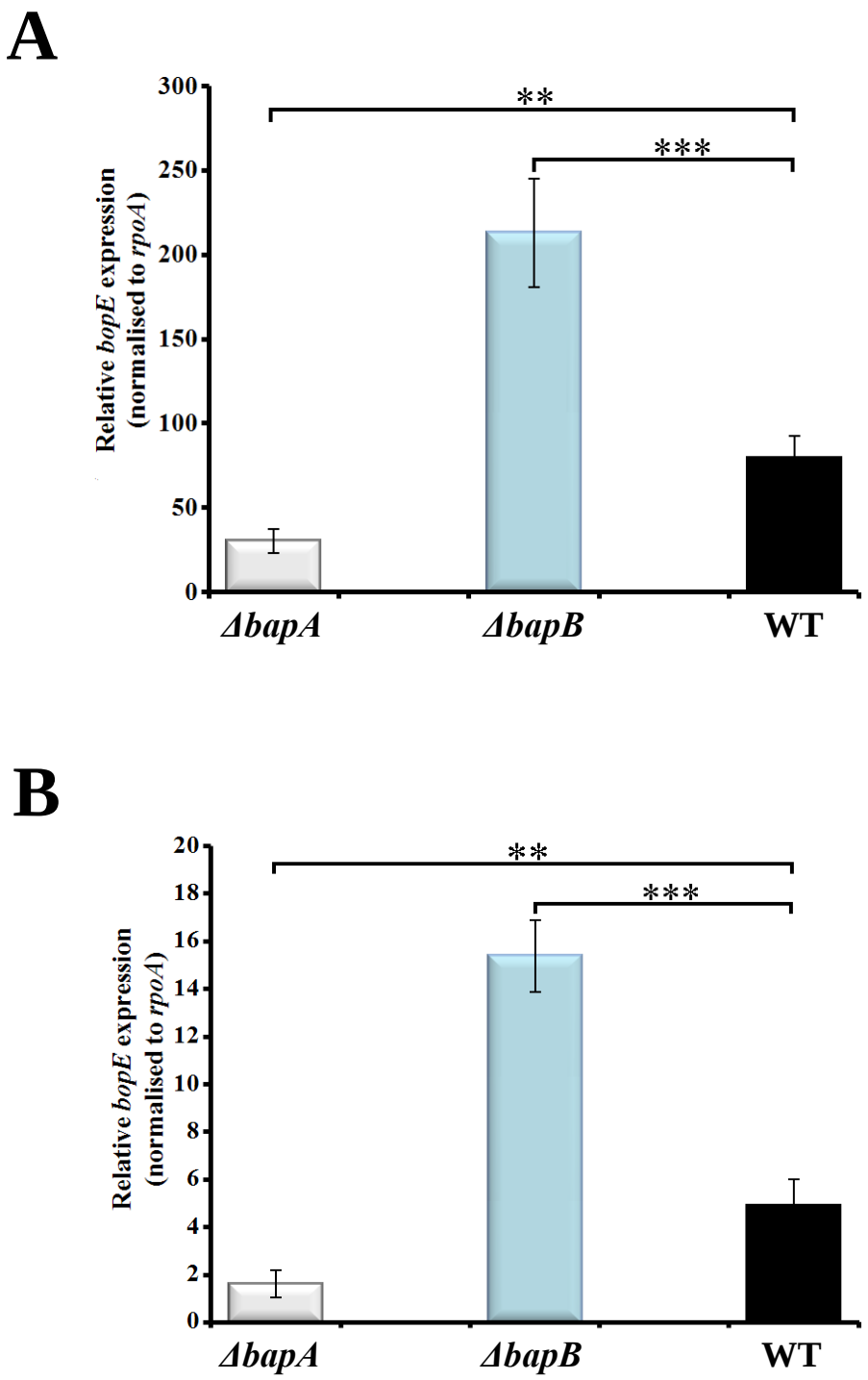

Figure 5.2.8 Transcription of *bopE* is increased in the K96243*ΔbapB* strain during mid (A) and late (B) exponential growth phase. Quantitative real-time RT-PCR was conducted on cDNA from the K96243*ΔbapA* (*ΔbapA*), K96243*ΔbapB* (*ΔbapB*) strains and the wild-type (WT) strain. The level of *bopE* transcription in each sample was normalised to the housekeeping gene *rpoA* expression. Data are expressed as mean ± SEM. Error bars represent the SEM from three technical replicates of biological duplicates (n = 2). ***P* < 0.001, ****P* < 0.0001.

```
BapB      MTAGPHLSDAAALAAAKTLLAGMLGVPEAQIAPPQRLLDDLAMDSLELIELAMELDERWN
IacP      -------MNMDIEARVKKVITSCIAVDVDSINGQTHLVEDLYADSLDLIDIVFGLSEEFD
                 :    * .*.:::. :.*   .*    :*::**  ***:**::.: *.*.::

BapB      IRLDRARLAEVATVADVAALLGAAARADDSGGA
IacP      ISCNENDLPDMMIFADICRVVKKSLESRV----
          *  :.  *.:: *.**:. ::  : .:
```

Figure 5.3.1 Amino acid sequence alignment of the *B. pseudomallei* BapB and the *Salmonella* IacP. Sequence similarity is shown with '**:**' or '**.**' to designate amino acids with strongly and weakly conserved properties, respectively. Sequence identity is shown with '*****' to designate identical amino acids.

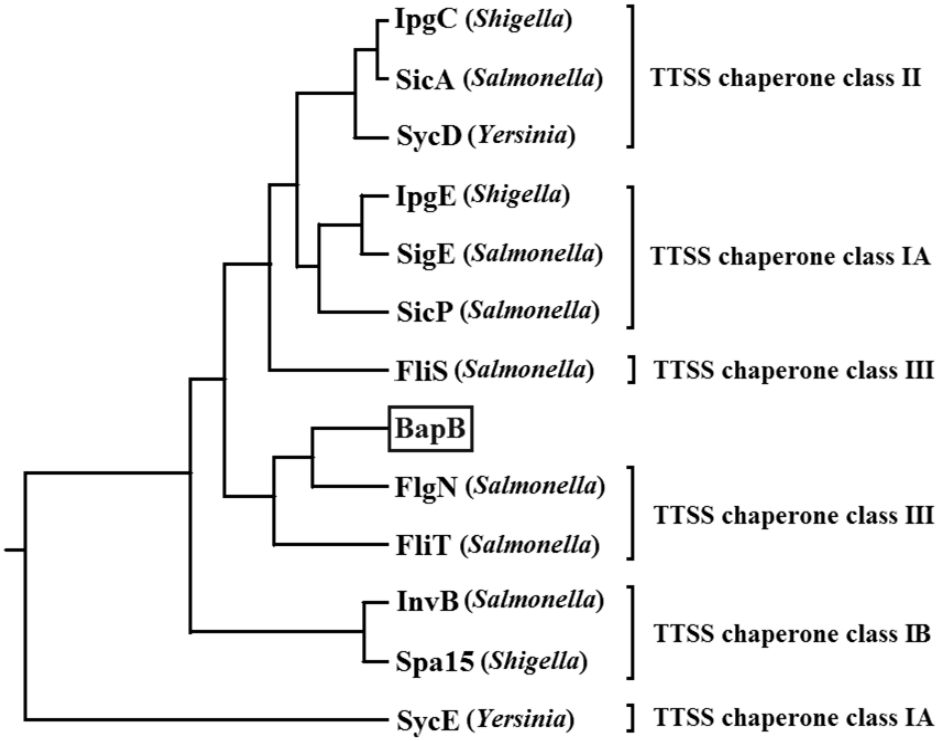

Figure 5.3.2 Phylogenetic tree analysis of representative different classes of TTSS chaperones (Parsot *et al.*, 2003) based on ClustalW alignment (www.genome.jp/tools/clustalw). BapB is highlighted in a box.

A

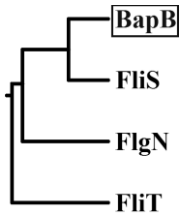

B

```
BapB    ------------------MTAGPH-LSDAAALAAAKTLLAGMLGVPEAQIAPP------
FliS    MYTASGIKAYAQVSVESAVMSASPHQLIEMLFDGANSALVRARLFLEQGDVVAKGEALSK
                          *:*.** * :    .* .:*: . * : :.::..

BapB    --------------QRLLDDLAMDSLELIELAMELDERWNIRLDRARLAEVATVADVAAL
FliS    AINIIDNGLKAGLDQEKGGEIATNLSELYDYMIRRLLQANLRNDAQAIEEVERLLSNIAE
                     *.  .::* :  ** :  :.   : *:* *   : **  : .  *

BapB    LGAAARADDSGGA--
FliS    AWKQISPKASFQESR
          .. *
```

Figure 5.3.3 Phylogenetic tree analysis of representative TTSS chaperone class III (A) and amino acid sequence alignment of the *B. pseudomallei* BapB and the *Salmonella* FliS (B). BapB is highlighted in a box. Sequence similarity is shown with '**:**' or '**.**' to designate amino acids with strongly and weakly conserved properties, respectively. Sequence identity is shown with '*****' to designate identical amino acids.

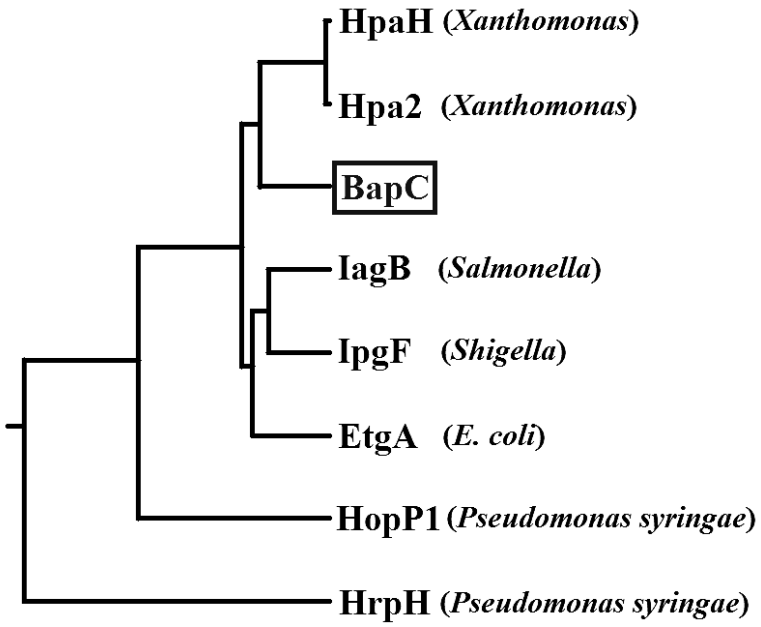

Figure 5.3.4 Phylogenetic relationship of TTSS-associated lytic transglycosylase enzymes from animal- and plant-pathogenic bacteria based on ClustalW alignment. The *B. pseudomallei* BapC is highlighted in a box.

A

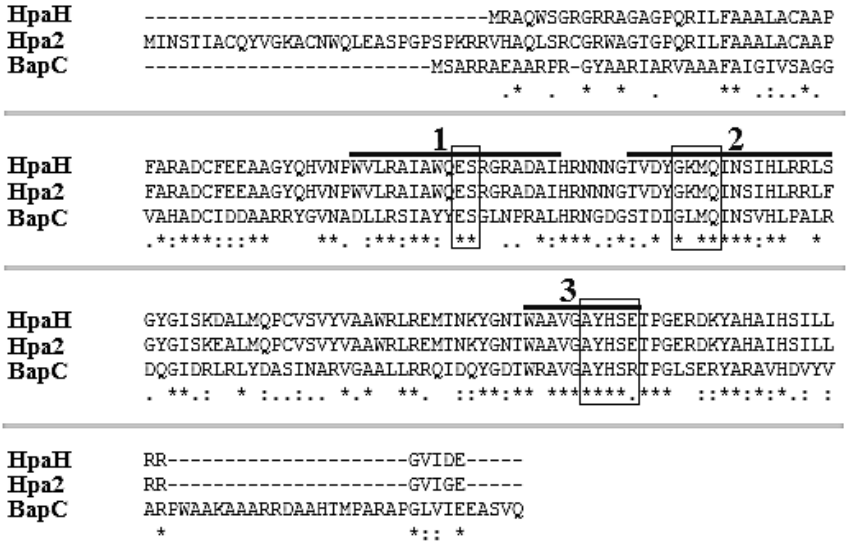

B

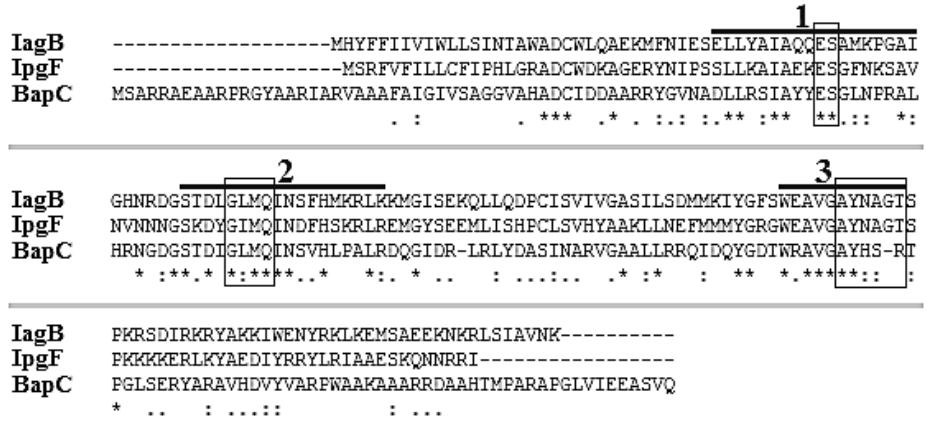

Figure 5.3.5 Amino acid sequence alignment of the *B. pseudomallei* BapC and the *X. campestris* pv. vesicatoria HpaH and *X. oryzae* pv. oryzae Hpa2 (A), and the IagB of *Salmonella* and IpgF of *Shigella* (B). Three conserved motifs of the LT domains are indicated by the boxes. Regions 1 and 3 are predictably to form α-helices and 2 is predictably to form the β-sheet. Residue E in α-helix regions (boxed) is the typical catalytic glutamate residue which is responsible for cleaving β-1,4 glycosidic bonds of bacterial peptidoglycan. Sequence similarity is shown with '**:**' or '**.**' to designate amino acids with strongly and weakly conserved properties, respectively. Sequence identity is shown with '*****' to designate identical amino acids.

A

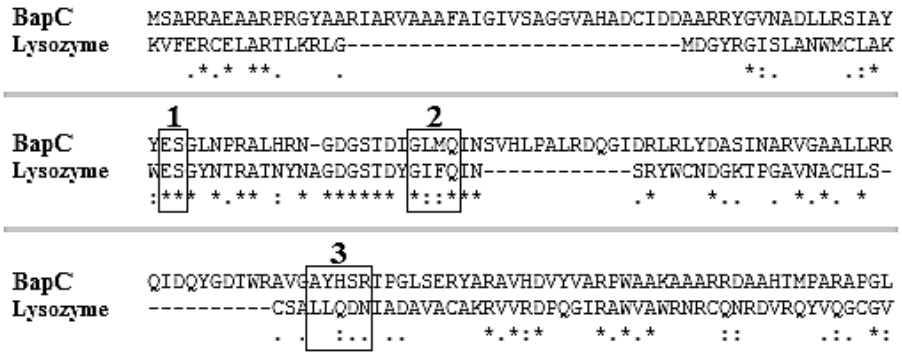

B

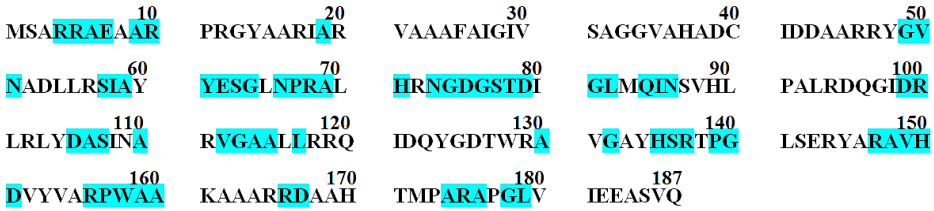

Figure 5.3.6 Amino acid sequence alignment of the *B. pseudomallei* BapC and amino acid residues involved in the conformational stability and folding of human lysozyme. (A) Sequence similarity is shown with '**:**' or '**.**' to designate amino acids with strongly conserved or weakly conserved properties, respectively. Identitied amino acids are shown with '*****'. Three conserved motifs of the LT domains are indicated by the blue boxes. Number 1 and 3 are part of α-helices and 2 is the β-sheet. The residue in α-helix 1 (boxed) is the typical catalytic glutamate residue which is responsible for cleaving β-1,4 glycosidic bonds of bacterial peptidoglycan. (B) Locations of amino acid sequence identity to human lysozyme of BapC are highlighted in blue.

Chapter 6

General discussion and future directions

Chapter 6: General discussion and future directions

The *B. pseudomallei* TTSS3 is a key virulence factor that consists of a structural injectisome, translocons, chaperones and effectors. Of all these TTSS3 molecules, the secreted effectors play direct roles in host cell interactions and modification of host cell functions in order to aid bacterial survival and replication within the host. In this study, the putative effectors BapA, BapB and BapC, encoded within the TTSS3 locus, were characterised with regard to their role as effectors and their importance in *B. pseudomallei* virulence.

In Chapter 3, the K96243*ΔbapA*, *ΔbapB* and *Δbap*C strains, and a K96243*Δbap*BC strain were generated by double cross-over allelic exchange. These mutant strains were characterised in order to identify the importance of these genes in bacterial pathogenesis. All mutants displayed reduced *in vivo* survival compared to the wild-type strain, and in initial trials all showed reduced virulence as infected mice displayed an increased time to death, suggesting that BapA, BapB and BapC may play a role in, but are not essential for, bacterial growth and virulence. In order to verify that the observed phenotypes were specifically due to inactivation of the *bap* genes, complementation was initially attempted using the replicating pBHR1 plasmid. All pBHR1 constructs showed low stability in *B. pseudomallei* with between 0% and 56% of the recombinant plasmids retained over 12 h in the absence of selection. The K96243*ΔbapB*[*bapB*] strain was the most stable and this construct partially restored the wild-type *in vivo* survival phenotype of the K96243*ΔbapB* strain. By using the same complementation approach, D'Cruze *et al.* (2011) also showed partial restoration of the wild-type phenotype of a *BPSL1394* mutant using *in vitro* macrophage infection assays. Due to the low stability of the pBHR1 constructs, complementation with this approach was not tested further. Instead, another complementation approach was attempted by using the transposon mini-Tn*7* vector. Although these complementation constructs were able to be mobilised into *B. pseudomallei*, no integration site could be definitely determined. Therefore, as complementation was not successful, four independently derived strains, K96243*ΔbapA*_2, *ΔbapB*_2, *ΔbapC*_2 and *ΔbapBC*_2, were generated as an alternative and these independent mutants used in direct virulence trials. The K96243*ΔbapA*_2 strain showed similar attenuation to the original mutant, indicating that the attenuation observed for the original mutant was likely due to inactivation of *bapA*. Thus, it can be concluded that *bapA* likely plays a role, either direct or indirect, in virulence of *B. pseudomallei*. Although we cannot rule out the possibility that both mutants have other mutations outside *bapA*, this should be the focus of future work. In contrast, the other

independent mutants revealed different attenuation levels from the corresponding original mutant, suggesting that BapB and BapC do not play a significant role in bacterial virulence in the BALB/c mouse model. However, it remains unclear why the original mutants behaved differently in the first animal experiments. The variable virulence trial data suggest that there may be additional mutations outside the regions subjected to mutagenesis and/or different susceptibility to *B. pseudomallei* infection of mice in each of the virulence trials. Accordingly, several additional experiments should be conducted. Complementation is the most complete method to assess the specific role of inactivated genes in generating a given phenotype(s). Therefore, further work should be done with the mini-Tn*7* complementation constructs in order to identify and confirm the integration positions of the mini-Tn*7* complemented mutant strains, for instance, by full genome sequencing. If each construct is shown to contain the appropriate integration then these strains should be used for competitive growth assays and virulence trials. The stability of the constructs would also need to be assessed by growth in the absence of antibiotics for up to 10 days (the normal duration of the mouse virulence trials). Alternatively, complementation could be achieved by generating complementation constructs in the pDM4 vector in such a way that they would be integrated into the genome.

In addition to further attempts at complementation, genome sequencing could be conducted on both the independently derived mutants and the original mutants to determine if there was any secondary mutation(s) in any of the strains. Another set of independently derived K96243*ΔbapB* and K96243*ΔbapC* strains could also be generated for assessing attenuation in comparison to the previous two mutants and the wild-type strain. In addition to the K96243*ΔbapBC* strain already generated, the K96243*ΔbapAB* and K96243*ΔbapABC* strains, could be generated and characterised in order to investigate the virulence of the bacteria when *bapAB* or *bapABC* have been inactivated.

In Chapter 4, the original K96243*ΔbapA*, *ΔbapB*, *ΔbapC* and *ΔbapBC* strains were further characterised for their possible function(s) in regards to subverting host cell functions. Several *in vitro* phenotypic assays were conducted based on previous TTSS studies. Disruption of *bapA*, *bapB*, *bapC* or even *bapBC* did not affect any of the following: bacterial invasion of the cultured lung epithelial cell line A549, bacterial survival and replication in the macrophage-like cell line RAW264.7, ability of bacteria to escape from host phagosomes, actin-mediated motility or MNGC formation. Thus, unlike other members of previously characterised TTSS3 genes (Cullinane *et al.*, 2008; D'Cruze *et al.*, 2011; Gong *et al.*, 2011), these genes do not play a role in

these functions. However, the K96243*ΔbapB* and K96243*ΔbapC* strains stimulated a statistically significant increase in TNF-α secretion from macrophage-like cells at 2 h p.i. whereas the K96243*ΔbapBC* strain stimulated a reduced TNF-α secretion at 4 and 6 h p.i., suggesting a possible role for *bapB* and *bapC* in stimulating the host immune systems which has been previously reported (Burtnick *et al.*, 2008; Hii *et al.*, 2008; Miao & Warren, 2010).

Pretreatment of RAW264.7 cells with IFN-γ prior to infection augments the antimicrobial activity of macrophages. The intracellular survival and replication of the K96243*ΔbapC* strain was significantly reduced in IFN-γ pre-treated RAW264.7 cells, suggesting that BapC may play a role in avoiding IFN-γ stimulation. The K96243*ΔbapC* strain, as well as the K96243*ΔbapA* and *ΔbapBC* strains, showed reduced IL-6 secretion from IFN-γ stimulated RAW264.7 cells, but only at 2 h p.i. However, all mutant strains stimulated a similar level of TNF-α secretion from IFN-γ pre-treated RAW264.7 cells as did the wild-type strain. To confirm and extend these results, several additional experiments should be carried out. All of the *in vitro* assays carried out in this study were performed in RAW264.7 cells, however previous TTSS3 studies (Burtnick *et al.*, 2008; Stevens *et al.*, 2002) have used another murine macrophage-like cell line J774.2 to perform the phenotypic assays. Thus, the intracellular survival and replication assays could be repeated in this cell line in order to identify if there are any differences in cellular behaviour from RAW264.7 cells. Furthermore, as the K96243*ΔbapC* strain showed altered intracellular replication in IFN-γ stimulated RAW264.7 cells, the K96243*ΔbapC*, K96243*ΔbapC*_2 and K96243*ΔbapC*[*bapC*] strains should also be tested in both normal and IFN-γ pre-treated macrophages. In addition, time-course experiments longer than 6 h p.i. should be conducted, based on previous studies showing that some TTSS3 mutants exhibit delayed phenotypes (Burtnick *et al.*, 2008). Importantly, the TNF-α and IL-6 secretion experiments should be repeated using the K96243*ΔbapC*, K96243*ΔbapC*_2 and K96243*ΔbapC*[*bapC*] strain, and the K96243*ΔbapBC* and K96243*ΔbapBC*_2 strains in both normal untreated macrophages and IFN-γ pre-treated macrophages. Based on the TNF-α and IL-6 assay results, other cytokines, for instance, IL-8, IL-1β and IL-10 (Alciato *et al.*, 2010; Burtnick *et al.*, 2008), should be assessed. The levels of IL-8 (Hii *et al.*, 2008) and IFN-γ (Paludan, 2000) secreted from infected phagocytic cells are likely to correlate with that of TNF-α. Furthermore, RAW264.7 cell cytotoxicity assays, measured by assessing the level of LDH release (Smith *et al.*, 2011), should also be carried out along with *in vitro* infection in order to verify that there was no unintentional effects from the

loss of cell integrity (Burtnick *et al.*, 2008). These assays could also show whether BapA, BapB and/or BapC play a role in causing host cell damage/death.

In Chapter 5, the function of BapA, BapB and BapC as TTSS3-dependent secreted effectors was assessed by following the secretion of TC-tagged proteins using the TC-FlAsH^{TM}-based fluorescence labelling technique. The FlAsH-labelling system was optimised for *B. pseudomallei* using the well characterised TTSS3 effector BopE, prior to testing of the TC-tagged BapA, BapB and BapC in whole samples or supernatants. In a similar manner to the positive control BopE, both BapA and BapC were observed to be secreted in a TTSS3-dependent manner, confirming that they are indeed true TTSS3 effectors. These data showed for the first time that BapA and BapC are TTSS3 effector proteins. However, no TC-tagged BapB could be detected either in whole cell or supernatant samples. It is possible that tagging of BapB at the C-terminal end altered the conformation of the protein and hindered the binding of the TC motif to the FlAsH compound. Alternatively, it is possible that BapB is not expressed under the conditions tested. Two possible TTSS stimulation conditions, congo red and high salt concentration (320 mM NaCl), which have been previously reported to stimulate the TTSS activity in *Shigella* (Bahrani *et al.*, 1997; Enninga *et al.*, 2005; Simpson *et al.*, 2010) and *B. pseudomallei* respectively (Pumirat *et al.*, 2010), were tested to see if they enhanced TTSS3 secretion via analysis of BopE secretion. High salt concentration increased the secretion of BopE whereas the addition of congo red did not.

Further experiments should be carried out to investigate the secretion of BapB. Firstly, the protein should be tagged at the N-terminal end and then FlAsH labelling used to analyse secretion. In addition, optimisation with regard to the generation of this construct could be considered, including adding or removing the linkers of the TC tag and/or using tandem repeat TC tags, for instance, CCPGCCPGCCPGCC, in order to help increase the flexibility and/or intensity of fluorescent complex formation as demonstrated elsewhere (Simpson *et al.*, 2010; VanEngelenburg & Palmer, 2008). Although the N-terminal region of almost all TTSS effectors is essentially required for the secretion/translocation, some effectors appear to have their functional domains at either the C-terminal or both N- and C-terminal regions, depending upon the interaction required during pathogenesis (Brown *et al.*, 2006; Diacovich *et al.*, 2009; Harrington *et al.*, 2003; Kim *et al.*, 2007; Myeni & Zhou, 2010; Terry *et al.*, 2008). Since amino acids 10 to 30 and 50 to 100 of TTSS effectors are predicted to be the location of secretion signal and chaperone/translocation binding sites, respectively (Löwer & Schneider, 2009), it would be important to characterise these regions of the newly identified effectors BapA and BapC.

Deletion or substitution variants within (made by site-directed mutagenesis) each of those regions in C-terminal TC-tag fusions should be constructed and subsequently analysed by FlAsH labelling to determine if these regions are required for the secretion/function of these two effectors. Moreover, the fluorescent secretion and production of the TC-tagged BapA and BapC should be assessed in other TTSS3 mutants (e.g. the *bipD* mutant) in order to confirm that BapA and BapC are secreted in a TTSS3-dependent manner. Alternatively, other reporter systems, for instance, the β-lactamase reporter system (Charpentier & Oswald, 2004), should be also used to investigate the translocation of BapA, BapB and/or BapC into host cells. This reporter system has been used successfully to monitor the translocation of effectors in many Gram-negative pathogens (Charpentier & Oswald, 2004; McCann *et al.*, 2007; Mills *et al.*, 2008). Moreover, direct FlAsH labelling of TC-tagged BapA, BapC and BopE should be carried out to monitor the secretion of these effectors in real-time throughout the bacterial infection process, since this approach has been successfully used in monitoring the secretion of *Shigella* and *Salmonella* effectors during bacterial invasion (Enninga *et al.*, 2005; Hoffmann *et al.*, 2010; VanEngelenburg & Palmer, 2008). This would allow direct visualisation of when and where these effectors are secreted during infection.

In order to determine if BapA, BapB and BapC were essential for the function of the TTSS3 system, the secretion of the effector BopE was analysed in each of the K96243*ΔbapA*, *ΔbapB*, *ΔbapC* and *ΔbapBC* strains. BapA, BapB and BapC were not essential for TTSS function as BopE was secreted from each of the mutant strains. However, the secretion and expression of BopE was substantially increased in the K96243*ΔbapB* strain, suggesting that BapB plays a role in regulation of the TTSS3 secretion machinery or in a direct interaction with BopE. Stevens *et al.* (2004) demonstrated that BopE does not play a role in virulence, intracellular replication and escape from host endosomes of *B. pseudomallei*. In this study, BopE secretion was altered in the K96243*ΔbapB* strain, but the mutant strain showed unaltered bacterial virulence, intracellular replication and escape from host endosomal vacuoles; this is in accordance with the results of Stevens *et al.* (2004) with respect to altered production of BopE. Bioinformatic analysis suggests that BapB may act as a TTSS3 chaperone preventing the premature secretion of one or more effectors. In this case, mutation of *bapB* would lead to premature secretion of BopE. Several TTSS chaperones in other Gram-negative bacteria have been reported to play a role in preventing premature secretion of their cognate effectors (Büttner, 2012; Parsot *et al.*, 2003). Indeed, *Shigella* IpgA and IpgE interact, stabilise and regulate the secretion of their cognate effectors IcsB and IpgD, respectively (Niebuhr *et al.*, 2000; Ogawa *et al.*, 2003). Moreover,

some chaperones can regulate multiple effectors, for example, *Salmonella* chaperone InvB regulates and stabilises its cognate effectors SopE2 and SipA, and also prevents the secretion of another effector SopE (Büttner, 2012; Parsot *et al.*, 2003). In contrast to the K96243*ΔbapB* strain, BopE secretion in the K96243*ΔbapA* strain exhibited a slight decrease in mid and late exponential growth phase, and *bopE* transcription was decreased in this mutant at both growth phases, suggesting that BapA may also interact with BopE, or BapA may play a minor or indirect role in transcription and/or secretion of BopE. To further investigate the function of BapA, BapB and BapC, and identify putative protein-protein interactions, especially between BapB and BopE, several experiments using different approaches should be carried out. Protein co-immunoprecipitation (Deng *et al.*, 2005) using bacterial supernatant samples, followed by normal or 2D SDS-PAGE and then Western immunoblotting or mass spectrometry would potentially identify the binding partners of each of the proteins (Ishidate *et al.*, 1986; Lara-Tejero *et al.*, 2011; Schraidt *et al.*, 2010). To further determine if BapA, BapB and BapC are expressed in a growth-dependent manner, both supernatant and whole cell lysate samples should be prepared from cells at different growth phases, proteins labelled with the FlAsH compound and then detected by fluorescence following separation by SDS-PAGE as described previously. Moreover, blue native-PAGE (Ehrbar *et al.*, 2003; Lara-Tejero *et al.*, 2011) could be used to determine native protein masses of BapA, BapB and BapC and to identify if they exist as part of larger protein complexes. Alternatively, BapA-, BapB- and BapC-specific antisera could be produced for analysing the localisation and interaction of any of these proteins using Western immunoblotting. Apart from protein-protein interaction assays, assays specific for functional characterisation of the ACP and LT domain of BapB and BapC, respectively, should be conducted. Amino acid residues in BapB contributing to its three-dimensional structure and interactions with various enzymes should be identified using site-direct mutagenesis followed by acyl-ACP synthetase assay as described previously (Flaman *et al.*, 2001). Muramidase activity assays (de la Mora *et al.*, 2007; Laible & Germaine, 1985) and zymogram analyses (Kohler *et al.*, 2007; Zahrl *et al.*, 2005) should also be carried out to determine the peptidoglycan degrading activity of BapC. Moreover, as *bopE* transcription was specifically increased in the K96243*ΔbapB* strain and slightly decreased in the K96243*ΔbapA* strain, *bopE* transcription should be assessed in either other mutants, including the K96243*ΔbapC* and *ΔbapBC*, the pBHR1 or the mini-Tn*7* complemented strains.

In summary, three *B. pseudomallei* TTSS3 proteins, namely BapA, BapB and BapC, were characterised in this study. BapA and BapC were shown to be secreted in a TTSS3-dependent

manner and are therefore new TTSS3 effector proteins. Also, BapB and possibly BapA appear to play a role in regulation of the BopE expression and secretion, suggesting that BapB may be a chaperone that controls BopE release. Furthermore, each of the proteins showed a minor role in *in vivo* growth of this bacterium, and BapA showed a possible role in bacterial virulence as two independently derived mutants both showed reduced virulence in the BALB/c mouse model. However, without successful complementation, the possibility that the tested *bapA* mutants might contain secondary mutations that play a role in the observed virulence reduction cannot be ruled out. Finally, BapB and BapC exhibited an involvement in stimulating host innate immune responses while BapA did not seem to be required for this function. Again, confirmation of these phenotypes by analysis of the independently derived mutants and/or complementation is required.

Bibliography

Bibliography

Abby, S. S. & Rocha, E. P. C. (2012). The non-flagellar type III secretion system evolved from the bacterial flagellum and diversified into host-cell adapted systems. *PLoS Genet* **8**, e1002983.

Adams, S. R., Campbell, R. E., Gross, L. A., Martin, B. R., Walkup, G. K., Yao, Y., Llopis, J. & Tsien, R. Y. (2002). New biarsenical ligands and tetracysteine motifs for protein labelling *in vitro* and *in vivo*: synthesis and biological applications. *J Am Chem Soc* **124**, 6063-6076.

Aizawa, S. I. (2001). Bacterial flagella and type III secretion systems. *FEMS Microbiol Lett* **202**, 157-164.

Akopyan, K., Edgren, T., Wang-Edgren, H., Rosqvist, R., Fahlgren, A., Wolf-Watz, H. & Fallman, M. (2011). Translocation of surface-localized effectors in type III secretion. *Proc Natl Acad Sci U S A* **108**, 1639-1644.

Alam, A., Miller, K. A., Chaand, M., Butler, J. S. & Dziejman, M. (2011). Identification of *Vibrio cholerae* type III secretion system effector proteins. *Infect Immun* **79**, 1728-1740.

Alciato, F., Sainaghi, P. P., Sola, D., Castello, L. & Avanzi, G. C. (2010). TNF-α, IL-6, and IL-1 expression is inhibited by GAS6 in monocytes/macrophages. *J Leukoc Biol* **87**, 869-875.

Aldridge, P. D. & Hughes, K. T. (2002). Regulation of flagellar assembly. *Curr Opin Microbiol* **5**, 160-165.

Aldridge, P. D., Karlinsey, J. E., Aldridge, C., Birchall, C., Thompson, D., Yagasaki, J. & Hughes, K. T. (2006). The flagellar-specific transcription factor, σ28, is the type III secretion chaperone for the flagellar-specific anti-σ28 factor FlgM. *Genes Dev* **20**, 2315-2326.

Allaoui, A., Ménard, R., Sansonetti, P. J. & Parsot, C. (1993). Characterization of the *Shigella flexneri ipgD* and *ipgF* genes, which are located in the proximal part of the *mxi* locus. *Infect Immun* **61**, 1707-1714.

Allwood, E. M., Devenish, R. J., Prescott, M., Adler, B. & Boyce, J. D. (2011). Strategies for intracellular survival of *Burkholderia pseudomallei*. *Front Microbiol* **2**, 170.

Alonso, S., Pethe, K., Russell, D. G. & Purdy, G. E. (2007). Lysosomal killing of *Mycobacterium* mediated by ubiquitin-derived peptides is enhanced by autophagy. *Proc Natl Acad Sci U S A* **104**, 6031-6036.

Alwis, P. A., Gong, L., Cullinane, M., Prescott, M., Devenish, R. J., Adler, B. & Boyce, J. D. (unpublished data). Fluorescent *Burkholderia pseudomallei* strains: a new tool for investigating intracellular pathogenesis.

Arjcharoen, S., Wikraiphat, C., Pudla, M., Limposuwan, K., Woods, D. E., Sirisinha, S. & Utaisincharoen, P. (2007). Fate of a *Burkholderia pseudomallei* lipopolysaccharide mutant in

the mouse macrophage cell line RAW264.7: possible role for the O-antigenic polysaccharide moiety of lipopolysaccharide in internalization and intracellular survival. *Infect Immun* **75**, 4298-4304.

Arnold, R., Brandmaier, S., Kleine, F., Tischler, P., Heinz, E., Behrens, S., Niinikoski, A., Mewes, H.-W., Horn, M. & other authors (2009). Sequence-based prediction of type III secreted proteins. *PLoS Pathog* **5**, e1000376.

Arnold, U. & Ulbrich-Hofmann, R. (1999). Quantitative protein precipitation from guanidine hydrochloride-containing solutions by sodium deoxycholate/trichloroacetic acid. *Anal Biochem* **271**, 197-199.

Atkins, T., Prior, R. G., Mack, K., Russell, P., Nelson, M., Oyston, P. C. F., Dougan, G. & Titball, R. W. (2002a). A mutant of *Burkholderia pseudomallei*, auxotrophic in the branched chain amino acid biosynthetic pathway, is attenuated and protective in a murine model of melioidosis. *Infect Immun* **70**, 5290-5294.

Atkins, T., Prior, R., Mack, K., Russell, P., Nelson, M., Prior, J., Ellis, J., Oyston, P. C. F., Dougan, G. & other authors (2002b). Characterisation of an acapsular mutant of *Burkholderia pseudomallei* identified by signature tagged mutagenesis. *J Med Microbiol* **51**, 539-553.

Atlas, R. M. (2003). Bioterrorism and biodefence research: changing the focus of microbiology. *Nat Rev Micro* **1**, 70-74.

Attree, O. & Attree, I. (2001). A second type III secretion system in *Burkholderia pseudomallei*: who is the real culprit? *Microbiology* **147**, 3197-3199.

Auerbuch, V., Lenz, L. L. & Portnoy, D. A. (2001). Development of a competitive index assay to evaluate the virulence of *Listeria monocytogenes actA* mutants during primary and secondary infection of mice. *Infect Immun* **69**, 5953-5957.

Bahrani, F. K., Sansonetti, P. J. & Parsot, C. (1997). Secretion of Ipa proteins by *Shigella flexneri*: inducer molecules and kinetics of activation. *Infect Immun* **65**, 4005-4010.

Bailie, M. B., Standiford, T. J., Laichalk, L. L., Coffey, M. J., Strieter, R. & Peters-Golden, M. (1996). Leukotriene-deficient mice manifest enhanced lethality from *Klebsiella pneumonia* in association with decreased alveolar macrophage phagocytic and bactericidal activities. *J Immunol* **157**, 5221-5224.

Bennett, J. C. Q., Thomas, J., Fraser, G. M. & Hughes, C. (2001). Substrate complexes and domain organization of the *Salmonella* flagellar export chaperones FlgN and FliT. *Mol Microbiol* **39**, 781-791.

Bernadsky, G., Beveridge, T. J. & Clarke, A. J. (1994). Analysis of the sodium dodecyl sulfate-stable peptidoglycan autolysins of select gram-negative pathogens by using renaturing polyacrylamide gel electrophoresis. *J Bacteriol* **176**, 5225-5232.

Blackburn, N. T. & Clarke, A. J. (2000). Assay for lytic transglycosylases: a family of peptidoglycan lyases. *Anal Biochem* **284**, 388-393.

Blackburn, N. T. & Clarke, A. J. (2001). Identification of four families of peptidoglycan lytic transglycosylases. *J Mol Evol* **52**, 78-84.

Blocker, A. J., Komoriya, K. & Aizawa, S.-I. (2003). Type III secretion systems and bacterial flagella: insights into their function from structural similarities. *Proc Natl Acad Sci U S A* **100**, 3027-3030.

Bobard, A., Mellouk, N. & Enninga, J. (2011). Spotting the right location - imaging approaches to resolve the intracellular localization of invasive pathogens. *Biochim Biophys Acta* **1810**, 297-307.

Breitbach, K., Klocke, S., Tschernig, T., van Rooijen, N., Baumann, U. & Steinmetz, I. (2006). Role of inducible nitric oxide synthase and NADPH oxidase in early control of *Burkholderia pseudomallei* infection in mice. *Infect Immun* **74**, 6300-6309.

Brett, P. J., Mah, D. C. & Woods, D. E. (1994). Isolation and characterization of *Pseudomonas pseudomallei* flagellin proteins. *Infect Immun* **62**, 1914-1919.

Briones, G., Hofreuter, D. & Galán, J. E. (2006). Cre reporter system to monitor the translocation of type III secreted proteins into host cells. *Infect Immun* **74**, 1084-1090.

Brown, N. F., Szeto, J., Jiang, X., Coombes, B. K., Finlay, B. B. & Brumell, J. H. (2006). Mutational analysis of *Salmonella* translocated effector members SifA and SopD2 reveals domains implicated in translocation, subcellular localization and function. *Microbiology* **152**, 2323-2343.

Brutinel, E. D. & Yahr, T. L. (2008). Control of gene expression by type III secretory activity. *Curr Opin Microbiol* **11**, 128-133.

Brutinel, E. D., Vakulskas, C. A. & Yahr, T. L. (2009). Functional domains of ExsA, the transcriptional activator of the *Pseudomonas aeruginosa* type III secretion system. *J Bacteriol* **191**, 3811-3821.

Buchrieser, C., Glaser, P., Rusniok, C., Nedjari, H., D'Hauteville, H., Kunst, F., Sansonetti, P. & Parsot, C. (2000). The virulence plasmid pWR100 and the repertoire of proteins secreted by the type III secretion apparatus of *Shigella flexneri*. *Mol Microbiol* **38**, 760-771.

Bucior, I., Pielage, J. F. & Engel, J. N. (2012). *Pseudomonas aeruginosa* pili and flagella mediate distinct binding and signalling events at the apical and basolateral surface of airway epithelium. *PLoS Pathog* **8**, e1002616.

Burtnick, M. N., Brett, P. J., Nair, V., Warawa, J. M., Woods, D. E. & Gherardini, F. C. (2008). *Burkholderia pseudomallei* type III secretion system mutants exhibit delayed vacuolar escape phenotypes in RAW264.7 murine macrophages. *Infect Immun* **76**, 2991-3000.

Büttner, D. (2012). Protein export according to schedule: architecture, assembly, and regulation of type III secretion systems from plant- and animal-pathogenic bacteria. *Microbiol Mol Biol Rev* **76**, 262-310.

Büttner, D. & He, S. Y. (2009). Type III protein secretion in plant pathogenic bacteria. *Plant Physiol* **150**, 1656-1664.

Byers, D. M. & Gong, H. (2007). Acyl carrier protein: structure-function relationships in a conserved multifunctional protein family. *Biochem Cell Biol* **85**, 649-662.

Ceballos-Olvera, I., Sahoo, M., Miller, M. A., Barrio, L. d. & Re, F. (2011). Inflammasome-dependent pyroptosis and IL-18 protect against *Burkholderia pseudomallei* lung infection while IL-1β is deleterious. *PLoS Pathog* **7**, e1002452.

Chan, D. I. & Vogel, H. J. (2010). Current understanding of fatty acid biosynthesis and the acyl carrier protein. *Biochem J* **430**, 1-19.

Chan, Y. Y. & Chua, K. L. (2005). The *Burkholderia pseudomallei* BpeAB-OprB efflux pump: expression and Impact on quorum sensing and virulence. *J Bacteriol* **187**, 4707-4719.

Chan, Y. Y., Tan, T. M. C., Ong, Y. M. & Chua, K. L. (2004). BpeAB-OprB, a multidrug efflux pump in *Burkholderia pseudomallei*. *Antimicrob Agents Chemother* **48**, 1128-1135.

Chan, Y. Y., Bian, H. S., Tan, T. M. C., Mattmann, M. E., Geske, G. D., Igarashi, J., Hatano, T., Suga, H., Blackwell, H. E. & other authors (2007). Control of quorum sensing by a *Burkholderia pseudomallei* multidrug efflux pump. *J Bacteriol* **189**, 4320-4324.

Chang, Y.-C. (1992). Efficient precipitation and accurate quantitation of detergent-solubilized membrane proteins. *Anal Biochem* **205**, 22-26.

Charpentier, X. & Oswald, E. (2004). Identification of the secretion and translocation domain of the Enteropathogenic and Enterohemorrhagic *Escherichia coli* effector Cif, using TEM-1 β-Lactamase as a new fluorescence-based reporter. *J Bacteriol* **186**, 5486-5495.

Cheng, A. C. & Currie, B. J. (2005). Melioidosis: epidemiology, pathophysiology, and management. *Clin Microbiol Rev* **18**, 383-416.

Chevallet, M., Diemer, H., Van Dorssealer, A., Villiers, C. & Rabilloud, T. (2007). Toward a better analysis of secreted proteins: the example of the myeloid cells secretome. *PROTEOMICS* **7**, 1757-1770.

Chieng, S., Carreto, L. & Nathan, S. (2012). *Burkholderia pseudomallei* transcriptional adaptation in macrophages. *BMC Genomics* **13**, 328.

Chilcott, G. S. & Hughes, K. T. (2000). Coupling of flagellar gene expression to flagellar assembly in *Salmonella enterica* serovar Typhimurium and *Escherichia coli*. *Microbiol Mol Biol Rev* **64**, 694-708.

Choi, K. H. & Kim, K. J. (2009). Applications of transposon-based gene delivery system in bacteria. *J Microbiol Biotechnol* **19**, 217-228.

Choi, K. H., DeShazer, D. & Schweizer, H. P. (2006). mini-Tn*7* insertion in bacteria with multiple *glmS*-linked *att*Tn*7* sites: example *Burkholderia mallei* ATCC 23344. *Nat Protoc* **1**, 162-169.

Choi, K. H., Gaynor, J. B., White, K. G., Lopez, C., Bosio, C. M., Karkhoff-Schweizer, R. R. & Schweizer, H. P. (2005). A Tn*7*-based broad-range bacterial cloning and expression system. *Nat Methods* **2**, 443-448.

Choi, K. H., Mima, T., Casart, Y., Rholl, D., Kumar, A., Beacham, I. R. & Schweizer, H. P. (2008). Genetic tools for select-agent-compliant manipulation of *Burkholderia pseudomallei*. *Appl Environ Microbiol* **74**, 1064-1075.

Chua, K. L., Chan, Y. Y. & Gan, Y. H. (2003). Flagella are virulence determinants of *Burkholderia pseudomallei*. *Infect Immun* **71**, 1622-1629.

Coburn, B., Sekirov, I. & Finlay, B. B. (2007). Type III secretion systems and disease. *Clin Microbiol Rev* **20**, 535-549.

Coombes, B. K. & Pilar, A. V. (2011). A fresh look at the type III secretion system: two-step model of effector translocation in pathogenic bacteria. *Front Microbiol* **2**, 113-115.

Copeland, M. F., Flickinger, S. T., Tuson, H. H. & Weibel, D. B. (2010). Studying the dynamics of flagella in multicellular communities of *Escherichia coli* by using biarsenical dyes. *Appl Environ Microbiol* **76**, 1241-1250.

Cornelis, G. R. (2006). The type III secretion injectisome. *Nat Rev Microbiol* **4**, 811-825.

Cornelis, G. R. & Van Gijsegem, F. (2000). Assembly and function of type III secretory systems. *Annu Rev Microbiol* **54**, 735-774.

Costa, S. C. P., Schmitz, A. M., Jahufar, F. F., Boyd, J. D., Cho, M. Y., Glicksman, M. A. & Lesser, C. F. (2012). A new means to identify type 3 secreted effectors: functionally interchangeable class IB chaperones recognize a conserved sequence. *mBio* **3**, e00243-00211.

Cuccui, J., Easton, A., Chu, K. K., Bancroft, G. J., Oyston, P. C. F., Titball, R. W. & Wren, B. W. (2007). Development of signature-tagged mutagenesis in *Burkholderia pseudomallei* to identify genes important in survival and pathogenesis. *Infect Immun* **75**, 1186-1195.

Cui, J., Yao, Q., Li, S., Ding, X., Lu, Q., Mao, H., Liu, L., Zheng, N., Chen, S. & Shao, F. (2010). Glutamine deamidation and dysfunction of ubiquitin/NEDD8 induced by a bacterial effector family. *Science* **329**, 1215-1218.

Cullinane, M., Gong, L., Li, X., Adler, N.-L., Tra, T., Wolvetang, E., Prescott, M., Boyce, J. D., Devenish, R. J. & other authors (2008). Stimulation of autophagy suppresses the intracellular survival of *Burkholderia pseudomallei* in mammalian cell lines. *Autophagy* **4**, 744-753.

Cullinane, M., Gong, L., Li, X., Adler, N.-L., Tra, T., Wolvetang, E., Prescott, M., Boyce, J. D., Devenish, R. J. & other authors (unpublished data). Stimulation of autophagy suppresses the intracellular survival of *Burkholderia pseudomallei* in mammalian cell lines.

Currie, B. J. (2003). Melioidosis: an important cause of pneumonia in residents of and travellers returned from endemic regions. *Eur Respir J* **22**, 542-550.

Currie, B. J., Jacups, S. P., Cheng, A. C., Fisher, D. A., Anstey, N. M., Huffam, S. E. & Krause, V. L. (2004). Melioidosis epidemiology and risk factors from a prospective whole-population study in northern Australia. *Trop Med Int Health* **9**, 1167-1174.

D'Cruze, T., Gong, L., Treerat, P., Ramm, G., Boyce, J. D., Prescott, M., Adler, B. & Devenish, R. J. (2011). Role for the *Burkholderia pseudomallei* type three secretion system cluster 1 *bpscN* gene in virulence. *Infect Immun* **79**, 3659-3664.

Darwin, K. H. & Miller, V. L. (1999). Molecular basis of the interaction of *Salmonella* with the intestinal mucosa. *Clin Microbiol Rev* **12**, 405-428.

Dasgupta, N., Lykken, G. L., Wolfgang, M. C. & Yahr, T. L. (2004). A novel anti-anti-activator mechanism regulates expression of the *Pseudomonas aeruginosa* type III secretion system. *Mol Microbiol* **53**, 297-308.

de la Mora, J., Ballado, T., González-Pedrajo, B., Camarena, L. & Dreyfus, G. (2007). The flagellar muramidase from the photosynthetic bacterium *Rhodobacter sphaeroides*. *J Bacteriol* **189**, 7998-8004.

De Lay, N. R. & Cronan, J. E. (2007). *In vivo* functional analyses of the type II acyl carrier proteins of fatty acid biosynthesis. *J Biol Chem* **282**, 20319-20328.

de Lorenzo, V., Herrero, M., Jakubzik, U. & Timmis, K. N. (1990). Mini-Tn*5* transposon derivatives for insertion mutagenesis, promoter probing, and chromosomal insertion of cloned DNA in gram-negative eubacteria. *J Bacteriol* **172**, 6568-6572.

Dean, P. (2011). Functional domains and motifs of bacterial type III effector proteins and their roles in infection. *FEMS Microbiol Rev* **35**, 1100-1125.

Deane, J. E., Abrusci, P., Johnson, S. & Lea, S. (2010). Timing is everything: the regulation of type III secretion. *Cell Mol Life Sci* **67**, 1065-1075.

Deane, J. E., Roversi, P., Cordes, F. S., Johnson, S., Kenjale, R., Daniell, S., Booy, F., Picking, W. D., Picking, W. L. & other authors (2006). Molecular model of a type III secretion system needle: Implications for host-cell sensing. *Proc Natl Acad Sci U S A* **103**, 12529-12533.

Deng, W., Li, Y., Hardwidge, P. R., Frey, E. A., Pfuetzner, R. A., Lee, S., Gruenheid, S., Strynakda, N. C. J., Puente, J. L. & other authors (2005). Regulation of type III secretion hierarchy of translocators and effectors in attaching and effacing bacterial pathogens. *Infect Immun* **73**, 2135-2146.

DeShazer, D., Brett, P. J. & Woods, D. E. (1998). The type II O-antigenic polysaccharide moiety of *Burkholderia pseudomallei* lipopolysaccharide is required for serum resistance and virulence. *Mol Microbiol* **30**, 1081-1100.

DeShazer, D., Brett, P. J., Carlyon, R. & Woods, D. E. (1997). Mutagenesis of *Burkholderia pseudomallei* with Tn*5*-OT182: isolation of motility mutants and molecular characterization of the flagellin structural gene. *J Bacteriol* **179**, 2116-2125.

DeShazer, D., Waag, D. M., Fritz, D. L. & Woods, D. E. (2001). Identification of a *Burkholderia mallei* polysaccharide gene cluster by subtractive hybridization and demonstration that the encoded capsule is an essential virulence determinant. *Microb Pathog* **30**, 253-269.

Diacovich, L., Dumont, A., Lafitte, D., Soprano, E., Guilhon, A.-A., Bignon, C., Gorvel, J.-P., Bourne, Y. & Méresse, S. (2009). Interaction between the SifA virulence factor and its host target SKIP is essential for *Salmonella* pathogenesis. *J Biol Chem* **284**, 33151-33160.

Druar, C., Yu, F., Barnes, J. L., Okinaka, R. T., Chantratita, N., Beg, S., Stratilo, C. W., Olive, A. J., Soltes, G. & other authors (2008). Evaluating *Burkholderia pseudomallei* Bip proteins as vaccines and Bip antibodies as detection agents. *FEMS Immunol Med Microbiol* **52**, 78-87.

Dunstan, R. A., Heinz, E., Wijeyewickrema, L. C., Pike, R. N., Purcell, A. W., Evans, T. J., Praszkier, J., Robins-Browne, R. M., Strugnell, R. A. & other authors (2013). Assembly of the type II secretion system such as found in *Vibrio cholerae* depends on the novel pilotin AspS. *PLoS Pathog* **9**, e1003117.

Ehrbar, K., Friebel, A., Miller, S. I. & Hardt, W.-D. (2003). Role of the *Salmonella* Pathogenicity Island 1 (SPI-1) protein InvB in type III secretion of SopE and SopE2, two *Salmonella* effector proteins encoded outside of SPI-1. *J Bacteriol* **185**, 6950-6967.

Ellis, T. N. & Beaman, B. L. (2004). Interferon-gamma activation of polymorphonuclear neutrophil function. *Immunology* **112**, 2-12.

Enninga, J. & Rosenshine, I. (2009). Imaging the assembly, structure and activity of type III secretion systems. *Cell Microbiol* **11**, 1462-1470.

Enninga, J., Mounier, J., Sansonetti, P. & Nhieu, G. T. V. (2005). Secretion of type III effectors into host cells in real time. *Nat Meth* **2**, 959-965.

Eriksson, S., Lucchini, S., Thompson, A., Rhen, M. & Hinton, J. C. D. (2003). Unravelling the biology of macrophage infection by gene expression profiling of intracellular *Salmonella enterica*. *Mol Microbiol* **47**, 103-118.

Ernst, R. K., Guina, T. & Miller, S. I. (1999). How intracellular bacteria survive: surface modifications that promote resistance to host innate immune responses. *J Infect Dis* **179**, S326-S330.

Estes, D. M., Dow, S. W., Schweizer, H. P. & Torres, A. G. (2010). Present and future therapeutic strategies for melioidosis and glanders. *Expert Rev Anti Infect Ther* **8**, 325-338.

Felgner, P. L., Kayala, M. A., Vigil, A., Burk, C., Nakajima-Sasaki, R., Pablo, J., Molina, D. M., Hirst, S., Chew, J. S. W. & other authors (2009). A *Burkholderia pseudomallei* protein microarray reveals serodiagnostic and cross-reactive antigens. *Proc Natl Acad Sci U S A* **106**, 13499-13504.

Fennelly, N. K., Sisti, F., Higgins, S. C., Ross, P. J., van der Heide, H., Mooi, F. R., Boyd, A. & Mills, K. H. G. (2008). *Bordetella pertussis* expresses a functional type III secretion system that subverts protective innate and adaptive immune responses. *Infect Immun* **76**, 1257-1266.

Figueira, R. & Holden, D. W. (2012). Functions of the *Salmonella* pathogenicity island 2 (SPI-2) type III secretion system effectors. *Microbiology* **158**, 1147-1161.

Firdausi Qadri, Shaikh Abu Hossain, Ivan Ciznar, Khaleda Haider, Âsa Ljungh, Torkel Wadstrom & Sack, D. A. (1988). Congo red binding and salt aggregation as indicators of virulence in *Shigella* species. *J Clin Microbiol* **26**, 1343-1348.

Flaman, A. S., Chen, J. M., Van Iderstine, S. C. & Byers, D. M. (2001). Site-directed mutagenesis of acyl carrier protein (ACP) reveals amino acid residues involved in ACP structure and acyl-ACP synthetase activity. *J Biol Chem* **276**, 35934-35939.

Forbes, M. L., Horsey, E., Hiller, N. L., Buchinsky, F. J., Hayes, J. D., Compliment, J. M., Hillman, T., Ezzo, S., Shen, K. & other authors (2008). Strain-specific virulence phenotypes

of *Streptococcus pneumoniae* assessed using the *Chinchilla laniger* model of otitis media. *PLoS ONE* **3**, e1969.

Francis, M. S., Lloyd, S. A. & Wolf-Watz, H. (2001). The type III secretion chaperone LcrH co-operates with YopD to establish a negative, regulatory loop for control of Yop synthesis in *Yersinia pseudotuberculosis*. *Mol Microbiol* **42**, 1075-1093.

Francis, M. S., Wolf-Watz, H. & Forsberg, Å. (2002). Regulation of type III secretion systems. *Curr Opin Microbiol* **5**, 166-172.

Fraser, G. M., González-Pedrajo, B., Tame, J. R. H. & Macnab, R. M. (2003). Interactions of FliJ with the *Salmonella* type III flagellar export apparatus. *J Bacteriol* **185**, 5546-5554.

Freeman, D. J., Falkiner, F. R. & Keane, C. T. (1989). New method for detecting slime production by coagulase negative staphylococci. *J Clin Pathol* **42**, 872-874.

French, C. T., Toesca, I. J., Wu, T.-H., Teslaa, T., Beaty, S. M., Wong, W., Liu, M., Schröder, I., Chiou, P.-Y. & other authors (2011). Dissection of the *Burkholderia* intracellular life cycle using a photothermal nanoblade. *Proc Natl Acad Sci U S A* **108**, 12095-12100.

Frey, U. H., Bachmann, H. S., Peters, J. & Siffert, W. (2008). PCR-amplification of GC-rich regions: 'slowdown PCR'. *Nat Protoc* **3**, 1312-1317.

Fujii, T., Cheung, M., Blanco, A., Kato, T., Blocker, A. J. & Namba, K. (2012). Structure of a type III secretion needle at 7-Å resolution provides insights into its assembly and signaling mechanisms. *Proc Natl Acad Sci U S A* **109**, 4461-4466.

Gaillard, M. E., Bottero, D., Castuma, C. E., Basile, L. A. & Hozbor, D. (2011). Laboratory adaptation of *Bordetella pertussis* is associated with the loss of type three secretion system functionality. *Infect Immun* **79**, 3677-3682.

Galan, J. E. & Collmer, A. (1999). Type III secretion machines: bacterial devices for protein delivery into host cells. *Science* **284**, 1322-1328.

Galan, J. E. & Wolf-Watz, H. (2006). Protein delivery into eukaryotic cells by type III secretion machines. *Nature* **444**, 567-573.

Galyov, E. E., Brett, P. J. & DeShazer, D. (2010). Molecular insights into *Burkholderia pseudomallei* and *Burkholderia mallei* pathogenesis. *Annu Rev Microbiol* **64**, 495-517.

Gan, Y. H. (2005). Interaction between *Burkholderia pseudomallei* and the host immune response: sleeping with the enemy? *J Infect Dis* **192**, 1845-1850.

Geddes, K., Cruz, F., III & Heffron, F. (2007). Analysis of cells targeted by *Salmonella* type III secretion *in vivo*. *PLoS Pathog* **3**, e196.

Getz, E. B., Xiao, M., Chakrabarty, T., Cooke, R. & Selvin, P. R. (1999). A comparison between the sulfhydryl reductants tris(2-carboxyethyl)phosphine and dithiothreitol for use in protein biochemistry. *Anal Biochem* **273**, 73-80.

Ghosh, P. (2004). Process of protein transport by the type III secretion system. *Microbiol Mol Biol Rev* **68**, 771-795.

Giepmans, B. N. G., Adams, S. R., Ellisman, M. H. & Tsien, R. Y. (2006). The fluorescent toolbox for assessing protein location and function. *Science* **312**, 217-224.

Gieseler, S., König, B., König, W. & Backert, S. (2005). Strain-specific expression profiles of virulence genes in *Helicobacter pylori* during infection of gastric epithelial cells and granulocytes. *Microb Infect* **7**, 437-447.

Glover, D. M. (1985). *DNA cloning: a practical approach*. Oxford, IRL Press.

Godfrey, A. J., Wong, S., Dance, D. A., Chaowagul, W. & Bryan, L. E. (1991). *Pseudomonas pseudomallei* resistance to beta-lactam antibiotics due to alterations in the chromosomally encoded beta-lactamase. *Antimicrob Agents Chemother* **35**, 1635-1640.

Gong, L., Cullinane, M., Treerat, P., Ramm, G., Prescott, M., Adler, B., Boyce, J. D. & Devenish, R. J. (2011). The *Burkholderia pseudomallei* type III secretion system and BopA are required for evasion of LC3-associated phagocytosis. *PLoS ONE* **6**, e17852.

Gong, L., Cullinane, M., Lai, S.-C., Treerat, P., Prescott, M., Adler, B., Boyce, J. D. & Devenish, R. J. (manuscript in preparation). *Burkholderia pseudomallei* type III secretion system cluster 3 ATPase BsaS: a chemotherapeutic target for small molecule ATPase inhibitors.

Gophna, U., Ron, E. Z. & Graur, D. (2003). Bacterial type III secretion systems are ancient and evolved by multiple horizontal-transfer events. *Gene* **312**, 151-163.

Gordon, M. A., Jack, D. L., Dockrell, D. H., Lee, M. E. & Read, R. C. (2005). Gamma interferon enhances internalization and early nonoxidative killing of *Salmonella enterica* serovar Typhimurium by human macrophages and modifies cytokine responses. *Infect Immun* **73**, 3445-3452.

Grant, S. G., Jessee, J., Bloom, F. R. & Hanahan, D. (1990). Differential plasmid rescue from transgenic mouse DNAs into *Escherichia coli* methylation-restriction mutants. *Proc Natl Acad Sci U S A* **87**, 4645-4649.

Griffin, B. A., Adams, S. R. & Tsien, R. Y. (1998). Specific covalent labeling of recombinant protein molecules inside live cells. *Science* **281**, 269-272.

Haglund, C. M. & Welch, M. D. (2011). Pathogens and polymers: microbe–host interactions illuminate the cytoskeleton. *J Cell Biol* **195**, 7-17.

Haque, A., Chu, K., Easton, A., Stevens, M. P., Galyov, E. E., Atkins, T., Titball, R. & Bancroft, G. J. (2006). A live experimental vaccine against *Burkholderia pseudomallei* elicits CD4+ T cell-mediated immunity, priming T cells specific for 2 type III secretion system proteins. *J Infect Dis* **194**, 1241-1248.

Ham, H., Sreelatha, A. & Orth, K. (2011). Manipulation of host membranes by bacterial effectors. *Nat Rev Micro* **9**, 635-646.

Hamad, M. A., Austin, C. R., Stewart, A. L., Higgins, M., Vázquez-Torres, A. & Voskuil, M. I. (2011). Adaptation and antibiotic tolerance of anaerobic *Burkholderia pseudomallei*. *Antimicrob Agents Chemother* **55**, 3313-3323.

Harper, M., Boyce, J. D., Wilkie, I. W. & Adler, B. (2004). Signature-tagged mutagenesis of *Pasteurella multocida* identifies mutants displaying differential virulence characteristics in mice and chickens. *Infect Immun* **71**, 5440-5446.

Harper, M., Cox, A. D., St. Michael, F., Wilkie, I. W., Boyce, J. D. & Adler, B. (2004). A heptosyltransferase mutant of *Pasteurella multocida* produces a truncated lipopolysaccharide structure and is attenuated in virulence. *Infect Immun* **72**, 3436-3443.

Harrington, A. T., Hearn, P. D., Picking, W. L., Barker, J. R., Wessel, A. & Picking, W. D. (2003). Structural characterization of the N terminus of IpaC from *Shigella flexneri*. *Infect Immun* **71**, 1255-1264.

Hayashi, F., Smith, K. D., Ozinsky, A., Hawn, T. R., Yi, E. C., Goodlett, D. R., Eng, J. K., Akira, S., Underhill, D. M. & other authors (2001). The innate immune response to bacterial flagellin is mediated by Toll-like receptor 5. *Nature* **410**, 1099-1103.

Hayden, H. S., Lim, R., Brittnacher, M. J., Sims, E. H., Ramage, E. R., Fong, C., Wu, Z., Crist, E., Chang, J. & other authors (2012). Evolution of *Burkholderia pseudomallei* in recurrent melioidosis. *PLoS ONE* **7**, e36507.

Hayes, C. S., Aoki, S. K. & Low, D. A. (2010). Bacterial contact-dependent delivery systems. *Annu Rev Genet* **44**, 71-90.

He, S. Y., Nomuraa, K. & Whittamc, T. S. (2004). Type III protein secretion mechanism in mammalian and plant pathogens. *Biochim Biophys Acta* **1694**, 181–206.

Hearps, A., Pryor, M., Kuusisto, H., Rawlinson, S., Piller, S. & Jans, D. (2007). The biarsenical dye Lumio™ exhibits a reduced ability to specifically detect tetracysteine-containing proteins within live cells. *J Fluorescence* **17**, 593-597.

Henke, W., Herdel, K., Jung, K., Schnorr, D. & Loening, S. A. (1997). Betaine improves the PCR amplification of GC-rich DNA sequences. *Nucl Acids Res* **25**, 3957-3958.

Herbst, S., Schaible, U. E. & Schneider, B. E. (2011). Interferon gamma activated macrophages kill *Mycobacteria* by nitric oxide induced apoptosis. *PLoS ONE* **6**, e19105.

Higginbotham, J. N., Lin, T. L. & Pruett, S. B. (1992). Effect of macrophage activation on killing of *Listeria monocytogenes*. Roles of reactive oxygen or nitrogen intermediates, rate of phagocytosis, and retention of bacteria in endosomes. *Clin Exp Immunol* **88**, 492–498.

Hii, C.-S., Sun, G. W., Goh, J. W. K., Lu, J., Stevens, M. P. & Gan, Y.-H. (2008). Interleukin-8 induction by *Burkholderia pseudomallei* can occur without Toll-like receptor signaling but requires a functional type III secretion system. *J Infect Dis* **197**, 1537-1547.

Hirano, T., Minamino, T. & Macnab, R. M. (2001). The role in flagellar rod assembly of the N-terminal domain of *Salmonella* FlgJ, a flagellum-specific muramidase. *J Mol Biol* **312**, 359-369.

Ho Lee, S. & Galan, J. E. (2003). InvB is a type III secretion-associated chaperone for the *Salmonella enterica* effector protein SopE. *J Bacteriol* **185**, 7279-7284.

Hoffmann, C., Gaietta, G., Zurn, A., Adams, S. R., Terrillon, S., Ellisman, M. H., Tsien, R. Y. & Lohse, M. J. (2010). Fluorescent labeling of tetracysteine-tagged proteins in intact cells. *Nat Protoc* **5**, 1666-1677.

Holden, M. T., Titball, R. W., Peacock, S. J., Cerdeno-Tarraga, A. M., Atkins, T., Crossman, L. C., Pitt, T., Churcher, C., Mungall, K. & other authors (2004). Genomic plasticity of the causative agent of melioidosis, *Burkholderia pseudomallei*. *Proc Natl Acad Sci U S A* **101**, 14240-14245.

Homma, M., Kutsukake, K., Hasebe, M., Iino, T. & Macnab, R. M. (1990). FlgB, FlgC, FlgF and FlgG. A family of structurally related proteins in the flagellar basal body of *Salmonella typhimurium*. *J Mol Biol* **211**, 465-477.

Hybiske, K. & Stephens, R. S. (2008). Exit strategies of intracellular pathogens. *Nat Rev Micro* **6**, 99-110.

Ibarra, J. A. & Steele-Mortimer, O. (2009). *Salmonella*--the ultimate insider. *Salmonella* virulence factors that modulate intracellular survival. *Cell Microbiol* **11**, 1579-1586.

Imada, K., Minamino, T., Kinoshita, M., Furukawa, Y. & Namba, K. (2010). Structural insight into the regulatory mechanisms of interactions of the flagellar type III chaperone FliT with its binding partners. *Proc Natl Acad Sci USA* **107**, 8812-8817.

Ishidate, K., Creeger, E. S., Zrike, J., Deb, S., Glauner, B., MacAlister, T. J. & Rothfield, L. I. (1986). Isolation of differentiated membrane domains from *Escherichia coli* and *Salmonella typhimurium*, including a fraction containing attachment sites between the inner and outer membranes and the murein skeleton of the cell envelope. *J Biol Chem* **261**, 428-443.

Jarvik, J. W. & Telmer, C. A. (1998). Epitope tagging. *Annu Rev Genet* **32**, 601-618.

Jensen, M. A., Fukushima, M. & Davis, R. W. (2010). DMSO and betaine greatly improve amplification of GC-rich constructs in *De Novo* synthesis. *PLoS ONE* **5**, e11024.

Johnson, S., Roversi, P., Espina, M., Olive, A., Deane, J. E., Birket, S., Field, T., Picking, W. D., Blocker, A. J. & other authors (2007). Self-chaperoning of the type III secretion system needle tip proteins IpaD and BipD. *J Biol Chem* **282**, 4035-4044.

Jones, A. L., Beveridge, T. J. & Woods, D. E. (1996). Intracellular survival of *Burkholderia pseudomallei*. *Infect Immun* **64**, 782-790.

Joo, H.-S. & Otto, M. (2012). Molecular basis of *in vivo* biofilm formation by bacterial pathogens. *Chem Biol* **19**, 1503-1513.

Journet, L., Agrain, C., Broz, P. & Cornelis, G. R. (2003). The needle length of bacterial injectisomes is determined by a molecular ruler. *Science* **302**, 1757-1760.

Justice, S. S., Hunstad, D. A., Cegelski, L. & Hultgren, S. J. (2008). Morphological plasticity as a bacterial survival strategy. *Nat Rev Micro* **6**, 162-168.

Kane, C. D., Schuch, R., Day, W. A. & Maurelli, A. T. (2002). MxiE regulates intracellular expression of factors secreted by the *Shigella flexneri* 2a type III secretion system. *J Bacteriol* **184**, 4409-4419.

Kawahara, K., Dejsirilert, S., Danbara, H. & Ezaki, T. (1992). Extraction and characterization of lipopolysaccharide from *Pseudomonas pseudomallei*. *FEMS Microbiol Lett* **96**, 129-133.

Kespichayawattana, W., Rattanachetkul, S., Wanun, T., Utaisincharoen, P. & Sirisinha, S. (2000). *Burkholderai pseudomallei* induces cell fusion and actin-associated membrane protrusion: a possible mechanism for cell-to-cell spreading. *Infect Immun* **68**, 5377-5384.

Kim, B. H., Kim, H. G., Kim, J. S., Jang, J. I. & Park, Y. K. (2007). Analysis of functional domains present in the N-terminus of the SipB protein. *Microbiology* **153**, 2998-3008.

Kim, J., Ahn, K., Min, S., Jia, J., Ha, U., Wu, D. & Jin, S. (2005). Factors triggering type III secretion in *Pseudomonas aeruginosa*. *Microbiology* **151**, 3575-3587.

Kim, J. S., Eom, J. S., Jang, J. I., Kim, H. G., Seo, D. W., Bang, I.-S., Bang, S. H., Lee, I. S. & Park, Y. K. (2011). Role of *Salmonella* pathogenicity island 1 protein IacP in *Salmonella enterica* serovar Typhimurium pathogenesis. *Infect Immun* **79**, 1440-1450.

Klug-Micu, G. M., Stenger, S., Sommer, A., Liu, P. T., Krutzik, S. R., Modlin, R. L. & Fabri, M. (2013). CD40L and IFN-γ induce an antimicrobial response against *M. tuberculosis* in human monocytes. *Immunology* **139**, 121-128.

Kohler, P. L., Hamilton, H. L., Cloud-Hansen, K. & Dillard, J. P. (2007). AtlA functions as a peptidoglycan lytic transglycosylase in the *Neisseria gonorrhoeae* type IV secretion system. *J Bacteriol* **189**, 5421-5428.

Koraimann, G. (2003). Lytic transglycosylases in macromolecular transport systems of Gram-negative bacteria. *Cell Mol Life Sci* **60**, 2371-2388.

Kuma, A., Matsui, M. & Mizushima, N. (2007). LC3, an autophagosome marker, can be incorporated into protein aggregates independent of autophagy: caution in the interpretation of LC3 localization. *Autophagy* **3**, 323-328.

Kutsukake, K. (1997). Hook-length control of the export-switching machinery involves a double-locked gate in *Salmonella typhimurium* flagellar morphogenesis. *J Bacteriol* **179**, 1268-1273.

Kutsukake, K., Ohya, Y. & Iino, T. (1990). Transcriptional analysis of the flagellar regulon of *Salmonella typhimurium*. *J Bacteriol* **172**, 741-747.

Laible, N. J. & Germaine, G. R. (1985). Bactericidal activity of human lysozyme, muramidase-inactive lysozyme, and cationic polypeptides against *Streptococcus sanguis* and *Streptococcus faecalis*: inhibition by chitin oligosaccharides. *Infect Immun* **48**, 720-728.

Langermans, J. A., van der Hulst, M. E., Nibbering, P. H. & van Furth, R. (1990). Activation of mouse peritoneal macrophages during infection with *Salmonella typhimurium* does not result in enhanced intracellular killing. *J Immunol* **144**, 4340-4346.

Langermans, J. A., Nibbering, P. H., van der Hulst, M. E. & van Furth, R. (1991). Microbicidal activities of *Salmonella typhimurium*- and interferon-gamma-activated mouse peritoneal macrophages. *Pathobiology* **59**, 189-193.

Langhorst, M. F., Genisyuerek, S. & Stuermer, C. A. O. (2006). Accumulation of FlAsH/Lumio green in active mitochondria can be reversed by β-mercaptoethanol for specific staining of tetracysteine-tagged proteins. *Histochem Cell Biol* **125**, 743-747.

Lara-Tejero, M., Kato, J., Wagner, S., Liu, X. & Galán, J. E. (2011). A sorting platform determines the order of protein secretion in bacterial type III systems. *Science* **331**, 1188-1191.

Leakey, A. K., Ulett, G. C. & Hirst, R. G. (1998). BALB/c and C57BL/6 mice infected with virulent *Burkholderia pseudomallei* provide contrasting animal models for the acute and chronic forms of human melioidosis. *Microb Pathog* **24**, 269-275.

Lever, M. S., Nelson, M., Stagg, A. J., Beedham, R. J. & Simpson, A. J. (2009). Experimental acute respiratory *Burkholderia pseudomallei* infection in BALB/c mice. *Int J Exp Pathol* **90**, 16-25.

Lincoln, J. A., Lefkowitz, D. L., Cain, T., Castro, A., Mills, K. C., Lefkowitz, S. S., Moguilevsky, N. & Bollen, A. (1995). Exogenous myeloperoxidase enhances bacterial phagocytosis and intracellular killing by macrophages. *Infect Immun* **63**, 3042-3047.

Lipscomb, L. & Schell, M. A. (2011). Elucidation of the regulon and *cis*-acting regulatory element of HrpB, the AraC-type regulator of a plant pathogen-like type III secretion system in *Burkholderia pseudomallei*. *J Bacteriol* **193**, 1991-2001.

Liu, B., Koo, G. C., Yap, E. H., Chua, K. L. & Gan, Y.-H. (2002). Model of differential susceptibility to mucosal *Burkholderia pseudomallei* infection. *Infect Immun* **70**, 504-511.

Lo, M., Bulach, D. M., Powell, D. R., Haake, D. A., Matsunaga, J., Paustian, M. L., Zuerner, R. L. & Adler, B. (2006). Effects of temperature on gene expression patterns in *Leptospira interrogans* serovar Lai as assessed by whole-genome microarrays. *Infect Immun* **74**, 5848-5859.

Logan, S. M. (2006). Flagellar glycosylation – a new component of the motility repertoire? *Microbiology* **152**, 1249-1262.

Logue, C.-A., Peak, I. R. A. & Beacham, I. R. (2009). Facile construction of unmarked deletion mutants in *Burkholderia pseudomallei* using *sacB* counter-selection in sucrose-resistant and sucrose-sensitive isolates. *J Microbiol Methods* **76**, 320-323.

Löwer, M. & Schneider, G. (2009). Prediction of type III secretion signals in genomes of Gram-negative bacteria. *PLoS ONE* **4**, e5917.

Machleidt, T., Robers, M. & Hanson, G. T. (2006). Protein labeling with FlAsH and ReAsH. *Methods Mol Biol* **356**, 209-220.

MacMicking, J., Xie, Q.-W. & Nathan, C. (1997). Nitric oxide and macrophage function. *Annu Rev Immunol* **15**, 323-350.

Madani, F., Lind, J., Damberg, P., Adams, S. R., Tsien, R. Y. & Graslund, A. O. (2009). Hairpin structure of a biarsenical−tetracysteine motif determined by NMR spectroscopy. *J Am Chem Soc* **131**, 4613-4615.

Markham, A. P., Birket, S. E., Picking, W. D., Picking, W. L. & Middaugh, C. R. (2008). pH sensitivity of type III secretion system tip proteins. *Proteins* **71**, 1830-1842.

Marlovits, T. C., Kubori, T., Sukhan, A., Thomas, D. R., Galan, J. E. & Unger, V. M. (2004). Structural insights into the assembly of the type III secretion needle complex. *Science* **306**, 1040-1042.

Matteï, P.-J., Faudry, E., Job, V., Izoré, T., Attree, I. & Dessen, A. (2011). Membrane targeting and pore formation by the type III secretion system translocon. *FEBS Journal* **278**, 414-426.

McCann, J. R., McDonough, J. A., Pavelka, M. S. & Braunstein, M. (2007). β-Lactamase can function as a reporter of bacterial protein export during *Mycobacterium tuberculosis* infection of host cells. *Microbiology* **153**, 3350-3359.

McCarter, L. L. (2006). Regulation of flagella. *Curr Opin Microbiol* **9**, 180-186.

McDermott, J. E., Corrigan, A., Peterson, E., Oehmen, C., Niemann, G., Cambronne, E. D. Sharp, D., Adkins, J. N., Samudrala, R. & Heffron, F. (2011). Computational prediction of type III and IV secreted effectors in Gram-negative bacteria. *Infect Immun* **79**, 23-32.

Meumann, E. M., Cheng, A. C., Ward, L. & Currie, B. J. (2012). Clinical features and epidemiology of melioidosis pneumonia: results from a 21-year study and review of the literature. *Clin Infect Dis* **54**, 362-369.

Miao, E. A. & Warren, S. E. (2010). Innate immune detection of bacterial virulence factors via the NLRC4 inflammasome. *J Clin Immunol* **30**, 502-506.

Mills, E., Baruch, K., Charpentier, X., Kobi, S. & Rosenshine, I. (2008). Real-Time analysis of effector translocation by the type III secretion system of Enteropathogenic *Escherichia coli*. *Cell Host Microbe* **3**, 104-113.

Milton, D. L., O'Toole, R., Horstedt, P. & Wolf-Watz, H. (1996). Flagellin A is essential for the virulence of *Vibrio anguillarum*. *J Bacteriol* **178**, 1310-1319.

Minamino, T., Yamaguchi, S. & Macnab, R. M. (2000). Interaction between FliE and FlgB, a proximal rod component of the flagellar basal body of *Salmonella*. *J Bacteriol* **182**, 3029–3036.

Miras, I., Hermant, D., Arricau, N. & Popoff, M. Y. (1995). Nucleotide sequence of *iagA* and *iagB* genes involved in invasion of HeLa cells by *Salmonella enterica* subsp. *enterica* ser. *Typhi*. *Res Microbiol* **146**, 17-20.

Moore, R., Tuanyok, A. & Woods, D. (2008). Survival of *Burkholderia pseudomallei* in water. *BMC Res Notes* **1**, 11-16.

Moore, R. A., DeShazer, D., Reckseidler, S., Weissman, A. & Woods, D. E. (1999). Efflux-mediated aminoglycoside and macrolide resistance in *Burkholderia pseudomallei*. *Antimicrob Agents Chemother* **43**, 465-470.

Moore, R. A., Reckseidler-Zenteno, S., Kim, H., Nierman, W., Yu, Y., Tuanyok, A., Warawa, J., DeShazer, D. & Woods, D. E. (2004). Contribution of gene loss to the pathogenic evolution of *Burkholderia pseudomallei* and *Burkholderia mallei*. *Infect Immun* **72**, 4172-4187.

Mota, L. J. & Cornelis, G. R. (2005). The bacterial injection kit: type III secretion systems. *Ann Med* **37**, 234-249.

Muangman, S., Korbsrisate, S., Muangsombut, V., Srinon, V., Adler, N.-L., Schroeder, G. N., Frankel, G. & Galyov, E. E. (2011). BopC is a type III secreted effector protein of *Burkholderia pseudomallei*. *FEMS Microbiol Lett* **323**, 75-82.

Muangsombut, V., Suparak, S., Pumirat, P., Damnin, S., Vattanaviboon, P., Thongboonkerd, V. & Korbsrisate, S. (2008). Inactivation of *Burkholderia pseudomallei bsaQ* results in decreased invasion efficiency and delayed escape of bacteria from endocytic vesicles. *Arch Microbiol* **190**, 623-631.

Mueller, C. A., Broz, P. & Cornelis, G. R. (2008). The type III secretion system tip complex and translocon. *Mol Microbiol* **68**, 1085-1095.

Myeni, S. K. & Zhou, D. (2010). The C terminus of SipC binds and bundles F-actin to promote *Salmonella* invasion. *J Biol Chem* **285**, 13357-13363.

Nambu, T., Minamino, T., Macnab, R. M. & Kutsukake, K. (1999). Peptidoglycan-hydrolyzing activity of the FlgJ protein, essential for flagellar rod formation in *Salmonella typhimurium*. *J Bacteriol* **181**, 1555-1561.

Ngauy, V., Lemeshev, Y., Sadkowski, L. & Crawford, G. (2005). Cutaneous melioidosis in a man who was taken as a prisoner of war by the Japanese during World War II. *J Clin Microbiol* **43**, 970-972.

Niebuhr, K., Jouihri, N., Allaoui, A., Gounon, P., Sansonetti, P. J. & Parsot, C. (2000). IpgD, a protein secreted by the type III secretion machinery of *Shigella flexneri*, is chaperoned by IpgE and implicated in entry focus formation. *Mol Microbiol* **38**, 8-19.

Nikaido, H. (1998). Antibiotic resistance caused by Gram-negative multidrug efflux pumps. *Clin Infect Dis* **27**, S32-S41.

Noël, L., Thieme, F., Nennstiel, D. & Bonas, U. (2002). Two novel type III-secreted proteins of *Xanthomonas campestris* pv. vesicatoria are encoded within the *hrp* pathogenicity island. *J Bacteriol* **184**, 1340-1348.

Novem, V., Shui, G., Wang, D., Bendt, A. K., Sim, S. H., Liu, Y., Thong, T. W., Sivalingam, S. P., Ooi, E. E. & other authors (2009). Structural and biological diversity of lipopolysaccharides from *Burkholderia pseudomallei* and *Burkholderia thailandensis*. *Clin Vaccine Immunol* **16**, 1420-1428.

O'Callaghan, J., Reen, F. J., Adams, C. & O'Gara, F. (2011). Low oxygen induces the type III secretion system in *Pseudomonas aeruginosa* via modulation of the small RNAs *rsmZ* and *rsmY*. *Microbiology* **157**, 3417-3428.

Ogawa, M., Suzuki, T., Tatsuno, I., Abe, H. & Sasakawa, C. (2003). IcsB, secreted via the type III secretion system, is chaperoned by IpgA and required at the post-invasion stage of *Shigella* pathogenicity. *Mol Microbiol* **48**, 913-931.

Pallen, M. J. & Gophna, U. (2007). Bacterial flagella and Type III secretion: case studies in the evolution of complexity. *Genome Dyn* **3**, 30-47.

Pallen, M. J., Beatson, S. A. & Bailey, C. M. (2005). Bioinformatics, genomics and evolution of non-flagellar type-III secretion systems: a Darwinian perpective. *FEMS Microbiol Rev* **29**, 201-229.

Paludan, S. R. (2000). Synergistic action of pro-inflammatory agents: cellular and molecular aspects. *J Leukoc Biol* **67**, 18-25.

Parsot, C., Hamiaux, C. & Page, A.-L. (2003). The various and varying roles of specific chaperones in type III secretion systems. *Curr Opin Microbiol* **6**, 7-14.

Peacock, S. J. (2006). Melioidosis. *Curr Opin Infect Dis* **19**, 421-428.

Peacock, S. J., Limmathurotsakul, D., Lubell, Y., Koh, G. C. K. W., White, L. J., Day, N. P. J. & Titball, R. W. (2012). Melioidosis vaccines: a systematic review and appraisal of the potential to exploit biodefense vaccines for public health purposes. *PLoS Negl Trop Dis* **6**, e1488.

Pelegrin, P., Barroso-Gutierrez, C. & Surprenant, A. (2008). P2X7 receptor differentially couples to distinct release pathways for IL-1β in mouse macrophage. *J Immunol* **180**, 7147-7157.

Pilatz, S., Breitbach, K., Hein, N., Fehlhaber, B., Schulze, J., Brenneke, B., Eberl, L. & Steinmetz, I. (2006). Identification of *Burkholderia pseudomallei* genes required for the intracellular life cycle and *in vivo* virulence. *Infect Immun* **74**, 3576-3586.

Plano, G. V., Day, J. B. & Ferracci, F. (2001). Type III export: new uses for an old pathway. *Mol Microbiol* **40**, 284-293.

Poole, K. (2001). Multidrug resistance in Gram-negative bacteria. *Curr Opin Microbiol* **4**, 500-508.

Pudla, M., Limposuwan, K. & Utaisincharoen, P. (2011). *Burkholderia pseudomallei*-induced expression of a negative regulator, sterile-α and armadillo motif-containing protein, in mouse macrophages: a possible mechanism for suppression of the MyD88-independent pathway. *Infect Immun* **79**, 2921-2927.

Pumirat, P., Cuccui, J., Stabler, R. A., Stevens, J. M., Muangsombut, V., Singsuksawat, E., Stevens, M. P., Wren, B. W. & Korbsrisate, S. (2010). Global transcriptional profiling of *Burkholderia pseudomallei* under salt stress reveals differential effects on the Bsa type III secretion system. *BMC Microbiol* **10**, 171-181.

Pumpuang, A., Chantratita, N., Wikraiphat, C., Saiprom, N., Day, N. P. J., Peacock, S. J. & Wuthiekanunb, V. (2011). Survival of *Burkholderia pseudomallei* in distilled water for 16 years. *Trans R Soc Trop Med Hyg* **105**, 598–600.

Qadri, F., Hossain, S. A., Ciznar, I., Haider, K., Ljungh, Â., Wadstrom, T. & Sack, D. A. (1988). Congo red binding and salt aggregation as indicators of virulence in *Shigella* species. *J Clin Microbiol* **26**, 1343-1348.

Rainbow, L., Hart, C. A. & Winstanley, C. (2002). Distribution of type III secretion gene clusters in *Burkholderia pseudomallei*, *B. thailandensis* and *B. mallei*. *J Med Microbiol* **51**, 374-384.

Ramli, N. S. K., Eng Guan, C., Nathan, S. & Vadivelu, J. (2012). The effect of environmental conditions on biofilm formation of *Burkholderia pseudomallei* clinical isolates. *PLoS ONE* **7**, e44104.

Ramos, H. C., Rumbo, M. & Sirard, J.-C. (2004). Bacterial flagellins: mediators of pathogenicity and host immune responses in mucosa. *Trends Microbiol* **12**, 509-517.

Rappl, C., Deiwick, J. & Hensel, M. (2003). Acidic pH is required for the functional assembly of the type III secretion system encoded by *Salmonella* pathogenicity island 2. *FEMS Microbiol Lett* **226**, 363-372.

Ray, K., Marteyn, B., Sansonetti, P. J. & Tang, C. M. (2009). Life on the inside: the intracellular lifestyle of cytosolic bacteria. *Nat Rev Micro* **7**, 333-340.

Reckseidler-Zenteno, S. L., DeVinney, R. & Woods, D. E. (2006). The capsular polysaccharide of *Burkholderia pseudomallei* contributes to survival in serum by reducing complement factor C3b deposition. *Infect Immun* **73**, 1106-1115.

Rietsch, A. & Mekalanos, J. J. (2006). Metabolic regulation of type III secretion gene expression in *Pseudomonas aeruginosa*. *Mol Microbiol* **59**, 807-820.

Ritz, M., Garenaux, A., Berge, M. & Federighi, M. (2009). Determination of *rpoA* as the most suitable internal control to study stress response in *C. jejuni* by RT-qPCR and application to oxidative stress. *J Microbiol Methods* **76**, 196-200.

Rodrigues, C. D. & Enninga, J. (2010). The 'when and whereabouts' of injected pathogen effectors. *Nat Meth* **7**, 267-269.

Saier, M. H., Jr. (2004). Evolution of bacterial type III protein secretion systems. *Trends Microbiol* **12**, 113-115.

Sanceau, J., Wijdenes, J., Revel, M. & Wietzerbin, J. (1991). IL-6 and IL-6 receptor modulation by IFN-gamma and tumor necrosis factor-alpha in human monocytic cell line (THP-1). Priming effect of IFN-gamma. *J Immunol* **147**, 2630-2637.

Sarkar-Tyson, M., Thwaite, J. E., Harding, S. V., Smither, S. J., Oyston, P. C. F., Atkins, T. P. & Titball, R. W. (2007). Polysaccharides and virulence of *Burkholderia pseudomallei*. *J Med Microbiol* **56**, 1005-1010.

Sarovich, D. S., Price, E. P., Von Schulze, A. T., Cook, J. M., Mayo, M., Watson, L. M., Richardson, L., Seymour, M. L., Tuanyok, A. & other authors (2012). Characterization of ceftazidime resistance mechanisms in clinical Isolates of *Burkholderia pseudomallei* from Australia. *PLoS ONE* **7**, e30789.

Sawasdidoln, C., Taweechaisupapong, S., Sermswan, R. W., Tattawasart, U., Tungpradabkul, S. & Wongratanacheewin, S. (2010). Growing *Burkholderia pseudomallei* in biofilm stimulating conditions significantly induces antimicrobial resistance. *PLoS ONE* **5**, e9196.

Scheurwater, E., Reid, C. W. & Clarke, A. J. (2008). Lytic transglycosylases: bacterial space-making autolysins. *Int J Biochem Cell Biol* **40**, 586-591.

Scheurwater, E. M. & Burrows, L. L. (2011). Maintaining network security: how macromolecular structures cross the peptidoglycan layer. *FEMS Microbiol Lett* **318**, 1-9.

Schraidt, O., Lefebre, M. D., Brunner, M. J., Schmied, W. H., Schmidt, A., Radics, J., Mechtler, K., Galán, J. E. & Marlovits, T. C. (2010). Topology and organization of the *Salmonella typhimurium* type III secretion needle complex components. *PLoS Pathog* **6**, e1000824.

Schroder, K., Hertzog, P. J., Ravasi, T. & Hume, D. A. (2004). Interferon-γ: an overview of signals, mechanisms and functions. *J Leukoc Biol* **75**, 163-189.

Schroeder, G. N. & Hilbi, H. (2008). Molecular pathogenesis of *Shigella* spp.: controlling host cell signaling, invasion, and death by type III secretion. *Clin Microbiol Rev* **21**, 134-156.

Scott, A. E., Twine, S. M., Fulton, K. M., Titball, R. W., Essex-Lopresti, A. E., Atkins, T. P. & Prior, J. L. (2011). Flagellar glycosylation in *Burkholderia pseudomallei* and *Burkholderia thailandensis*. *J Bacteriol* **193**, 3577-3587.

Serezani, C. H. C., Aronoff, D. M., Jancar, S., Mancuso, P. & Peters-Golden, M. (2005). Leukotrienes enhance the bactericidal activity of alveolar macrophages against *Klebsiella pneumoniae* through the activation of NADPH oxidase. *Blood* **106**, 1067-1075.

Simon, R., Priefer, U. & Pühler, A. (1983). A broad host range mobilization system for *in vivo* genetic engineering: transposon mutagenesis in Gram negative bacteria. *Biotechnology* **1**, 784-791.

Simpson, N., Audry, L. & Enninga, J. (2010). Tracking the secretion of fluorescently labeled type III effectors from single bacteria in real time. *Methods Mol Biol* **619**, 241-256.

Smith, S. M., Wunder, M. B., Norris, D. A. & Shellman, Y. G. (2011). A simple protocol for using a LDH-based cytotoxicity assay to assess the effects of death and growth inhibition at the same time. *PLoS ONE* **6**, e26908.

Soscia, C., Hachani, A., Bernadac, A., Filloux, A. & Bleves, S. (2007). Cross talk between type III secretion and flagellar assembly systems in *Pseudomonas aeruginosa*. *J Bacteriol* **189**, 3124-3132.

Stevens, J. M., Galyov, E. E. & Stevens, M. P. (2006). Actin-dependent movement of bacterial pathogens. *Nat Rev Micro* **4**, 91-101.

Stevens, J. M., Ulrich, R. L., Taylor, L. A., Wood, M. W., DeShazer, D., Stevens, M. P. & Galyov, E. E. (2005a). Actin-binding proteins from *Burkholderia mallei* and *Burkholderia thailandensis* can functionally compensate for the actin-based motility defect of a *Burkholderia pseudomallei bimA* mutant. *J Bacteriol* **187**, 7857-7862.

Stevens, M. P., Friebel, A., Taylor, L. A., Wood, M. W., Brown, P. J., Hardt, W.-D. & Galyov, E. E. (2003). A *Burkholderia pseudomallei* type III secreted protein, BopE, facilitates bacterial invasion of epithelial cells and exhibits guanine nucleotide exchange factor activity. *J Bacteriol* **185**, 4992-4996.

Stevens, M. P., Wood, M. W., Taylor, L. A., Monaghan, P., Hawes, P., Jones, P. W., Wallis, T. S. & Galyov, E. E. (2002). An Inv/Mxi-Spa-like type III protein secretion system in *Burkholderia pseudomallei* modulates intracellular behaviour of the pathogen. *Mol Microbiol* **46**, 649-659.

Stevens, M. P., Stevens, J. M., Jeng, R. L., Taylor, L. A., Wood, M. W., Hawes, P., Monaghan, P., Welch, M. D. & Galyov, E. E. (2005b). Identification of a bacterial factor required for actin-based motility of *Burkholderia pseudomallei*. *Mol Microbiol* **56**, 40-53.

Stevens, M. P., Haque, A., Atkins, T., Hill, J., Wood, M. W., Easton, A., Nelson, M., Underwood-Fowler, C., Titball, R. W., Bancroft, G. J. & Galyov, E. E. (2004). Attenuated virulence and protective efficacy of a *Burkholderia pseudomallei bsa* type III secretion mutant in murine models of melioidosis. *Microbiology* **150**, 2669-2676.

Stojkovic, B., Torres, E. M., Prouty, A. M., Patel, H. K., Zhuang, L., Koehler, T. M., Ballard, J. D. & Blanke, S. R. (2008). High-throughput, single-cell analysis of macrophage interactions with fluorescently labeled *Bacillus anthracis* spores. *Appl Environ Microbiol* **74**, 5201-5210.

Stroffekova, K., Proenza, C. & Beam, K. (2001). The protein-labeling reagent FLASH-EDT_2 binds not only to CCXXCC motifs but also non-specifically to endogenous cysteine-rich proteins. *Pflugers Arch* **442**, 859-866.

Sturm, A., Heinemann, M., Arnoldini, M., Benecke, A., Ackermann, M., Benz, M., Dormann, J. & Hardt, W.-D. (2011). The cost of virulence: retarded growth of *Salmonella* Typhimurium cells expressing type III secretion system 1. *PLoS Pathog* **7**, e1002143.

Sun, G. W. & Gan, Y.-H. (2010). Unraveling type III secretion systems in the highly versatile *Burkholderia pseudomallei*. *Trends Microbiol* **18**, 561-568.

Sun, G. W., Chen, Y., Liu, Y., Tan, G. Y., Ong, C., Tan, P. & Gan, Y. H. (2010). Identification of a regulatory cascade controlling type III secretion system 3 gene expression in *Burkholderia pseudomallei*. *Mol Microbiol* **76**, 677-689.

Suparak, S., Kespichayawattana, W., Haque, A., Easton, A., Damnin, S., Lertmemongkolchai, G., Bancroft, G. J. & Korbsrisate, S. (2005). Multinucleated giant cell formation and apoptosis in infected host cells is mediated by *Burkholderia pseudomallei* type III secretion protein BipB. *J Bacteriol* **187**, 6556-6560.

Szpirer, C. Y., Faelen, M. & Couturier, M. (2001). Mobilization function of the pBHR1 plasmid, a derivative of the broad-host-range plasmid pBBR1. *J Bacteriol* **183**, 2101-2110.

Tampakaki, A. P., Fadouloglou, V. E., Gazi, A. D., Panopoulos, N. J. & Kokkinidis, M. (2004). Conserved features of type III secretion. *Cell Microbiol* **6**, 805-816.

Tan, G.-Y. G., Liu, Y., Sivalingam, S. P., Sim, S.-H., Wang, D., Paucod, J.-C., Gauthier, Y. & Ooi, E.-E. (2008). *Burkholderia pseudomallei* aerosol infection results in differential inflammatory responses in BALB/c and C57Bl/6 mice. *J Med Microbiol* **57**, 508-515.

Tan, K. S., Chen, Y., Lim, Y. C., Tan, G. Y., Liu, Y., Lim, Y. T., Macary, P. & Gan, Y. H. (2010). Suppression of host innate immune response by *Burkholderia pseudomallei* through the virulence factor TssM. *J Immunol* **184**, 5160-5171.

Tangsudjai, S., Pudla, M., Limposuwan, K., Woods, D. E., Sirisinha, S. & Utaisincharoen, P. (2010). Involvement of the MyD88-independent pathway in controlling the intracellular fate of *Burkholderia pseudomallei* infection in the mouse macrophage cell line RAW264.7. *Microbiol Immunol* **54**, 282-290.

Taweechaisupapong, S., Kaewpa, C., Arunyanart, C., Kanla, P., Homchampa, P., Sirisinha, S., Proungvitaya, T. & Wongratanacheewin, S. (2005). Virulence of *Burkholderia pseudomallei* does not correlate with biofilm formation. *Microb Pathog* **39**, 77-85.

Terry, C. M., Picking, W. L., Birket, S. E., Flentie, K., Hoffman, B. M., Barker, J. R. & Picking, W. D. (2008). The C-terminus of IpaC is required for effector activities related to *Shigella* invasion of host cells. *Microb Pathog* **45**, 282-289.

Titball, R. W., Russell, P., Cuccui, J., Easton, A., Haque, A., Atkins, T., Sarkar-Tyson, M., Harley, V., Wren, B. & other authors (2008). *Burkholderia pseudomallei*: animal models of infection. *Trans R Soc Trop Med Hyg* **102 Suppl 1**, S111-S116.

Treerat, P., Widmer, F., Middleton, P. G., Iredell, J. & George, A. M. (2008). *In vitro* interactions of tobramycin with various nonantibiotics against *Pseudomonas aeruginosa* and *Burkholderia cenocepacia*. *FEMS Microbiol Lett* **285**, 40-50.

Tuanyok, A., Tom, M., Dunbar, J. & Woods, D. E. (2006). Genome-wide expression analysis of *Burkholderia pseudomallei* infection in a hamster model of acute melioidosis. *Infect Immun* **74**, 5465-5476.

Ulett, G. C., Ketheesan, N. & Hirst, R. G. (2000). Cytokine gene expression in innately susceptible BALB/c mice and relatively resistance C57BL/6 mice during infection with virulent *Burkholderia pseudomallei*. *Infect Immun* **68**, 2034-2042.

Ulett, G. C., Labrooy, J. T., Currie, B. J., Barnes, J. L. & Ketheesan, N. (2005). A model of immunity to *Burkholderia pseudomallei*: unique responses following immunization and acute lethal infection. *Microbes Infect* **7**, 1263-1275.

Ulrich, R. L., DeShazer, D., Brueggemann, E. E., Hines, H. B., Oyston, P. C. & Jeddeloh, J. A. (2004). Role of quorum sensing in the pathogenicity of *Burkholderia pseudomallei*. *J Med Microbiol* **53**, 1053-1064.

Utaisincharoen, P., Tangthawornchaikul, N., Kespichayawattana, W., Chaisuriya, P. & Sirisinha, S. (2001). *Burkholderia pseudomallei* interferes with inducible nitric oxide synthase (iNOS) production: a possible mechanism of evading macrophage killing. *Microbiol Immunol* **45**, 307-313.

Utaisincharoen, P., Anuntagool, N., Limposuwan, K., Chaisuriya, P. & Sirisinha, S. (2003). Involvement of beta interferon in enhancing inducible nitric oxide synthase production and antimicrobial activity of *Burkholderia pseudomallei*-infected macrophages. *Infect Immun* **71**, 3053-3057.

Utaisincharoen, P., Anuntagool, N., Arjcharoen, S., Limposuwan, K., Chaisuriya, P. & Sirisinha, S. (2004). Induction of iNOS expression and antimicrobial activity by interferon (IFN)-β is distinct from IFN-γ in *Burkholderia pseudomallei*-infected mouse macrophages. *Clin Exp Immunol* **136**, 277-283.

van Dissel, J. T., Stikkelbroeck, J. J., Michel, B. C., van den Barselaar, M. T., Leijh, P. C. & van Furth, R. (1987). Inability of recombinant interferon-gamma to activate the antibacterial activity of mouse peritoneal macrophages against *Listeria monocytogenes* and *Salmonella typhimurium*. *J Immunol* **139**, 1673-1678.

VanEngelenburg, S. B. & Palmer, A. E. (2008). Quantification of real-time *Salmonella* effector type III secretion kinetics reveals differential secretion rates for SopE2 and SptP. *Chem Biol* **15**, 619-628.

Wagner, S., Stenta, M., Metzger, L. C., Dal Peraro, M. & Cornelis, G. R. (2010). Length control of the injectisome needle requires only one molecule of Yop secretion protein P (YscP). *Proc Natl Acad Sci U S A* **107**, 13860-13865.

Walker, K. A. & Miller, V. L. (2004). Regulation of the Ysa type III secretion system of *Yersinia enterocolitica* by YsaE/SycB and YsrS/YsrR. *J Bacteriol* **186**, 4056-4066.

Warawa, J. & Woods, D. E. (2005). Type III secretion system cluster 3 is required for maximal virulence of *Burkholderia pseudomallei* in a hamster infection model. *FEMS Microbiol Lett* **242**, 101-108.

Whitmore, A. (1913). An account of a glanders-like disease occurring in Rangoon. *J Hyg (Lond)* **13**, 1-34.

Wiersinga, W. J. & van der Poll, T. (2009). Immunity to *Burkholderia pseudomallei*. *Curr Opin Infect Dis* **22**, 102-108.

Wiersinga, W. J., Currie, B. J. & Peacock, S. J. (2012). Melioidosis. *N Engl J Med* **367**, 1035-1044.

Wiersinga, W. J., van der Poll, T., White, N. J., Day, N. P. & Peacock, S. J. (2006). Melioidosis: insights into the pathogenicity of *Burkholderia pseudomallei*. *Nat Rev Micro* **4**, 272-282.

Winstanley, C., Hales, B. A. & Hart, C. A. (1999). Evidence for the presence in *Burkholderia pseudomallei* of a type III secretion system-associated gene cluster. *J Med Microbiol* **48**, 649-656.

Worrall, L. J., Lameignere, E. & Strynadka, N. C. J. (2011). Structural overview of the bacterial injectisome. *Curr Opin Microbiol* **14**, 3-8.

Wuthiekanun, V. & Peacock, S. J. (2006). Management of melioidosis. *Expert Rev Anti Infect Ther* **4**, 445-455.

Yabuuchi, E., Kosako, Y., Oyaizu, H., Yano, I., Hotta, H., Hashimoto, Y., Ezaki, T. & Arakawa, M. (1992). Proposal of *Burkholderia* gen. nov; and transfer of seven species of the *Pseudomonas* homology group II to the new genus, with the type species *Burkholderia cepacia* (Palleroni and Holmes 1981) comb. nov. *Microbiol Immunol* **36**, 1251–1275.

Yao, Q., Cui, J., Zhu, Y., Wang, G., Hu, L., Long, C., Cao, R., Liu, X., Huang, N., Chen, S. Liu, L. & Shao, F. (2009). Structural overview of the bacterial injectisome. *Proc Natl Acad Sci U S A* **106**, 3716-3721.

Yip, C. K., Kimbrough, T. G., Felise, H. B., Vuckovic, M., Thomas, N. A., Pfuetzner, R. A., Frey, E. A., Brett Finlay, B., Miller, S. I. & other authors (2005). Structural characterization of the molecular platform for type III secretion system assembly. *Nature* **435**, 702-707.

Yokoseki, T., Iino, T. & Kutsukake, K. (1996). Negative regulation by FliD, FliS, and FliT of the export of the flagellum-specific anti-sigma factor, FlgM, in *Salmonella typhimurium*. *J Bacteriol* **178**, 899-901.

Yu, F. S., Cornicelli, M. D., Kovach, M. A., Newstead, M. W., Zeng, X., Kumar, A., Gao, N., Yoon, S. G., Gallo, R. L. & other authors (2010a). Flagellin stimulates protective lung mucosal immunity: role of cathelicidin-related antimicrobial peptide. *J Immunol* **185**, 1142-1149.

Yu, Y.-C., Lin, C.-N., Wang, S.-H., Ng, S.-C., Hu, W. & Syu, W., Jr. (2010b). A putative lytic transglycosylase tightly regulated and critical for the EHEC type three secretion. *J Biomed Sci* **17**, 1-9.

Zahrl, D., Wagner, M., Bischof, K., Bayer, M., Zavecz, B., Beranek, A., Ruckenstuhl, C., Zarfel, G. E. & Koraimann, G. (2005). Peptidoglycan degradation by specialized lytic transglycosylases associated with type III and type IV secretion systems. *Microbiology* **151**, 3455-3467.

Zhang, L., Wang, Y., Picking, W. L., Picking, W. D. & De Guzman, R. N. (2006). Solution structure of monomeric BsaL, the type III secretion needle protein of *Burkholderia pseudomallei*. *J Mol Biol* **359**, 322-330.

Zhu, W., MaGbanua, M. M. & White, F. F. (2000). Identification of two novel *hrp*-associated genes in the *hrp* gene cluster of *Xanthomonas oryzae* pv. oryzae. *J Bacteriol* **182**, 1844-1853.

Appendices

Appendices

Appendix 1: Formulation and preparation of culture media

Cultural media were prepared, autoclaved and, unless otherwise indicated, stored at room temperature.

A1.1 Protocol for preparation of Luria-Bertani (LB) broth – 100 mL

- Tryptone 1 g
- Yeast extract 0.5 g
- NaCl 0.5 g
- dH_2O up to 100 mL

* Supplemented with ampicillin (100 μg/mL), chloramphenicol (20, 50 or 100 μg/mL), kanamycin (50 μg/mL or 1 mg/mL) or tetracycline (12.5 or 25 μg/mL) as required, after autoclaving.
* Supplemented with 5% (w/v) sucrose and/or 0.08% (w/v) congo red as required before autoclaving.
* Supplemented with 320 mM NaCl as required before autoclaving.

A1.2 Protocol for preparation of glycerol broth – 100 mL

- Heart infusion 3.7 g
- Glycerol 30 mL
- dH_2O up to 100 mL

A1.3 Protocol for preparation of super optimal broth (SOB) – 100 mL

- Tryptone 2 g
- Yeast extract 0.5 g
- NaCl 0.05 g
- KCl 0.02 g
- dH_2O up to 100 mL

Appendix 2: Formulation and preparation of buffers

Buffer solutions were prepared and, unless otherwise indicated, stored at room temperature.

A2.1 1 M Tris-hydrochloric acid (Tris-HCl), pH 7.5

- Tris base 121.14 g
- ddH_2O up to 1 L

Tris base (AMRESCO®, OH, USA) was dissolved in 700 mL of ddH_2O. The stock solution was adjusted to pH 7.5 with 37% (v/v) HCl. The final volume was brought to 1 L with ddH_2O.

A2.2 0.5 M Tris-hydrochloric acid (Tris-HCl), pH 6.8

- Tris base 60.57 g
- ddH_2O up to 1 L

Tris base was dissolved in 700 mL of ddH_2O. The stock solution was adjusted to pH 6.8 with 37% (v/v) HCl. The final volume was brought to 1 L with ddH_2O.

A2.3 50X Tris-acetate-EDTA (TAE)

- Tris base 242 g
- 50 mM EDTA, pH 8.0 100 mL
- Glacial acetic acid 57.1 mL
- ddH_2O up to 1 L

Tris base and EDTA were mixed and dissolved in 500 mL of ddH_2O. Glacial acetic acid was then added prior to bringing the final volume to 1 L with ddH_2O.

A2.4 1X TAE running buffer

- 50X TAE 20 mL
- ddH_2O up to 1 L

A2.5 10x DNA loading buffer

- 50X TAE 20 mL
- Sucrose 40 g
- Bromophenol blue 10 mg
- ddH_2O up to 100 mL

Bromophenol blue was purchased from Bio-Rad Laboratories (NSW, Australia). The loading buffer was prepared and stored at 4^oC.

A2.6 3 M sodium acetate (NaAc)

- sodium acetate (NaAc) 40.81 g
- ddH_2O up to 100 mL

NaAc was dissolved in 70 mL of ddH_2O. The pH was adjusted to pH 5.2 with glacial acetic acid. The final volume was brought to 100 mL with ddH_2O prior to autoclaving.

A2.7 10X Phosphate-buffered saline (PBS), pH 7.4

- NaCl 80 g
- KCl 2 g
- Na_2HPO_4 14.4 g
- KH_2PO_4 2.4 g
- ddH_2O up to 1 L

NaCl, KCl, Na_2HPO_4 and KH_2PO_4 were mixed and dissolved in 700 mL of ddH_2O. The pH was adjusted to 7.4 with 37% (v/v) HCl. The final volume was brought to 1 L with ddH_2O prior to autoclaving.

A2.8 1X PBS buffer, pH 7.4

- 10X PBS, pH 7.4 100 mL
- ddH_2O up to 1 L

The buffer was prepared and autoclaved before use.

A2.9 1X PBS/0.1% (v/v) Triton X-100

- 10X PBS, pH 7.4 100 mL
- Triton X-100 1 mL
- ddH_2O up to 1 L

The buffer was prepared and filtered through a 0.20 μM filter (Pall Life Science, NY, USA). The washing buffer was pre-warmed at 37^{o}C before use.

A2.10 1X PBS/0.5% (w/v) saponin

- 10X PBS, pH 7.4 100 mL
- Saponin 5 g
- ddH_2O up to 1 L

Saponin was purchased from Sigma-Aldrich (MO, USA). The buffer was prepared and filtered through a 0.20 μM filter. The washing buffer was pre-warmed at 37^{o}C before use.

A2.11 1X PBS/1% (w/v) bovine serum albumin (BSA)

- 10X PBS, pH 7.4 100 mL
- BSA 10 g
- ddH_2O up to 1 L

BSA (≥ 96%) was purchased from Sigma-Aldrich (MO, USA). The buffer was prepared and filtered through a 0.20 μM filter. The washing buffer was pre-warmed at 37°C before use.

A2.12 1X PBS/3.5% (w/v) paraformaldehyde (PFA)

- 16% (w/v) PFA 21.88 mL
- 10X PBS, pH 7.4 10 mL
- ddH_2O up to 100 mL

PFA (16% stock solution per ampoule, EM grade) was purchased from Electron Microscopy Sciences, Inc. (PA, USA). The buffer was prepared and filtered through a 0.20 μM filter prior to storing at -20°C until use.

A2.13 Resolving gel buffer, pH 8.8 (for SDS-PAGE analysis)

- Tris base 181.65 g
- Sodium dodecyl sulfate (SDS) 4 g
- ddH_2O up to 1 L

Tris base and SDS (AMRESCO®, OH, USA) were dissolved in 700 mL of ddH_2O. The stock solution was adjusted to pH 8.8 with 37% (v/v) HCl. The final volume was brought to 1 L with ddH_2O.

A2.14 Stacking gel buffer, pH 6.8 (for SDS-PAGE analysis)

- Tris base 60 g
- SDS 4 g
- ddH_2O up to 1 L

Tris base and SDS were dissolved in 700 mL of ddH_2O. The stock solution was adjusted to pH 6.8 with 37% (v/v) HCl. The final volume was brought to 1 L with ddH_2O.

A2.15 5X Laemmli sample buffer with β-mercaptoethanol (BME)

- 0.5 M Tris-HCl, pH 6.8 2.4 mL
- glycerol 2.5 mL
- 10% (w/v) SDS 2 mL
- 1% (w/v) bromophenol blue 1 mL
- BME 10 μL
- ddH_2O 1.1 mL

BME (14.3 M, the stock solution) was purchased from Sigma-Aldrich (MO, USA). This stock solution was prepared and stored at -20^{o}C.

A2.16 5X Laemmli sample buffer (no reducing agent)

- 0.5 M Tris-HCl, pH 6.8 2.4 mL
- glycerol 2.5 mL
- 10% (w/v) SDS 2 mL
- 1% (w/v) bromophenol blue 1 mL
- ddH_2O 1.1 mL

The stock solution was prepared and stored at -20^{o}C. Reducing agents were added before use as indicated.

A2.17 5X Tris-glycine running buffer (for SDS-PAGE analysis)

- Tris base 15 g
- Glycine 72 g
- SDS 5 g
- ddH_2O up to 1 L

A2.18 10X Transblot buffer (for Western blotting)

- Tris base 30.3 g
- Glycine 144.1 g
- ddH_2O up to 1 L

A2.19 1X Transblot buffer, working solution (for Western blotting)

- 10X Transblot buffer 100 mL
- Methanol 100 mL
- ddH_2O 800 mL

This working solution was prepared and kept in at 4^{o}C until use, and was reused up to three times.

A2.20 10X Tris-buffered saline (TBS), pH 7.4

- Tris base 121.2 g
- NaCl 175.4 g
- ddH_2O up to 1 L

Tris base and NaCl were dissolved in 700 mL of ddH_2O. The stock solution was adjusted to pH 7.4 with 37% (v/v) HCl. The final volume was brought to 1 L with ddH_2O.

A2.21 1X TBS/0.1% (v/v) Tween-20 buffer

- 10X TBS 100 mL
- Tween-20 1 mL
- ddH_2O up to 1 L

A2.22 Blocking buffer (for Western blotting)

- 1X TBS/0.1% Tween-20 20 mL
- Skim milk powder 1 g

The buffer was freshly prepared on the day of experiment.

A2.23 Coomassie Brilliant Blue staining

- Coomassie Brilliant Blue R-250 1 g
- Glacial acetic acid 100 mL
- Absolute ethanol 400 mL
- ddH_2O up to 1 L

Coomassie Brilliant Blue R-250 was purchased from Bio-Rad Laboratories (NSW, Australia).

A2.24 Destaining solution (for SDS-PAGE analysis)

- Glacial acetic acid 70 mL
- Absolute ethanol 400 mL
- ddH_2O up to 1 L

A2.25 RF1 buffer – 40 mL

- RbCl 0.48 g
- $MnCl_2$ 0.40 g
- 30 mM potassium acetate, pH 7.5 1.2 mL
- $CaCl_2 \cdot 2H_2O$ 0.06 g
- glycerol 6 mL

The buffer was prepared freshly on the day of experiment and carefully adjusted to pH 5.8 with 0.2 M acetic acid. The final volume was brought to 40 mL with ddH_2O prior to filter sterilisation using 0.20 μM filter (Pall Life Science, NY, USA). The buffer was placed on ice before use.

A2.26 RF2 buffer – 20 mL

- RbCl 0.02 g
- MOPS 0.4 mL

- $CaCl_2 \cdot 2H_2O$ 0.22 g
- glycerol 3 mL

The buffer was prepared freshly on the day of experiment and carefully adjusted to pH 6.8 with 0.1 M NaOH. The final volume was brought to 20 mL with ddH_2O prior to filter sterilisation using 0.20 μM filter. The buffer was placed on ice before use.

A2.27 Depurination solution – 50 mL

- 5 M HCl 2.5 mL
- ddH_2O up to 50 mL

5 M HCl was prepared by diluting stock HCl (37% w/w; 12 M) with ddH_2O e.g. 50 mL of stock HCl in 70 mL of ddH_2O.

A2.28 Denaturation solution

- 2 M NaOH 100 mL
- 5 M NaCl 120 mL
- ddH_2O up to 1 L

2 M NaOH was prepared by dissolving 80 g of NaOH in 1 L of ddH_2O. 5 M NaCl was prepared by dissolving 292.2 g of NaCl in 1 L of ddH_2O.

A2.29 Neutralisation solution

- Tris base 121.2 g
- NaCl 87.7 g
- ddH_2O up to 1 L

Tris base and NaCl were dissolved in 700 mL of ddH_2O. The stock solution was adjusted to pH 7.5 with 37% (v/v) HCl. The final volume was brought to 1 L with ddH_2O.

A2.30 20X Saline sodium citrate (SCC) buffer

- NaCl 175.3 g
- Sodium citrate 83.3 g
- ddH_2O up to 1 L

Sodium citrate and NaCl were dissolved in 700 mL of ddH_2O. The stock solution was adjusted to pH 7.0 with 37% (v/v) HCl. The final volume was brought to 1 L with ddH_2O.

A2.31 2X SCC solution

- 20X SCC 10 mL
- ddH_2O up to 100 mL

The buffer was freshly prepared before use.

A2.32 10X SCC solution

- 20X SCC 50 mL
- ddH_2O up to 100 mL

The buffer was freshly prepared before use.

A2.33 Pre-hybridisation solution (for Southern blotting)

- 20X SCC 7.5 mL
- Skim milk powder 0.5 g
- 10% (w/v) N-lauroylsarcosine 0.3 mL
- 10% (w/v) SDS 0.06 mL
- ddH_2O 22.14 mL

The buffer was prepared and incubated at 65^{o}C for 45 min to completely dissolve the skim milk powder. The buffer was stored at -20^{o}C until use.

A2.34 2X Wash solution (for Southern blotting)

- 20X SCC 100 mL
- 10% (w/v) SDS 10 mL
- ddH_2O up to 1 L

A2.35 0.2X Wash solution (for Southern blotting)

- 20X SCC 10 mL
- 10% (w/v) SDS 10 mL
- ddH_2O up to 1 L

A2.36 5X Maleic acid buffer, pH 7.5

- Maleic acid 58.04 g
- NaCl 43.82 g
- ddH_2O up to 1 L

Maleic acid and NaCl were dissolved in 500 mL of ddH_2O. The stock solution was adjusted to pH 7.5 with NaOH pellets. The final volume was brought to 1 L with ddH_2O. The stock solution was autoclaved before use.

A2.37 Washing buffer (for Southern blotting)

- 5X Maleic acid buffer, pH 7.5 100 mL
- Tween 20 1.5 mL
- ddH_2O up to 500 mL

A2.38 Blocking buffer (for Southern blotting)

- Washing buffer 200 mL
- Skim milk powder 2 g

The buffer was freshly prepared on the day of experiment.

A2.39 Detection solution (for Southern blotting)

- Tris base 12.1 g
- NaCl 5.85 g
- ddH_2O up to 1 L

Tris-base and NaCl were dissolved in 700 mL of ddH_2O. The stock solution was adjusted to pH 9.5 with 37% (v/v) HCl. The final volume was brought to 1 L with ddH_2O.

Appendix 3: Polymerase chain reaction (PCR) protocols and other reaction conditions

Table A3.1 Standard protocol for the preparation of PCR using Taq polymerase

PCR mixture	**1 reaction**
• 10X PCR reaction buffer* (with 25 mM Mg_2Cl)	2 µL
• DMSO	2 µL
• Forward primer (10 µM)	2 µL
• Reverse primer (10 µM)	2 µL
• 10 mM dNTPs	0.4 µL
• Taq polymerase	0.2 µL
• Sterile double distilled water	10.9 µL
• DNA template (10-500 pg)	0.5 µL
Total	**20 µL**

*****100 mM Tris-HCl, 500 mM KCl; pH 8.3

PCR cycling condition

Cycles	**Temp**	**Time**
1	94ºC	10 min
	94ºC	30 sec
35	X*ºC	30 sec
	72ºC	$X^{\#}$ min
1	72ºC	7 min
	10ºC	hold

X* = 58°C when DNA templates were extracted from *E. coli* strains, or 60°C when the templates were extracted from *B. pseudomallei* strains.

$X^{\#}$ = extension time depending on the expected size of DNA fragments, generally, 60 sec per 1 kilobase.

Table A3.2 Standard protocol for the preparation of PCR using Expand High Fidelity PCR system

PCR mixture	**1 reaction**
• 5X Expand High Fidelity PCR buffer (no Mg_2Cl)	2 µL
• 25 mM Mg_2Cl	4 µL
• DMSO	2 µL
• Forward primer (10 µM)	2 µL
• Reverse primer (10 µM)	2 µL
• 10 mM dNTPs	0.4 µL
• Expand High Fidelity Taq polymerase	0.2 µL
• Sterile double distilled water	6.9 µL
• DNA template (10-500 pg)	0.5 µL
Total	**20 µL**

PCR cycling condition

Cycles	**Temp**	**Time**
1	94ºC	2 min
	94ºC	30 sec
35	52-62ºC	30 sec
	72ºC	2 min
1	72ºC	$X^{\#}$ min
	10ºC	hold

$X^{\#}$ = extension time depending on the expected size of DNA fragments, generally, 60 sec per 1 kilobase.

Table A3.3 Standard protocol for the preparation of PCR using KOD polymerase

PCR mixture	**1 reaction**
• 10X KOD PCR buffer*	2.5 µL
• KOD 25 mM $MgSO_4$	1 µL
• DMSO	1.25 µL
• Betaine** (5 M)	12.5 µL
• Forward primer (10 µM)	1.5 µL
• Reverse primer (10 µM)	1.5 µL
• KOD dNTP mix	2.5 µL
• KOD polymerase	0.5 µL
• Sterile double distilled water	1.25 µL
• DNA template (10-500 pg)	0.5 µL
Total	**25 µL**

*1.2 M Tris-HCl, 100 mM KCl, 60 mM $(NH_4)_2SO_4$, 1% Triton X-100, 0.01% BSA, pH 8.0.

**Betaine was purchased from Sigma-Aldrich (MO, USA).

PCR cycling condition

Cycles	**Temp**	**Time**
1	93ºC	2 min
	93ºC	20 sec
35	58ºC	30 sec
	70ºC	$X^{\#}$ min
1	72ºC	7 min
	10ºC	hold

$X^{\#}$ = extension time depending on the expected size of DNA fragments, generally, 60 sec per 1 kilobase.

Table A3.4 Standard protocol for the preparation of nucleotide sequencing

PCR mixture	**1 reaction**
• BigDye premix*	2 µL
• DMSO	2 µL
• Forward or reverse primer (10 µM)	1 µL
• 10X PCR buffer**	1 µL
• Sterile double distilled water	9-12 µL
• DNA template (10-500 pg)	2-5 µL
Total	**20 µL**

* Applied Biosystems PRISM BigDye Terminator Mix v 3.1 (Life Technologies, Victoria, Australia)

**100 mM Tris-HCl, 500 mM KCl, pH 8.3.

PCR cycling condition

Cycles	**Temp**	**Time**
1	96ºC	1 min
	96ºC	10 sec
30	55ºC	5 sec
	60ºC	4 min
1	4ºC	2 min
	10ºC	hold

Table A3.5 Standard protocol for sequencing reaction clean-up using sodium acetate-ethanol method

In a standard 1.5 mL microfuge tube:

Sequencing clean-up mixture	**1 reaction**
• 3 M Sodium acetate, pH 5.2 (*Appendix 2, A2.6*)	3 µL
• 96% (v/v) ethanol	62.5 µL
• Sterile double distilled water	14.5 µL

The sequencing clean-up mixture solution was freshly prepared before mixing with 20 µL of cycle sequencing reaction and incubating at room temperature for 15 min. The reaction mixture was centrifuged at 11,337 x g (13,000 rpm) for 30 min, and the supernatant was discarded. Washing step was performed in 70% (v/v) ethanol, and the pellet was dried (with the lid open) at 70-90^{o}C for 1 min. The microfuge tube was allowed to cool prior to dropping off at Micromon (Monash University, Australia) for further analysis.

Table A3.6 PCR protocol for the preparation of DIG-labelled DNA probes using Taq polymerase

PCR mixture	DIG-labelled (1 reaction)	Non DIG-labelled (1 reaction)
• 10X PCR reaction buffer* (with 25 mM Mg_2Cl)	5 µL	5 µL
• DMSO	5 µL	5 µL
• Forward primer (10 µM)	2 µL	2 µL
• Reverse primer (10 µM)	2 µL	2 µL
• 10 mM dNTPs	2 µL	2 µL
• 10 mM DIG-labelled dNTPs	2 µL	-
• Taq polymerase	0.5 µL	0.5 µL
• Sterile double distilled water	30.5 µL	32.5 µL
• DNA template (10-500 pg)	1 µL	1 µL
Total	**50 µL**	**50 µL**

*****100 mM Tris-HCl, 500 mM KCl; pH 8.3

PCR cycling condition

Cycles	Temp	Time
1	94ºC	10 min
	94ºC	30 sec
35	60ºC	30 sec
	72ºC	$X^{\#}$ min
1	72ºC	7 min
	10ºC	hold

$X^{\#}$ = extension time depending on the expected size of DNA fragments, generally, 60 sec per 1 kilobase.